Coinage metal complexes bearing *mono*-supported borohydride ligands based on scorpionate scaffolds

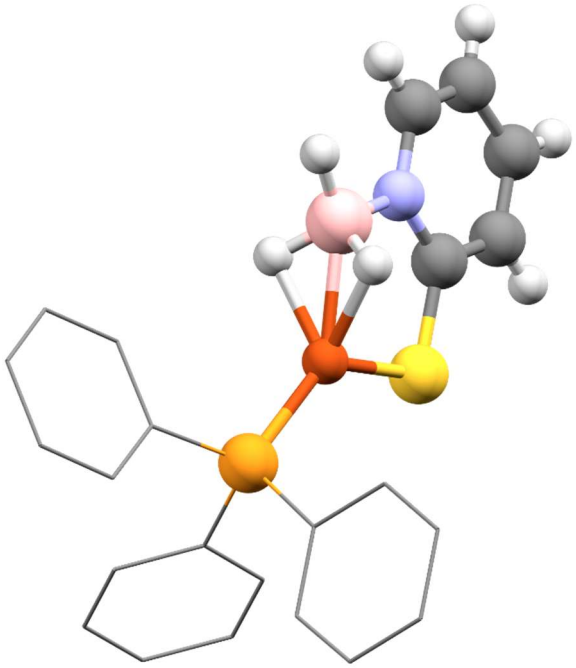

Simon David Thomas

A submission presented in partial fulfilment of the requirements of the University of South Wales/ Prifysgol De Cymru for the degree of Doctor of Philosophy

Supervised by
Dr Gareth Owen

September 2021

I: Acknowledgements

I would like to first thank my director of studies Dr. Gareth Owen for affording me the opportunity to undertake this research project, for his guidance during the project and his assistance in writing this thesis. In addition to Dr. Owen I would also like to thank the University of South Wales for providing the funding for this research. I extend my thanks to my supervisor's Dr Natasha Galea, Dr Suzy Kean and the staff at the Graduate School who have provided support throughout this project.

I would also like to express my gratitude to the technical staff at the University of South Wales who will not hesitate to offer their assistance when needed and have on numerous occasions lent equipment and chemicals and kept the NMR, ATR and other equipment running. I would also like to express my gratitude to Stephen Boyer, for his assistance with elemental analysis, Dr. Graham Tizzard for his assistance with obtaining crystal structures, The NMSF at Swansea University and Robin Hicks at Cardiff University for their assistance in running mass spectra.

I am grateful for the assistance from my group members Dr. Nildo Costa and Dr. Angelo Iannetelli for explaining new techniques and their assistance in the synthesis of the ligands used in this thesis. I would also like to that the rest of the group and everyone I shared an office with in GK111 for making this PhD fly by so fast. Last but certainly not least I am extremely grateful for the support I have received from friends and family, I will be forever grateful.

II: Abstract

Singly supported borohydride ligands, in comparison to scorpionate ligands are scarcely reported within the chemical literature. This thesis looks at select examples of the coordination of such ligands and compares the different supporting scaffolds and structural motifs between these ligands. It also draws comparisons with their neutral analogues, the supported borane ligand. Both supported borohydride and borane ligands can observe a range of coordination modes which are discussed. Using the available spectroscopic and diffraction data Chapter 2 explores the coordination of such ligands across a range of select examples throughout the chemical literature.

The coordination of singly supported borohydride ligands was then investigated. This thesis presents the first example of the coordination of a singly supported borohydride ligand to copper complexes in Chapter 3. The ligands utilised were based on known scorpionate scaffolds and were compared to their bis- and tris- counterparts. The coordination of the mono- ligands allows for the $[BH_n]^-$ unit to come into closer proximity to the metal centre. The addition of substitutions at the $[BH_n]^-$ moiety have also been shown to influence the coordination of the bridging B-H bonds. For example, the addition of a phenyl ring results in the bridging hydrogens being more protic in character and conversely a methyl substituent gives hydrogens that are more hydridic in character. Using the same metal, the nature of the supporting scaffolds is also investigated and compared.

Chapter 4 extends the investigation and reports the synthesis of silver complexes and the first examples of gold complexes of singly supported borohydride ligands. Such complexes were previously thought to be unachievable due to the reducing power of the $[BH_n]^-$ group. Comparisons between the supporting scaffolds and the addition of substituents to the borohydride group support the conclusions made in the previous chapter. In particular the coordination of the 7-azaindol-7-ylborate (Mai) scaffold demonstrates an unexpected coordination mode which is consistent across the copper and silver complexes. Comparisons of complexes down the coinage metal group reveals that coordination of the $[BH_n]^-$ group becomes weaker with the heavier metal centres.

The final results chapter, Chapter 5 explores the potential for the development of new supporting scaffolds for singly supported borohydride ligands, in particular those which are supported by carbenes. Carbenes were selected for their notorious election donating properties. This chapter explores the synthesis of carbenes and their pro-ligands which contain a vinyl group as a potential site for hydroboration. The synthesis of the precursors was found to be best achieved using the addition of $BrCH_2BPin$ to functionalised imidazoles. The pro-ligands were found to be uncharacteristically stubborn to deprotonation and did not form carbenes. Furthermore, the synthesis of the respective CAAC iminium precursor again did not deprotonate.

III: Contents

I: Abstract i

II: Contents iv

III: List of Figures vii

IV: List of Schemes ix

V: List of Tables xiii

VI: Abbreviations and symbols xiv

Chapter 1: Introduction 1
1.1Introduction 1
1.2 Metal ligand bonding 3
1.3 Scope of project 6
1.4 Early work on metal borohydride chemistry 9
1.4.1 Structural characterisation of tetra hydroborate ligands 10
1.4.2 Computational studies of tetrahydroborate as a ligand 12

Chapter 2: A review of metal complexes containing mono-supported borohydride and borane ligands 15
2.1 Introduction 15
2.2 Bonding features in singly supported BH_n ligands 17
2.3 Examples of mono- supported neutral borane ligands 21
2.3.1 Neutral one-atom supported borane ligands 21
2.3.2 Neutral three-atom supported borane ligands 25
2.4 Examples of mono- supported anionic borohydride ligands 41
2.4.1 Anionic two-atom supported borohydride ligands 42
2.4.2 Anionic three-atom supported borohydride ligands 45
2.4.3 An example of an anionic five-atom supported borohydride ligand 55
2.5 Review conclusions 57

Chapter 3: Synthesis and structure of copper complexes containing a supported anionic borohydride ligand with a 3-atom bridge 59
3.1 Introduction 59
3.2 Complexes based on a 2-mercaptopyridine scaffold 60
3.2.1 Synthesis of copper Mmp complexes 63
3.2.2 Synthesis of ^{R}Mmp ligands 72
3.2.3 Synthesis of copper ^{Ph}Mmp complexes 75
3.2.4 Synthesis of copper ^{Me}Mmp complexes 80
3.3 Complexes based on a 7-azaindole scaffold 84
3.3.1 Synthesis of copper Mai complexes 87
3.3.2 Synthesis of copper ^{Me}Bai complexes 97
3.4 Complexes based on a methimazole scaffold 102
3.4.1 Synthesis of ligands based on the methimazole scaffold 102
3.4.2 Synthesis of copper Mm complexes 104

3.4.3 Synthesis of copper Bm complexes 108
3.5 Chapter summary/conclusions 111

Chapter 4: Synthesis and structure of silver and gold complexes containing a supported anionic borohydride ligand with a 3-atom bridge 113
4.1 Introduction 113
4.2 Synthesis of silver complexes 118
4.2.1 Introduction 118
4.2.2 Mmp complexes 119
4.2.3 ^{R}Mmp complexes 124
4.2.4 Mai complexes 127
4.3 Synthesis of gold complexes 135
4.3.1 Examples of bis and tris complexes of gold 135
4.3.2 Synthesis of mono gold complexes 140
4.4 Summary, discussion and comparisons of complexes synthesised in chapter 3 and 4 144
4.5 Chapter conclusions 148

Chapter 5: Towards the synthesis of novel supported borane and borohydride-based ligands 149
5.1 Introduction 149
5.1.1 Hydroboration of vinyl phosphine ligands 152
5.2 The hydroboration route 154
5.2.1 Reactions of borane with vinyl imidazole 154
5.2.2 Synthesis of vinyl imidazolium salts 159
5.2.3 Reactions of borane with vinyl imidazolium salts 161
5.2.4 Synthesis vinyl functionalised carbenes 162
5.2.5 Synthesis of a rhodium carbene complex 165
5.3 An alternative method involving boron-containing alkylating reagents 168
5.3.1 Synthesis MeBPin imidazolium salts 174
5.3.2 Activation attempts 178
5.3.3 Reduction using $LiAlH_4$ 183
5.3.4 Synthesis of iminium salts bearing a pendant BPin moiety 187
5.4 Chapter conclusions 192

Chapter 6: Experimental 194
6.1 General experimental remarks 194
6.2 Synthesis and structure of copper complexes containing a supported anionic borohydride ligand with a 3-atom bridge 195
Synthesis of [Cu(Mmp)(PPh_3)] 195
Synthesis of [Cu(Mmp)(PCy_3)] 196
Synthesis of [Cu(^{Ph}Mmp)(PPh_3)] 198
Synthesis of [Cu(^{Ph}Mmp)(PCy_3)] 199
Synthesis of [Cu(^{Me}Mmp)(PPh_3)] 200
Synthesis of [Cu(^{Me}Mmp)(PCy_3)] 201
Synthesis of [Cu(Mai)(PPh_3)$_2$] 202
Synthesis of [Cu(Mai)(PCy_3)] 203
Synthesis of [Cu(^{Me}Bai)(PPh_3)] 204

Synthesis of [Cu(^{Me}Bai)(PCy_3)] 205
Synthesis of [Cu(Mm)(PPh_3)] 206
Synthesis of [Cu(Mm)(PCy_3)] 207
Synthesis of [Cu(Bm)(PPh_3)] 208
Synthesis of [Cu(Bm)(PCy_3)] 209
6.3 Synthesis of silver and gold complexes 210
Synthesis of [Ag(Mmp)(PPh_3)] 210
Synthesis of [Ag(Mmp)(PCy_3)] 211
Synthesis of [Ag(^{Me}Mmp)(PPh_3)] 212
Synthesis of [Ag(^{Me}Mmp)(PCy_3)] 213
Synthesis of [Ag(^{Ph}Mmp)(PPh_3)] 214
Synthesis of [Ag(^{Ph}Mmp)(PCy_3)] 215
Synthesis of [Ag(Mai)(PPh_3)$_2$] 216
Synthesis of [Ag(Mai)(PCy_3)] 217
Synthesis of [Au(Mmp)(PPh_3)] 218
Synthesis of [Au(Mai)(PPh_3)] 219
6.4 Carbene chapter 220
Synthesis of 5.12 220
Synthesis of 5.13 221
Synthesis of 5.14 222
Synthesis of 5.15 223
Synthesis of 5.34 224
Synthesis of 5.35 225
Synthesis of 5.36 226
Synthesis of 5.38 227
Synthesis of 5.39 228
Synthesis of 5.40 229
Synthesis of 5.41 230
Synthesis of 5.54 231
6.5 X-ray data tables 232

7. References 237

IV: List of Figures

Figure 1.1.	MO diagrams for L, X and Z ligands	3
Figure 1.2.	Structure and bonding in H_3^+	4
Figure 1.3.	Representations of the 3c-2e bond in H_3^+	4
Figure 1.4.	The structure of diborane	5
Figure 1.5.	The scorpionate analogy	6
Figure 1.6.	Mono-, bis- and tris- substituted borohydrides each demonstrating κ^3 coordination to a metal centre	7
Figure 1.7.	The notation utilise for scorpionate ligands	8
Figure 1.8.	Structure of $[Cu(PPh_2Me)_3(BH_4)]$	10
Figure 1.9.	A BH4 anion exhibiting η^2-B,H, κ^1-H, κ^2-H,H, η^3-H,B,H and κ^3-H,H,H coordination modes	12
Figure 1.10.	Coordination of BH_4 units in $[V(BH_4)_3(PMe_3)_2]$	13
Figure 1.11.	$[V(BH_4)_3(PMe_3)_2]$ showing (κ^1, κ^1, κ^1), (κ^2, κ^2, κ^2) and (κ^1, κ^2, κ^3) coordination modes	13
Figure 2.1.	Mono-, bis- and tris- substituted mono-supported BH_n ligands	17
Figure 2.2.	Hypothetical supported κ^3-H,H,H coordination of a mono-supported borohydride ligand	18
Figure 2.3.	Examples of both neutral and anionic metal boron complexes containing one, two and three atom supports	19
Figure 2.4.	Possible complexes based on the further reactivity of supported neutral and anionic boron-based ligands	20
Figure 2.5.	Synthesis of an analogous tungsten complex bearing the ligand 2.24	28
Figure 3.1.	^{11}B (left) and $^{11}B\{^1H\}$ (right) NMR of $[Cu(Mmp)(PPh_3)]$	64
Figure 3.2.	SC-XRD structures for complexes $[Cu(Mmp)(PCy_3)]$ (left) and $[Cu(Mmp)(PPh_3)]$ (right) showing a similar coordination mode for the Mmp ligand in both complexes	68
Figure 3.3.	^1H NMR spectra for $[Cu(^{Ph}Mmp)(PPh_3)]$	76
Figure 3.4.	SC-XRD structures for $[Cu(^{Ph}Mmp)(PCy_3)]$ (left) and $[Cu(^{Ph}Mmp)(PPh_3)]$ (right)	78
Figure 3.5.	SC-XRD structure for $[Cu(^{Me}Mmp)(PPh_3)]$	82
Figure 3.6.	^1H (red) and $^1H\{^{11}B\}$ (blue) NMR spectra for $[Cu(Mai)(PPh_3)_2]$ with a focus on the BH_3 resonance at 3.72 ppm	89
Figure 3.7.	SC-XRD structures for $[Cu(Mai)(PPh_3)_2]$ (left) and $[Cu(Mai)(PCy_3)]$ (right)	91
Figure 3.8.	SC-XRD structure of $[Cu(Mai)(PPh_3)_2]$ showing the distance of Cu from the closest point on the aza-plane(right) and the B(1)N(2)-N(1)Cu(1) torsion angles (right)	92
Figure 3.9.	SC-XRD structures illustrating the geometries of 2.90 (left), 2.91 (middle) and $[Cu(Mai)(PPh_3)_2]$ (right)	95
Figure 3.10.	SC-XRD structures for $[Cu(^{Me}Bai)(PPh_3)]$ (left), $[Cu(^{Me}Bai)(PCy_3)]$ (middle) and $[Cu(^{Me}Bai)_2]$ (right)	100
Figure 3.11	$^{31}P\{^1H\}$ spectra of $[Cu(Mm)(PCy_3)]$	105
Figure 3.12.	SC-XRD structure of $[Cu(Mm)(PCy_3)]$	106

Figure 3.13.	SC-XRD structure for [Cu(Bm)(PPh_3)]	109
Figure 4.1.	Left – Ligand scaffolds utilised in supported borohydride ligands Middle – Monomeric silver phosphine complex, Right – structure of a dimeric silver scorpionate compound	115
Figure 4.2.	$^{31}P\{^1H\}$ spectra of [Ag(Mmp)(PCy_3)] showing Ag^{107} and Ag^{109} splitting	120
Figure 4.3.	SC-XRD structure for [Ag(Mmp)(PCy_3)]	122
Figure 4.4.	^1H NMR spectra of [Ag(Mai)(PPh_3)$_2$]	129
Figure 4.5.	SC-XRD structures for [Ag(Mai)(PPh_3)$_2$] and [Ag(Mai)(PCy_3)]	130
Figure 4.6.	SC-XRD structures of [Ag(Mai)(PPh_3)$_2$] showing the torsion angles and extended 7-azaindole plane	132
Figure 4.7.	Idealised bond angles in Mmp and Mai chelates	134
Figure 4.8.	Selected examples of linear gold scorpionate compounds Left – [Au_3(o-$C_6F_4Br)_3$(Tp)], Middle – [Au(NHC)(Tp)] showing κ^1-N coordination of Tp, Right – [$Au_2(Bis^R)_2$]	136
Figure 4.9.	Selected examples of gold sulfur scorpionate complexes Left - [Au(Bm)(PEt_3)], Middle – the [Au_2(Bm)(PEt_2)] anion of molybdenum salt and Right – [Au(Bm)(PPh_3)]	137
Figure 4.10.	Examples of κ^1, κ^2 and κ^3 coordination to gold from the Tp scaffold Left – [Au(Tp^{R_2})(C_2H_4)] (4.6 and 4.7), middle [Au(Tp(CF_3)$_2$)(CO)] and Right – [Au(Tp(CF_3)$_2$)(N^tBu_3)]	138
Figure 4.11.	Example of a κ^3-N,N,N complex [Au(Tp*)(PPh^3)]	138
Figure 4.12	$^1H\{^{11}B\}$ spectra pf [Au(Mai)(PPh_3)]	142
Figure 5.1.	Structure of two (left) and three (right) atom bridged carbenes	149
Figure 5.2.	MO diagrams showing both Fischer and Schrock type carbenes	150
Figure 5.3.	A MO diagram showing both σ and π components in Wanzlick Ardeungo carbenes	150
Figure 5.4.	^{11}B spectra of the reaction between vinyl imidazole and borane showing formation of both boric acid and the vinyl imidazole adduct	155
Figure 5.5.	$^{13}C\{^1H\}$ NMR spectra showing C-Rh coupling in 5.15	166
Figure 5.6.	^1H NMR Spectra of 5.35	175
Figure 5.7.	^{11}B spectra indicating the formation of 5.42 *in situ*	183
Figure 5.4.	^1H NMR spectra of 5.54 in $CDCl_3$	189

V: List of Schemes

Scheme 1.1.	Conversion of trimethyl borate to sodium borohydride	9
Scheme 2.1.	One, two and three atom supports in supported borane/borohydride ligands	15
Scheme 2.2.	Addition of $LiBH_4$ to $[TiCl_2(salen)]$ resulting in the complex $[Ti(BH_4)_2(salen)]_2$	22
Scheme 2.3.	Addition of $NaBH_4$ across a C=S bond resulting in a supported neutral borane ligand	23
Scheme 2.4.	Addition of $NaBH_4$ to titanium dithiolate complex	24
Scheme 2.5.	Synthesis of a single carbon atom bridged neutral borane ligand using BH_3	24
Scheme 2.6.	Addition of BH_3 to diiron complex 2.19	26
Scheme 2.7.	Reactivity of the anionic ligand $[(BH_3)SCHS]^-$ with $[RuCl_2Cp^*]_2$ and subsequent addition of BH_3	26
Scheme 2.8.	Synthesis of chromium complexes bearing the ligand 2.24	27
Scheme 2.9.	Synthesis of the asymmetrical neutral borane ligand 2.33	29
Scheme 2.10.	Synthesis of a bis carbene bis borane neutral ligand	30
Scheme 2.11.	Deprotonation of the proligand $[(BH_3)mapyH]$ and subsequent reaction with $½[Rh(Cl)(cod)]_2$ to form the complex $[Rh\{(BH_3)mapy\}(cod)]$	32
Scheme 2.12.	Formation of both Mn and Ru complexes bearing the ligand $[(H_3B)mapy]$	33
Scheme 2.13.	Ruthenium and manganese complexes bearing the ligand $[(BH_3)iPrbzam]$	34
Scheme 2.14.	A cobalt complex bearing the dppm·BH_3 ligand	35
Scheme 2.15.	Synthesis of a rhodathiaborane dppm·BH_3 complex	36
Scheme 2.16.	Addition of the ligand dppm·BH_3 to $[RhCl(cod)_2]$ forming $[Rh(dppm·BH_3)(cod)]$ showing κ^3-P,H,H coordination	37
Scheme 2.17.	Addition of dppm·BH_3 to various metal complexes	38
Scheme 2.18.	Synthesis of manganese dppm·BH_3 complexes	39
Scheme 2.19.	Synthesis of an iron dppa·BH_3 complex	40
Scheme 2.20.	Tautomerism in methimazole	41
Scheme 2.21.	Synthesis of the anionic borohydride ligand based on a pyrazole scaffold	42
Scheme 2.22.	Coordination of a mono pyrazole ligand to silver	43
Scheme 2.23.	Synthesis of the ligand salt $K[Mp^{Ph_2}]$	43
Scheme 2.24.	Synthesis of copper complexes of $[MpPh_2]$	44
Scheme 2.25.	Synthesis of the ligand salts 2.74 and 2.75	45
Scheme 2.26.	Synthesis of the ligand salt 2.77	45
Scheme 2.27.	Synthesis of technetium and rhenium complexes containing monosubstituted borohydride ligands	47
Scheme 2.28.	Ligand substitution reactions representing exchange of the BH-M 3c-2e bond for an L-type ligand	48
Scheme 2.29.	Tautomerism in azaindole and synthesis of the ligand Mai	48
Scheme 2.30.	Synthesis and reactivity of the Mai ligand with rhodium centres	49

Scheme 2.31.	Synthesis of ligand salts 2.94 and 2.95	50
Scheme 2.32.	Manganese complexes of [(H_3B)abz] and [(H_3B)bbza]	51
Scheme 2.33	Synthesis of an Iridium complex bearing the ligand [H3B(mbt)]	52
Scheme 2.34.	Rhodium complexes of [(H_3B)mbt]	53
Scheme 2.35.	Synthesis and subsequent reactivity of the ligand Mmp with a rhodium nbd complex	54
Scheme 2.36.	Reactivity of [IrCl(IMes)$_2$(coe)] with $LiBH_4$ resulting in a supported borohydride intermediate	56
Scheme 3.1.	Synthesis of ligands [K(Tmp)] and [Na(Bmp)]	60
Scheme 3.2.	Synthesis of complex [Cu(Tmp)(PR_3)]	61
Scheme 3.3.	Synthesis of [Cu(Bmp)(PR_3)] complexes	62
Scheme 3.4.	Synthesis of ligand [Na(Mmp)] through intermediate 3.1	63
Scheme 3.5.	Synthesis of Cu(Mmp) complexes containing different phosphines	65
Scheme 3.6.	Tautomerism in the ligand [Na(Mmp)]	71
Scheme 3.7.	A Generic scheme for the Synthesis of functionalised borohydrides from boronic esters and acids	72
Scheme 3.8.	Synthesis of [Li(^{R}Mmp] ligands	73
Scheme 3.9.	Synthesis of [Cu(^{Ph}Mmp)(PR_3)] complexes	75
Scheme 3.10.	Synthesis of [Cu(^{Me}Mmp)(PR_3)] complexes	80
Scheme 3.11.	Tautomerism in 7-azaindole	84
Scheme 3.12.	Synthesis of the ligand K[Tai] and subsequent synthesis of [Cu(Tai)(PPh_3)]	84
Scheme 3.13.	Synthesis of the ligand [Na(Mai)]	85
Scheme 3.14.	Synthesis of the ligand [Li(^{Ph}Bai)]	86
Scheme 3.15.	Synthesis of [Cu(Mai)(PR_3)$_n$] complexes	88
Scheme 3.16.	Synthesis of the ligand salt [Li(MeBai)]	97
Scheme 3.17.	Synthesis of [Cu(^{Me}Bai)(PR_3)] complexes	98
Scheme 3.18.	Synthesis of the ligand Na[Tm]	102
Scheme 3.19.	Synthesis of the ligand [Li(Bm)]	103
Scheme 3.20.	Synthesis of ligand [Na(Mm)]	103
Scheme 3.21.	Synthesis of [Cu(Mm)(PR_3)] complexes (PR_3 = PPh_3 and PCy_3)	104
Scheme 3.22.	Synthesis of [Cu(Bm)(PR_3)] complexes (PR_3 = PPh_3 and PCy_3)	108
Scheme 4.1.	Synthesis of silver complexes bearing both tris and bis supported borohydride ligands based on methimazole	114
Scheme 4.2.	Synthesis of silver complexes reported by Rabinovich bearing the ligand Tm^{R}	116
Scheme 4.3.	Synthesis of the flexible scorpionate Na[^{mp}Bm] from Na[Bm] and subsequent addition to silver to make complex [Ag(^{mp}Bm)(PCy_3)] showing preference for κ3-S,S,H coordination over κ3-S,S,S	117
Scheme 4.4.	Synthesis of silver Mmp complexes	119

Scheme 4.5.	Synthesis of the [Ag(^{Me}Mmp)(PR_3)] complexes	124
Scheme 4.6.	Synthesis of the [Ag(^{Ph}Mmp)(PR_3)] complexes	125
Scheme 4.7.	Synthesis of complexes [Ag(Mai)(PPh_3)$_2$] and [Ag(Mai)(PCy_3)]	127
Scheme 4.8.	Synthesis of the complex [Au(Mmp)(PPh_3)]	141
Scheme 4.9.	Synthesis of the complex [Au(Mai)(PPh_3)]	141
Scheme 5.1.	Hydroboration of vinyl phosphine using 9-BBN and subsequent addition to [Rh(cod)Cl]$_2$ (R = Fu and Ph)	151
Scheme 5.2.	Anti-Markovnikov addition of a BH bond to an alkene	152
Scheme 5.3.	Synthesis of 5.9 using a series of borane precursors	154
Scheme 5.4.	Catalytic cycle for hydroboration using Wilkinson's catalyst	157
Scheme 5.5.	Reactivity of CatBH and 9-BBN with vinyl imidazole	158
Scheme 5.6.	Synthesis of vinyl imidazolium salts	160
Scheme 5.7.	Attempted hydroboration of vinyl imidazolium salts	161
Scheme 5.8.	Attempted hydroboration of vinyl imidazolium salts using CatBH and 9-BBN	161
Scheme 5.9.	Synthesis of the dimeric silver iodide carbene complex 5.13	163
Scheme 5.10.	Synthesis of the dicarbene complex 5.14	164
Scheme 5.11.	Use of the silver carbene complex 5.13 as a transmetalation reagent for the synthesis of the rhodium carbene complex 5.15	166
Scheme 5.12.	Hydroboration attempts of a rhodium vinyl-carbene complex	167
Scheme 5.13.	Hydroboration of a chloroalkene as reported in the literature	168
Scheme 5.14.	Expected reactivity for the hydroboration of a bromoalkene using Wilkinson's catalyst	169
Scheme 5.15.	Synthesis and attempted further reactivity of bromo benzene boronic acid pinacol ester	170
Scheme 5.16.	Synthesis of ligand 5.24 from salicylic aldehyde	170
Scheme 5.17.	Attempted copper cross coupling between 5.21 and imidazole	171
Scheme 5.18.	N-quaternarisation reactions involving 5.25	171
Scheme 5.19.	Formation of silver carbene complexes bearing a pendant BPin moiety	172
Scheme 5.20.	Synthesis of a rhodium (I) complex bearing a pendant BPin Moiety	173
Scheme 5.21.	N-quaternarisation reactions of functionalised imidazoles using $BrCH_2BPin$	175
Scheme 5.22.	Synthesis of pendant BPin imidazolium salts 5.38, 5.39 and 5.40	176
Scheme 5.23.	Counter ion exchange of Br^- for PF_6^- in 5.40	177
Scheme 5.24.	Addition of a base to imidazolium salts bearing both adducted and non-adducted BPin moiety's	178
Scheme 5.25.	Synthesis of the complexes [Rh(OAc)(cod)] and [Rh(OMe)(cod)]	180
Scheme 5.26.	Synthesis of the complexes [Cu(HMDS)]$_4$ and [Zn(HMDS)$_2$]	181
Scheme 5.27.	Addition and reactivity of 5.40 with different quantities of PhLi generating the proposed products 5.41A and 5.41B	182
Scheme 5.29.	Reduction of the BPin groups to BH_3^- using $LiAlH_4$	184

Scheme 5.30. Addition of DCM and CHCl3 to zwitterionic imidazolium BH_3^+ compounds 185
Scheme 5.31. Synthesis of an iminium salt containing the BPin moiety 188
Scheme 5.32. Reduction of the iminium salt 5.54 using $LiAlH_4$ 191

VI: List of Tables

Table 1.1.	V-B, B-H_b (bridging) and B-H_t (terminal) bond lengths in Å for isomers of $[V(BH4)_3(PMe_3)_2]$	14
Table 3.1.	Selected spectroscopic data for copper complexes based on a 2-mercaptopyridine scaffold	67
Table 3.2.	Selected bond lengths (Å) and angles (°) for $[Cu(Mmp)(PR_3)]$ complexes compared with $[Cu(Bmp)PPh_3]$	70
Table 3.3.	Selected spectroscopic data for the ligand $[Li(^{Ph}Mmp)]$ and $[Cu(^{Ph}Mmp)(PR_3)]$ complexes	77
Table 3.4.	Selected bond distances (Å) and bond angles (°) for $[Cu(^{Ph}Mmp)(PPh_3)]$ and $[Cu(^{Ph}Mmp)(PCy_3)]$	79
Table 3.5.	Selected spectroscopic data for the ligand $[Li(^{Me}Mmp)]$ and $[Cu(^{Me}Mmp)(PR_3)]$ complexes	81
Table 3.6.	Selected bond distances and angles for $[Cu(^{Me}Mmp)(PPh_3)]$	82
Table 3.7.	Selected spectroscopic data for the ligand salt Na[Mai] and $[Cu(Mai)(PR_3)_n]$ complexes	90
Table 3.8.	Selected bond lengths and angles for the ligand [Na(Mai)] and $[Cu(Mai)(PR_3)_n]$ complexes	94
Table 3.9.	Selected spectroscopic data for $[Cu(^{Me}Bai)(PR_3)]$ complexes and their comparison with $[Cu(^{Me}Bmp)(PR_3)]$ complexes	99
Table 3.10.	Selected bond lengths and distances for the ligand $[Li(^{Me}Bai)]$ and $[Cu(^{Me}Bai)]$ complexes	101
Table 3.11.	Selected spectroscopic data for the ligand [Na(Mm)] and $[Cu(Mm)(PR_3)]$ complexes	105
Table 3.12.	Selected crystallographic data for $[Cu(Mm)(PCy_3)]$	107
Table 3.13.	Selected spectroscopic data for [Li(Bm)] and $[Cu(Bm)(PR_3)]$ complexes	109
Table 3.14.	Selected bond distances and angles for $[Cu(Bm)(PPh_3)]$	110
Table 4.1.	Spectroscopic data for $[Ag(Mmp)(PR_3)]$ complexes synthesised and examples for comparison.	121
Table 4.2.	Selected bond distances (Å) and angles (°) for the complex $[Ag(Mmp)(PCy_3)]$	123
Table 4.3.	Spectroscopic data for silver complexes bearing the ligand ^{R}Mmp	126
Table 4.4.	Spectroscopic data for complexes $[Ag(Mai)(PPh_3)_2]$, $[Ag(Mai)(PCy_3]$ and examples for comparison.	128
Table 4.5.	Selected bond distances (Å) and angles (°) for the complexes $[Ag(Mai)(PPh_3)_2]$ and $[Ag(Mmp)(PCy_3)]$	133
Table 4.6.	Spectroscopic data for gold complexes bearing mono-supported borohydride ligands and free ligand salts for comparison.	142
Table 4.7.	Combined spectroscopic data for all complexes synthesised in chapters 3 and 4	145
Table 4.8.	Selected SC-XRD bond lengths for complexes in chapters 3 and 4	146

VII: Abbreviations and symbols

{^{n}A}	Denotes nucleus of decoupling experiment
μ	Bridging ligand
3c-2e	Three centre two electron
9-BBN	9-Borabicyclo(3.3.1)nonane
Ac	Acetyl
ai	7-azaindole
ATR	Attenuated total reflection
b	Bridging
Bn	Benzyl
CAAC	Cyclic alkyl amino carbene
Cat	Catechol
cm^{-1}	Wavenumbers
cod	1,5-cyclooctadiene
COSY	Correlation Spectroscopy
Cp	Cyclopentadienyl
Cp*	Pentamethylcyclopentadiene
Cy	Cyclohexyl
d	Doublet
DCM	Dichloromethane
dppe	1,2-Bis(diphenylphosphino)ethane
dppm	1,1-Bis(diphenylphosphino)methane
EI	Electron ionisation
ESI	Electrospray ionisation
Et	Ethyl
Fu	Furyl
h.h.w.	Half height width
HMBC	Heteronuclear multiple bond correlation
HMDS	Hexamethyldisilazane
HOMO	Highest occupied molecular orbital
HSQC	Heteronuclear single quantum correlation
Hz	Hertz
IR	Infrared spectroscopy
J	Denotes an NMR coupling constant
L	L-Type ligand
LUMO	Lowest unoccupied molecular orbital
M	Metal
m	Multiplet
m	Methimazole
m/z	Mass to charge ratio

mapy	2-methyl amino pyridyl
Me	Methyl
Mes	Mesitylene
mg	Milligram
mL	Millilitre
mmol	Millimole
MO	Molecular orbital
mp	2-mercaptopyridyl
MS	Mass spectrometry
nbd	2,5-Norbornadiene
nBu	n-Butyl group
NHC	N-heterocyclic carbene
NMR	Nuclear Magnetic Resonance Spectroscopy
Ph	Phenyl
Pin	Pinacol
pz	Pyrazole
QTAIM	Quantum Theory of Atoms in Molecules
RT	Room Temperature
salen	N,N'-Ethylenebis(salicylimine)
SC-XRD	Single crystal X-ray diffraction
t	Triplet (NMR) / terminal (IR/SC-XRD)
^{t}Bu	Tert-Butyl group
THF	Tetrahydrofuran
TLC	Thin layer chromatography
Tol	Toluene
vw	Very weak
w	Weak
X	X-type or anionic ligand
Xy	Xylyl
Z	Z-type ligand
δ ppm	Chemical shift value
η	Hapticity
κ	Denticity
π	Pi bond
σ	Sigma bond

VIII: Copyright Declaration

This is to certify that, except where specific reference is made, the work described in this thesis is the result of my own research. Neither this thesis, nor any part of it, has been presented, or is currently submitted, in candidature for any other award at this or any other University.

Signed 

Date 6th September 2021

Chapter 1: Introduction

1.1 Introduction

Organometallic chemistry is the study of metal complexes containing ligands with organic frameworks. This field encompasses a diverse range of compounds and their subsequent applications. This thesis focuses on the coordination chemistry of mono-supported borohydride ligands, an area of chemistry that has not been extensively explored. This chapter outlines the key concepts surrounding this area of chemistry such as metal ligand bonding, looking in detail at covalent bonding between ligand and metal. The chemistry surrounding both scorpionate ligands and the anionic tetrahydroborate ligand is also discussed as the main focus of this thesis, mono supported borohydrides lies between these two extremes.

Following on from the introduction, this thesis will then further explore examples of mono-supported borohydride ligands and their neutral analogues mono-supported boranes within the literature. The aim of the literature review is to provide an account of research undertaken in the area thus far, drawing on both recent and earlier examples. The properties of these ligands are explored through spectroscopic data and comparisons are made between neutral and anionic ligands.

Chapters 3 and 4 explore the coordination of mono supported borohydride ligands upon group 11 metal centres based on 2-mercaptopyridine, methimazole and 7-azaindole scaffolds. These chapters explore the differences between mono-, bis-, and tris- ligands through spectroscopic data. The ligands based on mercaptopyridine have also been functionalised at the boron centre to include either methyl or phenyl groups and the consequences of functionalisation were also investigated. Further comparisons were drawn by comparing isoleptic complexes of copper, silver, and gold.

Chapter 5 investigates the potential of utilising heterocyclic units containing carbene functional groups as three atom bridges to support a borohydride unit. It looks into several synthetic routes for the synthesis of such compounds such as hydroboration and N-quaternarisation with a pre

functionalised unit. The chapter then assesses the difficulty in the deprotonation of these compounds and explores the reactivity of the pro-ligands.

1.2 Metal ligand bonding

Covalent bonding between ligand and metal are traditionally described using Lewis structures. Lewis structures are derived from work by Lewis in 1924.[1] He described covalent bonds using a two-centre-two-electron model. This is where two electrons are shared between two atoms with overlapping orbitals to form a chemical bond. This is achieved between a ligand and a metal in three different ways, these are called L, X and Z-type ligands (Figure 1.1). In an L-type ligand both electrons that are present in the covalent bond originate from the ligand forming a dative bond with the metal. X-type ligands are where both ligand and metal contribute a single electron to the bond. Finally, Z-type ligands are where the metal contributes both electrons to the bond.[2] L and X type ligands are extensively studied throughout the chemical literature and form the basis for the majority of organometallic complexes reported. Z-type ligands on the other hand are rare and are not as prevalent in the literature as its counterparts.[3–5]

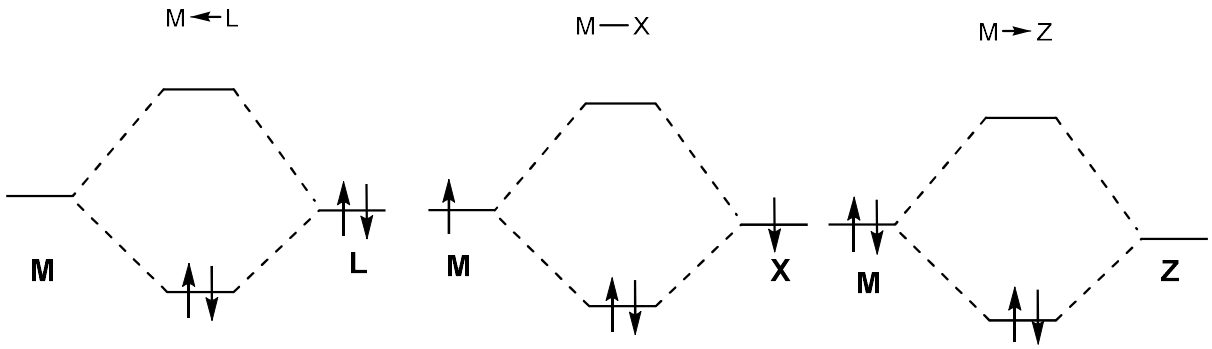

Figure 1.1. MO diagrams for L, X and Z ligands

Whilst the two centre two electron model holds up for the vast majority of metal ligand bonds, there are cases where this bonding model is not appropriate. A three centre two electron bond (3c-2e) is where two electrons are shared between three separate nuclei. The simplest molecule containing a three-centred two electron bond is $[H_3]^+$. $[H_3]^+$ is a cationic species in which the three hydrogen nuclei are organised in a triangular arrangement. This shape maximises the overlap between the orbitals in each of the three hydrogens. This results in the pair of electrons being efficiently shared between the

three hydrogen atoms. Figure 1.2 shows the connectivity in structure **1.1** and presents three equivalent bonding representations of $[H_3]^+$ as represented by **1.2, 1.3** and **1.4**. The dative bond originating from H_2 is drawn towards the protic species in each of these three separate representations. This shows that the electron deficiency of the proton is relieved by overlap of the σ-bonding orbital with the 1s orbital of H^+ and therefore the two electrons are shared across all three nuclei.

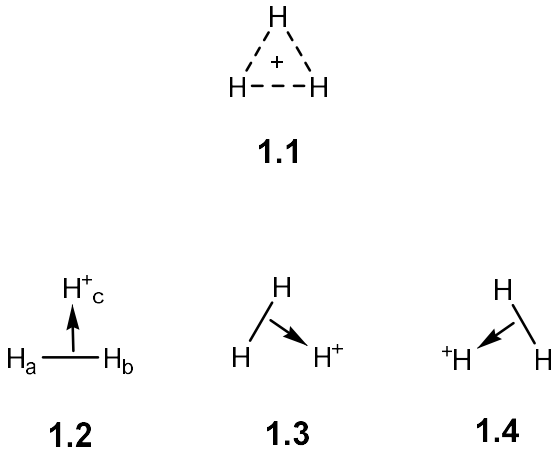

Figure 1.2. Structure and bonding in H_3^+

Representations of the three centred two electron bonds are made in a number of ways. Firstly, in **1.5** a dative bond is drawn from the H_2 bond to the third hydrogen atom, secondly as in **1.6** a half arrow could also be used from a 'bridging' hydrogen atom to represent the same species, and finally **1.7** demonstrates a dashed line to demonstrate the connectivity within the molecule (Figure 1.3). Although **1.5**, **1.6**, and **1.7** all drawn differently, they are all depictions of the same bonding arrangement. For simplicity, this thesis will use a dashed line as in **1.7** to represent the 3c-2e bonding mode from this point forward.

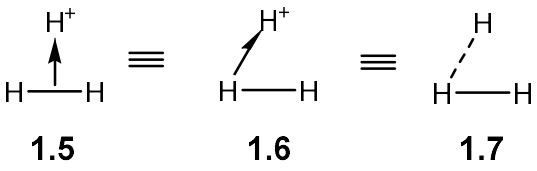

Figure 1.3. Representations of the 3c-2e bond in H_3^+

A further straightforward example in which 3c-2e bonds are present is that of diborane (Figure 1.4). The structure of diborane **1.8** was initially postulated as being similar to that of ethane. Early electron diffraction studies of the compound excluded the possibility of an analogous ethane structure. The confirmed structure of diborane consists of two BH_3 units in which a single BH bond per BH_3 monomer coordinates to the boron of the other BH_3 monomer in order relive the electron deficiency of the trivalent boron.[6,7] The coordination of the BH bond in this case is equivalent to a two-electron donor and therefore stabilises the electrophilic centre. This is in the same way that a base stabilises a borane in commercially available reagents such as BH_3·THF or BH_3·NMe_3

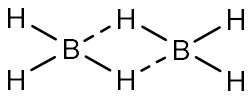

1.8

Figure 1.4. The structure of diborane

1.3 Scope of project

A key focus of organometallic chemistry is the fine tuning of metal centres through the use of ancillary ligands. Ancillary ligands have been used to control the geometry, coordination number, physical properties, and reactivity of metal centres. One such ligand architecture, scorpionate ligands, are recognised as one of the most flexible and have been used to carefully control the coordination sphere of metal centres.[8] The name scorpionate, coined by Trofimenko, is used to refer to tripodal ligand systems supported by either a sp^3 hybridised boron or carbon atom. The term scorpionate is an analogy which refers to the strength of each coordinating unit (Figure 1.5). Two claw like donors represent fixed points of attachment between ligand and metal. The third weaker donor is represented by a stinger which represents the reversible nature of the coordination (Figure 1.5). The interchange between bidentate and tridentate coordination modes (i.e. κ^2-L,L and κ^3-L,L,L) highlights the flexibility of these ligands which is important because many metal catalysed reactions proceed through ligand addition or dissociation steps. Because of this, scorpionate ligands and complexes thereof, have been well investigated and the key focus of many reviews.[9–13]

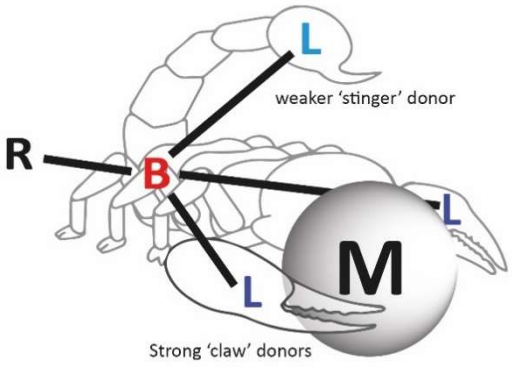

Figure 1.5. The scorpionate analogy

Whilst the bis- and tris- substituted borohydrides are extensively studied, there are few examples of mono-substituted borohydride ligands. To the best of our knowledge, no review has been undertaken for these complexes. This thesis intends to explore examples from across the literature of complexes containing mono-supported borohydrides and to draw comparisons with the chemistry of their

neutral mono-supported borane analogues. The metal complexes of supported borohydride ligands are of particular interest because of their propensity to undergo hydride migration from the ligand to the metal as previously demonstrated by our group.[14] Whilst the process of hydride migration has been investigated, little has been done to investigate the rationale as to why certain ligands undergo hydride migration more freely than other complexes. This thesis intends to explore the coordination chemistry of monosubstituted borohydride ligands **1.9** on coinage group metals and to compare them with the wider family of scorpionate ligands. Coinage group metals are host to a number of both bis-substituted **1.10** and tris-substituted **1.11** scorpionate ligand compounds (Figure 1.6). Using these, this thesis will explore the difference in the coordination of these ligands and draw comparisons across the whole family of supported borohydride ligands. Following on from this, we will attempt to expand the mono-substituted borohydride family by introducing new ligands utilising previously unused supports for borohydride ligands.

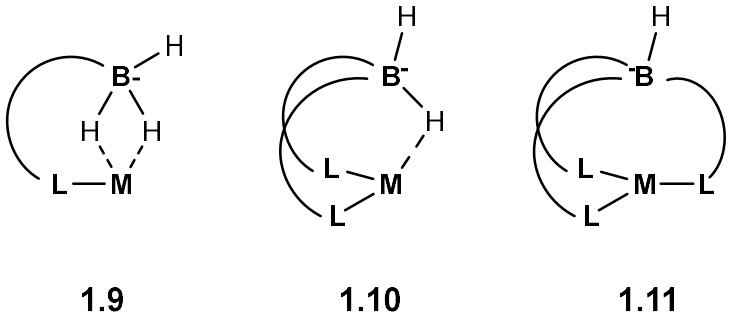

1.9 **1.10** **1.11**

Figure 1.6. Mono-, bis- and tris- substituted borohydrides each demonstrating κ^3 coordination to a metal centre

Scorpionate ligands are well defined in the literature and are regularly abbreviated to their shorthand terms. The ligand salt is presented as the cation first, typically an alkali metal, followed by parentheses and the prefix M, B or T. These are abbreviations for mono-, bis- or tris, respectively. The capital letter is then followed by an abbreviation for the supporting ligand scaffold, for example, mercaptopyridine is abbreviated to mp and 7-azaindole is abbreviated to ai. So, for example **Na[Bmp]** represents the sodium salt of a borohydride unit with two mercaptopyridine supports (Figure 1.7).

Figure 1.7. The notation utilise for scorpionate ligands

These abbreviations can be further embellished with substitutions either before or after the abbreviation for the ligand. Substitutions at the boron centre will be indicated by a superscript R before the ligand and substitutions on the supporting ligand are indicated using superscript after the ligand.

1.4 Early work on metal borohydride chemistry

Metal borohydrides are important reagents in synthetic chemistry which are used for a variety of chemical transformations.[15] Sodium borohydride, a reducing agent was first identified by Schlesinger and Brown in 1941.[16] The first synthesis of sodium borohydride was reported in 1936. It was wrongly identified as disodium diborane ($Na_2B_2H_6$). Further work in the field during the 1940's led to the discovery of aluminium borohydride,[17] beryllium borohydride[18] and lithium borohydride, all of which are used as reducing agents.[19] During the Second World War Schlesinger and Brown then focused their efforts on finding stable uranium compounds for safe handling, this led to the synthesis of the volatile compound uranium borohydride [$U(BH_4)_4$]. These advancements in the field led to an improved synthesis of sodium borohydride (Scheme 1.1). Scheme 1.1 shows the reaction of 4 equivalents of sodium hydride with one equivalent of methyl borate at 250 °C to form sodium borohydride and sodium methoxide.[20]

$$4\ NaH + B(OMe)_3 \xrightarrow{250\ ^oC} NaBH_4 + 3\ NaOMe$$

Scheme 1.1. Conversion of trimethyl borate to sodium borohydride

Following on from the discovery of metal borohydrides, further work was carried out to understand their reactivity. Sodium and lithium borohydrides were found to be good reducing agents. Sodium borohydride ($NaBH_4$) was found to reduce esters, aldehydes, and ketones whilst lithium borohydride ($LiBH_4$), in addition to the former also reduces alkyl halides, epoxides and amides. In 1945 came the discovery of a powerful reducing agent, lithium aluminium hydride ($LiAlH_4$). $LiAlH_4$ analogous to $LiBH_4$, has been extensively studied as a reducing agent and in conjunction with other boranes and borohydrides provides a basic tool kit for synthetic chemists in the reduction of a range of organic compounds, which are still extensively used to date. Due to their high hydrogen content and low molecular weight metal borohydrides have also been touted as potential hydrogen storage compounds.[21]

1.4.1 Structural characterisation of tetra hydroborate ligands

Structural characterisation of metal complexes bearing the ligand BH_4^- is typically achieved using single crystal X-ray diffraction (SC-XRD) studies. The complete unequivocal location of small atoms such as hydrogen, however, is not always possible. One such example of this can be traced back to studies involving Cu-H-B interactions in tetrahydroborate complexes in 1981. Three different studies reported the characterisation of the complex $[Cu(PPh_2Me)_3(BH_4)]$ **1.12** based on diffraction data. Two studies used X-ray diffraction data and a third utilised neutron diffraction data for their charactrisation.[22–24]

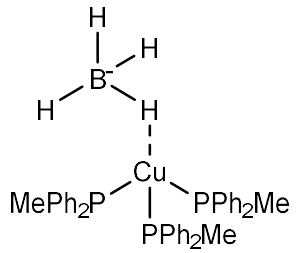

1.12

Figure 1.8. Structure of $[Cu(PPh_2Me)_3(BH_4)]$

Despite having the same complex, all three studies reported the BH_4 hydrogens in different locations and therefore, with different Cu-H-B bond angles. Whilst X-ray studies reported the Cu-H-B angles at approximately 170˚, the neutron diffraction solved structure gave the angle as 121.7˚. In this case, the neutron diffraction data provides a more reliable method of locating the B-H hydrogens. Neutrons are larger than x-rays and therefore have a greater probability of scattering with small atoms, thus, increasing the reliability in which they are located. The smaller X-rays used in diffraction studies are used to calculate an electron density map, in which, the location of the hydrogens are inferred. This can result in the misrepresentation of the true nature of the Cu-H-B bond, which is especially important in tetrahydroborate complexes in which the location of the hydrogens cannot be inferred from additional substituents. It is important to properly assess the nature of the B-H-M bond as this gives indication of the degree in which the BH donates it electrons to the metal centre. Unfortunately,

the accessibility and practicalities of using neutron diffraction does not allow for wide use of this technique and therefore X-ray diffraction is the more widely used technique. Improvements in X-ray diffraction has however, led to better degree of accuracy in locating hydrogens and therefore X-ray diffraction has become more reliable over time. The errors associated with X-ray diffraction will be expressed using the estimated standard deviations (e.s.d's) values obtained from the solved structures. The e.s.d's provide an indication of the precision of the last digit in a bond length. These values will be provided in parenthesis following a bond distance for example an e.s.d. of 0.0005 Å for a bond distance of 1.7332 Å will be represented as 1.7332(5) Å. For clarity, where available the e.s.d. values will be provided for all crystal structures. Whilst the majority of structures reported from the literature supply these values there are a few select examples in which this is not the case, therefore in some examples no e.s.d. values will be presented.

1.4.2 Computational studies of tetrahydroborate as a ligand

Borohydride as a ligand has many different coordination modes which depends on the metal and its coordination sphere. It can form between one and three, three centred two electron bonds between the metal and the B-H units. These bonds can be viewed in a number of ways. It can firstly be seen as an η^2-B-H **1.13**, coordinating via an agostic type bonding mode or as mostly coordinating from the hydrogen side of the bond due to the higher electronegativity of the hydrogen nuclei in comparison to boron. This latter mode is a κ^1-H type interaction **1.14** (Shimoi type). The true nature of the bond is thought to lie somewhere between these two extremes.[25–29] When two BH bonds coordinated to the metal centre it is considered as either two separate BH bonds coordinating in a κ^2-H,H manner (**1.15**) or as continuous η-coordination through a central boron atom (**1.16**), in either case this is known as a dihydroborate interaction. This thesis will refer to these bonding modes as both 3c-2e and using κ notation for simplicity.

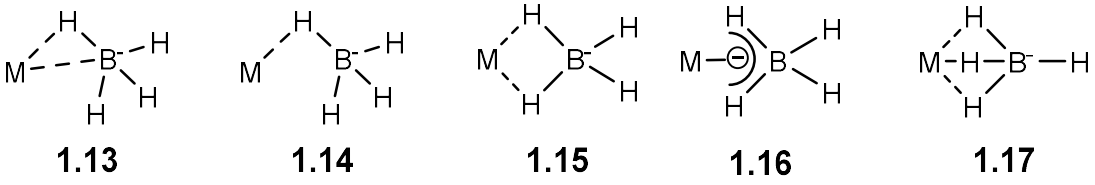

Figure 1.9. A BH_4 anion exhibiting η^2-B,H, κ^1-H, κ^2-H,H, η^3-H,B,H and κ^3-H,H,H coordination modes.

A vanadium complex containing three borohydride ligands was assessed by Lledos and Volatron.[30] Each ligand can coordinate to the metal via one (**1.14**), two (**1.15**) or three (**1.17**), three-centre two electron bonds. Therefore, there are 10 possible different isomers of compound **1.18.**[31] Each bonding mode is attributed to a number that represents the number of 3c-2e bonds for each respective tetrahydroborate ligand (Figure 1.10), for example (κ^1, κ^1, κ^1) **1.19**, (κ^2, κ^2, κ^2) **1.20** or (κ^1, κ^2, κ^3) **1.21**.

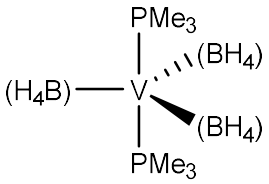

1.18

Figure 1.10. Coordination of BH_4 units in $[V(BH_4)_3(PMe_3)_2]$

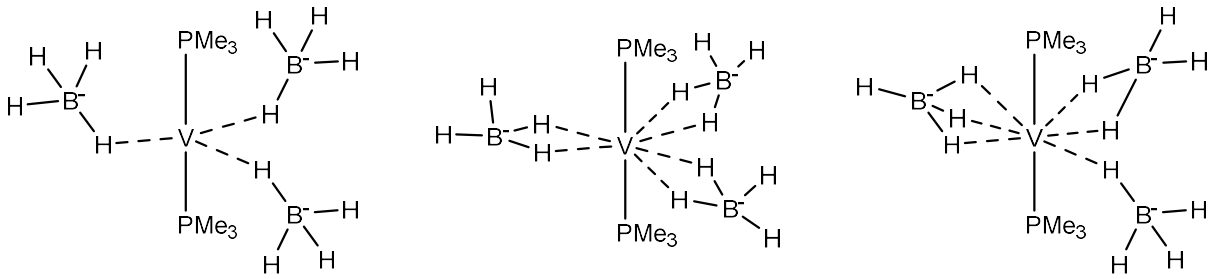

1.19 **1.20** **1.21**

Figure 1.11. $[V(BH_4)_3(PMe_3)_2]$ showing (κ^1, κ^1, κ^1), (κ^2, κ^2, κ^2) and (κ^1, κ^2, κ^3) coordination modes

The energies (kcalmol^{-1}) were calculated for each possible permutation. The isomer that was the lowest in energy was the (κ^2, κ^2, κ^2) isomer, as this complex is an 18-electron complex. There are small energy gaps of 1.1 and 8.1 kcalmol^{-1} between the (κ^2, κ^2, κ^2) isomer and isomers (κ^1, κ^2, κ^2) and (κ^2, κ^2, κ^3) respectively. This suggests that in solution these structures are readily accessible given the energy barrier between these transitions is consistently reported to be a low energy process.[32] Alternatively, the structure that had the largest energy difference from that of (κ^2, κ^2, κ^2) was (κ^1, κ^3, κ^3) at 39.8 Kcalmol^{-1}, followed by (κ^3, κ^3, κ^3) and (κ^1, κ^1, κ^1) with energy differences of 39.6 and 37.5 kcalmol^{-1}. Because of the high energy difference, it is unlikely that these isomers are present in solution. Further to this, the bond lengths were calculated for all structural isomers (see Table 1.1) and this showed the bond length decreases as the number of two centre three electron bonds increases. For example, in structures (κ^1, κ^1, κ^1), (κ^2, κ^2, κ^2) and (κ^3, κ^3, κ^3) the average of all 3 V-B distances decreases from 3.048 Å to 2.445 Å and finally 2.371 Å. The value for the (κ^3, κ^3, κ^3) is very close to the sum of the covalent radii of vanadium 1.53(8) Å and boron 0.84(3) Å[33] which is calculated as 2.37 Å, this gives a V-B distance

which is comparable to a V-B single bond. As the number of coordinating BH bonds increases the V-B bond distance decreases as a consequence of facilitating the coordination of each BH bond.

Table 1.1. V-B, B-H_b (bridging) and B-H_t (terminal) bond lengths in Å for isomers of $[V(BH_4)_3(PMe_3)_2]$

	(κ^1, κ^1, κ^1)	**(κ^2, κ^2, κ^2)**	**(κ^3, κ^3, κ^3)**
V-B	*3.048*	*2.445*	*2.371*
B-H_b	*1.364*	*1.252*	*1.225*
B-H_t	*1.203*	*1.198*	*1.190*

Chapter 2: A review of metal complexes containing mono-supported borohydride and borane ligands

2.1 Introduction

Metal boron complexes have previously been the subject of many excellent reviews.[34–37] Of which, few have mentioned mono-supported ligands containing B-H interactions.[5,38] Mono-supported borohydride and borane complexes are complexes in which a single ligand support is utilised in supporting an anionic or neutral BH_3 unit. The BH_3 unit can then coordinate to a metal centre through one or more of its B-H bonds. Unsupported borohydride complexes and scorpionate complexes have all previously been reviewed.[9–13,39,40] However, mono-substituted borohydrides, which lie between these two extremes, are less explored and have yet to be reviewed. When looking at the coordination of the neutral analogues, unsupported boranes, these again have been the subject of previous reviews.[41–43] However, their mono-supported counterparts again have yet to be a core focus of any review.

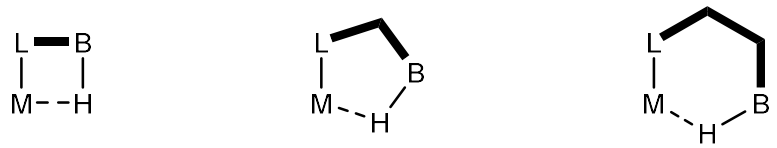

2.1 **2.2** **2.3**

Scheme 2.1. One, two and three atom supports in supported borane/borohydride ligands

This review intends to explore the coordination and chemistry of mono-supported ligands containing either an anionic borohydride or neutral borane moiety. It will focus on different supporting ligands including one- **2.1**, two- **2.2**, and three-atom bridges **2.3** (Figure 2.1). Further to this, we will explore the nature of the interactions of the BH_3 functional group with metal centres comparing both nuclear magnetic resonance and single crystal x-ray diffraction studies where available. We will also seek to explore the similarities and differences between both anionic and neutral ligands. Finally, we will

explore the reactivity of these complexes, both at the metal and on boron with scope to further investigate their properties and subsequently their reactivity with hydrogen.

2.2 Bonding features in singly supported BH_n ligands

Supported metal boranes and borohydrides are a flexible range of compounds which host a diverse range of interactions, of which, many different bonding modes have been described in the literature. It is therefore necessary to define these because their descriptions are not always consistent between publications. The precoordinated ligand supports the metal using one, two or three atom supporting bridges although theoretically this could increase to several more atoms. This ligand species or 'supporting ligand' assists in bringing the boron-based functional group into close proximity with the metal centre. Although functionalisation of these complexes with non-coordinating functional groups will make the respective bis- or tris-substituted borohydride complexes, the nomenclature in this thesis will refer to the complexes as mono- referring to the number of supporting ligands (Figure 2.1).

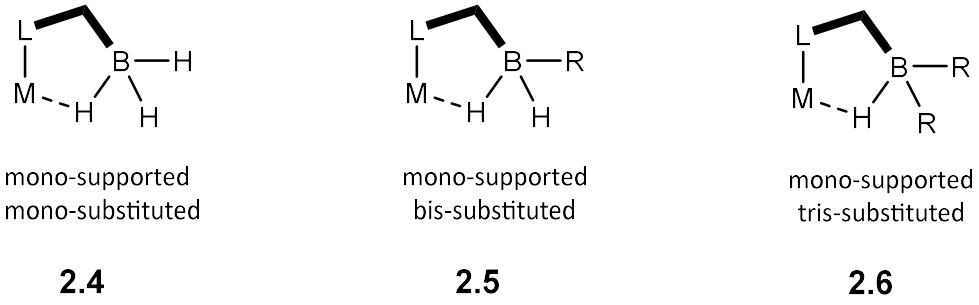

Figure 2.1. Mono-, bis- and tris- substituted mono-supported BH_n ligands

Therefore, in a tris-substituted mono-supported borohydride ligand as in **2.6**, the only possible mode of coordination for the borohydride moiety is κ^1-H. Less substituted borohydrides such as the structures shown in **2.4** and **2.6** can coordinate κ^2-H,H. One other possible mode is κ^3-H,H,H coordination, however, for this to occur the length of the supporting chain would have to be quite long to facilitate this (Figure 2.2).

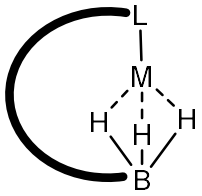

Long chain support

2.7

Figure 2.2. Hypothetical supported κ^3H,H,H coordination of a mono-supported borohydride ligand

Figure 2.3 shows the plausible modes of coordination for both neutral borane and anionic borohydride ligands which are supported by a precoordinated ligand. The first row in Figure 2.3 represents a single atom-supporting unit resulting in the formation of a 4-membered ring on coordination to a metal. The second row increases this by adding an atom to the supporting ring resulting in the formation of 5-membered rings in conjunction with the metal. Three atom supports will therefore result in the formation of a 6-membered ring. The first two columns of Figure 2.3 show the ligand supporting neutral boranes with κ^1-H coordination of the borane in column one and κ^2-H,H in column two. For the κ^2-H,H coordination mode of the borane unit, this creates an additional 4 membered M-H-B-H chelate in which a rigid structure is generated and the boron is brought into close proximity to the metal centre. The third and fourth columns are used to represent ligand supports in an anionic borohydride complex. Again, the difference between these two columns lies in the difference in coordination of the borohydride unit where the first column demonstrates κ^1-H coordination and the second κ^2-H,H. Whilst Figure 2.3 provides an extensive coverage of all the possible bonding motifs of these complexes, it is important to note that not all these compounds have been realised yet and some of the examples have yet to be reported. This chapter will look at select examples which have been reported so far.

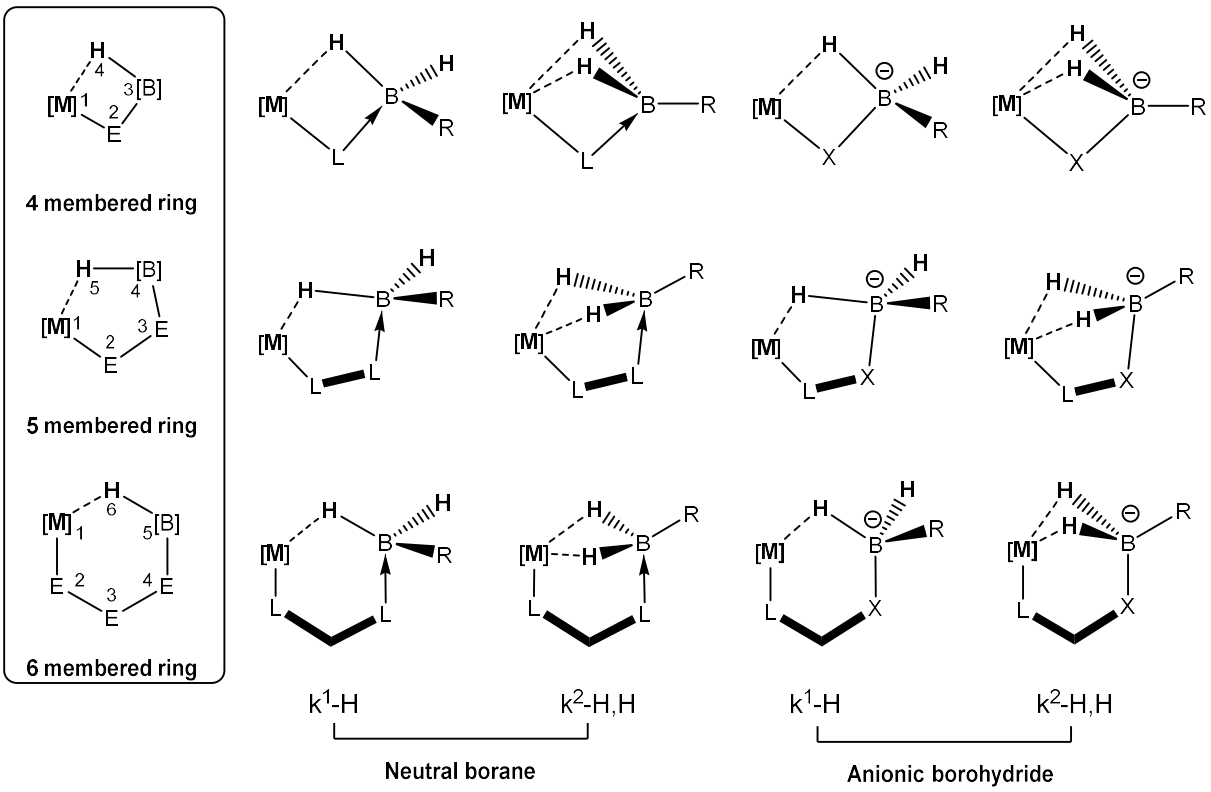

Figure 2.3. Examples of both neutral and anionic metal boron complexes containing one, two and three atom supports.

The importance of the number of atoms in the bridge between the supporting ligand and the metal becomes more apparent when you look at the potential reactivity and the resultant ring sizes. The reactivity of a neutral borane fragment with a metal centre occurs by the oxidative addition of the BH bond. The resultant ligand chelate will give the neutral boryl fragment coordinating to the metal through X-type metal ligand bond. Following the oxidative addition, the ring size of the chelate will reduce by one atom. In Figure 2.4, the potential structure **2.8** represents a two-atom supporting ligand bridge, which has reduced from a 5 membered ring to a 4 membered ring and, a 3-atom supporting chain will be reduced from a 6 membered ring to a 5 membered ring. Moving to the second column shows the resultant complexes **2.9** and **2.11** from the reactivity of the supported anionic borohydride ligands, this is where a hydride migrates from the boron to a metal resulting in a metal hydride and the formation of a Z-type interaction between the metal and the ligand. Again, this reduces the ring size by a single atom and sees the same decrease in ring size. The reduction in ring size which is most favoured is the transition between 6 and 5 membered rings.

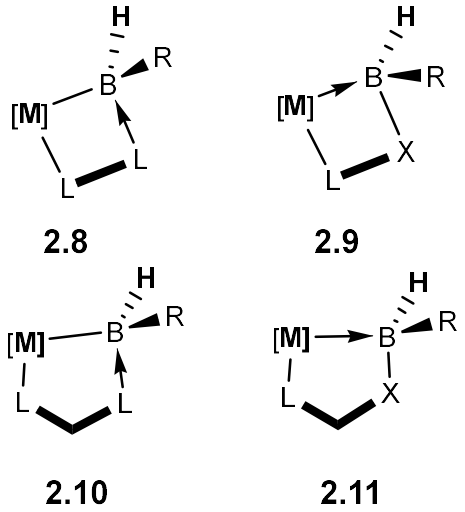

Figure 2.4. Possible complexes based on the further reactivity of supported neutral and anionic boron-based ligands

2.3 Examples of mono- supported neutral borane ligands

2.3.1 Neutral one-atom supported borane ligands

One of first examples of a fully characterised and supported BH_3 unit that interacts with a metal is that of **$[Ti(BH_4)_2(salen)]_2$**, the structure was reported in 1982 by Floriani (Scheme 2.2).[44] **$[TiCl_2(salen)]$** was reacted with $LiBH_4$ in THF. This resulted in the addition of a BH bond across the each of the imine functionalities and subsequent elimination of LiCl. The resultant complex **$[Ti(BH_4)_2(salen)]_2$**. supports two BH_3 units via a dative bond from each of the nitrogen donors on the salen ligand. The supported BH_3 unit then forms a four-membered chelate where a single 2c-3e bond is formed between the metal and the BH bond. A single BH bond coordinates above the equatorial plane and the other coordinates below the equatorial plane. BH stretching bands were observed at 2460, 2410 and 2325 cm^{-1} with the latter attributed to the bridging BH's. BH hydrogens were located by SC-XRD analysis and this showed the bridging boron-hydrogen bond lengths as 1.23(12) and 1.42(12) Å and the terminal BH's were 0.99(14), 0.84(13), 1.33(13) and 1.11(13) Å. Inconsistencies in the BH bond lengths was attributed to the difficulties in locating hydrogens in single crystal x-ray diffraction studies. The bridging hydrogens are generally longer than that of the terminal hydrogens indicating a weakening of the terminal BH bond as the consequence of the formation of 3c-2e bonds.

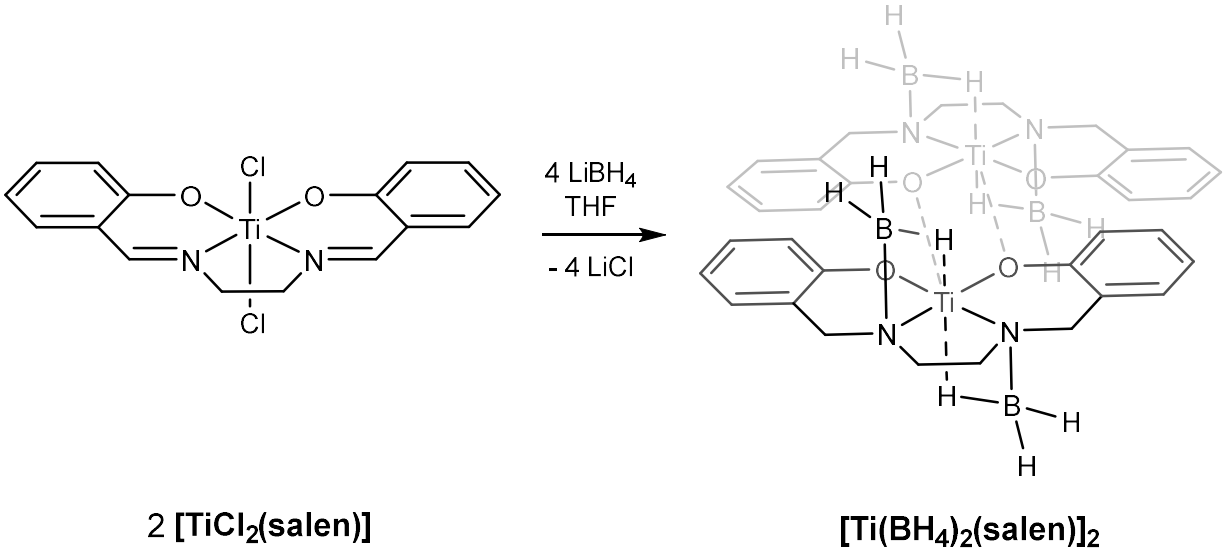

*Scheme 2.2. Addition of $LiBH_4$ to two equivalents of **$[TiCl_2(salen)]$** resulting in the complex **$[Ti(BH_4)_2(salen)]_2$***

Another early example where addition of the borohydride anion to an existing metal ligand framework results in the formation of a singly supported neutral borane complex, is the addition of $NaBH_4$ to **2.12** (Scheme 2.3). This results in the synthesis of the supported borohydride iron complex **2.13**. This is achieved through the release of NaCl and addition of the $[BH_4]^-$ unit across the C=S bond.[45] In complex **2.13** the BH_3 unit is present as a neutral species which is supported by a dative bond from the lone pair on the sulfur atom. The complex itself gives rise to two B-H absorption bands at 2480 and 2400 cm^{-1}. The ^1H NMR shows a single broad peak at −13.7 ppm for the BH_3 protons indicating rapid exchange is taking place between terminal and bridging hydrogens in solution. The chemical shift value indicates that a significant 3c-2e interaction is present between the BH bond and the metal centre. X-ray crystal data shows that the BH_3 unit is coordinated through a single 3c-2e bond. The bridging B-H bond distance exhibits a longer bond length of 1.28(4) Å when compared to that of the terminal BH's bond distances of 1.16(4) and 1.11(4) Å. The iron centre adopts an octahedral geometry in which all 6 coordination sites are occupied, of which the BH bond occupies a single site. Upon addition of CO or PMe_3, to solutions of the complex, no reactivity is observed. This suggests that the BH_3 unit protects the coordination site with each BH bonds acting as a 2-electron donor in place of each L-type ligand. However, when pyridine added to the reaction mixture the BH_3 unit was abstracted

in the presence of carbon monoxide or trimethyl phosphine, this resulted in the BH's former coordination site being occupied by either a single CO or PMe_3 ligand. This reactivity shows that neutral BH_3 units can be abstracted using a Lewis base.

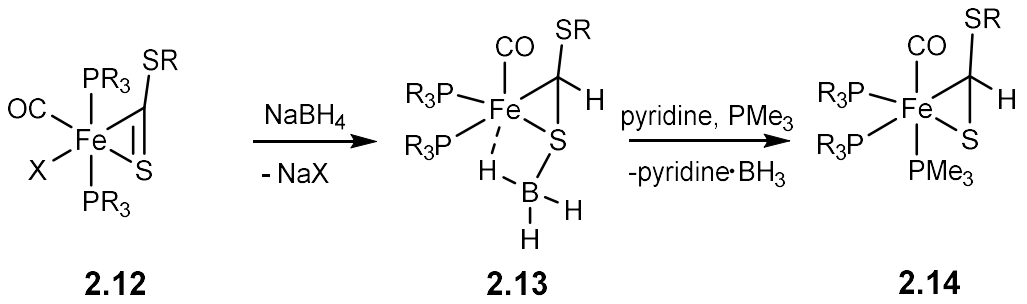

2.12 **2.13** **2.14**

Scheme 2.3. Addition of $NaBH_4$ across a C=S bond resulting in a supported neutral borane ligand

Stephan also demonstrated an example of a sulfur supported BH_3 complex where a titanium cyclopentadienyltitatium dithiolate species **2.15** reacts with $NaBH_4$ to form the supported borane complex **2.16**. In this case, one of the hydrogen atoms on boron is transferred to the metal centre (Scheme 2.4).[46] Again, the borane unit is supported by the lone pair of a ligated sulfur atom and the complex forms a dimer, as observed previously with the **$[Ti(BH_4)(salen)]_2$** complex.[44] This supported borane has a single 3c-2e bond. Room temperature ^1H NMR studies showed a single BH_3 resonance at −0.7 ppm, the BH_3 resonance could not be resolved into separate peaks on cooling. This indicates that the exchange between terminal and bridging hydrogens will occur readily at temperatures down to −70 °C. The Ti-H bond distance in the bridging unit is reported as 1.90 Å which is considerably longer than the terminal Ti-H bond which is shorter at 1.45 Å but this is expected due to the different bonding mode.

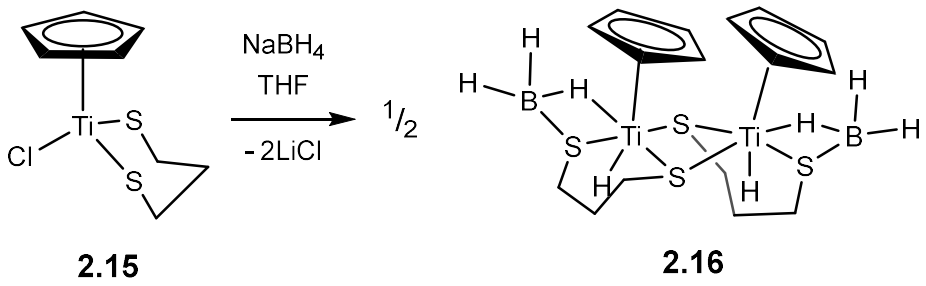

Scheme 2.4. Addition of $NaBH_4$ to titanium dithiolate complex

A ruthenium pincer complex was also found to support a metal BH interaction in an example reported by Gusev (Scheme 2.5).[47] In the reaction of complex **2.17** with BH_3·THF, the Ru-C bond is partially ruptured by the binding of BH_3 to the X-type coordinated carbon donor. This results in the formation of the 18 VE compound **2.18**. The Ru-C distance in the resultant complex is 2.291(14) Å. This represents a weaker coordination in comparison to the precursor [c.f. 2.108(4) Å]. The borane is supported through an interaction with the coordinating carbon of the aromatic ring with a C-B bond distance of 1.63(2) Å which is consistent with the C-B bond distances in dimesityl borohydride.[48] The C-B bond is removed from the aromatic plane by 24.8°. This does not appear to have any inherent effect on the aromaticity or the bond lengths within the ring itself. The borane unit is coordinated to the metal via a single 3c-2e bond. This is observed in the ^{1}H NMR spectrum where the B-H-Ru bridging hydrogen is present at −4.3 ppm and the terminal B-H's are present at 2.5 ppm. Integration confirms that a single B-H coordinates and that there is no rapid exchange between terminal and bridging protons in solution at room temperature. The bridging Ru-H distance is reported as 1.617 Å whilst the terminal Ru-H is significantly shorter at 1.344 Å.[47]

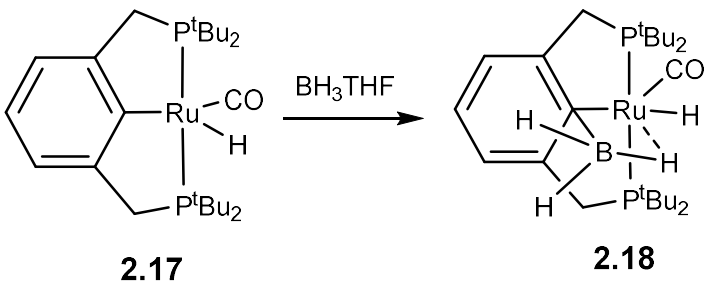

Scheme 2.5. Synthesis of a single carbon atom bridged neutral borane ligand using BH_3

2.3.2 Neutral three-atom supported borane ligands

Surprisingly to date, to the best of our knowledge, there are no neutral two-atom mono supported borane ligands. Therefore, this review will now discuss the most widely reported subset of ligand in this chapter, three-atom supported neutral borane ligands. In studies by Rauchfuss associated with that of Fe-Fe hydrogenases, the dinuclear compound **2.19** was found to react with one equivalent of BH_3·THF (Scheme 2.6).[49] The pendant amine unit of the azadithiolate group from **2.19** formed a dative bond with the BH_3 acceptor resulting in complex **2.20**. In complex **2.20** there was no interaction between the metal and the RN·BH_3 group. The IR data collected for **2.20** was very similar to that of the starting material and little to no change was observed in the CO stretching frequencies. The R group on the azadithiolate moiety contained either a methyl or a hydrogen substituent, for the hydrogen compound no further reactivity took place but when R = Me a ligand substitution reaction was performed. The adducted azadithiolate group forms a chelate utilising a single BH bond that interacts with the metal through a single 3c-2e bond. This reactivity was confirmed by changes in the IR spectrum. X-ray quality crystals of **2.21** were analysed by SC-XRD which confirmed that a single BH bond interacted with the iron centre. The BH bond had a slightly elongated B-H distance of 1.22(2) Å, which is 0.15 Å longer than the terminal BH bonds in the structure. VT NMR studies showed that at –40 °C the BH_3 protons are inequivalent with resonances of −17.8 (1H) and 2.05 (2H) ppm further confirming that a single BH_3 interacts with the iron centre. At 40 °C the BH_3 signal collapses into a single peak indicating free rotation of the BH_3 protons in solution on an NMR timescale.[49] The activation energy for the rotation of the BH_3 unit was calculated to be 13.6 kcalmol^{-1}.

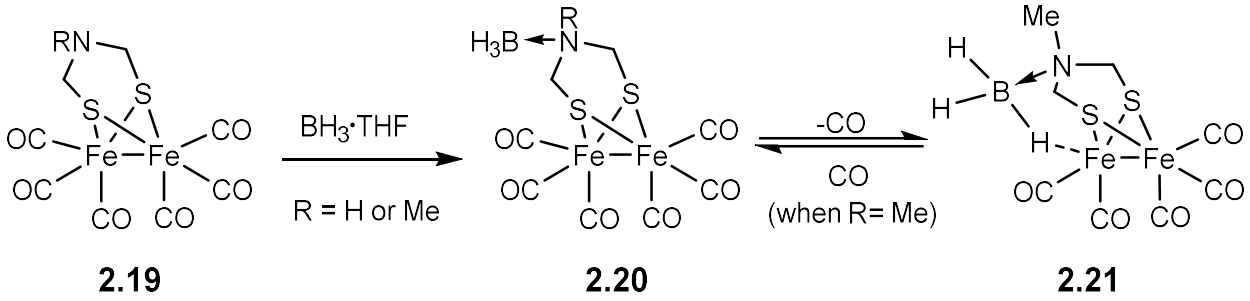

2.19 **2.20** **2.21**

*Scheme 2.6. Addition of BH_3 to diiron complex **2.19***

Ghosh added the ligand salt Na[(BH_3)SCHS] to **[Ru(μ-Cl)$_2$Cp*]** resulting in compound **2.22** (Scheme 2.7).[50] For the complex **2.22**, ^{11}B NMR studies confirmed the absence of boron from the compound and SC-XRD structure analysis confirmed that the compound was **2.22**. Ghosh tested the reactivity of this compound with small molecules and reveals that on treatment with BH_3·THF, a new complex, **2.23** was synthesised in a 61% yield. The $^{11}B\{^1H\}$ NMR spectrum of **2.23** revealed a resonance at 19.1 ppm which is a significant downfield shift in comparison to the anionic ligand salt Na[(BH_3)SCHS] at −24.9 ppm.[51] The X-ray structure showed a single [(BH_3)·SCHS] ligand coordinated to a single ruthenium centre through a sulfur donor and a dihydroborate interaction. The Ru-B bond distance was recorded as 2.143(12) Å which is shorter when compared to other ruthenium BH_2 complexes.[50]

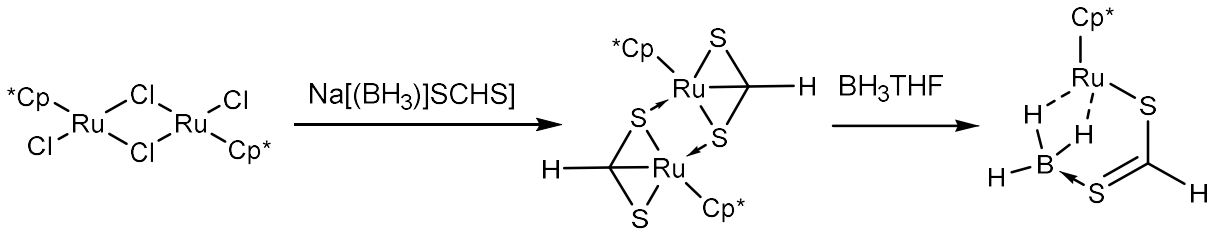

[Ru(μ-Cl)2Cp*] **2.22** **2.23**

Scheme 2.7. Reactivity of the anionic ligand [(BH_3)SCHS]$^-$ with [$RuCl_2$Cp]$_2$ and subsequent addition of BH_3*

The phosphonyl-substituted zwitterion **2.24** (Scheme 2.8) ordinarily coordinates to chromium via an L type interaction via the phosphine donor, however, η^5 coordination via the aromatic ring such as in complex **2.27** can also occur.[52] In a study by Gudat, the ligand **2.24** was reacted directly with a BH_3·THF solution to form the protected phosphine ligand **2.25**. On coordination of the ligand **2.24** to the

chromium centre it forms two products, one of which has the same coordination mode as **2.27**, and the other results in a phosphine supported B-H-Cr three centre two electron bond in **2.26**. The same interaction was achieved by the addition of BH_3·THF to the complex **2.29** which is formed through intermediate **2.28**. Complexes **2.26** and **2.29** were characterised *in situ* therefore no X-ray or pure NMR data for these complexes are available. However, an analogous reaction using tungsten was completed and resulted in the formation of complex **2.30** which was fully characterised (Figure 2.5). The ^1H NMR spectrum showed a single resonance for the BH_3 protons at −1.33 ppm. Complex **2.30** shows a single two centred two electron bond coordinated via a phosphine supported BH_3 bond the bridging W-HB distance was 2.022 Å and the B-H bond distances were reported as 1.145 (b), 1.149 (t) and 0.890 (t) Å. These are unexpected inconsistencies between both terminal and bridging B-H distances as both terminal BH's are expected to be in the same region as each other, the reported inconsistency is most likely due to the poor reliability of X-ray in locating hydrogens.[52]

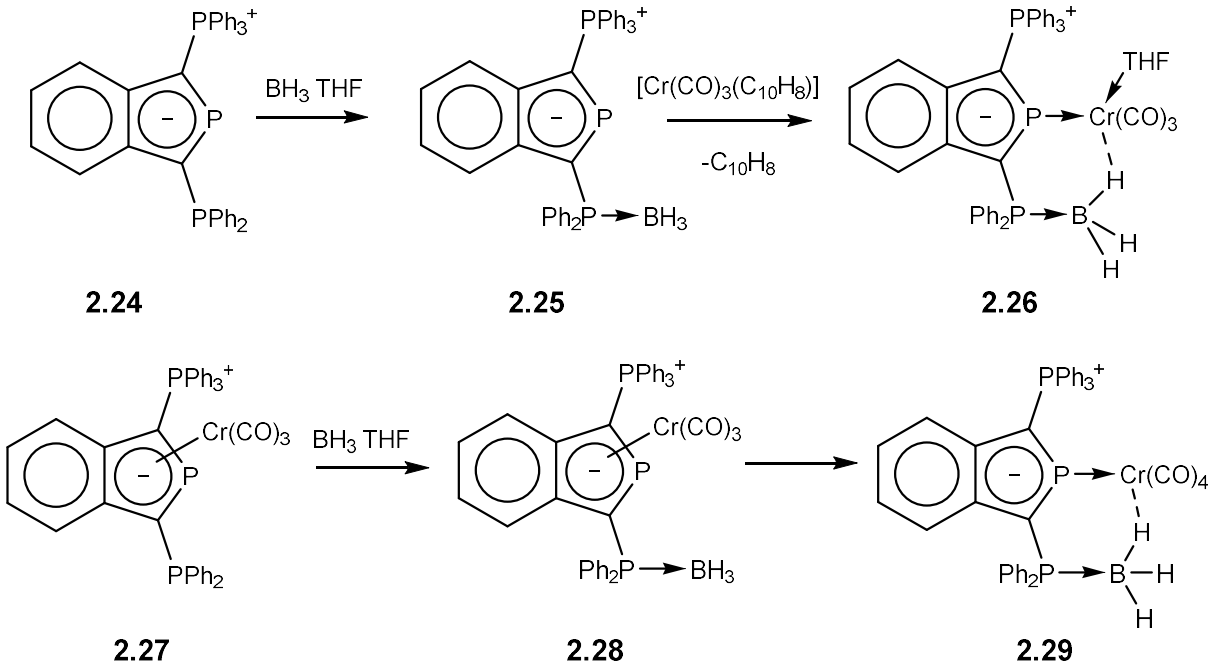

*Scheme 2.8. Synthesis of chromium complexes bearing the ligand **2.24***

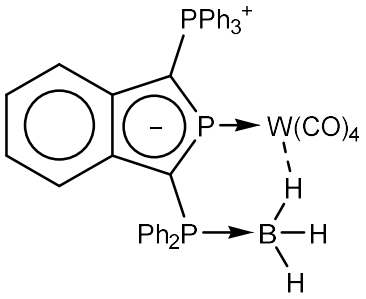

2.30

*Figure 2.5. Synthesis of an analogous tungsten complex bearing the ligand **2.24***

A further example of bis phosphine supported BH_3 ligands is that of the unsymmetrical ligand **2.33** reported by Gouygou (Scheme 2.9).[53] This ligand is synthesised by the reaction of **2.32** with a dibenzophospholylithum reagent catalysed by a 5% mol equivalent of [$Pd(OAc)_2$]/dppf]. This ligand shows three equivalent protons in the ^1H NMR spectrum at 1.34 ppm and a $^{11}B\{^1H\}$ resonance at −38.4 ppm. The synthesis of the corresponding rhodium complexes **2.34** was achieved by the addition of the ligand **2.33** to $[RhCl(cod)]_2$ followed by of $AgBF_4$. **2.34** was assessed by a ^1H $\{^{11}B,^{31}P\}$ NMR experiment which revealed that the BH_3 group rotated freely in solution at 298 K, in which as a single peak was observed at −0.09 ppm. On cooling, the interaction becomes static, on the NMR timescale at 188 K, with two separate resonances observed at 2.26 and −1.14 ppm. The $^{11}B\{^1H\}$ spectra at room temperature had a single resonance at −26.03 ppm which again represents a downfield shift in comparison to the uncoordinated ligand. X-ray quality crystals were obtained by metathesis with $NaBPh_4$ and studied via SC-XRD. This again showed that in the solid state the complex **2.34** had a static dihydroborate interaction and the B-H distances are 1.13(3), 1.24(3) and 1.00(3) Å which suggests an asymmetric interaction.[53,54]

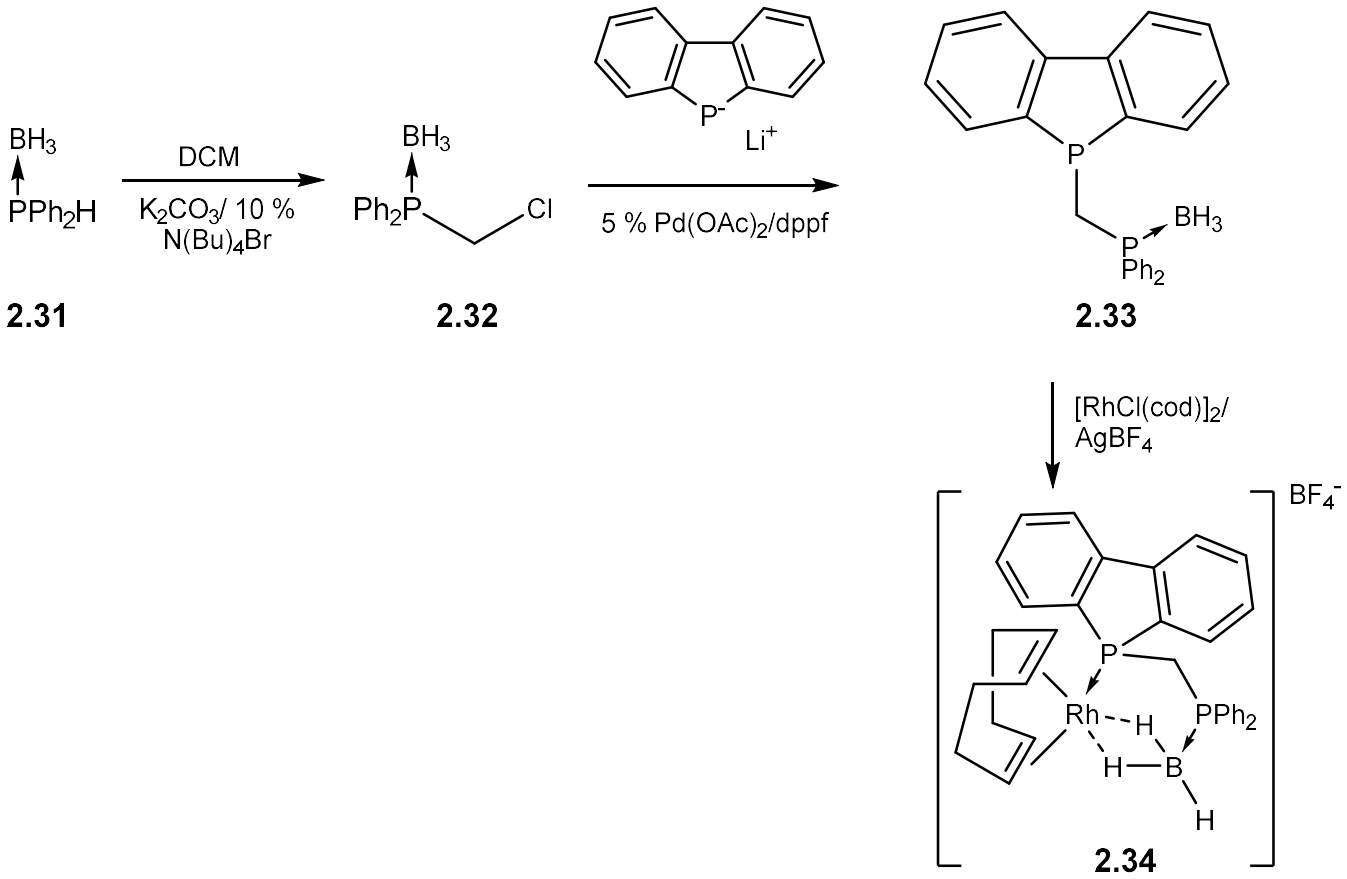

*Scheme 2.9. Synthesis of the asymmetrical neutral borane ligand **2.33***

In a study by Siebert, the synthesis of ligand **2.36** was achieved via the addition of two equivalents of BH_3·THF to the bis imidazole **2.35** (Scheme 2.10).[55] This resulted in the formation of a Lewis adduct between both nitrogen donors and a BH_3 unit. The pro-ligand **2.36** was subsequently activated via deprotonation of the acidic CH proton, with two equivalents of ^{n}BuLi. This resulted in the bis carbene **2.37** which was observed via NMR in solution. The reaction of a solution of **2.37** with one equivalent of $TiCp_2Cl_2$ or $ZrCp_2Cl_2$ resulted in complexes **2.38** and **2.39** respectively. Complex **2.38** is an air sensitive red powder and on exposure to air the complex immediately turns green. The instability of this compound was attributed to its electron count as it remains a 16-electron compound, as no B-H-M coordination is observed. Two separate ^{1}H NMR environments were observed for the methylene protons and Cp rings. This occurs due to shape of the coordinated ligand being distorted from the coordination plane and therefore the ligand bends closer to one of the Cp rings and further from the other resulting in separate chemical environments. Complex **2.39** is a colourless solid that does not

react with air. In this complex, NMR studies showed single resonances for the methylene and Cp protons suggesting that there is little to no bending of the ligand. Two separate boron resonances were observed at −17.8 and −20.9 ppm in comparison to complex **2.38** in which a single resonance at −22.3 ppm was observed. This confirms that the borane units are in separate environments suggesting different coordination modes for both BH_3 units. No data was reported for BH_3 resonances in solution, however, it was stated that this is fixed in solution. SC-XRD studies showed that a single borane unit is coordinated via a single two centre three electron bond, the bridging hydrogen Zr-H distance is 2.16(2) Å in comparison to the borane that does not interact with the metal at 3.290 Å is considerably shorter, confirming that only one B-H-M bond is present.[55] The stability of this compound is therefore attributed to its 18 valence electron count as a consequence of the coordination of the B-H bond to the metal centre.

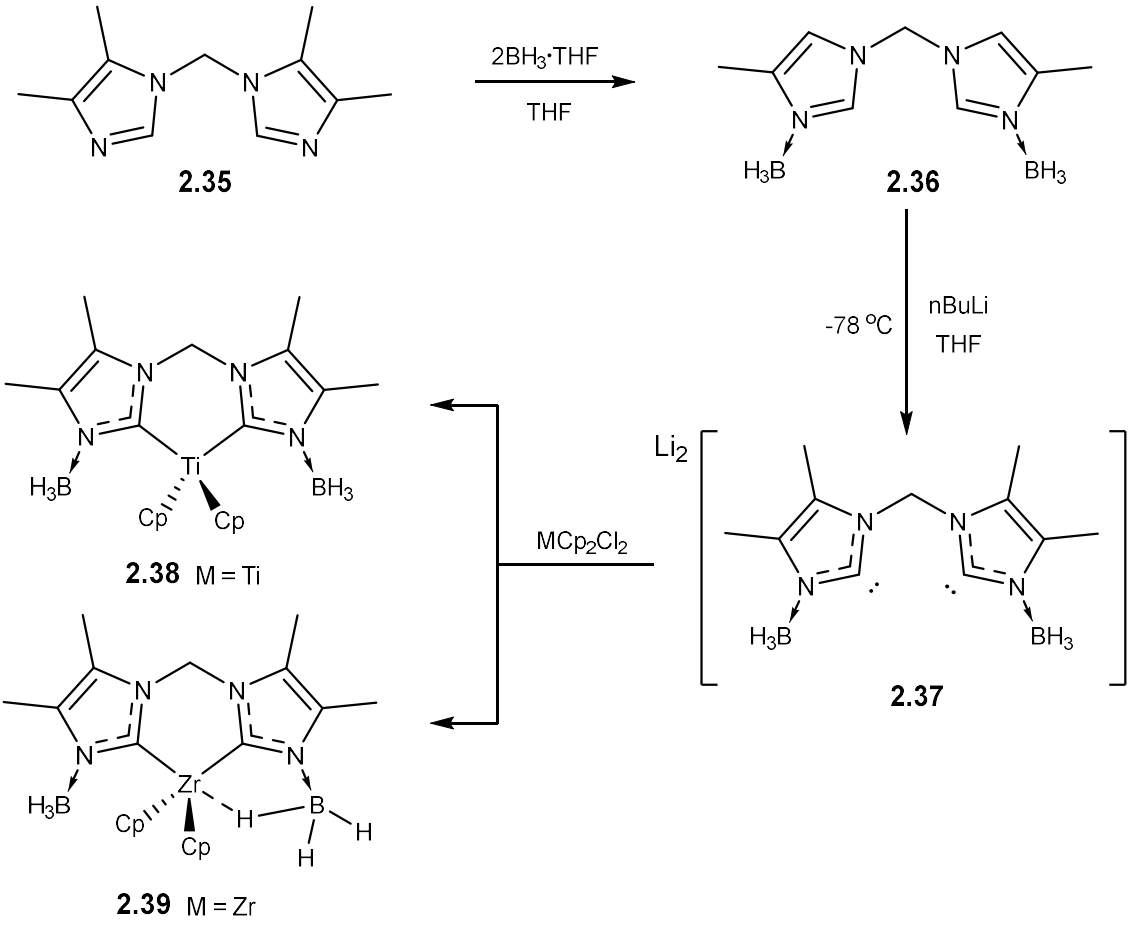

Scheme 2.10. Synthesis of a bis carbene bis borane neutral ligand

The pro-ligand HmapyBH$_3$ (**2.40**) was synthesised by the addition of BH$_3$·THF to a solution of 2-methyl amino pyridine (Hmapy) in toluene at −78 °C by Cabeza (Scheme 2.11).[56] The resultant product was obtained by removal of volatiles under reduced pressure and subsequent washing with hexanes. ^{1}H NMR studies of this ligand showed a single broad peak at 3.11 ppm that resolves into a sharp singlet in the ^{1}H{^{11}B} NMR spectrum. In the ^{11}B NMR spectrum, a quartet was observed at −16.1 ppm. The deprotonation of Hmapy(BH$_3$) was achieved by the addition of KHMDS in the presence of either $^1/_2$[IrCl(cod)]$_2$ or $^1/_2$[RhCl(cod)]$_2$. Each metal precursor was added to generate the corresponding [Rh{(BH$_3$)mapy}(cod)] **2.41** or [Ir{(BH$_3$)mapy}(cod)] **2.42** complexes, respectively. The solid produced from this reaction was removed via filtration and washed with hexanes. ^{11}B NMR studies for both complexes revealed, in comparison to the ligand downfield shifts for the Rh and Ir complexes at −10.0 and 0.6 ppm, respectively. SC-XRD structures were obtained for both complexes, the [Rh{(BH$_3$)mapy}(cod)] complex has a M-B distance of 2.257(4) Å and BH distances of 1.09(4) (t), 1.18(4) (b) and 1.17(4) (b) Å. This confirms that two of the BH bonds are elongated and therefore interact with the rhodium centre through two 3c-2e bonds. In [Ir{(BH$_3$)mapy}(cod)], the Ir-B distance was slightly shorter at 2.218 Å, the B-H distances in the [Ir{(BH$_3$)mapy}(cod)] complex were recorded as 1.08(5) (t), 1.33(6) (b) and 1.26(6) (b) Å. In this complex there are small differences between the bridging BH's this is due to experimental error associated with the difficulties of locating hydrogens in X-ray crystallography. In this case, however, Van der Maelen indicates a high degree of confidence in these values. Using DFT-optimised structures without symmetry restraints, the lowest energy structure contains a dihydroborate interaction that remains asymmetric and the differences in the XRD structure are not due to experimental error. Quantum theory of atoms in molecules (QTAIM) studies suggested that the asymmetry is in fact due to the very narrow bite angle of the ligand, which was found to be 62° in the rhodium complex and 70° in iridium complex resulting in an inefficient overlap with two equatorial sites of a trigonal bipyramidal complex. ^{1}H NMR studies of the [Rh{(BH$_3$)mapy}(cod)] complex showed very broad peaks for the BH$_3$ protons at 3.19 and −1.65 ppm whilst the BH$_3$ protons for [Ir{(BH$_3$)mapy}(cod)] were found to be sharp peaks at 5.02 and −3.34 ppm.

This difference in peak shape indicates that the BH_3 group in the iridium complex **2.42** is static and the Rh complexes (**2.41**) BH_3 group has a greater deal of free rotation in solution and VT NMR studies show that at higher temperatures there is a greater deal of free rotation.

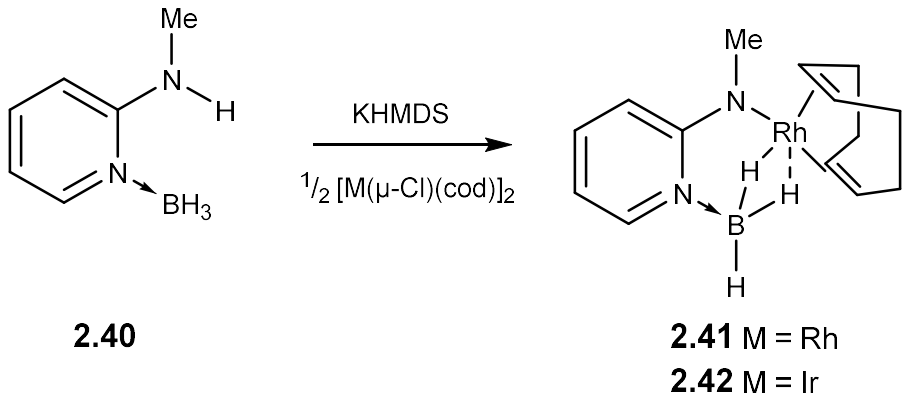

2.40

2.41 M = Rh
2.42 M = Ir

Scheme 2.11. Deprotonation of the proligand [(BH₃)mapyH] and subsequent reaction with ½[Rh(Cl)(cod)]₂ to form the complex [Rh{(BH₃)mapy}(cod)]

Further extending the complexes containing the ligand (BH_3)mapy, Van der Maelen treated toluene solutions of K[(BH_3)mapy] with one equivalent of either $[MnBr(MeCN)_2(CO)_3]$ or $[RuHCl(CO)(P^iPr_3)_2]$ (Scheme 2.12).[29] The addition of the ligand to these complexes results in the formation the potassium halide salt KX (X = Cl or Br) and the subsequent loss of two MeCN ligands, in the case of the manganese complex, and for ruthenium a single triisopropyl phosphine ligand was lost. On coordination to manganese the IR spectra shows two separate carbonyl bands and $^{13}C\{^1H\}$ NMR experiments observed two separate carbonyl NMR environments in a 2:1 intensity which suggests facial coordination of the ligand. The ^1H NMR spectra indicates a static dihydroborate interaction as the BH_3 group is present as two separate environments in the ^1H NMR at 4.31 and −10.71 ppm. SC-XRD studies observed the B-H bond distances as 1.09(2) (t), 1.21(2) (b) and 1.24(2) (b) Å. The slight difference in the B-H bond distances in the bridging B-H bonds in this case is not supported by DFT optimised structures which showed the B-H distances as the same and therefore the slight differences are attributed to experimental error. On coordination of the ligand to ruthenium the ^1H NMR spectra showed that the BH_3 protons were in three separate environments at 4.45 (t), −4.35 (b) and −6.52 (b) ppm. The CO, P^iPr_3 and hydride ligands were located by SC-XRD structure analysis, this also confirmed the

dihydroborate interactions. The structure appeared to suggest in this case a symmetrical κ^2-H,H interaction with B-H bond distances of 1.12 (t), 1.28 (b) and 1.28 (b) Å. However, this symmetrical interaction was not consistent with DFT calculations which indicated an asymmetric interaction.

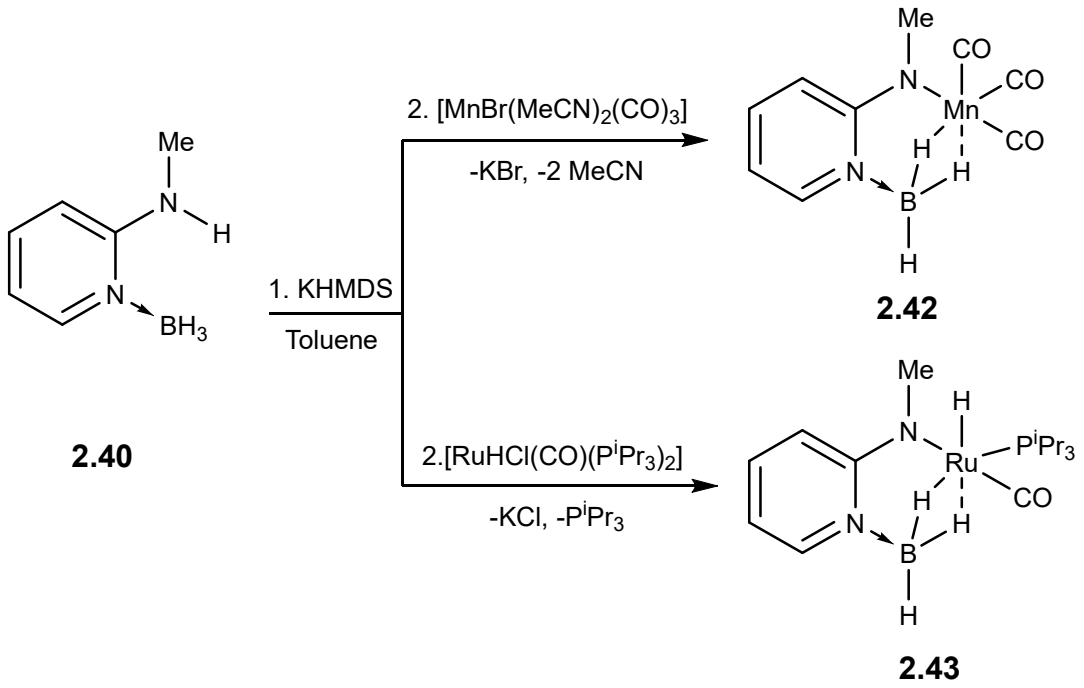

Scheme 2.12. Formation of both Manganese and Ruthenium complexes bearing the ligand [(H_3B)mapy]

The ligand [(BH_3)^{i}Pr$_2$bzam] was synthesised by the Van der Maelen group (Scheme 2.13).[28] The synthesis was achieved by the addition of phenyl lithium to a solution of N,N'-bis(isopropyl)carbodiimide **2.44** followed by quenching with H_2O. Subsequent addition of borane, from BH_3·THF, results in the bis(isopropyl)benzamidine borane adduct **2.46**. The pro-ligand was then characterised fully by NMR. In the ^{1}H NMR spectra the BH_3 protons were present as a very broad quartet at 2.64 ppm and in the ^{11}B experiment a single resonance confirmed the chemical shift of the boron nucleus at −23.60 ppm. The free ligand is generated by the addition of LiHMDS to (BH_3)^{i}Pr$_2$bzamH which is then added to either $^1/_2$[$RuCl_2Cp^*$]$_2$ or [$MnBr(CO)_3(MeCN)_2$]. In the case of manganese, the complex generated is [Mn(^{i}Pr$_2$bzamBH_3)$(CO)_3$] **2.48**. The ligand (BH_3)^{i}Prbzam replaces the two former MeCN ligands that were lost in the reaction. NMR studies showed a static dihydroborate interaction in the ^{1}H spectra with BH_3 resonances recorded at 4.83 and −9.88 ppm. SC-

XRD studies revealed the bond distances as 1.34(6), 1.08(6) and 1.13(6) Å. In the case of ruthenium, the ligand is coordinated via the nitrogen and two B-H-Ru bridges. The $^{11}B\{^{1}H\}$ NMR resonance was located at −16.4 ppm which is shifted downfield from that of the free ligand. The ^{1}H NMR of **2.47** again suggests a static interaction this is confirmed by SC-XRD structure analysis with a Ru-B bond distance of 2.173(3) Å and BH distances of 1.13(3) (t), 1.29(3) (b) and 1.32(2) (b) Å.

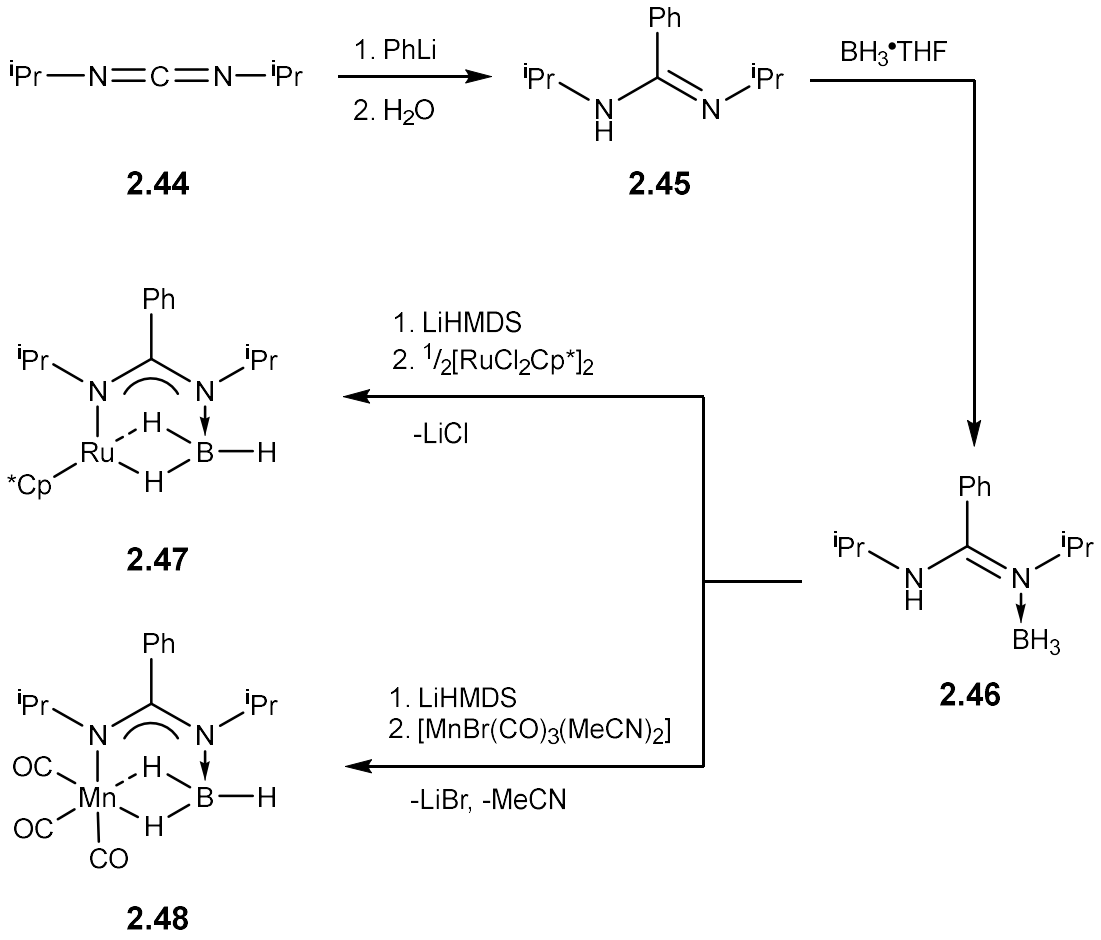

Scheme 2.13. Ruthenium and manganese complexes bearing the ligand [(BH$_3$)iPrbzam]

The ligand dppm has a very small bite angle due to its methylene bridge, the bite angle can be extended by adding a BH_n unit extending the ring size of any potential chelate from 4 atoms to 5, if bonded directly via the boron, this was extended to 6 atoms, if the BH bonds form 3c-2e bonds interacting with the metal centre. In an early example presented by Puddephatt, the reduction of cobalt dichloride or cobalt dibromide using sodium borohydride whilst in the presence of CO resulted in the synthesis of a base stabilised X-type metal boryl bond (Scheme 2.14).[57] This side product,

complex **2.49** was separated by hand picking black crystals. The structure of the complex **2.49** contains a distorted trigonal bipyramidal centre with two CO ligands, and a pendant dppm ligand a κ^2-P,B, bound dppm·BH_2. SC-XRD studies were successful in locating the hydrogens revealing a tetrahedral geometry around the boron centre. In addition to this, Puddelphatt states that the Co-B bond distance was expected to fall in the range of 2.00 – 2.15 Å based on previously reported examples,[58] however, the complex **2.49** gave a longer than the expected length at 2.227(6) Å. The dppm ligand provides steric shielding to the boryl moiety whilst simultaneously providing electron density to the cobalt centre giving greater stability to the boryl group. This is an example which shows the binding motif of the neutral borane ligand after reactivity has occurred.

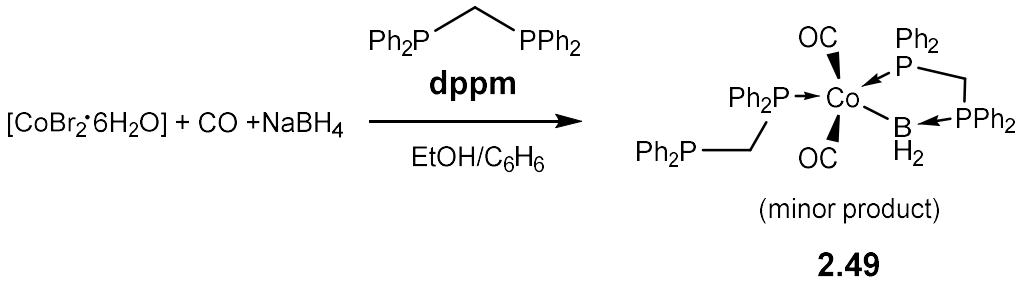

*Scheme 2.14. Synthesis of Puddelphat's cobalt complex **2.49** bearing the dppm·BH_3 ligand*

Barton synthesised a rhodathiaborane complex which contained two dppm ligands **2.51** (Scheme 2.15).[59] One dppm ligand is coordinated through both phosphine donors with the other ligand coordinated via a single phosphine donor (whilst the other remains pendant). The reaction of this complex with a 20-fold excess of BH_3·THF results in the insertion of a BH_3 unit between the Rh-P bond resulting in a dppm·BH_3 with a single donating phosphine to the metal centre whilst the other phosphine is occupied in dative bonding to the Lewis acidic BH_3 unit. The second pendant phosphine ligand was abstracted as dppm·$(BH_3)_2$. The Rh-B bond was recorded as 2.323 Å, the reported distance is above the sum of the covalent radii for a rhodium and boron 2.26 Å distance.[33] Room temperature NMR studies of this complex show that the BH_3 protons are all equivalent suggesting that the BH_3 unit is freely rotating in solution.

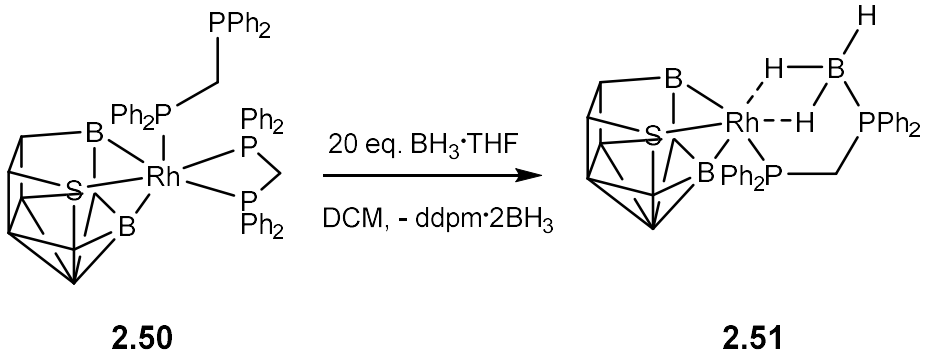

2.50 **2.51**

*Scheme 2.15. Synthesis of the rhodathiaborane dppm·BH_3 complex **2.51**.*

Weller and Ingleson synthesised a rhodium dppm·BH_3 complex **2.52** by the direct addition of dppm·BH_3 to $[RhCl(cod)]_2$ in the presence of a halide abstractor (Scheme 2.16).[60] The resulting cationic complex also contained cyclooctadiene (cod) as an ancillary ligand on the coordination sites opposite to the dppm·BH_3 chelate. Attempts to grow single crystals for X-ray diffraction with the PF_6 salt proved unsuccessful but subsequent metathesis with $Na[BPh_4]$ yielded X-ray quality crystals. Single crystal X-ray diffraction studies of the $[BPh_4]^-$ salt revealed that the BH_3 unit coordinates to the metal centre with two, 3c-2e bonds. The Rh-B distance was reported to be 2.313(3) Å which is similar to that reported by Barton.[59] In this study, the hydrogen atoms were located within the degree of certainty associated with X-ray studies. Again, as previously reported in the BH_3 unit, both bridging BH's elongate, further to this the P-B-H angles are compressed resulting in a distorted tetrahedral arrangement. This distortion is said to facilitate efficient bonding between the BH_3 group and the metal centre. Comparison of the Rh-C bond lengths associated with the cod ligand shows that the olefin trans to the BH_3 unit Rh-C bond lengths are significantly shorter than that of the trans phosphine Rh-C bond lengths. This suggests that the carbon trans to BH_3 is more labile in comparison to the carbon that is trans phosphine. The weaker bonding of the BH_3 unit to the rhodium is supported by VT NMR studies of the complex, at room temperature. The BH_3 protons show only one resonance at −0.25 ppm which demonstrates rapid exchange of the BH_3 hydrogens bound to the rhodium centre on an NMR timescale. On cooling to −50 ˚C, the single peak collapses and two new environments are

observed at 2.25 ppm and −1.48 ppm with a ratio of 1:2 respectively further supporting the evidence for the dihydroborate bonding mode.

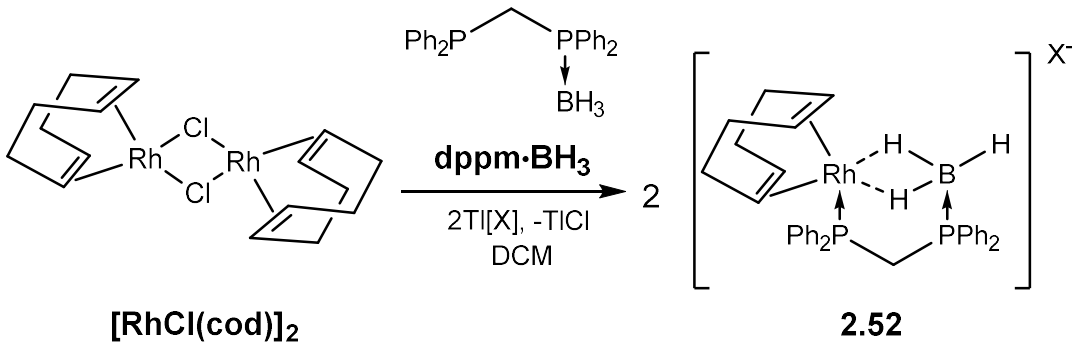

*Scheme 2.16. Addition of the ligand **dppm·BH₃** to **[RhCl(cod)₂]** forming [Rh(dppm·BH₃)(cod)] showing κ³-P,H,H coordination*

Further work by Weller extended knowledge on the dppm·BH_3 ligand to chromium and ruthenium centres.[61] Addition of dppm·BH_3 to [$Cr(CO)_4$(nbd)] **2.53** resulted in the formation of [$Cr(CO)_4$(η^1-H_3B·dppm)] **2.54** (Scheme 2.17). This complex only has a single BH agostic interaction, this is because **2.54** is formally an 18-electron complex when including the B-H-M bond and thus the complex has a saturated coordination sphere. In the solid state, the six membered chelate adopts a chair conformation. This conformation is fluxional in solution as the methylene protons are equivalent in room temperature NMR studies. The Cr-H bond length is longer than previously reported BH-Cr distances but significantly shorter than a CH-Cr bond. The Cr-B distance was recorded as 2.800(2) Å which is similar to that reported for unsupported R_3P·BH_3 compounds. This shows that in tethered BH_3 ligands the dppm chelate has little influence on the nature of coordination of the BH_3 unit in comparison to the coordination of unsupported BH_3·L complexes. Further extending the scope of the ligand to ruthenium, the complex **2.57** was prepared by reacting [Ru(Cp)$(NCMe)_3$]PF_6 with a either trimethyl phosphine or trimethoxy phosphine followed by the addition of the ligand dppm·BH_3. This again results in a BH_3 unit coordinated via one 3c-2e bond. If no PR_3 is added prior to the addition of dppm·BH_3 then the ligand is coordinated via two 3c-2e. This further establishes the BH unit as a formally 2-electron donor as a single BH bond can occupy the same coordination site as a phosphine.

Addition of one equivalent of phosphine or CO results in a shift from κ^2 to κ^1 coordination of the BH_3 unit to generate **2.56**. The Ru-B distance is significantly shorter in the κ^2 complex **2.55** at 2.180 Å than that of the κ^1 complexes **2.56** and **2.57** with bond distances of 2.520(4) Å and 2.499(8) Å respectively.

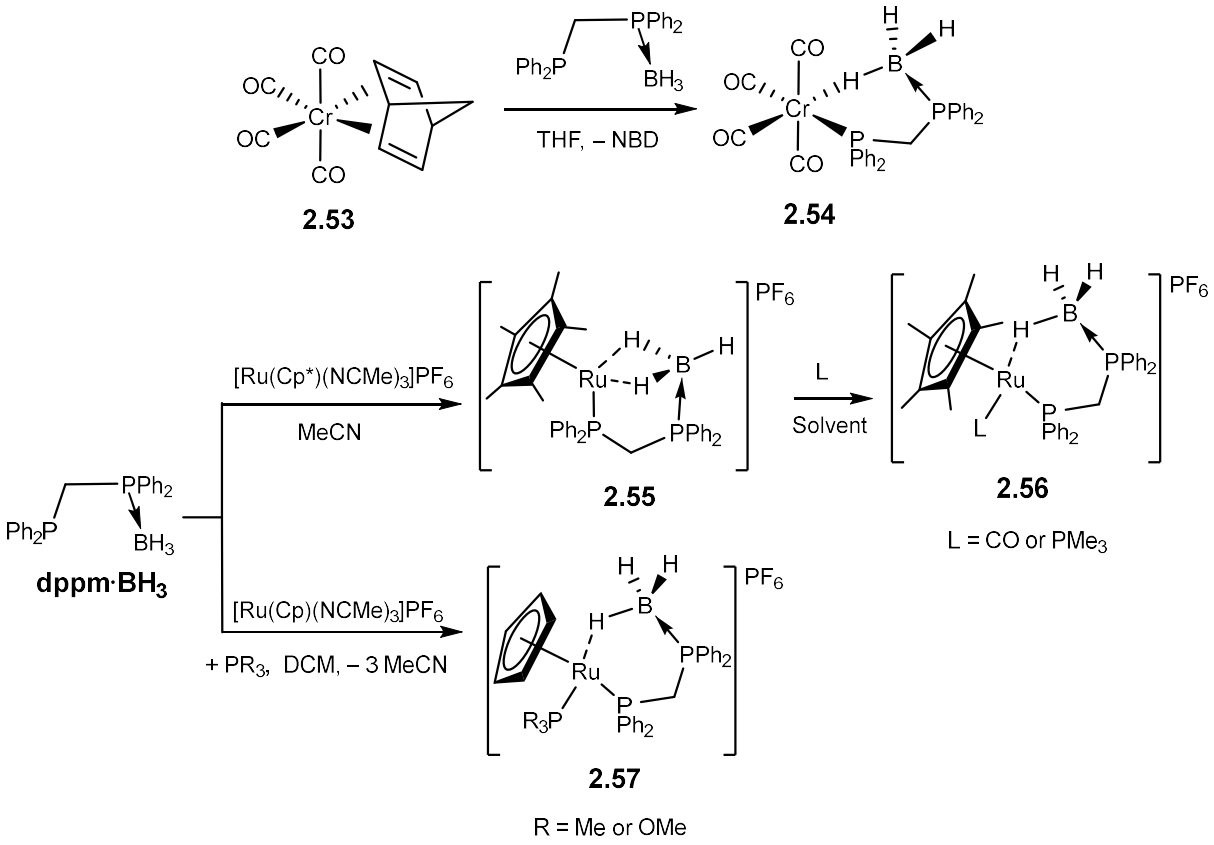

Scheme 2.17. Addition of the dppm·BH_3 ligand to chromium and ruthenium centres demonstrating both κ^3-P,H,H and κ_2-P,H coordination.

Again, studies by Weller described the treatment of]$Mn(CO)_5Br$] (**2.58**) with a halide abstractor ($Na[BAr^F_4]$) which results in the formation of complex **2.59** in which two CO ligands and a halide are replaced by the dppm·BH_3 ligand (Scheme 2.18).[62] This chelating ligand coordinates via the free phosphine and two, 3c-2e B-H bonds. This coordination mode was confirmed by X-ray diffraction studies, the B-Mn distance was found to be 2.146(4) Å. In addition to this, room temperature NMR studies revealed two separate resonances for the terminal and bridging BH's at 4.99 and −9.08 ppm respectively. Therefore, exchange between bridging and terminal hydrogens does not take place at room temperature. The ^{11}B NMR resonance for the uncoordinated dppm·BH_3 ligand is −37.1 ppm. On

coordination to manganese, this undergoes a significant downfield shift to 16.7 ppm. This downfield shift suggests a significant Mn-B interaction within the dihydroborate interaction. The addition of one equivalent of CO at room temperature, however, disrupts this interaction and produces complex **2.60** in which, a single 3c-2e bond is present. The NMR studies of this reaction show that the product undergoes rapid exchange between the terminal and bridging hydrogens at room temperature, which becomes static at 190 K on the NMR timescale. The ^{11}B NMR spectrum for **2.60** has a single resonance which shows a significant upfield shift to −37. 5 ppm. This is very close to the chemical shift observed for the free dppm·BH_3 ligand at −37.1 ppm. This shows a significant change in the strength of coordination between the two complexes. In comparison, the $^{31}P\{^1H\}$ experiments show little deviation between the two complexes **2.59** and **2.60** with chemical shift values of 15.6 and 16.0 ppm respectively. The dihydroborate interaction in this case results in a much more electron deficient boron, demonstrating the strong donating properties of this chelate.

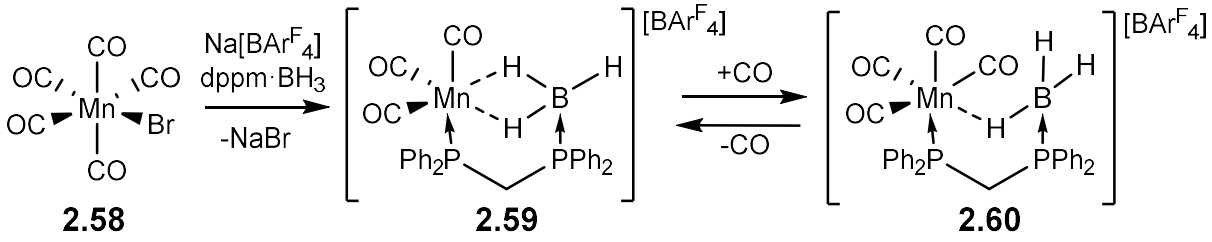

Scheme 2.18. Synthesis of manganese dppm·BH_3 complexes

The reaction of $NaBH_4$ with iron (II) chloride and dppa **2.61** in an ethanol/acetonitrile mixture was presented in a study by Langer (Scheme 2.19).[63] The reaction results in the formation of complex **2.62**, NMR studies of **2.62** show four separate phosphine resonances indicating that each phosphorous is in a unique environment, the ^1H NMR spectra shows three broad unique proton environments for the BH_3 unit distinguishing between terminal and both bridging hydrogens at −17.23, −10.27 and 0.44 ppm, this is due to one proton being trans phosphine and the other trans metal hydride. The presence of three separate environments in ^1H NMR spectra confirms there is no exchange between terminal and bridging hydrogens in the interaction. Further analysis of the BH bonds was provided using IR

spectroscopy, in which, two separate bands were observed for terminal and bridging BH bonds at 2425 and 2257 cm^{-1} respectively. X-ray diffraction studies were performed on crystals obtained by the slow diffusion of n-hexane into a solution **2.62** in DCM. These studies confirmed the coordination mode as a dihydroborate interaction, with one bridging hydrogen atom trans to a hydride ligand and the other trans phosphine, contained within the same plane as the three other coordinating phosphines. The Fe-B distance of 2.072(6) Å was in agreement with previously reported iron dihydroborate complexes.[64–67]

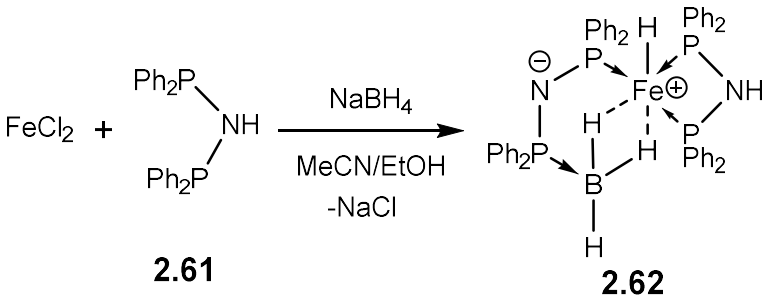

Scheme 2.19. Synthesis of an iron(II) dppa·BH_3 complex

2.4 Examples of mono- supported anionic borohydride ligands

Mono supported borohydride ligands in comparison to borohydride based scorpionates (i.e. bis- and tris-supported systems) are less prevalent in the literature. Having explored their neutral analogues in supported borane compounds, this review will now look at their anionic counterpart's mono supported borohydride ligands.

The most prevalent method of synthesis for mono supported borohydride ligands is achieved by the addition of a borohydride salt to a heterocyclic compound that contains a protic hydrogen capable of being substituted for a $[BH_n]^-$ unit and a donor atom. The presence of these two functional groups can also result in two tautomeric structures which readily interchange, this is due to the fact that protic hydrogens are readily supported by heteroatoms which can also act as donors. Scheme 2.20 shows the two tautomeric structures for methimazole (**2.63** and **2.64**), in which, the protic hydrogen is exchanged between two donor atoms such as a nitrogen or a sulfur donor. The addition of the $[BH_n]^-$ anion to the heterocycle is typically achieved in excess in order to reduce the possibility of formation of both bis- and tris- ligand although this is not always the case. The borohydride unit in these ligands are supported by a covalent bond typically between a heteroatom and the boron of the borohydride, this differs in comparison to the neutral borane analogues in which a dative bond supports a neutral BH_3 unit.

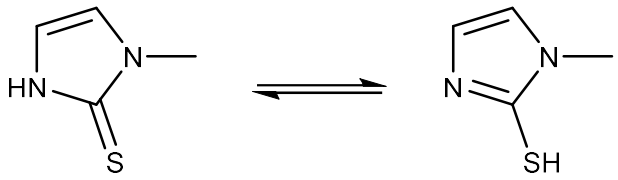

2.63 **2.64**

Scheme 2.20. Tautomerism in methimazole

2.4.1 Anionic two-atom supported borohydride ligands

As discussed at the start of this review the number of atoms between the metal and the boron in the supporting bridge can have an impact on the subsequent reactivity of the ligand at the metal centre. This section will proceed in the same manner as the previous section and start with the lowest number of supporting atoms and finish with the highest number of supporting atoms. The first example of the synthesis of a two-atom supported borohydride in this review is the synthesis of a pyrazole supported mono-ligand **2.66** (Scheme 2.21).[68] Santini showed that the synthesis of ligand salt **2.66** is achieved at room temperature. This is a lot milder in comparison to previous reported mono ligands. In this case, it appears that the mono ligand is the favoured product from this reaction as it is stated both **2.65** and $NaBH_4$ are added in a 1:1 molar ratio. In the IR spectrum, stretching frequencies observed in the B-H region for this ligand at 2357, 2318 and 2271 cm^{-1}, further analysis in the ^1H NMR spectra shows a single environment for the BH_3 protons at 2.10 ppm.

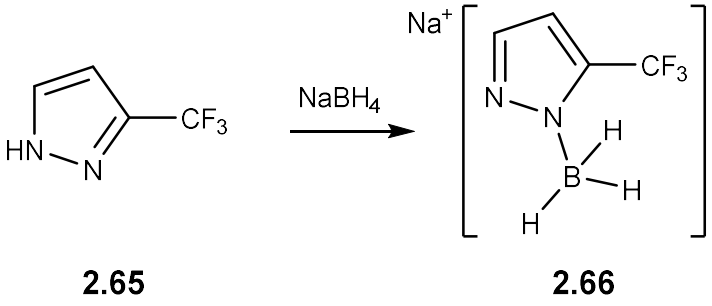

2.65 **2.66**

Scheme 2.21. Synthesis of the anionic borohydride ligand based on a pyrazole scaffold

Following its synthesis, the methanol stable ligand **2.66** was reacted with one equivalent of silver(I) nitrate and two equivalents of phosphine to afford their respective silver complexes **2.67** in methanol (Scheme 2.22). The phosphines used for this reaction were PPh_3, $P(o\text{-}Tol)_3$, $P(m\text{-}Tol)_3$ and $P(p\text{-}Tol)_3$. When the reaction was attempted without phosphine, this resulted in the reduction of the metal to metallic silver. Complexes **2.67** have slightly higher B-H stretching frequencies in comparison to the ligand salt **2.66** which are present in the region of 2302 – 2429 cm^{-1}. The shift in IR stretching frequencies in comparison to the free ligand is due to coordination of the ligand to the metal centre,

no observable resonance was located for the BH_3 protons which could indicate exchange between terminal and bridging protons in solution. X-ray quality crystals were obtained for PPh_3 and $P(p\text{-}Tol)_3$ complexes, diffraction studies demonstrated that the BH_3 unit is coordinated via a single 2c-3e bond to the metal. The bridging Ag-H distance were recorded as 2.07 and 2.17 Å respectively. The Ag-B distance was also reported as 2.941 and 2.952 Å.[68]

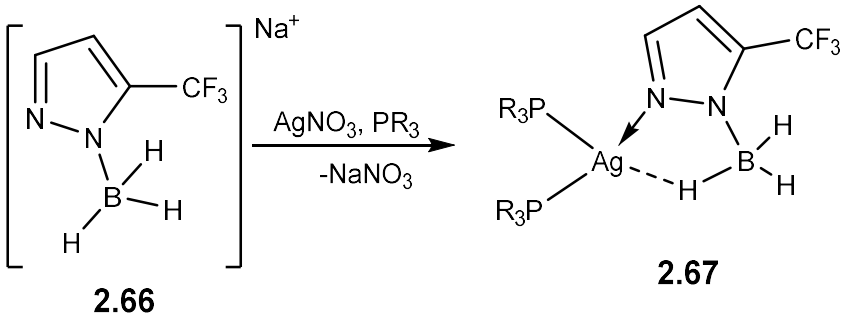

2.66 **2.67**

Scheme 2.22. Coordination of a mono pyrazole ligand to silver

The ligand [Mp^{Ph2}] was synthesised in DMF with an excess of $NaBH_4$ at 130 °C (Scheme 2.23). The excess $NaBH_4$ ensures that none of the corresponding bis or tris ligand is formed. Temperatures more than 130 °C also result in the slow formation of the bis ligand. The excess 3,5, diphenyl pyrazole is extracted with DCM and Et_2O resulting in the pure product **2.69**. The IR spectrum of the ligand salt **2.69** showed two BH absorption bands at 2304 and 2271 cm^{-1}. The presence of BH_3 protons in the ligand is confirmed in the ^{11}B NMR spectra with a quartet at −4.2 ppm and a very broad quartet in the ^1H spectrum at 2.44 pm in CD_3OD.

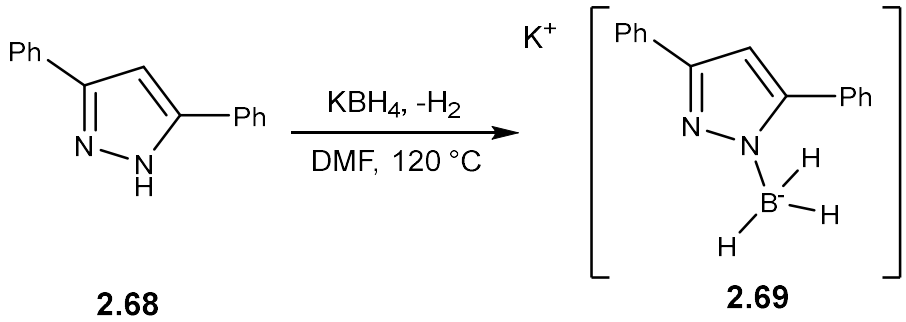

2.68 **2.69**

Scheme 2.23. Synthesis of the ligand salt K[Mp^{Ph2}]

In a study by Bouwman, the copper complexes of Mp^{Ph2} are synthesised in air from the $[CuI(PR_3)_2]_2$ dimer (where $PR_3 = PPh_3$, ½ dppe or dppbz) whilst stirring at room temperature in DCM.[69] This reaction results in the products $[Cu(Mp^{Ph2})(PPh_3)_2]$, $[Cu(Mp^{Ph2})(dppe)]_2$ and $[Cu(Mp^{Ph2})(dppbz)]$ which were purified by THF/n-hexane precipitation. IR studies showed the presence of B-H stretching bands in the region of 2014 - 2066 cm^{-1} indicating the presence of both terminal and bridging BH bonds. ^1H NMR studies in CD_2Cl_2 all gave single environments for the BH_3 protons at 3.13, 2.99 and 3.03 ppm for the three complexes, $[Cu(Mp^{Ph2})(PPh_3)_2]$, $[Cu(Mp^{Ph2})(dppe)]_2$ and $[Cu(Mp^{Ph2})(dppbz)]$, respectively. This suggests that rapid exchange occurs between terminal and bridging protons in solution. ^{11}B resonance for each of the complexes were found to be −0.74, −0.58 and −0.81 ppm for $[Cu(Mp^{Ph2})(PPh_3)_2]$, $[Cu(Mp^{Ph2})(dppe)]_2$ and $[Cu(Mp^{Ph2})(dppbz)]$, respectively. SC-XRD studies of each of the complexes show that the coordination of each of the ligands is through an L-type interaction from the nitrogen donor to the metal centre and a single 3c-2e bond originating from the bridging B-H. Upon coordination of the B-H, the B-H bond distance is slightly elongated when compared to terminal BH's. The Cu-B distances for each complex is 2.774, 2.874 and 2.732 Å for $[Cu(Mp^{Ph2})(PPh_3)_2]$, $[Cu(Mp^{Ph2})(dppe)]_2$ and $[Cu(Mp^{Ph2})(dppbz)]$, respectively.

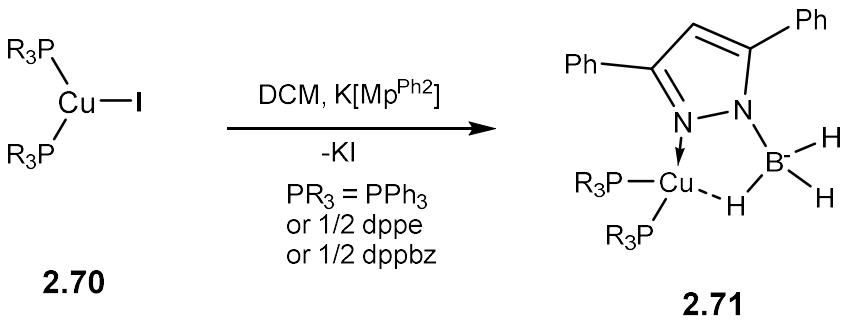

Scheme 2.24. Synthesis of copper complexes of $[Mp^{Ph2}]$

2.4.2 Anionic three-atom supported borohydride ligands

Santos demonstrated that the slow addition of **2.72** or **2.73** to a suspension of excess sodium borohydride in THF at 50 °C results in the respective formation of either **2.74** or **2.75** (Scheme 2.25).[70] A similar reaction was also successfully attempted with **2.76** where R = Me or Bm (1-[4((2-methoxyphenyl)-1-piperazi-nyl)butyl]-2-mercaptoimidazole and **2.76** with yields of 34 – 83%. ^{11}B NMR spectroscopic analysis of the ligands showed resonances at −19.0, −19.3 and −20.3 ppm for **2.74**, **2.75** and **2.77** respectively. Interestingly, it was noted that each of the ligands synthesised (**2.74**, **2.75** and **2.77**) are water soluble and stable molecules and the BH_3 group does not undergo hydrolysis to boronic acids. This was important for this research as the ligands were synthesised with objective of developing new radio pharmaceuticals.

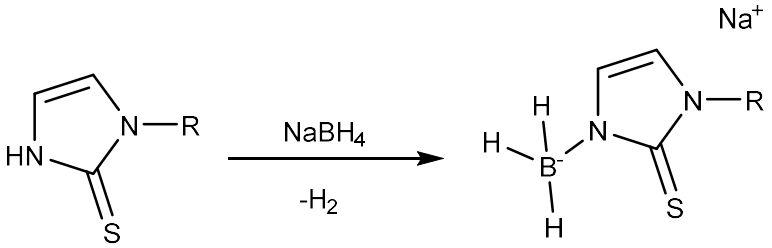

2.72 R = Me
2.73 R = Bm

2.74 R = Me
2.75 R = Bm

*Scheme 2.25. Synthesis of the ligand salts **2.74** and **2.75***

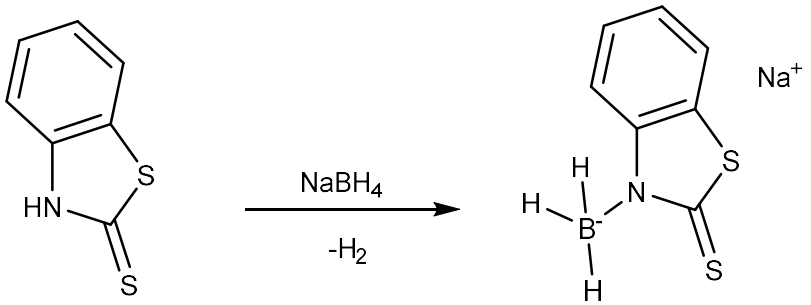

2.76 **2.77**

*Scheme 2.26. Synthesis of the ligand salt **2.77***

Following on from the ligand synthesis, in distilled water, Santos prepared complexes of rhenium from ligands **2.74**, **2.75** and **2.77** and a technetium-99 complex was made using ligand **2.74** (Scheme 2.27). The resultant complexes **2.80**, **2.81**, **2.82** and **2.83** all observe static dihydroborate metal interactions where the bridging hydrogens remain fixed and there is no exchange with the terminal B-H. Two separate environments are reported for the terminal and bridging hydrogens with the chemical shift of the latter observed between −5.48 and −6.04 ppm showing that the bridging hydrogens are more hydridic in nature due to their static interaction with the metal centres. The ^{11}B NMR resonances have been shifted downfield from their respective ligands and fall within the range of 8.2 – 12.1 ppm, this shift is most likely due to the formation of a significant M-B interaction within the dihydroborate interaction. SC-XRD studies solved the structure for complexes **2.80**, **2.81** and **2.83**. These confirmed the coordination of the BH_3 motif to the metal via two 3c-2e bonds. In **2.80**, the ^{99}Tc-H distances were found to be 1.95(3) and 1.90(2) Å. These are much longer than that of the bis complex [Tc(Bm)$(CO)_3$], in which, only a single three-centre two-electron bond is formed (κ^3-S,S,H coordination) with the reported Tc-H distance of 1.65(6) Å.[71] The Re-H distances found in **2.81** are slightly longer at 2.0(1) and 1.9(1) Å and are within agreement with that of a standalone borohydride ligand coordinated with a dihydroborate interaction with distances of 1.80(6) and 1.93(6) Å.[72] The M-B distances for complexes **2.80**, **2.81** and **2.83** are 2.329(2), 2.30(1) and 2.31(1) Å, respectively. This displays a slightly longer length for the technetium-99 complexes than that of the rhenium complexes.

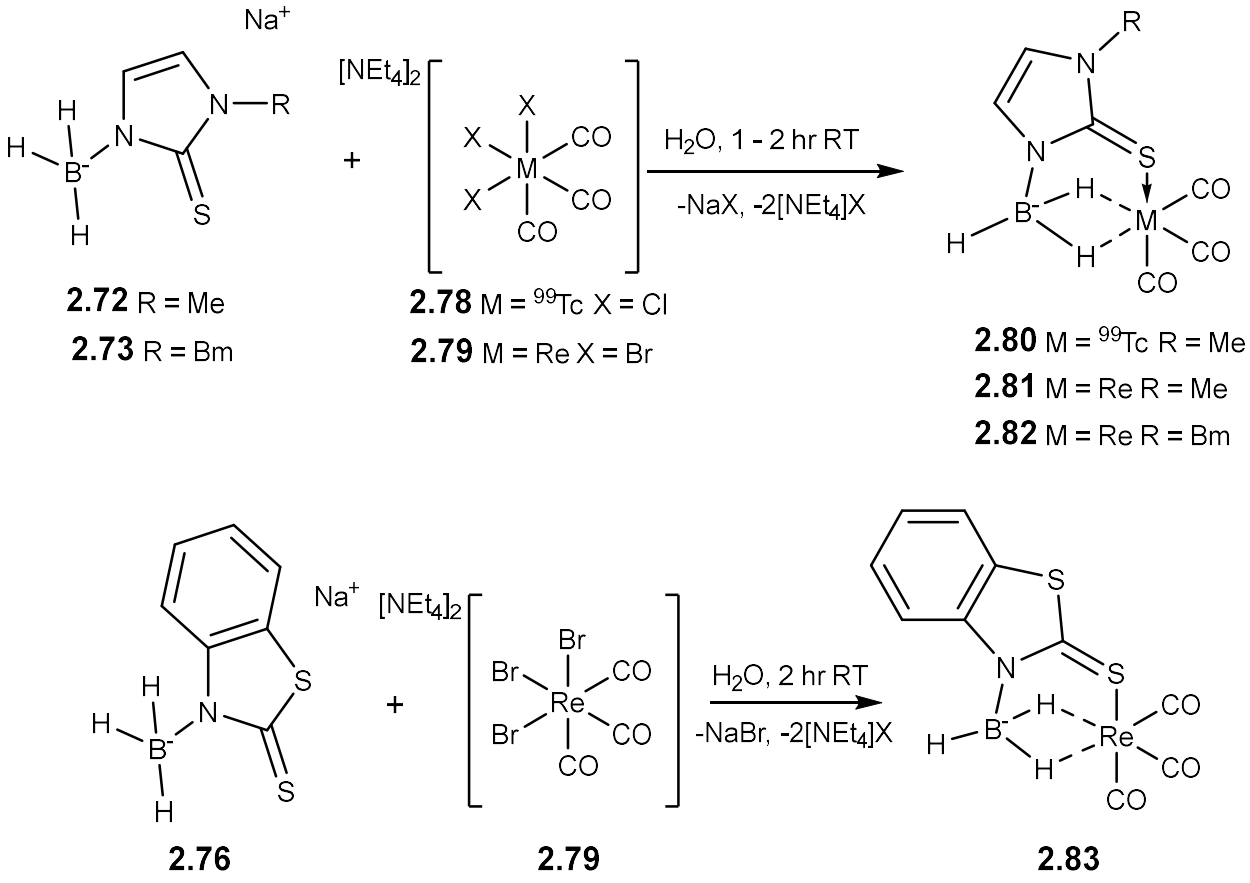

Scheme 2.27. Synthesis of technetium and rhenium complexes containing monosubstituted borohydride ligands

Following on from the synthesis of the complexes, Santos decided to explore the reactivity of the complex **2.81** (Scheme 2.28). To a solution of **2.81** in toluene was added, one equivalent or either PPh_3, ^tBuNC or $CNCH_2COOEt$. On addition of a ligand (PPh_3, ^tBuNC or $EtOOH_2NC$) to **2.81** a single 3c-2e bond is replaced by the ligand to make the resultant complexes **2.84**, **2.85** and **2.86**. Infrared spectroscopic studies show B-H's bands corresponding to each complex in both terminal and bridging modes, with bands at 2415 (t) and 2027 (b) cm^{-1} for **2.84**, 2398 (t) and 2128 (b) cm^{-1} for **2.85** and at 2428 (t) and 2207 (b) cm^{-1} for **2.86**. Room temperature ^1H NMR studies for each of the rhenium complexes observed single resonances at −0.47, −0.21 and −0.10 ppm for complexes **2.84**, **2.85** and **2.86,** respectively. On cooling to 190 K each of the respective peaks separates into its terminal and bridging peaks representing a static interaction with an integration of 2(terminal H's): 1 (bridging H's) thus confirming the flexibility of the BH_3 group depending on temperature. A SC-XRD structure was

obtained for **2.84**, the Re-B bond distance increases to 2.779(6) Å, again which is consistent with the change in coordination mode and the B-H distances are recorded as 1.34(5) (b), 1.16(6) (t) and 1.08(4) (t) Å. This shows clearly that the bridging BH is interacting with the rhenium centre as there is an elongation of the bridging BH in the solid state.[73]

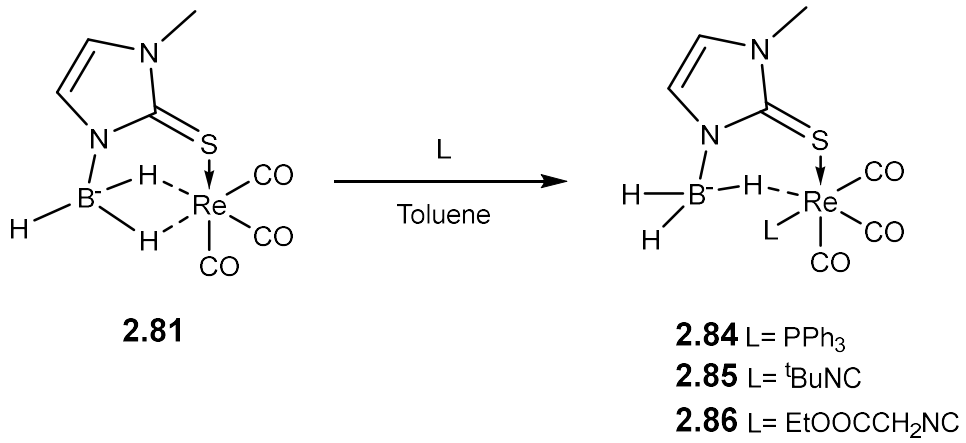

Scheme 2.28. Ligand substitution reactions representing exchange of the BH-M 3c-2e bond for an L-type ligand

Following on from the use of mercaptoimidazole, Hill used a 7-azaindole scaffold to synthesise a new monosubstituted ligand (Scheme 2.29).[74] Azaindole again has two tautomeric forms (**2.87** and **2.88**) in which the hydrogen atoms are located on either one of two nitrogen atoms. The reaction of excess borohydride with azaindole in refluxing in dioxane results in the formation of ligand salt **2.89**.

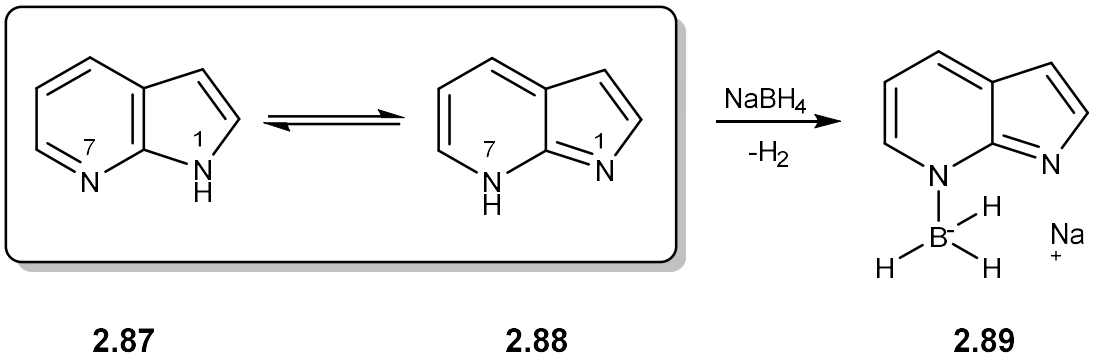

Scheme 2.29. Tautomerism in azaindole and synthesis of the ligand Mai

Surprisingly, the location of the BH_3^- is on the less basic pyridine ring of azaindole unit, which is in contrast to *bis* and *tris* scorpionate ligands based on azaindole scaffolds where the nitrogen in position

7 supports the $[BH_n]^-$ unit.[75,76] Reaction of the ligand salt **2.89** with metal precursors $[RhCl(CO)(PPh_3)_2]$ and $[RhCl(PPh_3)_3]$ results in two separate complexes (Scheme 2.30). The first complex **2.91** has only one 2c-3e bond and the second of which **2.90** has two 2c-3e bonds this is because a PPh_3 ligand is displaced by a B-H bond but a CO ligand is not. On the addition of CO to **2.90** one of the BH-M interactions is displaced resulting in formation of **2.91**. This again cements the idea that the BH-M bond acts as a two electron donor, this substitution is typical for these complexes.[59,77] The complex **2.90** has a Rh-B distance of 2.378 Å which is consistent with rhodium dihydroborate interactions.[59,60] In comparison the complex **2.91**, **2.90** has a bond length Rh-B distance is significantly longer at 3.083 Å, this is also significantly longer than that of Rh(dppm·BH_3) complexes containing a single 3c-2e bond. This is most likely due to the steric effects of the ligand. Surprisingly, in solution NMR studies of **2.90** shows only a single resonance for the BH_3 protons whereas **2.91** has two separate environments, previous examples have shown the opposite of this where dihydroborate complexes tend to have more static interactions which, is not the case for this complex. Hill states that this is because in **2.91** free rotation requires distortion of the rigid azaindole scaffold and therefore it will be a comparatively higher energy process when compared to the more flexible dppm·BH_3 ligands. In addition to this free rotation in **2.91** may result in a κ^3-N,H,H coordination which would violate the 18-electron rule.

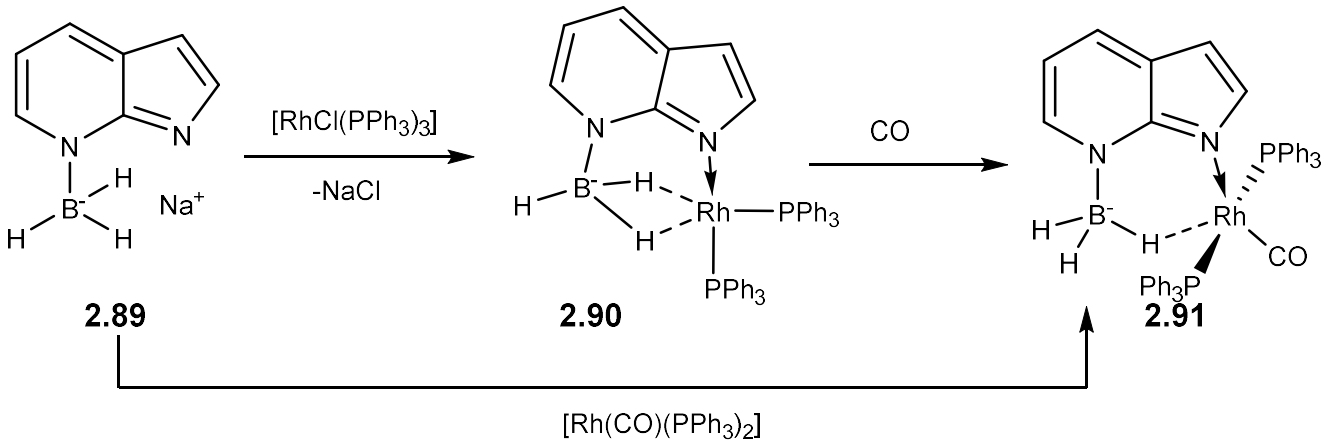

Scheme 2.30. Synthesis and reactivity of the Mai ligand with rhodium centres

The ligands **2.94** and **2.95** were synthesised by stirring in THF at various temperatures (Scheme 2.31). For the synthesis of **2.94**, $NaBH_4$ and bis-(benzothiazole-2-yl)amine (**2.92)** were reacted in a 1:1 molar

ratio at room temperature which suggests that the ligand **2.94** is the favoured product of the reaction. Again a 1:1 molar ratio was used for the synthesis of **2.95** however, the reaction was stirred at 60 °C. Spectroscopic data for the ligands show stretching bands that indicate terminal BH's at 2525 cm^{-1} for **2.94** and 2523 and 2355 cm^{-1} for **2.95**. $^{11}B\{^{1}H\}$ NMR studies in $CDCl_3$ of both ligands give resonances at −25.0 and −18.0 ppm for **2.95** and **2.94**, respectively. The ^{1}H NMR resonances for the BH_3 protons were recorded as 2.19 and 2.60 ppm for **2.94** and **2.94**.

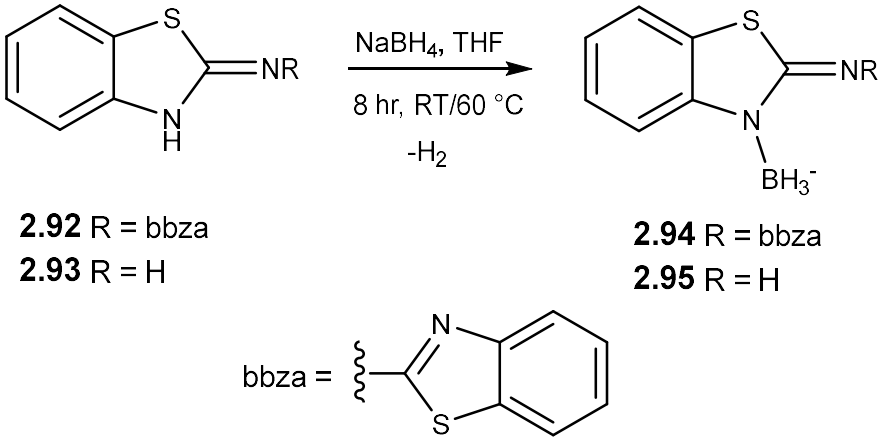

*Scheme 2.31. Synthesis of ligand salts **2.94** and **2.95***

The addition of $[Mn_2(CO)_{10}]$ in toluene to a solution of either **2.94** or **2.95**, was studied by Ghosh (Scheme 2.32).[78] The reaction which was carried out in THF results in the formation of complexes **2.96** and **2.97** which were both yellow solids. IR spectroscopy on both compounds showed both terminal and bridging BH stretching bands at 2515 and 2037 cm^{-1} for **2.96** and at 2363 and 2038 cm^{-1} for **2.97**. Room temperature ^{11}B NMR studies of both complexes in $CDCl_3$ indicate significant downfield shifts to 13.4 and 17.3 ppm for **2.97** and **2.96** respectively indicating that the coordination of the BH_3 unit to the metal is strong. This is further supported by the ^{1}H NMR data where the BH_3 protons have separated indicating no free rotation at room temperature in solution. For **2.97**, the chemical shifts were 4.41(t), −9.64(b) and −9.81(b) ppm and for **2.96**, 4.11(t) and −9.69(b) ppm. This confirms the presence of a static dihydroborate interaction in each of the complexes. SC-XRD studies also show dihydroborate interactions and the coordination of the ligand from the C=NR group. The Mn-B distances were recorded as 2.182(2) and 2.138(5) Å for **2.97** and **2.96** respectively, again the bridging

BH's are elongated when compared to the terminal BH's. Both complexes undergo ligand substitution replacing a single CO ligand with one equivalent of phosphine when added to the complex, this further confirms the strength of the dihydroborate ligand as there is no change in coordination when a second ligand is added.

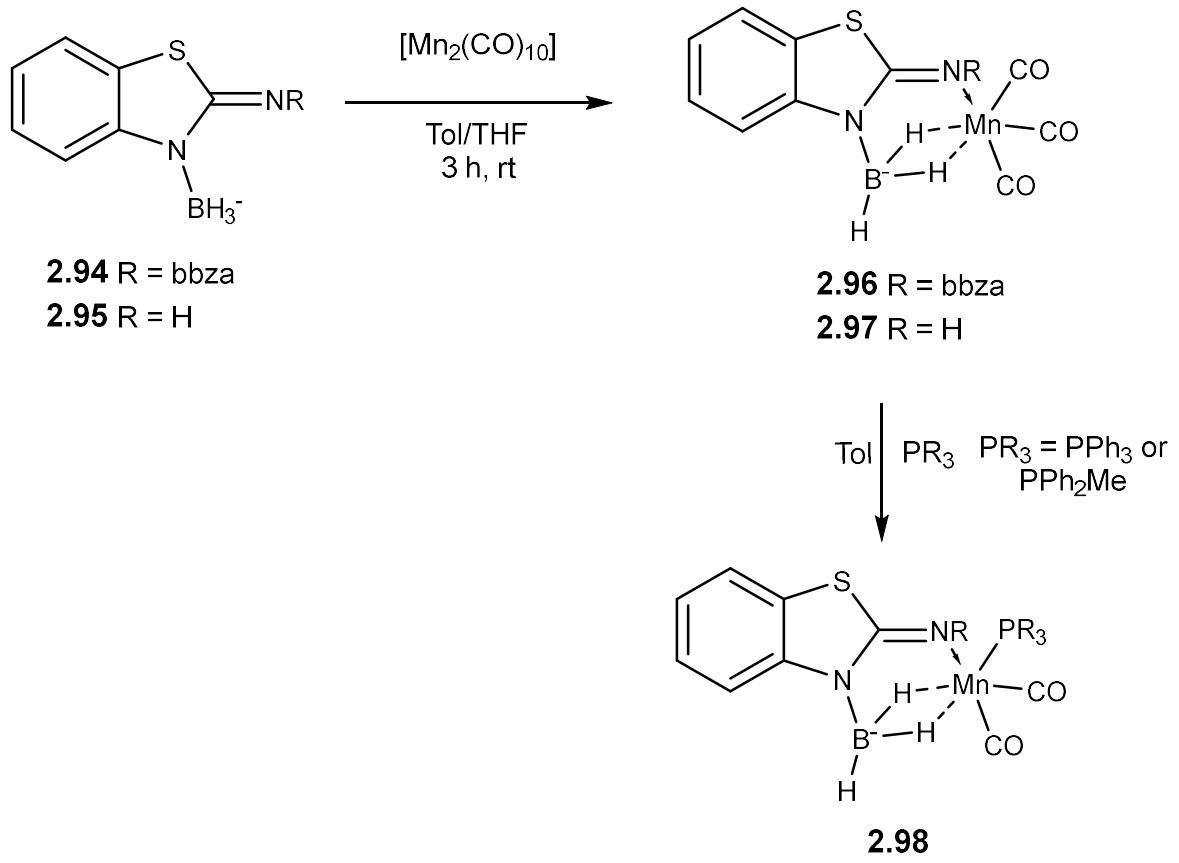

Scheme 2.32. Manganese complexes of [(H₃B)abz] and [(H₃B)bbza]

In another study by Ghosh, the ligand salt Na[(H₃B)mbt] was added directly to **[IrCl₂Cp*]₂** in toluene at −78 °C (Scheme 2.33). This resulted in the formation of complex **2.99**.[79] **2.99** was isolated as a yellow powder after purification by column chromatography. Only terminal stretching bands were reported for this complex at 2433 cm^{-1} in the IR spectrum and only a single environment at −4.96 ppm is present for the BH_3 protons in the ^1H NMR spectrum. Ghosh sates, however, that this single environment corresponds to the bridging BH's and therefore suggests that the interaction is of a fixed nature. SC-XRD data confirms the presence of a dihydroborate interaction between the BH_3 and the metal with a single terminal hydrogen pointing away. The distance of the iridium from the boron was recorded

as 2.214(6) Å and the three separate B-H distances are 1.07(4) (t), 1.39(3) (b) and 1.31(4) (b) the clear elongation of the BH bonds confirms their interaction with the metal. The corresponding rhodium complex was also synthesised in this study, however, in this case the synthesis was achieved by the addition of BH_3·THF to the metal precursor **2.100** in THF at 50 °C for one hour. Two products were isolated from the reaction by silica gel column, a yellow powder **2.101** in a 21% yield and an orange powder **2.102** in a 23% yield. Of interest to this review was **2.101** as it is the isoleptic rhodium complex of **2.99**. The spectroscopic data for **2.99** revealed only a terminal BH stretching band in the IR spectra at 2465 cm^{-1}. Within the ^1H NMR spectrum a bridging BH resonance was tentatively assigned at −2.07 ppm. The dihydroborate interaction was again confirmed by the SC-XRD structure which indicated a Rh-B bond distance of 2.241(6) Å and BH distances of 1.08(4) (t), 1.19(5) (b) and 1.23(4) (b). This was in comparison to the iridium complex a slightly weaker dihydroborate interaction due to the decreased lengthening on the B-H bonds.

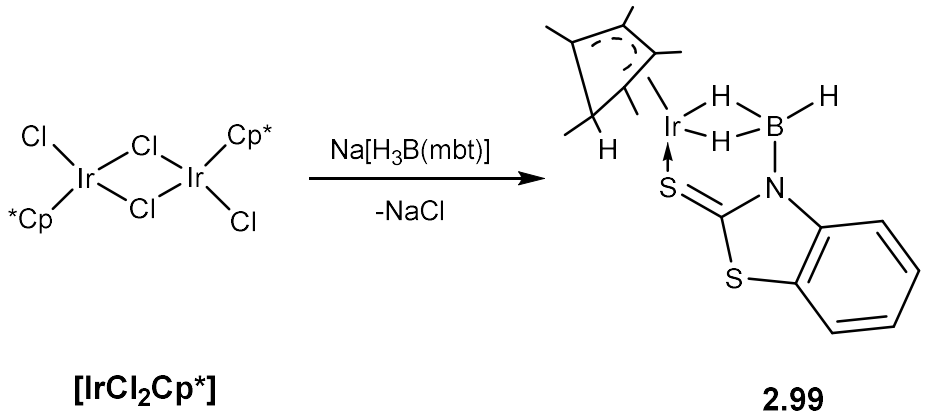

Scheme 2.33. Synthesis of an Iridium complex bearing the ligand [H_3B(mbt)]

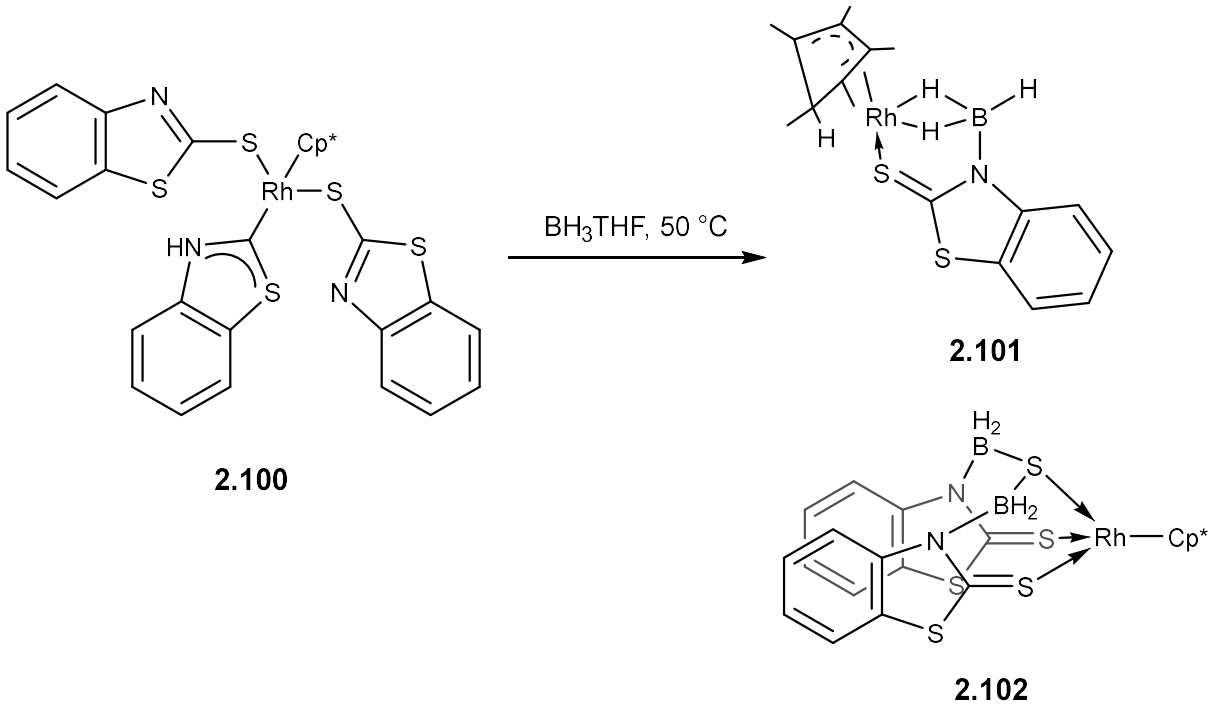

Scheme 2.34. Rhodium complexes of [(H3B)mbt]

Further expanding the family of *mono* scorpionate ligands, the Owen group synthesised a mercapto pyridine-based ligand (Scheme 2.35), the ligand was synthesised via the proposed sulfur borane intermediate **2.104** with excess borohydride, this is then transferred to the nitrogen as a borohydride unit.[14] It was shown that the ligand **2.105** was added to $[RhCl(nbd)]_2$ to form complex **2.106** at room temperature. The BH_3 protons were found to be fixed in solution with proton NMR resonances of 2.89 and −2.72 ppm. On heating the resonances began to collapse at 55 °C, only a single broad signal at −1.75 ppm was present corresponding to BH hydrogens. SC-XRD studies show the boron hydrogen distances to be 1.14(2), 1.14(2) and 1.14(2) Å for both terminal and bridging protons. On addition of carbon monoxide, a hydrogen from the BH_3 unit undergoes hydride migration to the metal to form the proposed intermediate **2.107**. This results in the formation of a Z-type interaction between the boron and the metal. The process by which a hydride migrates from a boron to a metal centre resulting in the formation of a Z-type interaction was first reported in 1999 by Hill and Owen.[80] However, this was the first such reported example for a mono substituted borohydride.

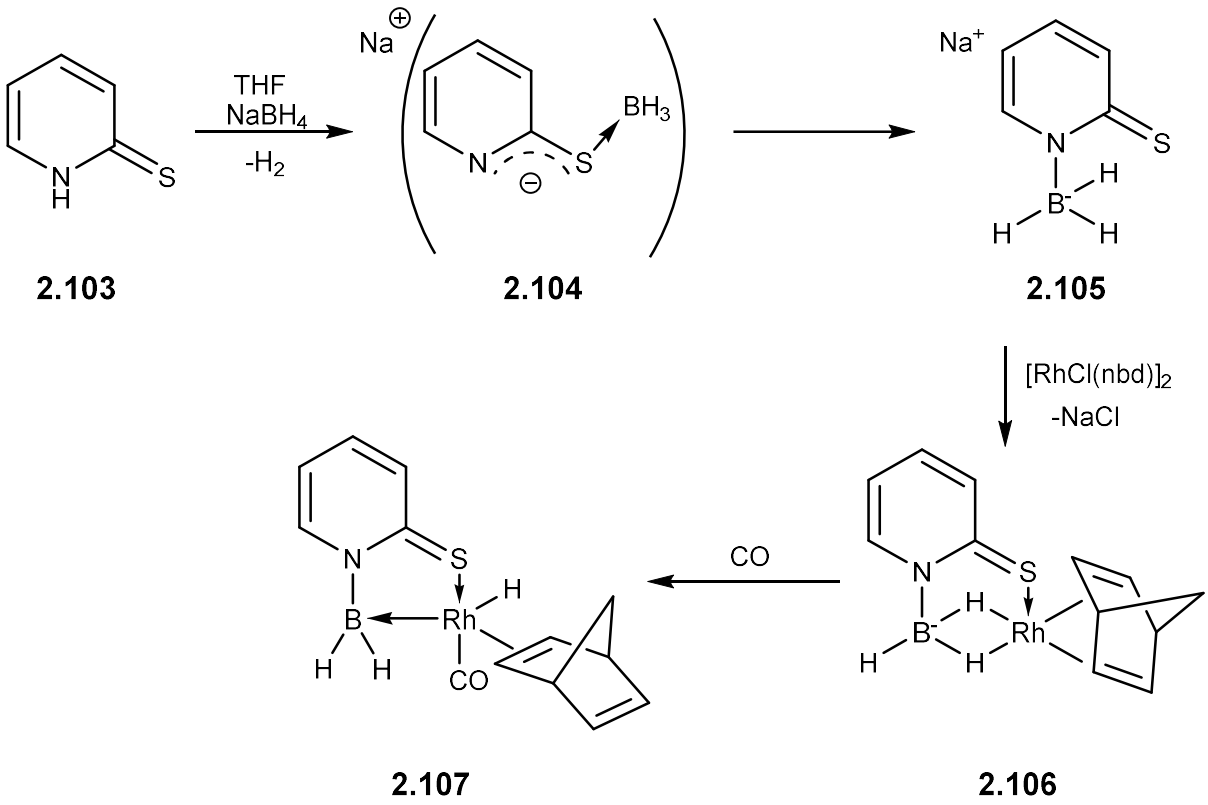

Scheme 2.35. Synthesis and subsequent reactivity of the ligand Mmp with a rhodium nbd complex

2.4.3 An example of an anionic five-atom supported borohydride ligand

Aldridge synthesised the metal complex **2.108** which is formed by the oxidative addition of a CH bond from a methyl group on the mesitylene moiety of [IrCl(IMes)$_2$(coe)] (Scheme 2.36). The coe ligand is lost through ligand dissociation.[81] On addition of $LiBH_4$ to the iridium complex **2.108,** the synthesis of the supported borohydride complex **2.110** is achieved through suggested intermediate **2.109**. Intermediate **2.109** has the tetrahydroborate unit coordinated through a dihydroborate interaction. Further transformation of this intermediate leads to an intramolecular migration and the formation of **2.110** in which the 4-coordinate borohydride unit is supported by the methylene group on the mesitylene ring. The iridium complex **2.110** exhibits a resonance at −38.7 ppm in the ^{11}B NMR spectrum which is close to where an uncoordinated $[BH_4]^-$ anion would be expected. Two separate B-H stretching bands at 2412 and 2175 cm^{-1} were observed indicating the presence of both terminal and bridging B-H's. This is consistent with the ^1H NMR spectrum which shows three separate resonances at −7.14, −6.74 and −0.42 ppm. The SC-XRD structure is also in agreement where the Ir-B distance was found to be 2.253(7) Å and the s B-H distances were recorded as 1.421, 1.349 and 1.17 Å. This gives an indication of an asymmetric interaction is due to the separate NMR environments for each BH_3 proton. Over time on addition of excess $LiBH_4$ to **2.110** results in the slow formation of the lithium salt **2.111** over a period of 7 days.

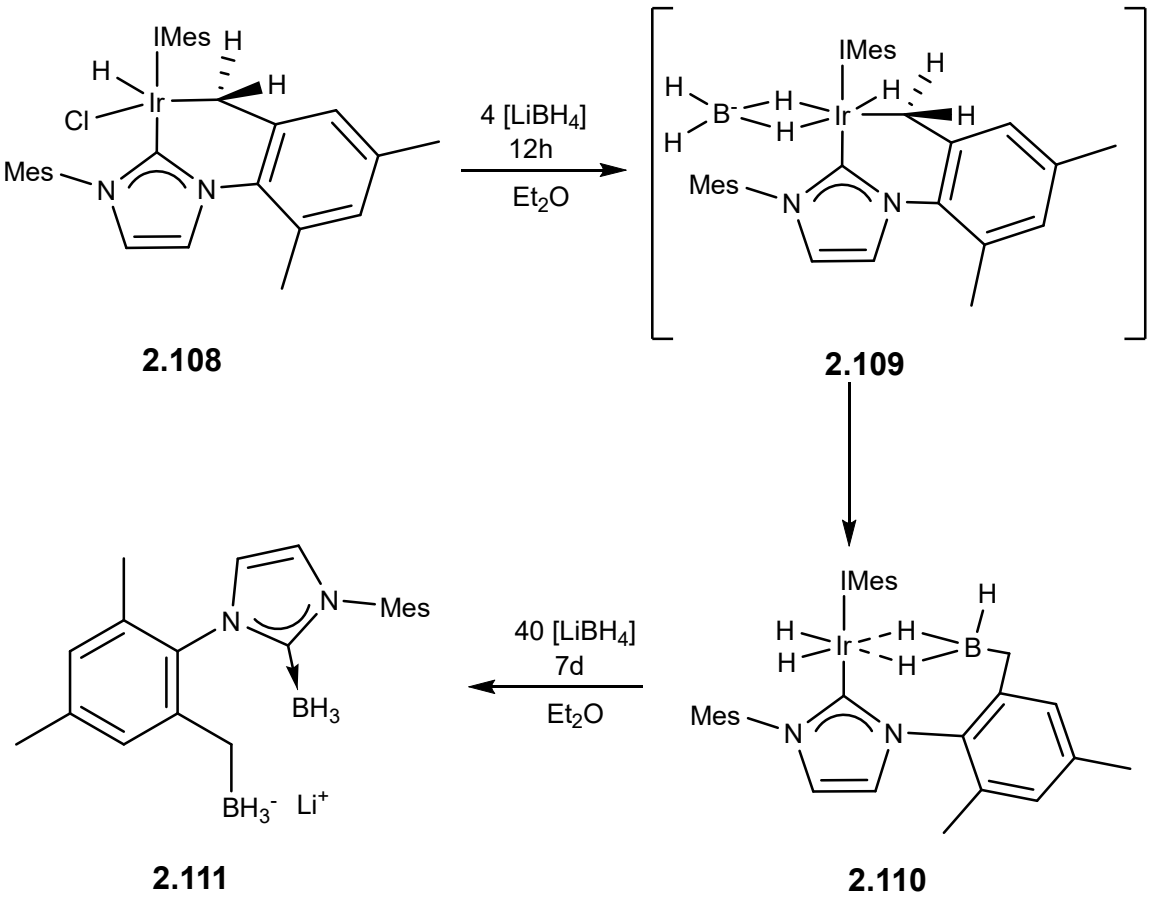

Scheme 2.36. Reactivity of [IrCl(IMes)$_2$(coe)] with LiBH$_4$ resulting in a supported borohydride intermediate

2.5 Review conclusions

This literature review has explored a diverse set of examples surrounding the chemistry of supported anionic borohydride and neutral borane ligands. The difference between the two examples lies in the method of attachment of the BH_n unit to the ligand support. Neutral boranes are supported by a dative bond and anionic borohydrides are supported by a covalent bond. Both examples are capable of coordinating to a metal centre via 3c-2e bonds. The 3c-2e bonds originates from the coordination of a B-H bond from the BH_3 functional group. Both examples have supporting scaffolds of varying length, although some of which, have yet to be realised. One key difference in reactivity of these complexes is the propensity for the abstraction of the neutral BH_3 fragment. Abstraction of the BH_3 unit is achieved using two L-type donor ligands, one to coordinate to the BH_3 and the second to replace the BH-M interaction. In comparison, the anionic BH_3^- unit shows no examples of abstraction, this because breaking of a B-X covalent bond leads to the formation of unstable charged fragments.

Overall, the coordination of the BH_3 unit in solution is flexible and is capable of freely rotating as observed by solution state NMR studies. This interaction may also be static, which, again is observed through the NMR spectroscopic data. The nature of the interaction is dependent on a number of factors. These include what ligand support has been used, the nature of the metal and its coordination sphere and finally the temperature of the solution. Both neutral and anionic ligands have examples of both static and freely rotating BH_3 groups. One other difference in the mode of coordination is the number of BH-M interactions. This literature review has seen examples of both κ^1-H, and κ^2-H,H interactions with respect to the BH_3 group. The mode of coordination is mostly dependent on the coordination sphere and valence electron count of the metal centre. Less saturated metal centres and lower valence electron counts are more likely to support κ^2-H,H interactions. The BH-M interaction can also be considered formally as a two-electron donor for electron counting purposes. The BH-M bond is both capable of substituting and being replaced by two electron (L-type) donors as seen in many examples throughout this review.

One very interesting example, by our group has shown the ability of the [BH_n] moiety to react at metal centres. Hydride migration has previously been seen in complexes bearing bis- and tris-substituted borohydride ligands and recently been expanded to mono-substituted ligands. Three atom supports have provided the greatest potential for hydride migration because these support five membered rings involving a M-B bond. This shows the potential of supported BH_3 ligands and therefore warrants further investigation.

To conclude, this chapter has explored the chemistry of singly supported neutral and anionic BH_3 ligands by providing a wide range of examples from the literature. The nature of the BH-M interaction for several complexes has been explored and can be considered as a two-electron donor. Further reactivity of these complexes, although these examples are scarce, provides justification for continued investigations into complexes of these types.

Chapter 3: Synthesis and structure of copper complexes containing a supported anionic borohydride ligand with a 3-atom bridge

3.1 Introduction

Borohydride ligands supported by one or more donor groups have been the focus of many research projects.[32,82–89] Supported borohydride ligands are generally known as scorpionates. This term is used to describe their mode of coordination.[90–92] The name scorpionate refers to two 'claw' like binding motifs and a third, sometimes weaker, binding site. Typically, scorpionates take the form of both bis- and tris-substituted borohydride ligands.[93–95] This family of ligands has been extended to their less substituted analogues monosubstituted borohydride ligands. Scorpionate and mono- substituted borohydride ligands are of interest as the borohydride unit can undergo a variety of transformations at the metal centre.[3–5,80,96,97]

Of particular interest is the process of reversible hydride migration and its potential applications in catalysis. The process of hydride migration between a ligand and a metal centre has been demonstrated on only a few metals such as rhodium, iridium, palladium, platinum and nickel.[75,97–100] Whilst work has been carried out in understanding the reactivity of these ligands on expensive platinum group metals, little work has been done on understanding the overall coordination of these ligands and the differences between mono, bis and tris.[101,102] This chapter aims to compare the coordination of mono-, bis- and tris- substituted borohydride ligands to copper using a variety of different scaffolds. As there are no previous examples of anionic mono- supported borohydride ligands coordinating to copper, this chapter will look to explore their synthesis and draw comparisons with literature examples of bis- and tris- ligands using the same supporting scaffolds. Using spectroscopic data collected from these complexes, this chapter will assess the trends associated with the coordination of mono-, bis- and tris- ligands. The data collected will be of particular interest in assessing the capability of each ligand to react or undergo transformations at a metal centre.

3.2 Complexes based on a 2-mercaptopyridine scaffold

The ligands Tmp and Bmp, which were first synthesised by our group in 2009 (Scheme 3.1) are supported by a 2-mercaptopyridine supporting unit.[93] The ligand salt **K[Tmp]** was prepared by heating a fourfold excess of 2-mercaptopyridine (**mpH**) in a xylene suspension with KBH_4 to 170 °C under nitrogen for 48 hours. After washing with THF and drying under vacuum, **K[Tmp]** was provided as a yellow powder with a yield of 74%. **Na[Bmp]** was prepared using a 50:50 mixture of toluene and THF, again with 2-mercaptopyridine, but this time with two equivalents with respect to $NaBH_4$. The mixture was heated to reflux overnight, and the resultant solid was washed with toluene to give the ligand **Na[Bmp]** with a yield of 85%.

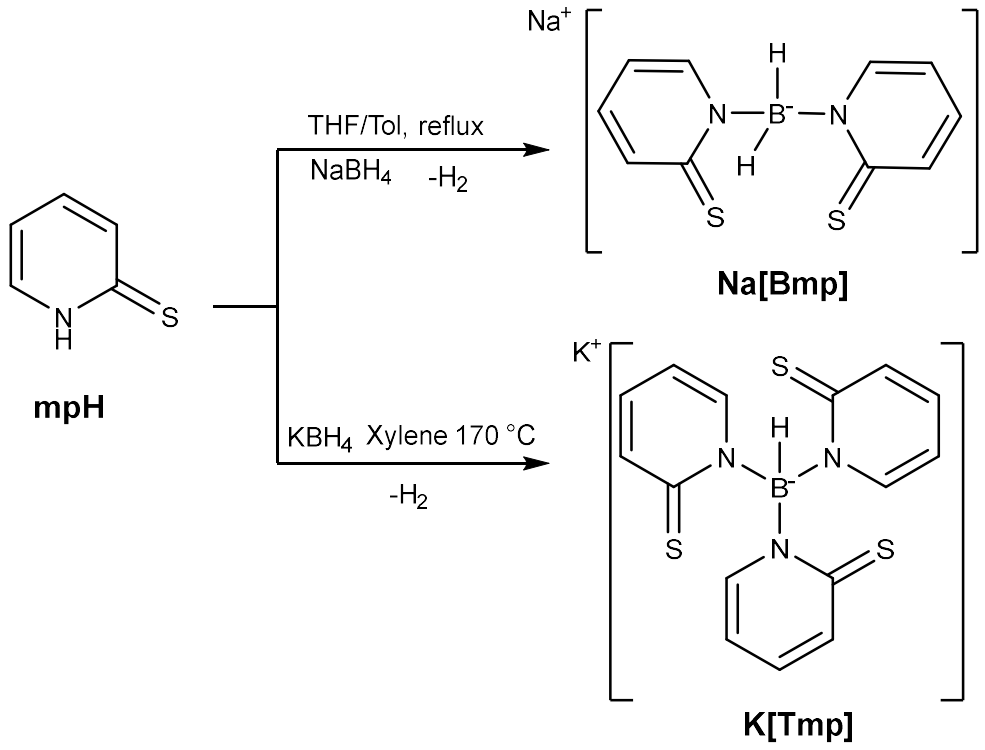

Scheme 3.1. Synthesis of *ligands* **[K(Tmp)]** and **[Na(Bmp)]**

To date only copper complexes of Tmp have been synthesised. In these cases, both PPh_3 and PCy_3 were utilised as co-ligands with one equivalent of CuCl in methanol. This led to the formation of yellow solid products over 2 hours. Subsequent washing with methanol, diethyl ether and extraction into DCM to give both products in good yields **[Cu(Tmp)(PPh_3)]** (80%) and **[Cu(Tmp)(PCy_3)]** (87%) (Scheme

3.2). The spectroscopic data for **[Cu(Tmp)(PPh$_3$)]** and **[Cu(Tmp)(PCy$_3$)]** was consistent with a κ^3-S,S,S coordination mode, this shows that there is no interaction between the copper and the BH hydrogen. This is because the boron centre adopts a tetrahedral arrangement in which the hydrogen points away from the metal centre.

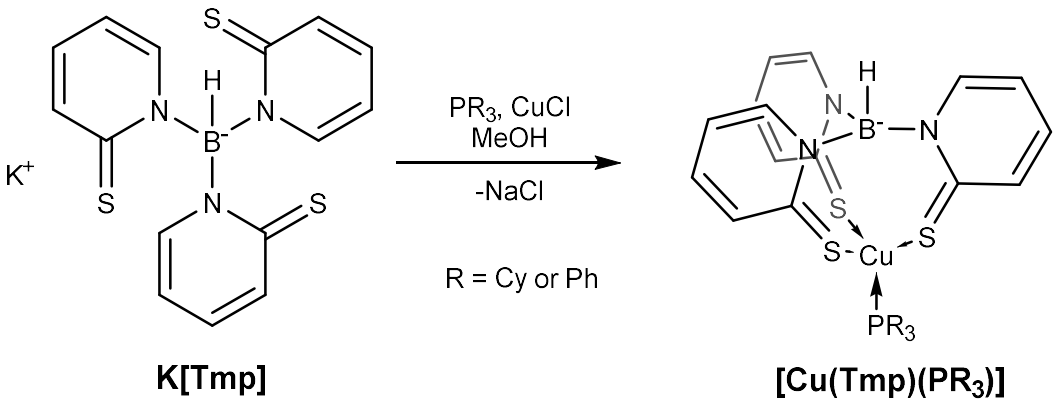

Scheme 3.2. Synthesis of complex **[Cu(Tmp)(PR$_3$)]**

Unlike Tmp, the ligand Bmp has previously been studied across a range of different metals, on addition of the ligand Bmp to $[RhCl(cod)]_2$ and $[IrCl(cod)]_2$ the intermediates [Rh(Bmp)(cod)] and [Ir(Bmp)(cod)] were proposed and were suggested to coordinate in a κ^3-S,S,H fashion. Subsequent reactivity of the ligand at the metal centre revealed that both [Rh(Bmp)(cod)] and [Ir(Bmp)(cod)] undergo hydride migration to form M-B Z-type interactions.[103] This reactivity was then replicated on platinum and palladium.[102,104] Bmp complexes of calcium, strontium, barium,[105] ruthenium,[106] rhenium and technetium[78] have also been prepared. With regards to copper, the corresponding Bmp complexes were prepared in a similar procedure to that of the Tmp copper complexes. Na[Bmp] was added with one equivalent of phosphine and copper (I) chloride to form their respective copper complexes in methanol (Scheme 3.3). The products were purified by washing with methanol and hexanes and is obtained as a yellow solid in good yields of 83% **[Cu(Bmp)(PPh$_3$)]** and 84% **[Cu(Bmp)(PCy$_3$)]**. The X-ray structure for **[Cu(Bmp)(PCy$_3$)]** was solved and showed that in the solid state the Bmp ligand coordinated to the metal via two sulfur donors and one B-H-M interaction (κ^3 - S,S,H). The interaction was said to be weak as both BH protons were equivalent in the ^{1}H NMR spectra.

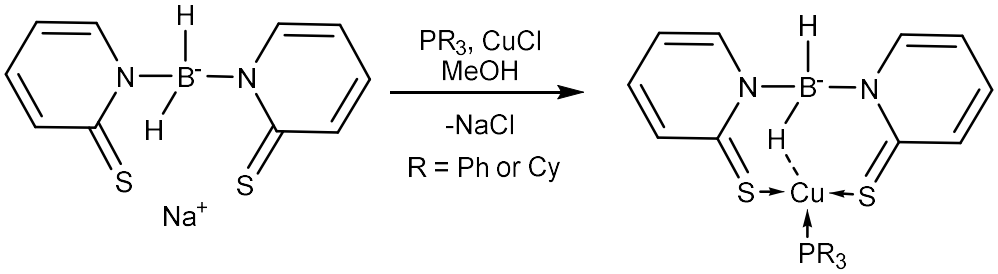

Scheme 3.3. Synthesis of [Cu(Bmp)(PR_3)] complexes

3.2.1 Synthesis of copper Mmp complexes

To date only one complex of the ligand mono mercaptopyridine (Mmp) has been reported.[14] The ligand was synthesised following the procedure previously outlined by the Owen group using an excess of $NaBH_4$ with respect to the mercaptopyridine. This results in the formation of the ligand **Na[Mmp]** which is formed via the intermediate **3.1** (Scheme 3.4). The ligand salt **Na[Mmp]** was purified via sequential removal of solvent in *vacuo* to form a concentrated solution*,* subsequent addition of hexane ensured that all $NaBH_4$ precipitated out of solution. The reported synthesis of the ligand was followed according to the literature synthesis and the spectroscopic data was in agreement with that of published data for the synthesised compound.

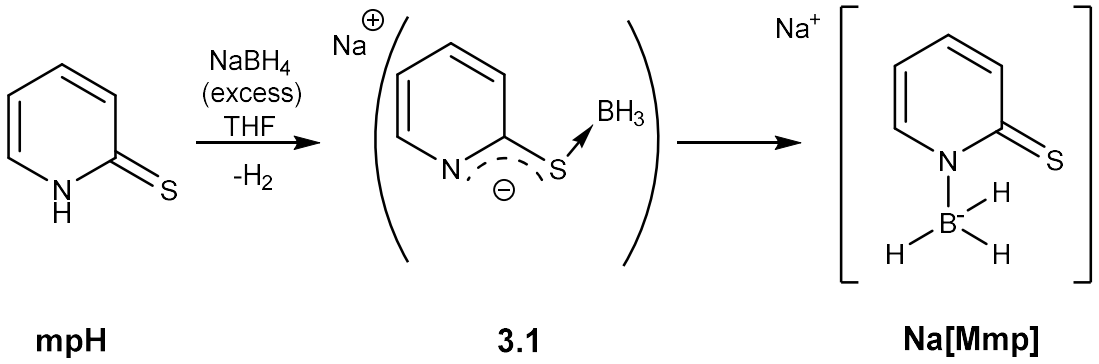

Scheme 3.4. Synthesis of ligand [Na(Mmp)] through intermediate **3.1**

Given the successful synthesis of the copper complexes bearing the ligands Bmp and Tmp.[93] It was decided to further extend the family of copper complexes pertaining to the mercaptopyridine support and explore the coordination of the mono mercaptopyridine ligand to copper. This chapter herein describes the synthesis of previously unreported copper complexes containing the Mmp ligand.

The synthesis of three new copper complexes **[Cu(Mmp)(PPh_3)]**, **[Cu(Mmp)(PCy_3)]** and **[Cu(Mmp)(dppe)]** was achieved by the reaction of stoichiometric quantities of CuCl, **[Na(Mmp)]** and either triphenyl phosphine (PPh_3), tricyclohexyl phosphine (PCy_3) or 1,2-bis(diphenylphosphino)ethane (dppe) (Scheme 3.5). All reagents were added into methanol and stirred over a 24-hour period, after which time the product had precipitated out of solution as a pale-

yellow powder. The air stable products were obtained in good yields (68, 65 and 73% respectively). The infrared spectra of the complexes were recorded using an attenuated total reflectance (ATR) spectrometer in the solid state. The spectra for these complexes each present two separate stretching bands suggesting that both bridging and terminal BH's were present. These bands appear at 2078, 2081 and 2085 cm^{-1} for bridging B-H's and 2378, 2439 and 2448 cm^{-1} for terminal B-H's (Table 3.1). The stretching frequencies for the terminal B-H bonds are close to the value reported for the free ligand salt at 2307 cm^{-1}.[107] The bridging BH's have lower energy wavelengths in comparison to the terminal B-H bonds which indicates a weakening of the B-H bond and the formation and coordination of a 3c-2e bond to the copper centre.

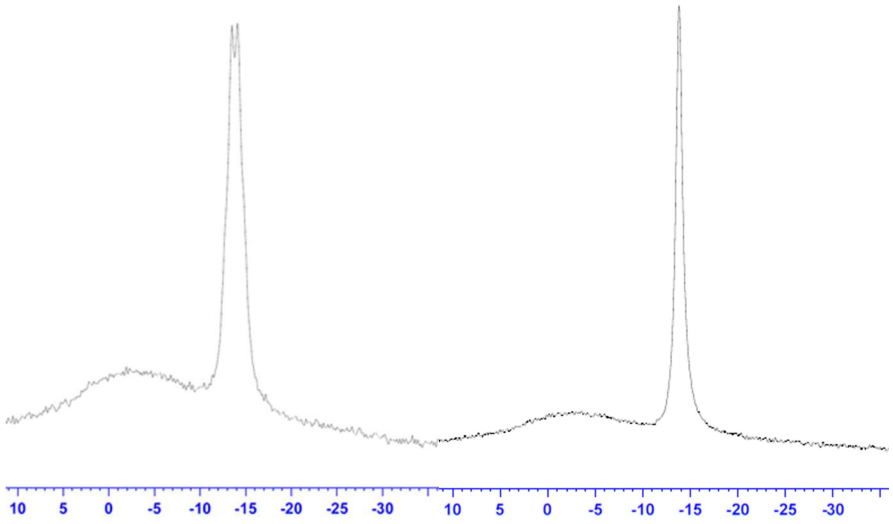

Figure 3.1. ^{11}B *(left) and* $^{11}B\{^{1}H\}$ *(right) NMR of* ***[Cu(Mmp)(PPh$_3$)]***

^{11}B NMR studies in $CDCl_3$ show little deviance from the chemical shift of the ligand (−14.1 ppm), with chemical shifts between −14.5 to −13.4 ppm. These slight differences in the chemical shift of the quartet do not provide sufficient evidence for the confirmation of the formation of a new complex. There are, however, clear observable differences in the $^{1}J_{BH}$ coupling constants of the BH_3^- quartet. The $^{1}J_{BH}$ value for the ligand salt Na[Mmp] is reported as 93 Hz. In the complexes **[Cu(Mmp)dppe]**, **[Cu(Mmp)PPh$_3$]** and **[Cu(Mmp)PCy$_3$]**, the measured $^{1}J_{BH}$ coupling constants decreases to 45 Hz, 75 Hz and 82 Hz, respectively. In comparison to the rhodium complex [Rh(Mmp)(nbd)], the ^{11}B NMR

chemical shifts are more up field when compared to a resonance at −7.8 ppm which in comparison is a strong M-H-B interaction in relation to the copper complexes.[14] The $^{11}B\{^{1}H\}$ NMR resonances in all cases resolve from a quartet to a singlet (Figure 3.1) confirming the presence of 3 hydrogen substituents around each of the boron nuclei. The half-height width (h.h.w.) of the NMR peaks also decreases. The h.h.w also differs between the free ligand and the metal complexes with the ligand reported and confirmed at 44 Hz and copper complexes synthesised had h.h.w.'s of 158 Hz, 113 Hz and 90 Hz for **[Cu(Mmp)dppe]**, **[Cu(Mmp)PPh$_3$]** and **[Cu(Mmp)PCy$_3$]**, respectively. The ^{11}B NMR data suggests that the Mmp ligand is weakly coordinated to the metal, this is because there is little to no observable change in the chemical shift of the BH_3^- environment. This shows that the boron is not losing significant electron density, in comparison to a stronger interaction which would show a more downfield resonance.

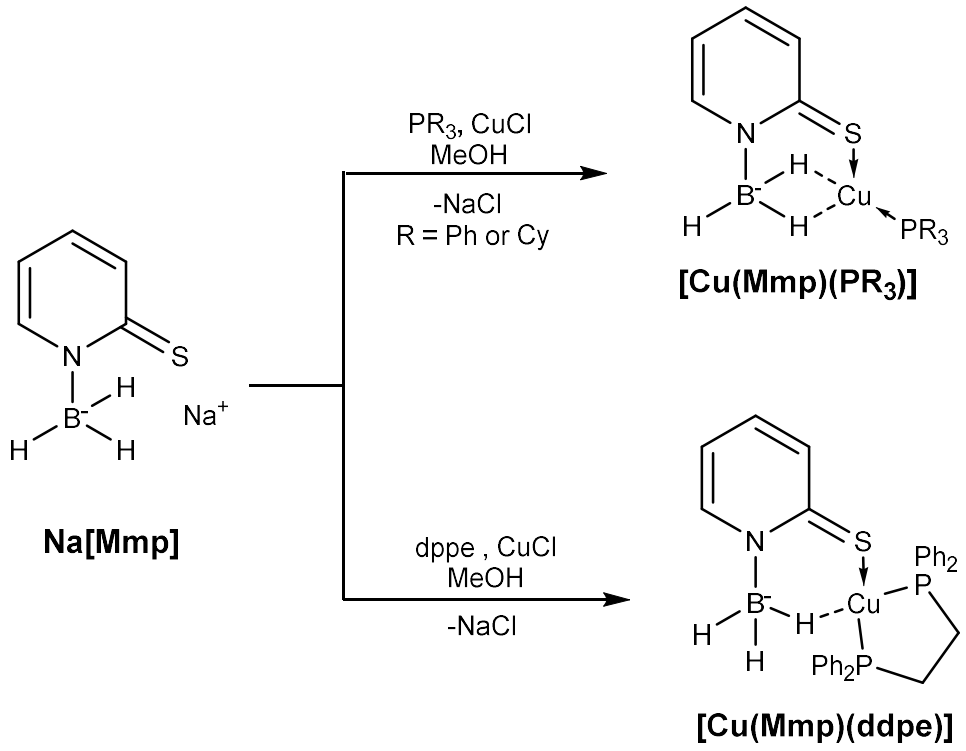

Scheme 3.5. Synthesis of Cu(Mmp) complexes containing different phosphines

^{1}H NMR spectroscopic data for the complexes show BH_3 resonances as broad quartets for each copper complex between 2.42 and 2.69 ppm (Table 3.1). These ^{1}H NMR resonances each integrate to 3 hydrogens, the equivalence of all three hydrogens indicate that there is rapid exchange between terminal and bridging hydrogens, which, on cooling to −60 °C does not resolve into separate peaks. This indicates that at low temperatures on the NMR timescale the exchange between terminal and bridging protons is still fast, and the BH hydrogens are not static in solution. This again suggests a much weaker interaction in comparison to the [Rh(Mmp)(nbd)] complex which has two distinct BH environments representing a static dihydroborate interaction. The corresponding resonances for [Rh(Mmp)(nbd)] observed at, −2.72 and 2.89 ppm, resolve into a single broad BH_3 peak at −1.75 ppm on heating to 55 °C. Upon coordination to the copper centre, it was revealed that the aromatic protons of the Mmp ligand had shifted downfield in comparison to the ligand salt **[Na(Mmp)]**. In **[Cu(Mmp)PPh$_3$]** and **[Cu(Mmp)dppe]** complexes there were overlapping protons attributed to both the phenyl rings of the phosphine ligand and a single mercaptopyridine proton. The presence of each environment was unambiguously confirmed via correct integration along with COSY and HSQC experiments. ^{1}H{^{11}B} NMR studies demonstrate that the broad BH_3 quartet in the ^{1}H spectra is due to boron coupling since it collapses into a singlet. Coordination of the phosphine ligand in each case was confirmed by ^{31}P{^{1}H} NMR spectroscopy in which a downfield shift was observed in comparison to the respective free ligands, giving singlets at 4.8, 27.2 and −5.4 ppm for the complexes **[Cu(Mmp)(PPh$_3$)]**, **[Cu(Mmp)(PCy$_3$)]** and **[Cu(Mmp)(dppe)],** respectively. In comparison, the corresponding Bmp complexes, **[Cu(Bmp)(PPh$_3$)]** and **[Cu(Bmp)(PCy$_3$)]**, recorded ^{31}P{^{1}H} resonances of 1.7 and 19.0 ppm respectively. Both were upfield in comparison to the Mmp complexes indicating that the coordination of the phosphine ligands to the Bmp copper complexes is weaker. Comparing the more substituted tris- and bis scorpionate ligands to the mono-supported borohydride ligands shows that each ligand remains tridentate in the copper mono-phosphine complexes. For example, the borohydride ligands in each of the complexes **[Cu(Mmp)(PPh$_3$)]**, **[Cu(Bmp)(PPh$_3$)]** and **[Cu(Tmp)(PPh$_3$)**] all exhibit κ^3 coordination. The difference between the coordination of each ligand is that moving from Tmp then

subsequently to Bmp and Mmp removes a mercaptopyridine donor arm in each step which results in a κ-S coordination site being exchanged for 'κ-H' coordination through a 3c-2e bond. Given that the phosphine resonance gives an indication of the overall strength of the chelate, comparisons can therefore be made between mono-, bis- and tris-supported borohydride ligands based on this metric. For example, in the complex **[Cu(Tmp)(PPh$_3$)]** where the Tmp ligand coordinates in a κ^3-S, S, S fashion the phosphine resonance is observed at −2.4 ppm, in comparison to this the complex **[Cu(Bmp)(PPh$_3$)]** displays a more downfield shift at 1.7 ppm, the ligand in this case coordinates κ^3-S, S, H to the metal. Finally, the newly synthesised complex **[Cu(Mmp)(PPh$_3$)]** continues the trend of more downfield resonances observed at 4.8 ppm. The coordination of this ligand is again κ^3 with κ^3-S, H, H coordination. This trend shows that the 3c-2e bond, although in its own right a two-electron donor, is weaker in comparison to κ-S coordination and therefore the ancillary phosphine NMR resonance reflects greater electron donation in order to compensate for this difference. This difference may be accounted for by sulfur's lone pair of elections which may provide additional electron donation to the metal centre.

Table 3.1. Selected spectroscopic data for copper complexes based on a 2-mercaptopyridine scaffold. *NMR chemical shifts record as ppm and (h.h.w.) in Hz. Powder film IR data in cm^{-1}, (t)-terminal and (b)-bridging BH's. n.o – Peak not observed.*

Compound	^{11}B{^{1}H} NMR	^{31}P{^{1}H} NMR	^{13}C{^{1}H} NMR *C*=S	^{1}H{^{11}B} NMR B*H*$_n$	IR B–H
Na[Mmp]	−14.1 (44)	-	181.3	2.11	2307
[Cu(Mmp)(PPh$_3$)]	−13.9 (113)	4.8	175.9	2.64	2439 (t) / 2078 (b)
[Cu(Mmp)(PCy$_3$)]	−13.4 (90)	27.2	176.1	2.42	2448 (t) / 2085 (b)
[Cu(Mmp)(dppe)]	−14.54	−5.4	176.2	2.69	2378 (t) / 2081 (b)
Na[(Bmp)]	−3.7 (211)	-	182.6	3.64	2438, 2370
[Cu(Bmp)(PPh$_3$)]	0.7 (265)	1.7	n.o.	4.12	2425
[Cu(Bmp)(PCy$_3$)]	−0.7 (248)	19.0	178.2	3.99	2374
K[(Tmp)]	4.4 (560)	-	182.5	4.83	2468
[Cu(Tmp)(PPh$_3$)]	−0.1 (412)	−2.4	178.3	n.o.	2458
[Cu(Tmp)(PCy$_3$)]	−0.5 (331)	17.4	181.0	5.86	n.o.

X-ray quality single crystals for **[Cu(Mmp)PPh$_3$]** and **[Cu(Mmp)PCy$_3$]** were grown from the slow evaporation of a concentrated methanol and diethyl ether solution. The solved structures (Figure 3.2) showed disorder with respect to the position of ligand Mmp where the ligand is rotated 180˚ in the

minor component when compared to the major component, in the ratios of 56:44 and 79:21, respectively. Each complex confirms the presence of a single phosphine and a single Mmp ligand coordinated to a copper atom. The BH_3 hydrogens were located within the degree of certainty associated with X-ray crystallography and shows that the BH_3 unit coordinating to the metal via two 3c-2e bonds (in a BH_2Cu motif). The remaining hydrogen (H(1AC)) is pointing away from the copper centre and does not interact with it. This is consistent with the solid-state IR data collected which shows two separate BH stretching bands as described above. Taking into account the boron atom as the centre of the dihydroborate interaction, the coordinated sulfur and phosphorus, the structure of these compounds is a distorted trigonal planar arrangement. The sum of the angles around the copper centre is 359.72° and 359.97° for **[Cu(Mmp)PPh$_3$]** and **[Cu(Mmp)PCy$_3$]**, respectively. This distorted arrangement is formed due to the tight chelate of the Mmp ligand. Considering the boron and the sulfur as points of attachment, the S-Cu-B bond angles for the chelate are 89.2(2)° for **[Cu(Mmp)PPh$_3$]** and 89.7(4)° for **[Cu(Mmp)PCy$_3$]**. The solution state NMR spectroscopic data suggests that the interaction is weak in solution, however, in the solid-state crystal structure the BH_3 unit is held in close proximity to the meal centre via the mercaptopyridine unit.

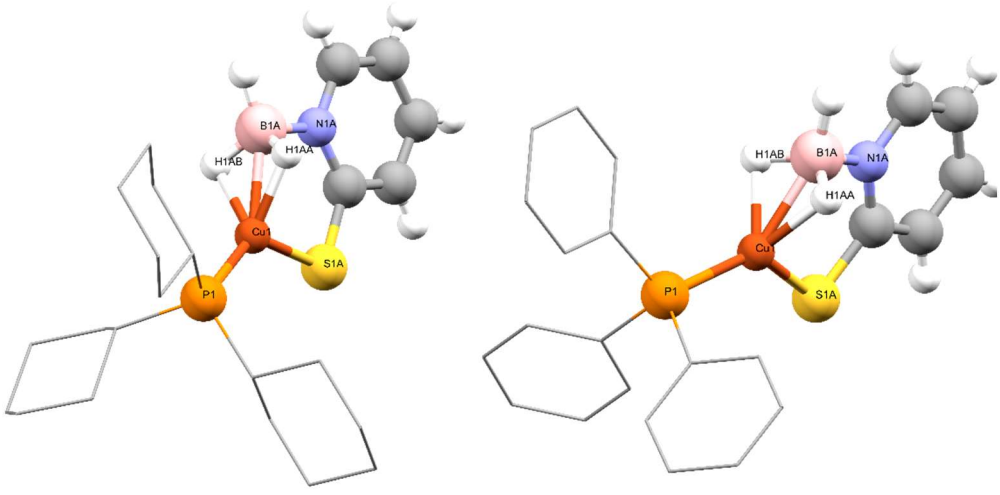

Figure 3.2. SC-XRD structures for complexes **[Cu(Mmp)(PCy$_3$)]** (left) and **[Cu(Mmp)(PPh$_3$)]** (right) showing a similar coordination mode for the Mmp ligand in both complexes. Hydrogens on Cy and Ph rings have been omitted for clarity.

The Cu-B distances within **[Cu(Mmp)(PPh$_3$)]** are 2.113(17) and 2.229(14) Å for the major and minor component, respectively and for **[Cu(Mmp)(PCy$_3$)]** they are 2.153(15) and 2.10(3) Å. These distances are shorter than that of the corresponding bis ligand complex **[Cu(Bmp)(PPh$_3$)]** which has a Cu-B distance of 2.7479(15) Å. This is consistent with the change in coordination mode of the BH_3 unit from κ^1-H to κ^2-H,H. The Cu-B distances for the **[Cu(Mmp)(PR$_3$)]** complexes lie closely to that of a previously unsupported κ^2-H,H $H_3B{\cdot}NMe_3$ ligand on coordination to a β-diketiminate copper(I) complex which was reported to be 2.152(2) Å.[108,109] Another contributing factor to the shorter distance is the greater flexibilty that the mono ligand provides since there is no second supporting ligand fixing the distance at which the boron atom remains from the metal. The B-H bond distances are consistent with that reported for the bis complexes (Table 3.2), both terminal and bridging hydrogens for the **[Cu(Mmp)(PPh$_3$)]** and **[Cu(Mmp)(PCy$_3$)]** complexes fall within the region of 1.14 to 1.18 Å and the terminal and bridging BH's all fall within the estimated standard deviations for the bond distances. Therefore, there is no noticable difference between the terminal and bridging hydrogens in these cases. Typically, as observed in the review chapter, B-H bond lengths elongate upon interaction with a metal centre, so having no observable difference is surprising and could suggest that in comparison this interaction is weaker. In the complex **[Cu(Bmp)(PPh$_3$)]**, the bond distance for terminal B-H was 1.090(18) Å and the bridging was 1.150(17) Å. This difference is only slight but highlights the elongation of the bridging B-H bond on coordination to copper. Therefore, when moving to a dihydroborate interaction in copper complexes, the elongation of both B-H bonds may not be observable as seen in the **[Cu(Mmp)(PPh$_3$)]** and **[Cu(Mmp)(PCy$_3$)]** complexes.

Table 3.2. Selected bond lengths (Å) and angles (°) for [Cu(Mmp)(PR_3)] complexes compared with [Cu(Bmp)PPh_3]

	[Cu(Mmp)(PPh_3)]	**[Cu(Mmp)(PCy_3)]**	**[Cu(Bmp)(PPh^3)]**
Cu(1)-P(1)	2.1789(4)	2.1876(4)	2.216(3)
Cu(1)-B(1)	2.113(17) / 2.229(14)[i]	2.153(16) / 2.10(3)	2.7479(15)
Cu(1)-S(1)	2.205(2) / 2.221(4)	2.2523(12) / 2.296(12)	2.255(4) / 2.248(4)
C(1)-S(1)	1.7515(17) / 1.722(2)	1.7244(17) / 1.751(13)	1.707(14) / 1.708(14)
B(1)-N(1)	1.551(8) / 1.465(10)	1.602(16) / 1.61(2)	1.592(2) / 1.583(18)
N(1)-C(1)	1.3506(19) / 1.3506(19)	1.3550(19) / 1.3550(19)	1.3649(17) / 1.3648(19)
B(1)-H(1AA)	1.17(2) / 1.18(2)	1.16(2) / 1.16(2)	-
B(1)-H(1AB)	1.16(2) / 1.18(2)	1.17(2) / 1.15(2)	1.090(18) (terminal)
B(1)-H(1AC)	1.17(2) / 1.17(2)	1.14(2) / 1.15(2)	1.150(17) (bridging)
Cu(1)-H(1AA)	1.75(3) / 1.81(4)	1.75(2) / 1.68(8)	1.832(17)
Cu(1)-H(1AB)	1.81(3) / 1.85(4)	1.81(2) / 1.82(8)	-
S(1)-Cu(1)-P(1)	129.93(3) / 134.69(5)	129.93(3) / 135.9(3)	111.88(15) / 124.56(14)
S(1)-Cu(1)-B(1)	89.2(2) / 87.3(2)	89.7(4) / 90.2(5)	82.29(3) / 80.27(3)
P(1)-Cu(1)-B(1)	140.5(2) / 137.5(3)	140.3(4) / 133.9(6)	135.64(3)
Σ angles around Cu	359.63 / 359.49	359.93 / 360.0	350.4
C(1)-S(1)-Cu(1)	99.53(9) / 99.14(16)	99.53(8) / 96.2(5)	106.49(5) / 109.83(5)
N(1)-B(1)-Cu(1)	110.0(8) / 108.7(7)	107.0(8) / 110.3(13)	95.36 / 99.09

i - complexes where two values are given include the major component followed by a / and the minor component

The ligand Mmp has two different possible resonance forms, the first a thiopyridone spieces supporting a borohydride **3.2** and the second a pyridine-2-thiolate borane adduct **3.3** (Scheme 3.6). The degree as to which resonance form is more prominent has been determined via the C-S and N-B bond distances. The shorter the C-S bond distance, the more thiopyridone in character and the longer the distance, the more thiolate in character. The **[Cu(Mmp)(PPh_3)]** C-S distances are 1.7515(17) Å (major) and 1.722(2) Å (minor) this suggests that the major component is more thiolate in character than the minor component and indicates that there are two isomers within the structure. This explains the reason behind the large variation in Cu-B distances between the major and minor components. When compared to copper complexes beraring the ligand **mpH** the major component lies above the typical range for C=S bond distances (1.67 – 1.72 Å) reported for these complexes.[110–116] It does however fall within the range of the C-S distances of copper thiophenolate complexes which typically fall within the reigion of 1.74 – 1.77 Å.[117–119] The **[Cu(Mmp)(PCy_3)]** crystal structure shows a C-S distance for the major component of 1.7244(17) Å whilst in the minor component of a distance of 1.751(13) Å was measured. This shows that the major component in this stucture is more thiolate in

character than the minor component. Both Cu(Mmp) complexes, however, give shorter C-S distances and are therefore more thiolate in character in comparison to the complex **[Cu(Bmp)(PPh$_3$)]** whose C-S distances are 1.707(14) and 1.708(14) Å.

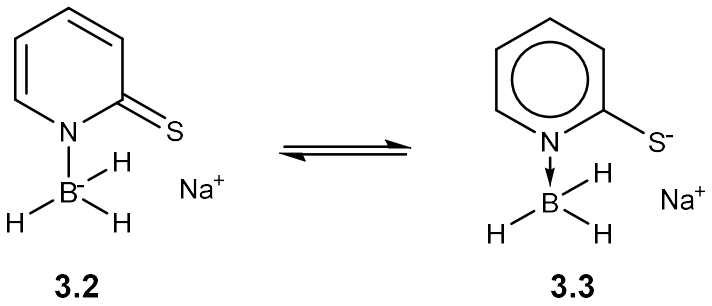

3.2 **3.3**

Scheme 3.6. Tautomerism in the ligand [Na(Mmp)]

The full characterisation of the compounds **[Cu(Mmp)(PPh$_3$)]** and **[Cu(Mmp)(PCy$_3$)]** represent the first examples of the coordination of a mono-supported borohydride ligand to copper. In doing so this has shown the versatility of the coordination of the $[BH_n]^-$ unit between both bis and mono substituted examples.

3.2.2 Synthesis of ^{R}Mmp ligands

Whilst the coordination of Mmp to copper has provided an interesting insight into the bonding to copper, previous work by our group has shown that exchanging the terminal BH for a new functional group can have an effect on the reactivity and bonding between the ligand and the metal. It is therefore necessary to further probe this family of ligands by introducing functional groups to the BH_n unit. Using copper as a base metal or benign example can potentially improve our understanding into the coordination and subsequent reactivity of these compounds.

The synthesis of functionalised borohydrides is achieved by the reduction of the corresponding borohydride using $LiAlH_4$ in THF.[120] This reaction was carried out using methyl and phenyl boronic acid following the procedure previously set out by Brown. It was noted however, that cooling to 0 °C for the reaction of $LiAlH_4$ with methyl boronic acid was insufficient on a large scale as large quantities of gas were released, therefore the reaction temperature was lowered to −78 °C, the solution was then slowly warmed to 0 °C over a period of a few hours. The work up for the reaction involving phenyl boronic acid was straightforward involving a filtration to remove the excess $LiAlH_4$ and subsequent evaporation of solvent in *vacuo* yielded a white solid. The removal of solvent for the methyl derivative took several weeks to complete and involved additional steps such as using a dynamic vacuum and cooling overnight in a freezer to aid in precipitation.

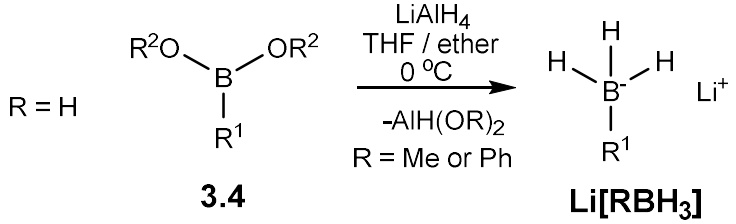

Scheme 3.7. A generic scheme for the synthesis of functionalised borohydrides from boronic esters and acids.

Following the procedure for the synthesis of **[Na(Mmp)]** in which $NaBH_4$ is utilised, in a procedure developed by our group, $NaBH_4$ can be substituted for both **[$LiBH_3Me$]** and **[$LiBH_3Ph$]** involving a two-

fold excess with respect to the lithium borohydride (Scheme 3.8).[121] The reaction between **mpH** and **[LiPhBH$_3$]** was left to stir for 72 hours at room temperature. Monitoring the reaction by ^{11}B NMR spectroscopy reveals an intermediate present as a broad triplet at −15.5 ppm which has previously been attributed to be the mercaptopyridine adduct of [PhBH$_2$]. The presence of the product in the ^{11}B NMR **Li[^{Ph}Mmp]** was confirmed by a triplet at −7.4 ppm. After 72 hours, it was confirmed that the reaction had indeed reached completion by the complete disappearance of the intermediate peak in the ^{11}B NMR spectra and the subsequent disappearance of the peak associated with the acidic proton in the ^{1}H NMR spectra corresponding to **mpH**. The ^{1}H and ^{11}B NMR spectra of the product was in agreement with that reported by our group thus confirming that the ligand had indeed been synthesised. Again, the reaction between **mpH** and **[LiMeBH$_3$]$^-$** was initially carried out at room temperature, the reaction however was more vigorous, and no intermediate was observed in solution Despite this, the reaction was also left for 72 hours to ensure completion. Confirmation of the presence of the product in solution came from solution-state ^{1}H and ^{11}B NMR studies which were in agreement with previously reported values for the ligand salt **[Li(^{Me}Mmp)]**.

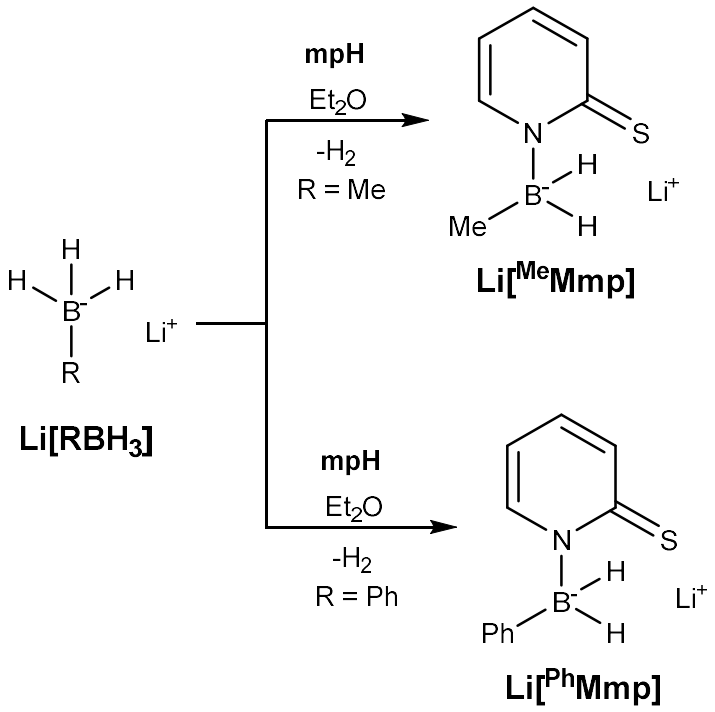

Scheme 3.8. Synthesis of [Li(^{R}Mmp] ligands

The synthesis of these ligand salts allows for the opportunity to further explore the synthesis and properties of complexes bearing the ligands ^{Ph}Mmp and ^{Me}Mmp. This would help gain insight into the effect that such groups have on the coordination of the $[BH_n]^-$ unit to the metal centre. Using this data may present greater opportunities for the fine tuning of ligand properties and to design such systems whereby hydride migration may be more accessible in cheaper and more readily available transition metal complexes.

3.2.3 Synthesis of copper ^{Ph}Mmp complexes

The synthesis of the complexes **[Cu(^{Ph}Mmp)(PPh$_3$)]** and **[Cu(^{Ph}Mmp)(PCy$_3$)]** was achieved by adapting the synthesis of **[Cu(Mmp)(PR$_3$)]** and replacing the ligand salt **Na[Mmp]** with the ligand salt **Li[^{Ph}Mmp].** The reaction was again, carried out under nitrogen using methanol as a solvent in which, after 24 hours of stirring the product precipitated out of solution as a pale-yellow powder. Subsequent drying of the complexes was performed under vacuum which achieved good yields of 76 and 83% for **[Cu(^{Ph}Mmp)(PPh$_3$)]** and **[Cu(^{Ph}Mmp)(PCy$_3$)]** respectively.

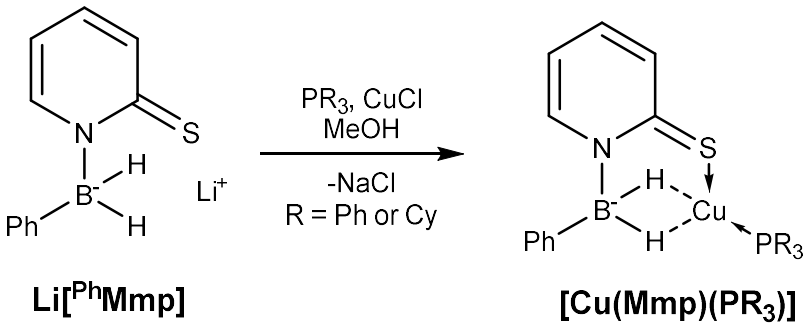

Scheme 3.9. Synthesis of **[Cu(^{Ph}Mmp)(PR$_3$)]** complexes

The IR spectroscopic data for these complexes show BH stretching bands in the region expected for bridging BH's. The infrared spectrum of **[Cu(^{Ph}Mmp)(PPh$_3$)]** shows two separate BH stretching frequencies at 2039 and 1987 cm^{-1}. These are both much lower than that expected of terminal BH's (2300 to 2500 cm^{-1}) therefore confirming the presence of a dihydroborate interaction. The presence of two separate bands indicates the presence of asymmetry within the structure. **[Cu(^{Ph}Mmp)(PCy$_3$)]** shows a single weak band at 2068 cm^{-1} again suggesting that only bridging BH's are present. This suggests that both BH bonds are involved in bonding with the copper centre as no terminal BH's are observed. This, of course is in contrast to those in the **[Cu(Mmp)(PR$_3$)]** complexes which exhibit stretching frequencies at 2439 and 2448 cm^{-1}. The ^{11}B NMR resonances are presented in the spectrum as broad singlets, these peaks should present as triplets due to the coupling of the BH_2 protons however the splitting pattern is not discernible. Nevertheless, there is a clear difference in the half-height widths between the ^{11}B and ^{11}B{^{1}H} spectra of each resonance. The half-height width of each

peak decreases from 317 Hz to 203 Hz in **[Cu(^{Ph}Mmp)(PPh$_3$)]** and from 1144 Hz to 526 Hz in **[Cu(^{Ph}Mmp)(PCy$_3$)]**. The ^{11}B{^{1}H} NMR resonance for the ^{Ph}Mmp ligand shifts downfield slightly upon coordination to the metal suggesting that there is an interaction between the boron and copper centres. This is only a small change of between 0.52 and 0.83 ppm but is more significant when compared to copper complexes bearing the unmodified Mmp ligand in which the range of the chemical shifts that are recorded encompass the chemical shift reported of the ligand salt. No change in coupling constant could be established due to the broad nature of the signals. However, the half-height widths of each peak increases from 55 Hz to 202 Hz and 526 Hz for the coordinated ligand.

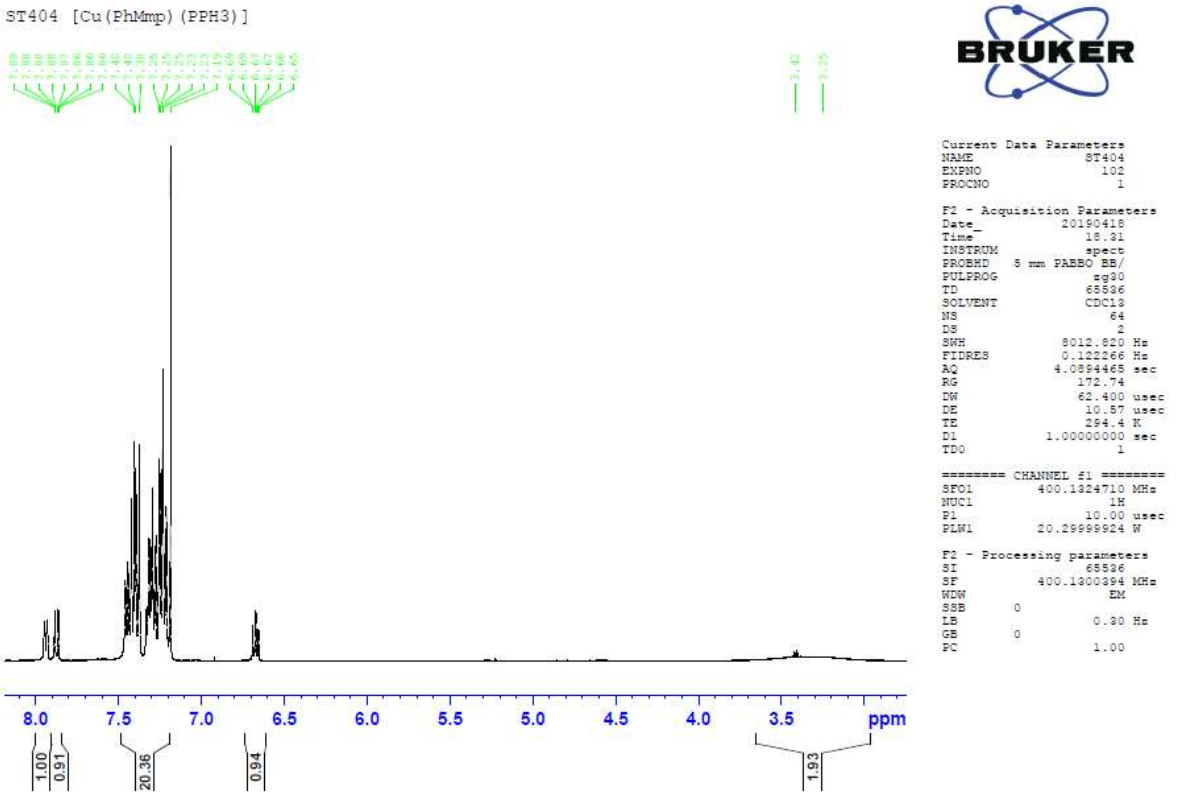

*Figure 3.3. ^{1}H NMR spectra for **[Cu(^{Ph}Mmp)(PPh$_3$)]***

The BH_2 protons are present as a very broad resonance in the ^{1}H spectra (Figure 3.3), but when ^{11}B decoupling is applied the very broad peak resolves into a sharp singlet which clearly integrates to 2 hydrogens confirming that both BH_2 protons are in the same environment in solution at 298 K. The corresponding BH_2 signals in the ^{1}H{^{11}B} NMR spectra resolve into singlets at 3.32 and 3.06 ppm for

the **[Cu(^{Ph}Mmp)(PPh$_3$)]** complexes, respectively. These chemical shift values are slightly downfield from the Mmp ligand where the BH_3 resonances are at 2.64 and 2.12 ppm. This indicates that the BH_2 protons are less hydridic in character.

Table 3.3. Selected spectroscopic data for the ligand [Li(^{Ph}Mmp)] and [Cu(^{Ph}Mmp)(PR$_3$)] complexes. *NMR chemical shifts record as ppm and (h.h.w.) in Hz. Powder film IR data in cm^{-1}, (t)-terminal and (b)-bridging BH's*

Compound	^{11}B{^{1}H} NMR (h.h.w)	^{31}P{^{1}H} NMR	^{13}C{^{1}H} NMR *C*=S	^{1}H{^{11}B} NMR B*H*$_n$	IR B–H
[Li(^{Ph}Mmp)]	−6.26 (55)	-	182.4	3.22	2263
[Cu(^{Ph}Mmp)PPh$_3$]	−5.74 (202)	10.1	175.6	3.32	2039 (b, w)
[Cu(^{Ph}Mmp)PCy$_3$]	−5.43 (526)	28.8	173.3	3.06	2068 (b, w)

The ^{31}P{^{1}H} NMR spectroscopic data confirms the coordination of both PPh_3 (10.1 ppm) and PCy_3 (28.8 ppm) to copper with downfield shifts from that of their respective free ligands. In comparison to the **[Cu(Mmp)(PR$_3$)]** complexes, both **[Cu(^{Ph}Mmp)(PPh$_3$)]** (4.8 ppm) and **[Cu(^{Ph}Mmp)(PCy$_3$)]** (27.2 ppm), have ^{31}P{^{1}H} resonances that are shifted more downfield. This suggests that the coordination of the phosphine to the **[Cu(^{Ph}Mmp)(PR$_3$)]** complexes is stronger. Stronger phosphine coordination could indicate a weaker overall coordination of the ^{Ph}Mmp ligand to the copper centre. The NMR spectra unambiguously confirms the presence of **[Cu(^{Ph}Mmp)(PPh$_3$)]** and **[Cu(^{Ph}Mmp)(PCy$_3$)]** in solution. MS data was obtained using an atmospheric solids analysis probe and both complexes were observed as $[M\text{-}H]^+$ ions, *m/z* = 524.08 (PPh_3) and 542.22 (PCy_3).

X-ray quality crystals were grown from the slow evaporation of a methanol solution for each of the compounds, resulting in single colourless blocks. The 3-D structure was solved using SC-XRD, both BH_2 protons were located by difference map and refined with a riding model. There was no disorder for **[Cu(^{Ph}Mmp)(PPh$_3$)]** but some minor disorder for **[Cu(^{Ph}Mmp)(PCy$_3$)]**. In **[Cu(^{Ph}Mmp)(PCy$_3$)]**, a single cyclohexyl ring bonded to atom P1 was located in two locations with a ratio of 91:09. Both copper centres are coordinated to a single ^{Ph}Mmp ligand and a single PR_3 ligand. The ^{Ph}Mmp ligand is coordinated to the ligand via the sulfur atom and two 3c-2e bonds originating from each of the B-H bonds.

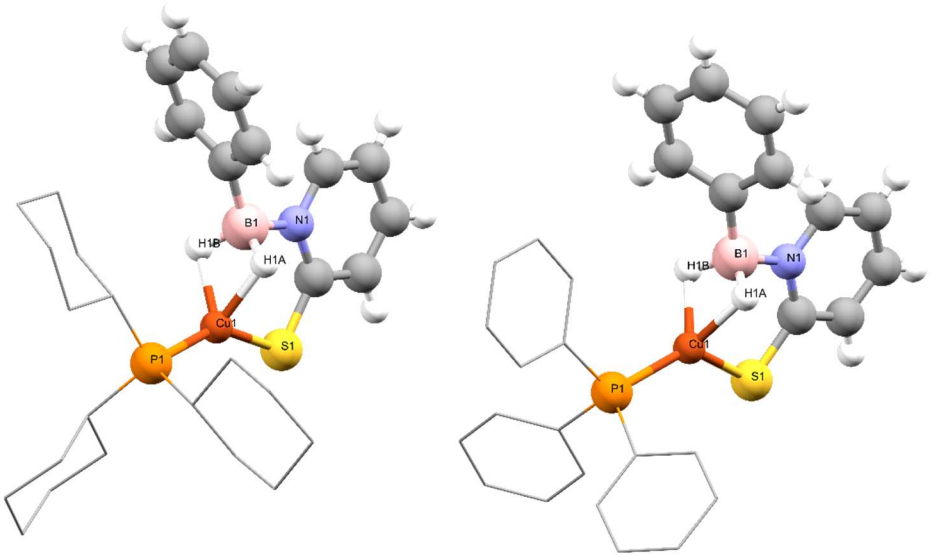

Figure 3.4. SC-XRD structures for **[Cu(^{Ph}Mmp)(PCy$_3$)]** (left) and **[Cu(^{Ph}Mmp)(PPh$_3$)]** (right). Hydrogens on Cy and Ph rings have been omitted for clarity.

The Cu-P bond distances in **[Cu(^{Ph}Mmp)(PPh$_3$)]** and **[Cu(^{Ph}Mmp)(PCy$_3$)]** were found to be 2.1748(8) Å and 2.1867(7) Å, respectively. This exhibits little variation being marginally shorter from that of the **[Cu(Mmp)(PR$_3$)]** complexes. Within the ligand itself the Ph ring situated on the borohydride moiety appears to be orientated to near perpendicular angles with respect to the mp ring, this was measured using the N(1)B(1)-C(6)C(7) torsion angles which have been measured as 67.7(2)° and 82.1(3)° for **[Cu(^{Ph}Mmp)(PPh$_3$)]** and **[Cu(^{Ph}Mmp)(PCy$_3$)]** complexes, respectively.

Table 3.4. Selected bond distances (Å) and bond angles (°) for **[Cu(^{Ph}Mmp)(PPh$_3$)]** and **[Cu(^{Ph}Mmp)(PCy$_3$)]**

	[Cu(^{Ph}Mmp)(PPh$_3$)]	**[Cu(^{Ph}Mmp)(PCy$_3$)]**
Cu(1)-P(1)	2.1748(8)	2.1867(7)
Cu(1)-B(1)	2.185(2)	2.230(3)
Cu(1)-S(1)	2.2197(9)	2.2074(7)
C(1)-S(1)	1.721(2)	1.722(2)
B(1)-N(1)	1.584(2)	1.578(3)
N(1)-C(1)	1.373(2)	1.376(3)
B(1)-H(1A)	1.17(2)	1.18(2)
B(1)-H(1B)	1.18(2)	1.18(2)
B(1)-C(6)	1.599(2)	1.604(4)
Cu(1)-H(1A)	1.79(2)	1.80(2)
Cu(1)-H(1B)	1.79(2)	1.85(2)
S(1)-Cu(1)-P(1)	131.80(4)	146.42(2)
S(1)-Cu(1)-B(1)	89.80(5)	89.04(7)
P(1)-Cu(1)-B(1)	138.28(5)	124.40(7)
$\Sigma_{\text{angles around Cu}}$	359.88	356.86
C(1)-S(1)-Cu(1)	100.54(6)	101.37(7)
N(1)-B(1)-Cu(1)	106.40(9)	106.2(1)
N(1)-B(1)-C(6)-C(7)	67.7(2)	82.1(3)

The B-H distances were recorded as 1.18(2), 1.17(2) for **[Cu(^{Ph}Mmp)(PPh$_3$)]** and 1.18(2), 1.18(2) Å for **[Cu(^{Ph}Mmp)(PCy$_3$)]** are similar in length to the **[Cu(Mmp)(PR$_3$)]** complexes. This trend continues for the corresponding Cu-H distances. The copper-boron distance for **[Cu(^{Ph}Mmp)(PPh$_3$)]** is 2.158(2) Å, this distance is consistent with the Cu-B distances of previously reported copper complexes bearing the ligand $[BH_4]^-$ coordinating in a κ^2-H,H manner in which copper boron distances of between 2.08 and 2.34 Å have been reported.[122–125] This is longer than the major component of **[Cu(Mmp)(PPh$_3$)]** 2.113(17) Å this suggests a weaker interaction which is consistent with NMR data. The Cu-B distance is a much more reliable indicator due to the difficulties in locating hydrogen atoms in SC-XRD solved structures. The **[Cu(^{Ph}Mmp)(PCy$_3$)]** Cu-B distance (2.230(3) Å) is longer than the PPh_3 complex again suggesting that its 3c-2e bonds are weaker. This is consistent with the trend observed for the Mmp complexes. Unlike the Mmp complexes there is no noticeable difference in the C-S bond lengths of 1.721(2) in **[Cu(^{Ph}Mmp)(PPh$_3$)]** and for **[Cu(^{Ph}Mmp)(PCy$_3$)]** 1.722(2) Å. However, both complexes appear to be more thione in character than both the major component of **[Cu(Mmp)PPh$_3$]** with a C-S distance of 1.7515(17) Å but within the region of error for **[Cu(Mmp)PCy$_3$]** C-S distance 1.7244(17) Å.

3.2.4 Synthesis of copper ^{Me}Mmp complexes

The reaction of Li[^{Me}Mmp] with one equivalent of phosphine and copper chloride in methanol proceeded over 24 hours and resulted in the formation of a pale-yellow powder. The powder was obtained with yields of 40% and 65% for **[Cu(^{Me}Mmp)(PPh$_3$)]** and **[Cu(^{Me}Mmp)(PCy$_3$)]**, respectively (Scheme 3.10).

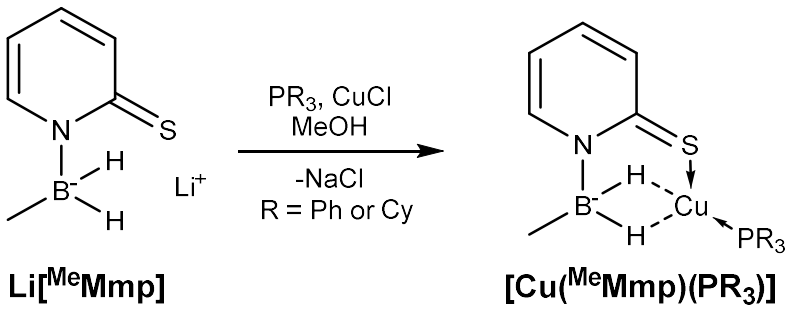

Scheme 3.10. Synthesis of **[Cu(^{Me}Mmp)(PR$_3$)]** complexes

The ^{1}H and ^{13}C{^{1}H} NMR spectra were assigned using COSY, HSQC and HMBC experiments, the presence of the target product in solution was confirmed by correct integration and chemical shift values for the ^{Me}Mmp and PPh$_3$ ligands in the ^{1}H NMR spectra. A single resonance was observed in the ^{11}B NMR spectra for both complexes corresponding to the BH_2^- group of the coordinated ligands. Again, this should appear as a triplet, however, the presence of hydrogen around the boron was confirmed by measuring the h.h.w. for both ^{11}B and ^{11}B{^{1}H} spectra. The h.h.w. decreases from 284 and 286 to 165 and 166 Hz for **[Cu(^{Me}Mmp)(PPh$_3$)]** and **[Cu(^{Me}Mmp)(PCy$_3$)]** respectively. This confirms the presence of ^{1}H nuclei around the boron. The broad peak representing the BH_2 protons in the ^{1}H NMR spectra also resolves to a sharper singlet in the ^{1}H{^{11}B} spectra again confirming that the broad signal is due to the presence of boron. The ^{11}B{^{1}H} NMR resonance for the coordinated ligand was shifted from −10.62 to −8.87 and −8.59 ppm. This suggests that the boron has lost electron density which could be due to the coordination of the $[RBH_2]^-$ unit to the copper centre. The ^{1}H{^{11}B} NMR shifts for the ^{Me}Mmp ligand salt and complexes are −2.17, −2.46 and −2.17 ppm for **[Li(^{Me}Mmp)]**, **[Cu(^{Me}Mmp)(PPh$_3$)]** and **[Cu(^{Me}Mmp)(PCy$_3$)]**. This represents an upfield shift from ^{Ph}Mmp ligands and

complexes suggesting that the BH protons are more hydridic in character, this could be due to the electron donating ability of the methyl group present on the BH_2^- moiety.

There is one single resonance in the $^{31}P\{^1H\}$ NMR spectrum for the **[Cu(^{Me}Mmp)PPh$_3$]** complex. This is located at 8.8 ppm confirming the coordination of the phosphorus ligand to the copper centre. This is shifted upfield from the **[Cu(^{Ph}Mmp)(PPh$_3$)]** complex where the resonance is recorded at 10.1 ppm. This is suggestive of weaker coordination and again suggests that the ^{Me}Mmp ligand is a stronger electron donating ligand than the ^{Ph}Mmp as the PPh_3 ligand gives a more shielded resonance. The PCy_3 complex is also slightly more upfield at 28.0 ppm in comparison to 28.8 ppm. $[M\text{-}H]^+$ ions for both complexes were detected using an atmospheric solids analysis probe. These were detected at *m/z* = 462.06 and 480.20 for **[Cu(^{Me}Mmp)(PPh$_3$)]** and **[Cu(^{Me}Mmp)(PCy$_3$)],** respectively.

Table 3.5. Selected spectroscopic data for the ligand [Li(^{Me}Mmp)] and [Cu(^{Me}Mmp)(PR$_3$)] complexes. NMR chemical shifts record as ppm and (h.h.w.) in Hz. Powder film IR data in cm^{-1}, (t)-terminal and (b)-bridging BH's

Compound	$^{11}B\{^1H\}$ NMR	$^{31}P\{^1H\}$ NMR	$^{13}C\{^1H\}$ NMR *C*=S	$^{1}H\{^{11}B\}$ NMR B*H*$_n$	IR B–H
[Li(^{Me}Mmp)]	−10.62 (70)	-	179.7	−2.17	2226
[Cu(^{Me}Mmp)(PPh$_3$)]	−8.87 (165)	8.8	175.8	−2.46	2016 (b, vw)
[Cu(^{Me}Mmp)(PCy$_3$)]	−8.59 (166)	28.0	174.4	−2.17	2032 (b, w)

X-ray quality crystals for **[Cu(^{Me}Mmp)(PPh$_3$)]** were grown via slow evaporation of a concentrated methanol solution. There was no disorder present in the structure. To the copper centre, there is a single PPh_3 and ^{Me}Mmp ligand coordinated in a distorted trigonal planar arrangement. The ^{Me}Mmp ligands coordinates to the copper via an L-type interaction originating from the sulfur donor and a dihydroborate interaction originating from the anionic $R[BH_2]^-$ moiety. Both B-H bonds donate electrons to the metal centre. The Cu-P bond distance is 2.1829(3) Å. This is slightly larger than that of the Cu-P bond distance in the complex **[Cu(^{Ph}Mmp)(PPh$_3$)]** 2.1748(8) Å and also the complex **[Cu(Mmp)(PPh$_3$)]** 2.1789(4) Å suggesting a slightly weaker interaction, this indicates that the presence of the methyl group has a greater effect at relieving the electron deficiency of the copper centre as the phosphine does not need to coordinate as strongly as it does in other ^{R}Mmp complexes. The sum

of the bond angles around the copper centre is 358.6° which is slightly distorted from the idealised 360°.

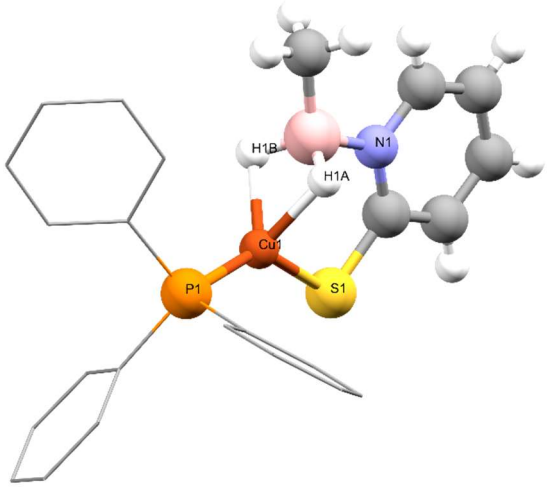

Figure 3.5. SC-XRD structure for **[Cu(^{Me}Mmp)(PPh$_3$)].** Hydrogens on Ph rings have been omitted for clarity.

Table 3.6. Selected bond distances and angles for [Cu(^{Me}Mmp)(PPh$_3$)]

	[Cu(^{Me}Mmp)(PPh$_3$)]
Cu(1)-P(1)	2.1829(3)
Cu(1)-B(1)	2.194(1)
Cu(1)-S(1)	2.2256(3)
C(1)-S(1)	1.727(1)
B(1)-N(1)	1.589(1)
N(1)-C(1)	1.366(2)
B(1)-H(1A)	1.17(2)
B(1)-H(1B)	1.18(2)
B(1)-C(6)	1.604(2)
Cu(1)-H(1A)	1.78(2)
Cu(1)-H(1B)	1.83(2)
S(1)-Cu(1)-P(1)	138.66(2)
S(1)-Cu(1)-B(1)	89.88(4)
P(1)-Cu(1)-B(1)	130.06(4)
$\Sigma_{\text{angles around Cu}}$[4]	358.6
C(1)-S(1)-Cu(1)	100.52(4)
N(1)-B(1)-Cu(1)	105.51(8)

Both BH hydrogens were located in the crystal structure and showed that the BH_2 unit coordinated to the metal via two 3c-2e bonds. The B-H bonds 1.17(2) and 1.18(2) Å are similar in length to both ^{Ph}Mmp and Mmp complexes and the Cu-H distances of 1.78(2) and 1.83(2) Å are also in the same range for

those complexes. The Cu-B bond distance was found to be 2.194(1) Å which again appears typical for both mono supported ligands with a dihydroborate interaction.

3.3 Complexes based on a 7-azaindole scaffold

Scorpionate ligands containing azaindole scaffolds were first reported in 2005 by Wang.[76] The potassium salt of the ligand Tai (Tris(7-azaindole)borate) was prepared by reacting freshly ground KBH_4 and excess 7-azaindole (**3.5**) with heating to 180 °C. SC-XRD studies determined that the BH unit is attached via each of the pyrrole rings of the supporting 7-azaindole moiety. Scorpionate ligands based on an azaindole scaffold can form B-N bonds from either of the two nitrogen functionalities on the heterocycle this is because 7-azaindole is present as two tautomers **3.5** and **3.6** (Scheme 3.11).

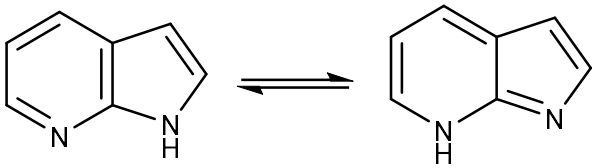

3.5 **3.6**

Scheme 3.11. Tautomerism in 7-azaindole

Copper and zinc complexes were synthesised containing the Tai ligand. The copper complex was synthesised by reacting $[Cu(MeCN)_2(PPh_3)_2]BF_4$ in a 1:1 molar ratio with **K[Tai]** in DCM in which the product **[Cu(Tai)(PPh$_3$)]** precipitated out of solution as crystals over a period of days (Scheme 3.12).

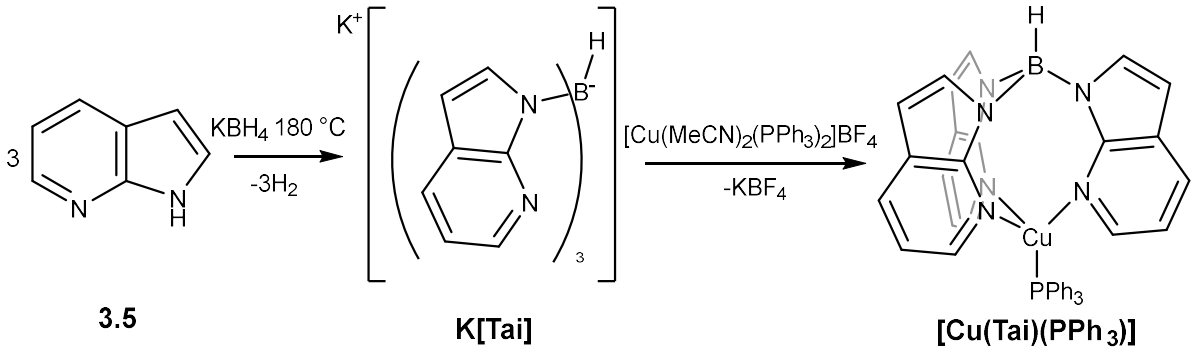

3.5 **K[Tai]** **[Cu(Tai)(PPh$_3$)]**

Scheme 3.12. Synthesis of the ligand **K[Tai]** and subsequent *synthesis* of **[Cu(Tai)(PPh$_3$)]**

Ever since the first initial synthesis of Tai, limited examples of metal complexes bearing this ligand have been reported, this includes [Ru(Tai)Cp*][88], [Rh(Tai)(cod)], [Ir(Tai)(cod)],[75,126] [Rh(Tai)(nbd),[127]

[Ru(Tai)Cp] and [Ru(Tai)CpCO].[128] These complexes demonstrate the flexibility of the Tai scorpionate observing both κ^3-N,N,N and κ^3-N,N,H coordination in which the BH bond is able to form strong agostic interactions. These complexes have also demonstrated the ability of the hydride to migrate from boron to metal centre to form a Z-type interaction between the boron and metal centre. Following on from the synthesis of Tai, Hill and Wagler synthesised the first mono azaindole scorpionate Mai.[74] The synthesis was achieved by reacting excess $NaBH_4$ with 7-azaindole in dioxane under refluxing conditions. Crystal structure data for [Na(Mai)]·0.5dioxane shows that the BH_3 unit was bonded to the pyridine nitrogen of azaindole moiety, this is in contrast to the Tai ligand whose B-N bond is located on the pyrrole ring.

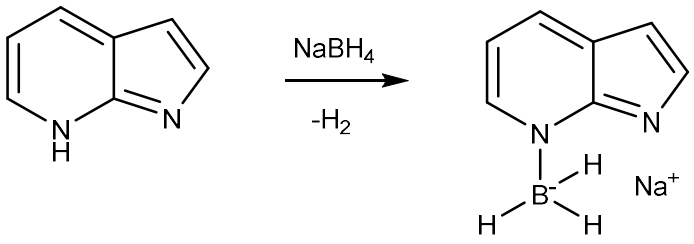

3.6 **Na[Mai]**

Scheme 3.13. Synthesis of the ligand [Na(Mai)]

Hill reported the synthesis of $[Rh(Mai)(PPh_3)_2CO]$ and $[Rh(Mai)(PPh_3)_2]$. These at the time of writing are the only reported Mai complexes reported to date. In 2009 Owen reported the synthesis of the ligand salt **Li[^{Ph}Bai]**.[75] Synthesis is achieved by reacting $Li[PhBH_3]$ with 7-azaindole in a 1:2.5 ratio in toluene at 120 °C for 48 hours, the reaction mixture was subsequently filtered and chilled to −30 °C after which time the product precipitated out as pale yellow crystals. This was the first example of a bis scorpionate based on an azaindole scaffold. There has been no reported synthesis of a non-substituted Bai ligand. The procedure for the synthesis of the ligand has since been altered and further derivatives have been synthesised, [^{Mes}Bai], [^{Napth}Bai][129,130] and [^{Me}Bai].[101]

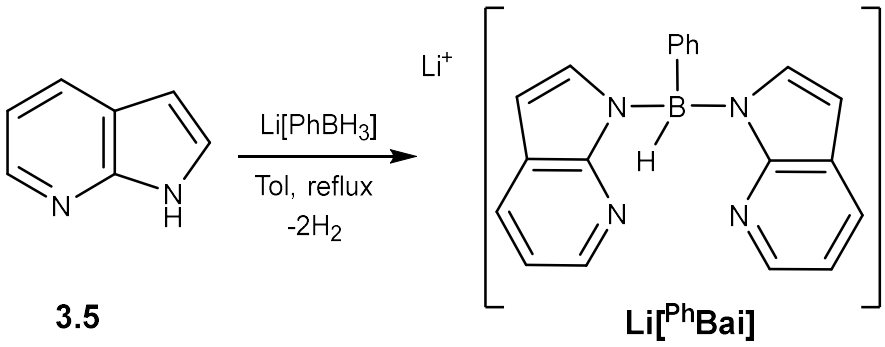

Scheme 3.14. Synthesis of the ligand [Li(^{Ph}Bai)]

3.3.1 Synthesis of copper Mai complexes

The successful synthesis of copper Mmp complexes represents the first examples of mono-supported borohydride ligands coordinating to copper. Further exploration discovered that the BH bond's coordination to the metal centre is influenced by adding a non-coordinating substituent such as a phenyl ring or a methyl group to the borohydride moiety. The synthesis of the corresponding mono-azaindole supported borohydride (Mai) complexes were therefore explored. The Mai scaffold has both a nitrogen support for the borohydride unit and additionally coordinates to metal centres through a dative bond involving a second nitrogen group.

The investigation of the Mai complexes has been used to assess their coordination to copper. Metrics such as Cu-B distances can be compared in order to ascertain its properties in relation to the mercaptopyridine scaffold as a supporting unit. Further to this, as previously discussed the ligand Tai has been utilised in the complex **[Cu(Tai)(PPh_3)]** and comparisons are made through the family of ligands.

Applying the same method for the synthesis of the **[Cu(Mmp)(PR_3)]** complexes (as outlined in sub-section 3.2.1) equimolar quantities of CuCl, **Na[Mai]** and either triphenyl- or tricyclohexyl-phosphine were left to stir for 24 hours in methanol (Scheme 3.15). After which time, it was observed that a pale green powder had precipitated out of solution in both triphenylphosphine and tricyclohexylphosphine reactions. NMR spectroscopic analysis of both precipitated products was performed by the uptake into $CDCl_3$ to make a concentrated solution. Of particular significance, was the relative integration of the phenyl rings in the triphenylphosphine complex which suggested that two equivalents of triphenylphosphine were present in the complex, this confirmed that the product was **[Cu(Mai)(PPh_3)$_2$]**. This was not the case when adding PCy_3 as a ligand. The NMR spectra of **[Cu(Mai)(PCy_3)]** remained consistent with our previous observations with only one equivalent of phosphine adding to the copper centre. The yields obtained for these reactions were good, 99% **[Cu(Mai)(PPh_3)$_2$]** (with respect to PPh_3 since this was now the limiting reagent) and 65%

[Cu(Mai)(PCy$_3$)] which is similar in yield to the previously described **[Cu(Mmp)(PR$_3$)]** complexes. Powder infrared spectroscopy data collected for both compounds show two separate BH stretching bands which confirms the presence of both terminal and bridging BH's are present (Table 3.7). Again, this is consistent with the observations made in **[Cu(Mmp)(PR$_3$)]** complexes.

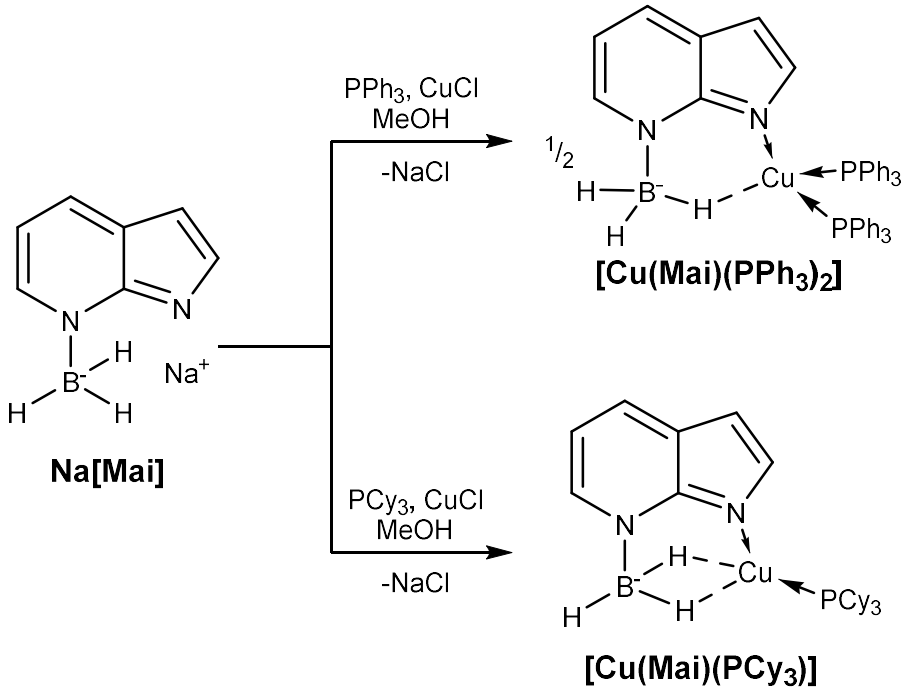

Scheme 3.15. Synthesis of [Cu(Mai)(PR$_3$)$_n$] complexes

Both complexes were comprehensively studied using ^{1}H, ^{1}H{^{11}B}, ^{11}B, ^{11}B{^{1}H}, ^{13}C{^{1}H}, ^{31}P{^{1}H}, COSY, HSQC and HMBC NMR experiments in $CDCl_3$. Upon coordination to the metal, the CH protons on the azaindole ring experience slight downfield shifts. Each CH environment on the azaindole ring was assigned using a combination of ^{1}H and COSY experiments and confirmed the presence of the azaindole within the structure. The ^{11}B{^{1}H} resonances for each complex were observed at −15.9 **[Cu(Mai)(PPh$_3$)$_2$]** and −15.4 ppm **[Cu(Mai)(PCy$_3$)]**. This again represents a downfield shift and indicates reduced electron density around the boron through coordination to the metal. A similar shift in the ^{11}B{^{1}H} spectra for [Rh(CO)(PPh$_3$)$_2$(Mai)] was observed at −15.1 ppm.[74] In the ^{11}B NMR experiments the shape of the peak implies the presence of a quartet, however, the splitting is ill-defined and not resolved. The presence of hydrogen substituents around the boron were therefore confirmed by

comparing the difference in h.h.w. between both the ^{11}B and $^{11}B\{^1H\}$ experiments for both **[Cu(Mai)(PPh$_3$)$_2$]** and **[Cu(Mai)(PCy$_3$)]** complexes. The h.h.w's. were reduced from 317 and 305 Hz in the ^{11}B spectra to 131 and 118 Hz in the $^{11}B\{^1H\}$ spectra, for both **[Cu(Mai)(PPh$_3$)$_2$]** and **[Cu(Mai)(PCy$_3$)]** complexes respectively. The reduction in half height widths (h.h.w.'s) between these two experiments, to a more uniform singlet therefore confirms that the boron has hydrogen substituents attached. Further to this, the BH_3 resonance in the ^1H spectra was very broad with individual resonances assigned at 3.72 ppm for **[Cu(Mai)(PPh$_3$)$_2$]** and 3.93 ppm for **[Cu(Mai)(PCy$_3$)]**, this then resolves to a sharp singlet in the $^1H\{^{11}B\}$ NMR spectra for both complexes confirming one chemical environment for these BH_3 protons in solution.

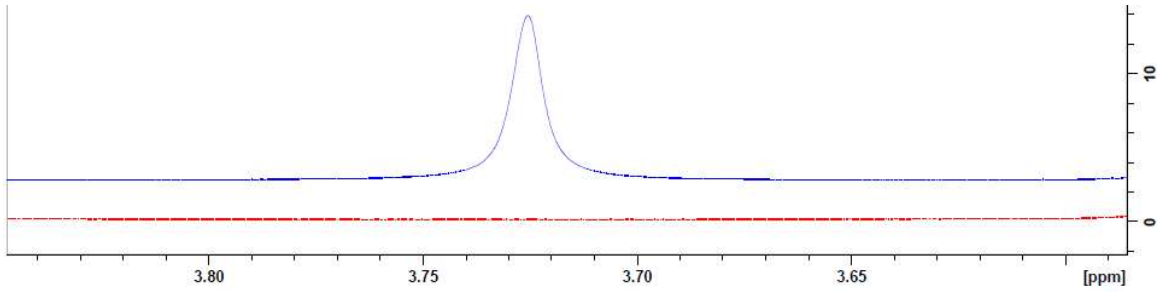

*Figure 3.6. ^1H (red) and $^1H\{^{11}B\}$ (blue) NMR spectra for **[Cu(Mai)(PPh$_3$)$_2$]** with a focus on the BH_3 resonance at 3.72 ppm*

In comparison to **[Cu(Mmp)(PR$_3$)]** complexes, the **[Cu(Mai)(PPh$_3$)$_2$]** and **[Cu(Mai)(PCy$_3$)]** BH_3 protons are more protic in character. $^{31}P\{^1H\}$ NMR data confirms the coordination of PPh_3 (2.4) and PCy_3 (23.0 ppm) to the copper centre as they are shifted downfield from their respective free ligands. These values are in line with the values for **[Cu(Mmp)(PPh$_3$)]** 4.8 and **[Cu(Mmp)(PCy$_3$)]** 27.2 ppm albeit slightly downfield suggesting a weaker Cu-P bond in each case. MS data was collected using ASAP solids probe with both complexes observing a mixture of [M-H] and [M+H] ions with the [M-H] being the major ion peak in both cases m/z = 455.09 **[Cu(Mai)(PPh$_3$)$_2$]** and 473.23 **[Cu(Mmp)(PCy$_3$)]** .

Table 3.7. Selected spectroscopic data for the ligand salt Na[Mai] and [Cu(Mai)(PR_3)$_n$] complexes. *NMR chemical shifts record as ppm and (h.h.w.) in Hz. Powder film IR data in cm^{-1}, (t)-terminal and (b)-bridging BH's*

Compound	$^{11}B\{^1H\}$ NMR	$^{31}P\{^1H\}$ NMR	$^1H\{^{11}B\}$ NMR BH_n	IR B–H
[Na(Mai)]	−16.8	-	2.4	2320
[Cu(Mai)(PPh_3)$_2$]	−15.9 (131)	2.4	3.72	2375 (t) / 2104 (b)
[Cu(Mai)(PCy_3)]	−15.4 (305)	23.0	3.93	2368 (t) / 2115 (b)

Single, colourless, block shaped crystals were grown directly by slow evaporation of the reaction mixture, from which, SC-XRD structures were obtained for both complexes (Figure 3.6). The structure for the **[Cu(Mai)(PCy_3)]** complex remains consistent with our observations for both the **[Cu(Mmp)(PR_3)]** and **[Cu(^{R}Mmp)(PR_3)]** complexes, in which a single tricyclohexylphosphine ligand is coordinated to the copper centre and the mono-supported borohydride (Mai) ligand coordinates via its 'L-type' nitrogen donor and through a dihydroborate interaction. Again, considering the boron as the point of attachment for the dihydroborate interaction, the complex adopts a trigonal planar geometry with the sum of the bond angles calculated as 359.56°. In the case of the **[Cu(Mai)(PPh_3)$_2$]** complex, the single crystal structure confirms that two triphenylphosphine ligands are indeed coordinating to the copper centre. The coordination of the Mai ligand in the complex **[Cu(Mai)(PPh_3)$_2$]**, in contrast to the coordination observed for **[Cu(Mai)(PCy_3)]** and the copper complexes bearing the ligand Mmp synthesised in previous sections of this thesis, which adopts a different mode of coordination. The coordination of the Mai ligand to the copper centre has two points of attachment, a single L-type interaction originates from the nitrogen donor and a single B-H 3c-2e bond between the ligand and the metal is observed (i.e. a κ^2-N,H coordination). The 3c-2e bond in this case is formally considered as a two electron donor for electron counting purposes. The geometry of the complex appears to be a slightly distorted trigonal pyramidal arrangement. The sum of the bond angles on the trigonal plane, in which both phosphine ligands and the nitrogen donor coordinate to the copper centre has been calculated as 355.06°, and the B-H hydrogen coordinates to the copper centre near

to a right angle with respects to the equatorial plane in the axial position with the N-Cu-H bond angle measured as 91.1(6)° (Table 3.8).

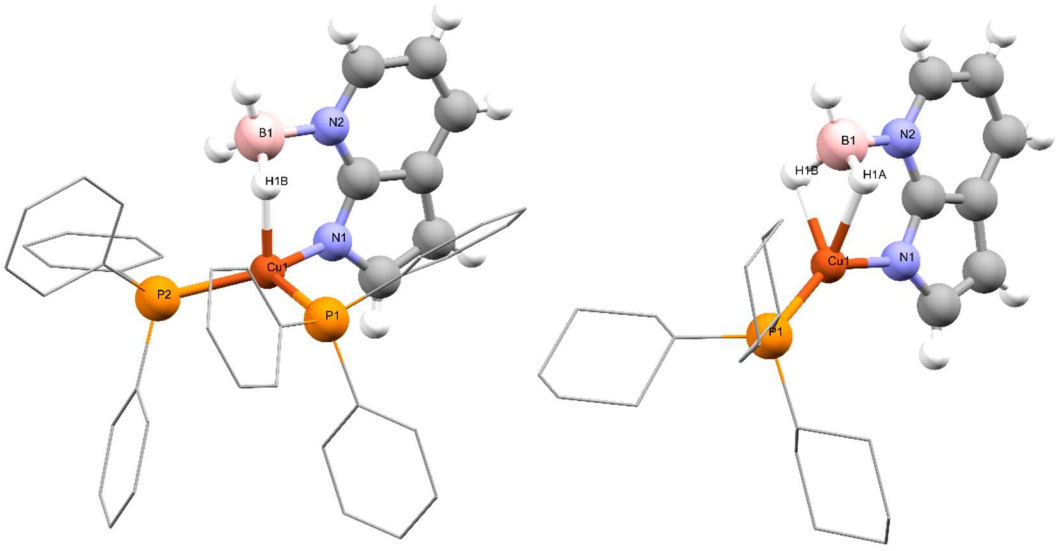

Figure 3.7. SC-XRD structures for **[Cu(Mai)(PPh$_3$)$_2$]** (left) and **[Cu(Mai)(PCy$_3$)]** (right). Hydrogens on Cy and Ph rings have been omitted for clarity.

Upon further inspection of the Mai ligand in both complexes, differences can be seen in the coordination of the nitrogen to the copper centres. The coordination of the nitrogen donor was as expected in **[Cu(Mai)(PCy$_3$)]** where the N-Cu bond continues at approximately 180° from the aromatic plane. Examination of the N-Cu bond in the **[Cu(Mai)(PPh$_3$)$_2$]** complex revealed a different situation. The N-Cu bond in **[Cu(Mai)(PPh$_3$)$_2$]** does not extend at a straight angle but has contorted from its expected configuration (Figure 3.7). This was measured using the BN-NCu torsion angles (Table 3.8) in which for the complex **[Cu(Mai)(PPh$_3$)$_2$]** the recorded angle was 23.08(8)°. This is a significant deviation from the expected angle of 0° and remains in contrast to the **[Cu(Mai)(PCy$_3$)]** complex which a torsion angle of 0.95(6)° was measured. By extending the aromatic plane of the azaindole ring the distance from which the copper centre has deviated from its expected position can also be calculated. This was achieved by measuring the distance of the copper atom from the closest point on the extended azaindole plane (Figure 3.7). This distance was calculated for both **[Cu(Mai)(PPh$_3$)$_2$]** (0.776

Å) and **[Cu(Mai)(PCy$_3$)]** (0.008 Å) complexes. The large distance observed for the **[Cu(Mai)(PPh$_3$)$_2$]** complex appears to be a significant deviation especially when compared to the **[Cu(Mai)(PCy$_3$)]** complex. In order to put these values into context these distances were also calculated for the previously reported Mai complexes prepared by Hill.[74] As outlined in Chapter 2, Hill demonstrated the κ^3-N,H,H (asymmetric) coordination of the Mai ligand in the complex [Rh(Mai)(PPh$_3$)$_2$] (**2.90**) in which, the distance from closest point on the extended azaindole plane was calculated as 0.234 Å. To this complex in C_6D_6, Hill added 1 atmosphere of CO which generated the complex [Rh(Mai)(CO)(PPh$_3$)$_2$] (**2.91**), the addition of a single equivalent of CO results in a change of coordination of the Mai ligand from κ^3-N,H,H to κ^2-N,H. The change in coordination mode reduces the calculated distance from the closest point on the extended azaindole plane to 0.078 Å. This shows that the addition of substituents to the metal centre can have an effect on the distortion of the N-Cu bond, but the distortion is not solely influenced by the change in coordination mode of the ligand, rather by the coordination sphere of the metal centre.

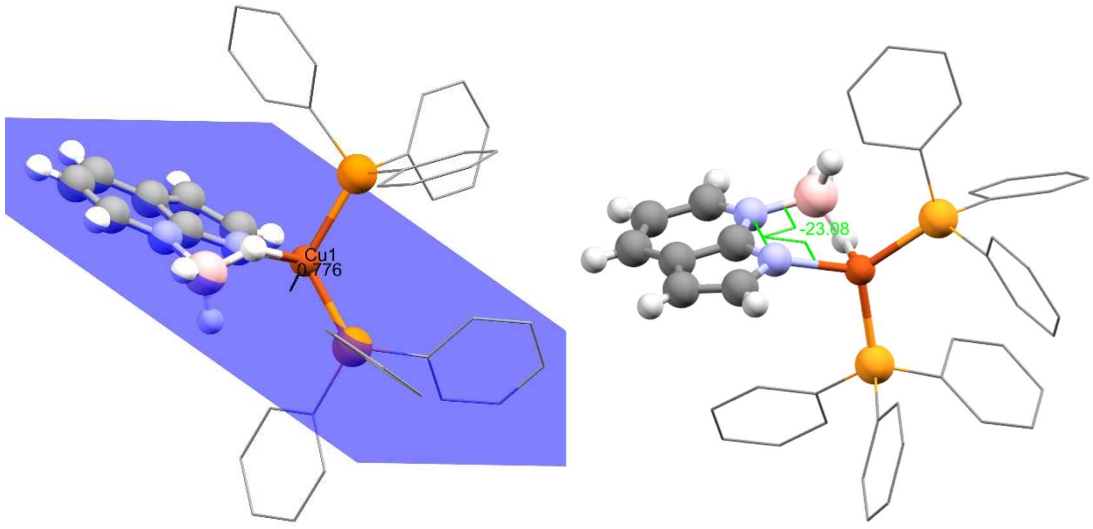

Figure 3.8. SC-XRD structure of **[Cu(Mai)(PPh$_3$)$_2$]** showing the distance of Cu from the closest point on the az*a-plane(right) and the B(1)N(2)-N(1)Cu(1) torsion angles (right). Hydrogens on Ph rings have been omitted for clarity.*

In the case of the copper complexes **[Cu(Mai)(PPh$_3$)$_2$]** and **[Cu(Mai)(PCy$_3$)]**, the addition of an extra phosphine in the **[Cu(Mai)(PPh$_3$)$_2$]** complex might be attributed to an increased insolubility of the bis

phosphine complex, or an increased solubility of the mono complex therefore driving the reaction towards the precipitation of the **[Cu(Mai)(PPh_3)$_2$]** complex. This scenario seems unlikely as it has not been observed in any of the Mmp complexes or even in **[Cu(Mai)(PCy_3)]**. It appears that this difference may be due to steric and electronic effects of the phosphine ligand. Comparing the Cu-B distances for both **[Cu(Mai)(PCy_3)]** and **[Cu(Mmp)(PCy_3)]** reveals that the Mai ligand is less effective at bringing the boron into close proximity with the metal centre with a Cu-B distance of 2.334(1) Å. This is in contrast to the Mmp complex which records a shorter distance of 2.153(16) Å. This difference is due to the deviation in hybridisation between the nitrogen and sulfur donors. The sulfur donor is able to support tighter angles as a sp^3 hybridised centre, thus bringing the $[BH_n]^-$ unit into closer proximity to the metal centre. The Mai ligand which has a sp^2 hybridised nitrogen donor atom is capable of supporting wider angles. For example, in the complex **[Cu(Mmp)(PCy_3)]**, the C-S-Cu bond angle is 99.53(8)° (Table 3.2) however in the complex **[Cu(Mmp)(PCy_3)]**, the corresponding C-N-Cu bond angle is 116.44(7)°. Therefore in the case of **[Cu(Mai)(PPh_3)$_2$]**, despite the use of a single equivalent of phosphine, the reduced steric influence of the boron based ligand at the metal centre allows for the coordination of an additional phosphine. This is in order to satisfy the electron deficiency as a result of the reduced proximity of the $[BH_n]^-$ group to the metal centre. This would also explain the difference between the two Mai complexes given that the PCy_3 ligand has both a larger cone angle and is reported to be a stronger electron donor.[131,132] Therefore, only a single equivalent of PCy_3 is required to stabilise the copper centre.

Table 3.8. Selected bond lengths and angles for the ligand [Na(Mai)] and [Cu(Mai)(PR_3)$_n$] complexes

	[Na(Mai)]·0.5dioxane	**[Cu(Mai)(PPh_3)$_2$]**	**[Cu(Mai)(PCy_3)]**
Cu(1)-P(1)	-	2.2772(6)	2.1835(3)
Cu(1)-P(2)	-	2.2493(4)	-
Cu(1)-B(1)	-	2.657(2)	2.334(1)
Cu(1)-N(1)	-	2.022(1)	1.957(1)
C(7)-N(1)	1.353(3)	1.352(2)	1.346(1)
N(2)-B(1)	1.580(3)	1.564(2)	1.566(2)
C(7)-N(2)	1.366(2)	1.355(2)	1.349(1)
B(1)-H(1A)	1.16(2)	1.12(2)	1.17(2)
B(1)-H(1B)	1.13(2)	1.21(2)	1.17(2)
B(1)-H(1C)	1.15(2)	1.13(2)	1.09(2)
Cu(1)-H(1A)	-	-	1.97(2)
Cu(1)-H(1B)	-	1.84(2)	1.93(2)
Cu(1)-^{aza}plane	-	0.776	0.008
P(1)-Cu(1)-N(1)	-	109.18(4)	143.35(3)
P(2)-Cu(1)-N(1)	-	128.09	-
P(1)-Cu(1)-P(2)	-	117.79	-
N(1)-Cu(1)-B(1)	-	75.11(5)	82.20(4)
P(1)-Cu(1)-B(1)	-	100.49(4)	134.01(4)
$\Sigma_{angles\ around\ Cu}$	-	355.06*	359.56
Cu(1)-N(1)-C(7)	-	118.19(9)	116.44(7)
Cu(1)-B(1)-N(2)	-	94.49(4)	100.01(7)
N(1)-Cu(1)-H(1B)	-	91.1(6)	89.9(5)
B(1)-N(2)-N(1)-Cu(1)	-	−23.08(8)	−0.95(6)

* Sum of bond angles calculated are calculated around the trigonal plane.

The Cu-P bond distances in **[Cu(Mai)(PPh_3)$_2$]** were found to be 2.2772(6) and 2.2493(4) Å. These distances are both longer in comparison to the complex **[Cu(Mmp)(PPh_3)]** (2.1789(4) Å). This shows that the two phosphine donors in the **[Cu(Mai)(PPh_3)$_2$]** complex are more weakly coordinating since there is a reduced requirement for both phosphines to relive the electron deficiency at the metal centre due to the presence of an extra phosphine ligand. Looking to the PCy_3 complexes, the Cu-P bond length for **[Cu(Mai)(PCy_3)]** was recorded as 2.1835(3) Å which is marginally shorter than the complex **[Cu(Mmp)(PCy_3)]** (2.1876(4) Å). This does, however, continue to illustrate the increased requirement for the PCy_3 ligand to satisfy the electron deficiency in the **[Cu(Mai)(PCy_3)]** complex due to its method of support.

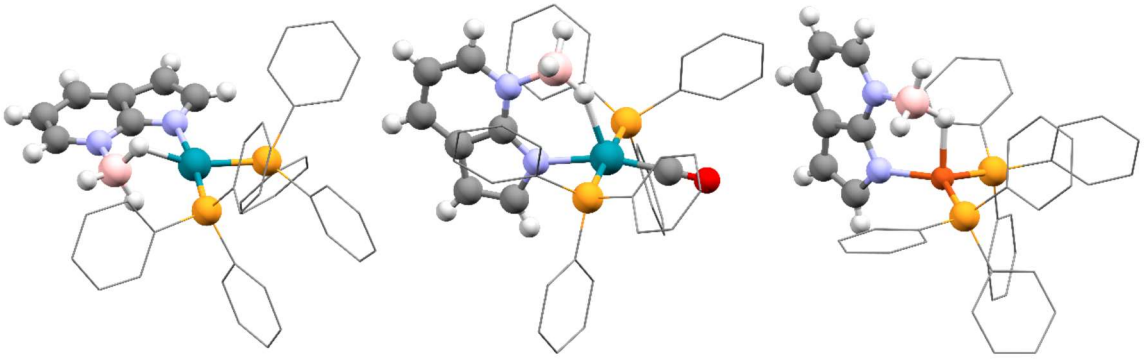

*Figure 3.9. SC-XRD structures illustrating the geometries of **2.90** (left), **2.91** (middle) and **[Cu(Mai)(PPh$_3$)$_2$]** (right). Both solvent and hydrogens have been ommitted for clarity.*

Looking further into the coordination of the $[BH_3]^-$ unit to the metal centre, in the complex **[Cu(Mai)(PCy$_3$)],** the bridging BH's bond distances were recorded as 1.17(2) and 1.17(2) Å and the terminal BH bond distance was 1.09(2) Å. These distances show some difference between both the terminal and bridging BH's, which is in contrast to what was observed for the **[Cu(Mmp)(PCy$_3$)]** complex, in which no significant difference was observed. Again, the Cu-H distances in **[Cu(Mai)(PCy$_3$)]** place the bridging hydrogens further from the copper centre (1.97(2) and 1.93(2) Å) compared with **[Cu(Mmp)(PCy$_3$)]** (1.75(3) and 1.81(4) Å). When looking at the **[Cu(Mai)(PPh$_3$)$_2$]** complex, the change in coordination mode (in comparison to **[Cu(Mai)(PCy$_3$)]**) from κ^3-N,H,H to κ^2-N,H results in only a single BH bond being elongated (1.21(2) Å), when compared to the terminal BH bonds (1.12(2) and 1.13(2) Å). As there is only a single bridging BH bond this is orientated towards the metal resulting in a shorter Cu-H bond distance of 1.84(2) for the **[Cu(Mai)(PPh$_3$)$_2$]** complex. This comparatively shorter bond suggests that, in the case of the **[Cu(Mai)(PPh$_3$)$_2$]** complex, the distortion of the N-Cu bond occurs in order to facilitate more efficient bonding of the BH bond to the metal centre. Referring back to the study by Hill[74] on rhodium complexes bearing the ligand Mai, the rhodium complexes give Rh-H distances of 2.13(3) and 1.88(2) Å for [Rh(Mai)(PPh$_3$)$_2$] (**2.90**) and 2.05(2) Å for [Rh(Mai)(CO)(PPh$_3$)$_2$] (**2.91**). The asymmetric interaction in **2.90** in which the biggest N-M 'distortion' for rhodium complexes is observed again results in a reduced M-H bond distance. This asymmetric interaction therefore allows for the Mai ligand to facilitate a square planar geometry in the rhodium complex (Figure 3.8).

In complex **2.91,** the geometry of the complex is a square pyramidal complex in which on the equatorial plane the Mai nitrogen, coordinates trans CO and both phosphines coordinate trans to each other. Finally, the BH bond coordinates in the axial position and no contortion is required in order to facilitate this. Accordingly, for the synthesised complex **[Cu(Mai)(PPh_3)$_2$]** the contortion of the N-Cu bond observed in the SC-XRD studies appears to occur in order to satisfy the geometric constraints of the metal centre. The trigonal pyramidal conformation therefore allows for the BH bond to come into closer proximity to the metal centre at the axial coordination site (Figure 3.8).

3.3.2 Synthesis of copper ^{Me}Bai complexes

For comparative purposes, copper complexes bearing the ligand ^{Me}Bai were also synthesised. The synthesis and spectroscopic data will therefore aid in the comparison of both Mai and Tai complexes. The ligand salt **Li[^{Me}Bai]·2MeCN** was synthesised according to the procedure set out by Owen (Scheme 3.16).[98] The presence of the ligand in the solution state was unambiguously confirmed by comparing ^{11}B and ^{1}H NMR spectra.

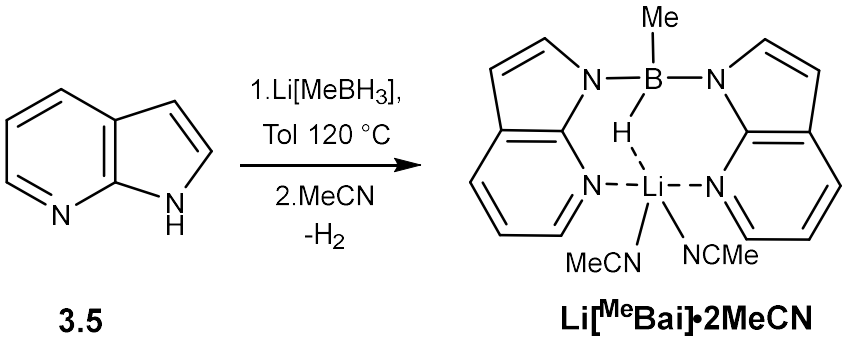

Scheme 3.16. Synthesis of the ligand salt [Li(^{Me}Bai)]

The synthesis of the copper complexes bearing the ligand ^{Me}Bai was carried out using standard Schlenk line techniques. Equimolar quantities of CuCl, PR_3 and **Li[^{Me}Bai]·2MeCN** were added in methanol and left to stir for at least 24 hours to allow for completion. The product had precipitated out of solution as a pale green powder and was present in good yields **[Cu(^{Me}Bai)(PPh_3)]** (55%) and **[Cu(^{Me}Bai)(PCy_3)]** (59%). Initial confirmation of the formation of the copper ^{Me}Bai complexes came from the infrared spectra for both **[Cu(^{Me}Bai)(PPh_3)]** and **[Cu(^{Me}Bai)(PCy_3)]**. Each complex exhibits a single BH stretching band at 2095 cm^{-1} **[Cu(^{Me}Bai)(PPh_3)]** and 2091 cm^{-1} **[Cu(^{Me}Bai)(PCy_3)]**. The presence of a single stretching band of this frequency indicates that the lone BH bond of the borohydride unit is coordinated to a copper centre as opposed to the non coordinating BH bond ligand salt **Li[^{Me}Bai]·2MeCN** (2359 cm^{-1}, Table 3.9).

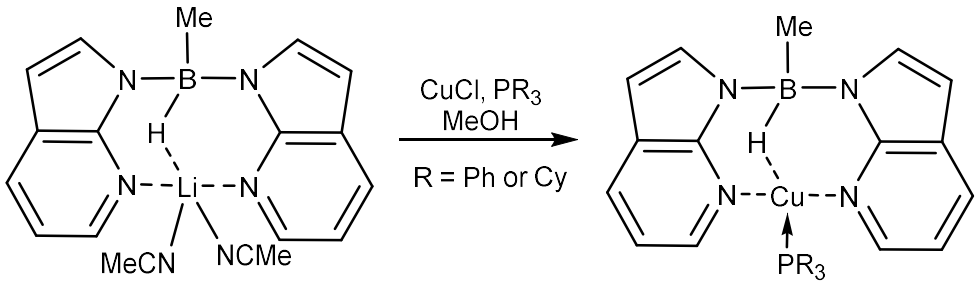

Li[^{Me}Bai]•2MeCN **[Cu(^{Me}Bai)(PR_3)]**

Scheme 3.17. Synthesis of **[Cu(^{Me}Bai)(PR_3)]** complexes

The products **[Cu(^{Me}Bai)(PPh_3)]** and **[Cu(^{Me}Bai)(PCy_3)]** were each dissolved in $CDCl_3$ and studied by various NMR experiments including ^{1}H, ^{11}B, ^{13}C and ^{31}P nuclei. In the ^{11}B spectra, the BH resonances were shifted downfield to −7.64 for **[Cu(^{Me}Bai)(PPh_3)]** and −8.39 ppm for **[Cu(^{Me}Bai)(PCy_3)]** in comparison to the ligand salt which was present at −9.72 ppm. This gives further indication of the coordination of the BH bond to the copper centre. The splitting of the BH resonances in the ^{11}B NMR spectra confirmed the presence of hydrogen around the boron as the doublet which resolved into a singlet in the $^{11}B\{^{1}H\}$ experiments, followed by a reduction in h.h.w. for each complex. Upon coordination to rhodium and iridium centres the ^{11}B resonance experiences a more significant downfield shift giving resonances of −5.0 to −0.8 ppm for rhodium complexes and −0.2 ppm for iridium complexes.[98] The BH environments for both **[Cu(Bmp)(PPh_3)]** and **[Cu(Bmp)(PCy_3)]** complexes (Table 3.9) in the ^{1}H NMR spectra each give, a single, broad peak which was resolved to a singlet in the $^{1}H\{^{11}B\}$ experiment. This again, confirms the presence of boron nuclei bonded to the hydrogen atom of that environment. The $^{31}P\{^{1}H\}$ NMR spectra confirms the coordination of both triphenyl and tricyclohexyl phosphine ligands to the copper centres, in which, both complexes give resonances shifted downfield from that of the free ligands. These resonances were recorded as 1.26 and 24.0 ppm for both **[Cu(Bmp)(PPh_3)]** and **[Cu(Bmp)(PCy_3)]** respectively, these resonances are consistent with the coordination of phosphines in both **[Cu(Bmp)(PPh_3)]** and **[Cu(Bmp)(PCy_3)]** in which the reported resonances 1.71 and 19.0 ppm respectively. The mass spectra recorded for both complexes showed

that each complex loses a fragment containing boron giving the following ions m/z = 560.12 [M-^{Me}BH]$^{+}$ for **[Cu(^{Me}Bai)(PPh$_3$)]** and m/z = 461.21 [M-BHaza] for **[Cu(^{Me}Bai)(PCy$_3$)]**.

Table 3.9. Selected spectroscopic data for **[Cu(^{Me}Bai)(PR$_3$)]** complexes and their comparison with **[Cu(^{Me}Bmp)(PR$_3$)]** complexes. *NMR chemical shifts record as ppm and (h.h.w.) in Hz. Powder film IR data in cm^{-1}, (t)-terminal and (b)-bridging BH's*

Compound	^{11}B{^{1}H} NMR	^{31}P{^{1}H} NMR	^{1}H{^{11}B} NMR BH_n	IR B–H
[Li(^{Me}Bai)]	−9.72	-	4.23	2359
[Cu(^{Me}Bai)(PPh$_3$)]	−7.64 (134)	1.26	4.99	2095 (b)
[Cu(^{Me}Bai)(PCy$_3$)]	−8.39 (165)	23.99	4.29	2091 (b)
[Cu(Bmp)(PPh$_3$)]	0.71	1.71	3.64	2354(t)
[Cu(Bmp)(PCy$_3$)	−0.70	19.0	3.99	2374(t)

X-ray quality crystals were grown directly from the slow evaporation of a filtered reaction solution. The structure of both complexes were as expected. Additionally, crystals of **[Cu(^{Me}Bai)$_2$]** were present in the reaction mixture for **[Cu(^{Me}Bai)(PCy$_3$)]**. The hydrogen on the BH unit for all structures were located in the difference map using a riding model. The structure for **[Cu(^{Me}Bai)(PCy$_3$)]** had disorder present in the positions of two of the cyclohexyl rings with a ratio of 68:32. The structure of the **[Cu(^{Me}Bai)(PR$_3$)]** complexes both adopt distorted tetrahedral arrangements (Figure 3.9). The ^{Me}Bai ligand coordinates with a κ^3-N,N,H mode with a facial arrangement with a single phosphine occupying the final coordination site. The **[Cu(^{Me}Bai)$_2$]** complexes also adopts this coordination mode but has an octahedral arrangement where the two ^{Me}Bai ligands coordinate in a facial arrangement and with all coordinated nitrogen donors *trans* to a nitrogen on the other ^{Me}Bai ligand and each of the B-H units coordinate trans to each other in both axial positions.

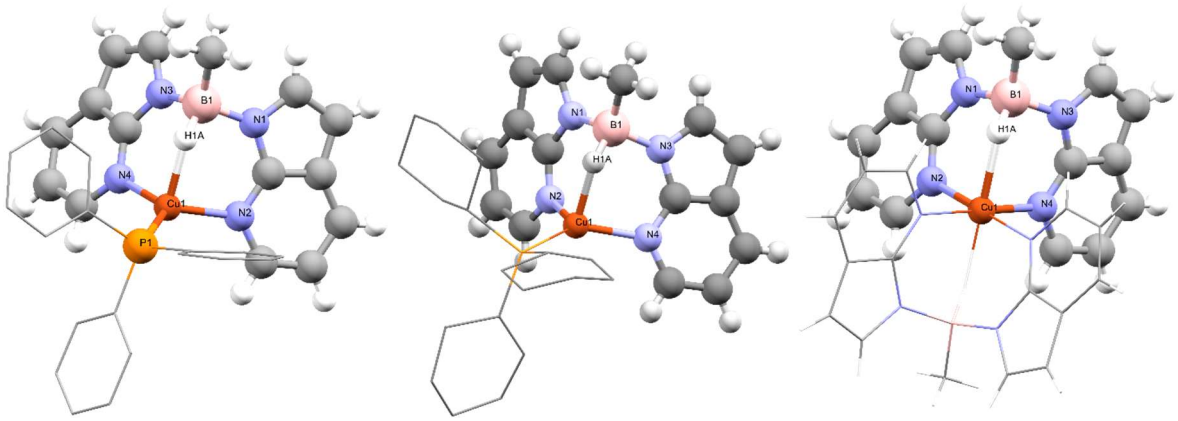

Figure 3.10. SC-XRD structures for **[Cu(^MeBai)(PPh3)]** (left), **[Cu(^MeBai)(PCy3)]** (middle) and **[Cu(^MeBai)2]** (right). Hydrogens on Cy and Ph rings have been omitted for clarity.

The Cu-P bond distance for **[Cu(^MeBai)(PPh3)]** is 2.1834(4) Å. This is shorter than for its respective Bmp complex **[Cu(Bmp)(PPh3)]** which is 2.216(3) Å and closer to that reported for the **[Cu(Mmp)(PPh3)]** complex 2.1789(4) Å. This suggests that ^{Me}Bai is weakly donating in comparison to Bmp, this could be due to steric factors or that copper(I) prefers a softer sulfur donor. The Cu-P bond distance for **[Cu(^MeBai)(PCy3)]** is 2.1802(6) Å. Again, this is close to that found in **[Cu(Mmp)(PPh3)]** which is 2.1876(4) Å. It is also close to the Cu-P distance of its respective Mai complex **[Cu(Mai)(PCy3)]** which is 2.1835 Å suggesting that the additon of an extra 7-azaindole does not releive any electron deficiency from the copper centre. The M-B bond distances for **[Cu(^MeBai)(PPh3)]** (2.776 Å), **[Cu(^MeBai)(PCy3)]** (2.763 Å) and **[Cu(^MeBai)2]** (2.944 Å) are longer than that of the **[Cu(Mai)(PCy3)]** complex 2.334 Å. This represents a change in coordination mode from a dihydroborate interaction in **[Cu(Mai)(PCy3)]** to a sinlge 3c-2e bond coordinating in the copper complexes bearing the ligand ^{Me}Bai. The Cu-B distances for these complexes also show that the **[Cu(^MeBai)2]** complex has a slightly elongated Cu-B distance of 2.944 Å when compared to the Cu-B distances recorded for the for **[Cu(^MeBai)(PPh3)]** (2.776 Å) and **[Cu(^MeBai)(PCy3)]** (2.763 Å) complexes. The B-H distances of 1.18 Å **[Cu(^MeBai)(PPh3)]**, 1.23 Å **[Cu(^MeBai)(PCy3)]** and 1.18 Å **[Cu(^MeBai)2]** are similar to that of the bridging BH's of the **[Cu(Mai)(Cy3)]** complex 1.17 and 1.17 Å confirming that the BH's are bridging with the copper centre these lengths are also slightly longer when compared to the crystal structure for the ligand **[Li(^MeBai)]·2MeCN** in which a bond distance of 1.15 Å has been recorded. The Cu-H distances of 1.85(2) Å in

[Cu(^{Me}Bai)(PPh$_3$)] and 1.84(2) Å **[Cu(^{Me}Bai)(PCy$_3$)]** are shorter than the distances for **[Cu(Mai)(PCy$_3$)]** 1.97 and 1.93 Å, this contrast in Cu-H distances is attributed to the different cooridination modes κ^3-N,N,H vs. κ^3-N,N,H. The Cu-H distance for **[Cu(^{Me}Bai)$_2$]** is much longer at 2.08 Å, again this is most likely due to the saturated coordination sphere.

Table 3.10. Selected bond lengths and distances for the ligand **[Li(^{Me}Bai)]** and **[Cu(^{Me}Bai)]** complexes

	[Li(^{Me}Bai)]·2MeCN	**[Cu(^{Me}Bai)(PPh$_3$)]**	**[Cu(^{Me}Bai)(PCy$_3$)]**	**[Cu(^{Me}Bai)$_2$]**
Cu(1)-P(1)	-	2.1834(4)	2.1802(6)	-
Cu(1)-B(1)	-	2.776(2)	2.763(2)	2.944
Cu(1)-N(2)	-	2.20(1)	2.074(2)	2.017
Cu(1)-N(4)	-	2.015(1)	1.996(2)	2.032
N(1)-B(1)	1.569(1)	1.549(2)	1.560(3)	1.560(4)
N(3)-B(1)	1.563(1)	1.564(2)	1.565(2)	1.553(3)
B(1)-C(15)	1.612(2)	1.609(2)	1.602(3)	1.606(3)
B(1)-H(1A)	1.15(1)	1.18(2)	1.23(2)	1.18(3)
Cu(1)-H(1A)	-	1.85(2)	1.84(2)	2.08
N(2)-Cu(1)-N(4)	-	107.78(5)	99.78(7)	89.77
P(1)-Cu(1)-N(2)	-	125.16(4)	118.87(5)	-
P(1)-Cu(1)-N(4)	-	123.95(4)	137.37(5)	-
Cu(1)-H(1A)-B(1)	-	131(1)	127(1)	127
Cu(1)-N(4)-C(14)	-	118.71(9)	116.9(1)	122.2
Cu(1)-N(2)-C(7)	-	119.01(9)	117.6(1)	122.8

3.4 Complexes based on a methimazole scaffold

3.4.1 Synthesis of ligands based on the methimazole scaffold

The first reported synthesis of a scorpionate ligand based on 3-methyl-imidazoline-2-thione was the ligand **Na[Tm]** reported by Reglinski in 1999.[133] Four equivalents of methimazole **3.7**, were added to one equivalent of $NaBH_4$ and heated directly to 160 °C (Scheme 3.18). The reaction had reached completion once three mol of H_2 gas was produced and the resultant solid was purified by Soxhlet extraction into chloroform. Since Reglinski's initial synthesis, the ligand Tm has attracted a great deal of attention.[134–143] The methyl substituent has previously changed to a variety of functional groups and has been the subject of two reviews.[12,94] In particular, work by Hill and Owen in 1999 showed that the ligand could undergo hydride migration to form a Z-type interaction between the metal and the boron.[80] Previous examples for copper Tm based complexes include the synthesis of $[Cu(Tm^{tBu})(PPh_3)]$, $[Cu(Tm^{tBu})]$[144] and $[Cu(Tm^{Et})(PPh_3)]$.[145] These complexes feature tBu or Et groups in place of the methyl substituent on the nitrogen.

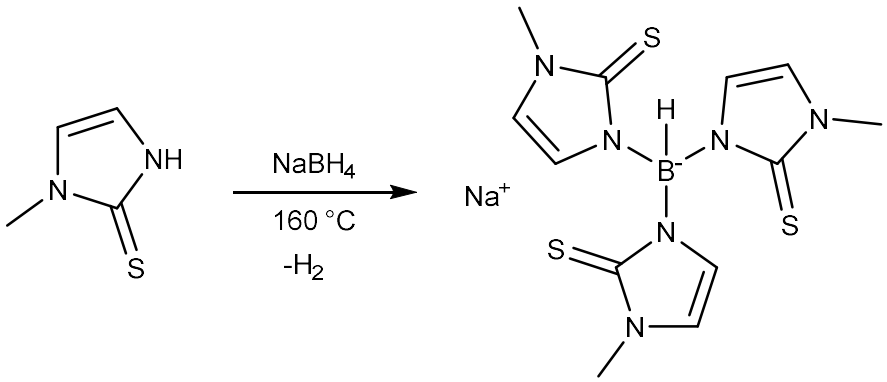

3.7 **Na[Tm]**

Scheme 3.18. Synthesis of the ligand **Na[Tm]**

Further to this in 2000, Parkin reported the synthesis of the first bis-supported ligand, Bm.[146] The ligand salt was synthesised by reacting methimazole with $LiBH_4$ in a 2.4:1 molar ratio in toluene at 50 °C, resulting a white solid which is purified by washing with ether and chloroform (Scheme 3.19). The ligand Bm is also well documented in literature.[71,140,147–150]

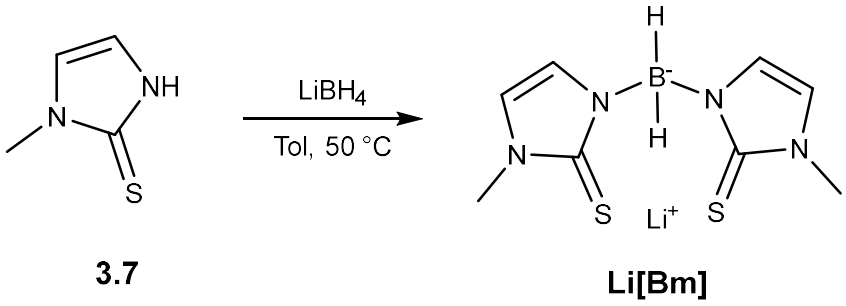

3.7 **Li[Bm]**

Scheme 3.19. Synthesis of the ligand [Li(Bm)]

Completing the family of ligands, the corresponding mono ligand was reported Santos in 2006 (Scheme 3.20).[70] Methimazole was added dropwise to a suspension of $NaBH_4$ in excess at 50 °C and is stirred for 3 hours, the product was purified by successive crystallisations from THF/hexane. The yield for this reaction is low 34%. When this ligand was targeted by ourselves, we were unable to improve upon this yield. This is because the ligand Na[Bm] is present as a by-product and has a similar solubility to **Na[Mm]**. To date only complexes of rhenium and technetium of the ligand Mm have been reported.[70,73]

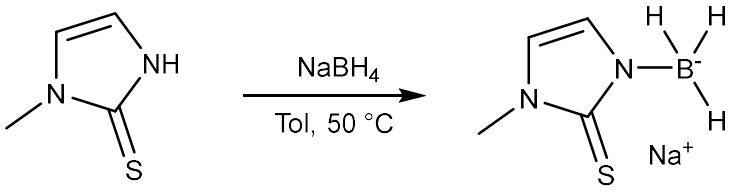

3.7 **Na[Mm]**

Scheme 3.20. Synthesis of ligand [Na(Mm)]

3.4.2 Synthesis of copper Mm complexes

The ligand salt **Na[Mm]** was stirred under nitrogen with equimolar quantities of copper (I) chloride and triphenyl phosphine or tricyclohexyl phosphine in methanol. After 24 hours of stirring the resultant product was filtered and washed with cold methanol to give the product an off-white solid. The products **[Cu(Mm)(PPh_3)]** and **[Cu(Mm)(PCy_3)]** were synthesised in good yields of 64% and 55%, respectively. The product, analysed by powder film IR gave BH stretching bands of 2434 and 2091 (PPh_3) and, 2450 and 2091 cm^{-1} (PCy_3) this indicates as with the Mmp and Mai copper complexes that there are both terminal and bridging BH's present.

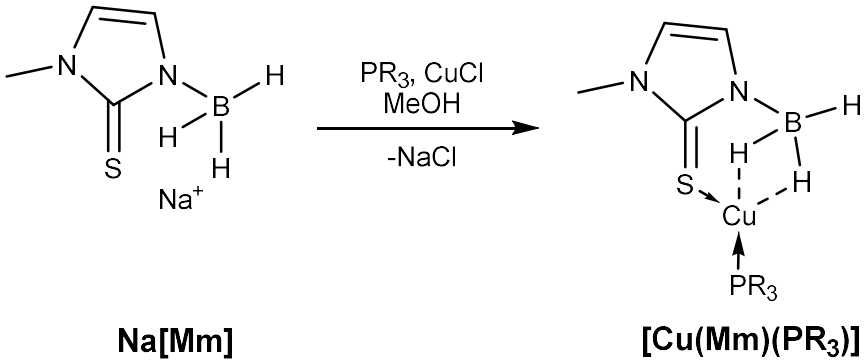

Scheme 3.21. Synthesis of **[Cu(Mm)(PR_3)]** complexes (PR_3 = PPh_3 and PCy_3)

Each product was dissolved in $CDCl_3$ and analysed by NMR spectroscopy. The ^1H NMR spectrum of both products shows that the protons of the methimazole ring experience a slight downfield shift to that of the free ligand suggesting that there is reduced electron density due to the coordination of the ligand. The BH_3 protons are present as a broad peak that resolves to a singlet in the $^1H\{^{11}B\}$ NMR spectra, confirming that the hydrogens are attached to the boron. The $^1H\{^{11}B\}$ resonance for the BH_3 protons were found at 2.38 ppm for **[Cu(Mm)(PPh_3)]** and 2.17 ppm for **[Cu(Mm)(PCy_3)].** These are more hydridic in character than that of the BH_3 protons for the corresponding Mai complexes (3.72 and 3.93 ppm) and Mmp complexes (2.64 and 2.42 ppm). Upon coordination to the metal there is, again, little change in the $^{11}B\{^1H\}$ chemical shift from −19.0 (Na[Mm]), however, the $^1J_{BH}$ coupling constant is reduced from 91 to 85 **[Cu(Mm)(PPh_3)]** and 81 Hz **[Cu(Mm)(PCy_3)]**.

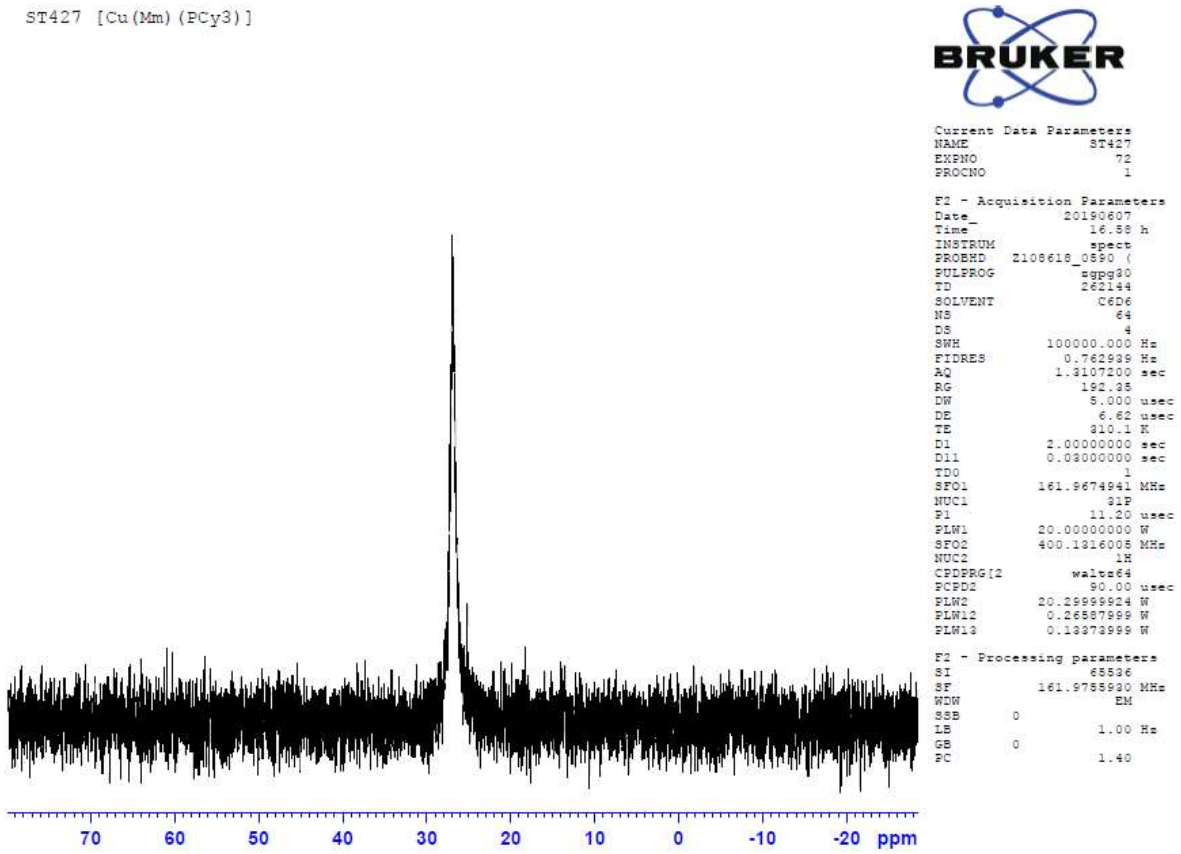

Figure 3.11. $^{31}P\{^{1}H\}$ *spectra of* ***[Cu(Mm)(PCy$_3$)]***

The $^{31}P\{^{1}H\}$ spectra confirms the coordination of each of the phosphines with resonances recorded at 6.8 ppm for **[Cu(Mm)(PPh$_3$)]** and 24.5 ppm for **[Cu(Mm)(PCy$_3$)]** (Figure 3.10) as they experience downfield shifts from that of the free ligand. Both complexes were analysed using an atmospheric solids analysis probe mass spectrometry. Both complexes gave $[M\text{-}H]^+$ ions *m/z* = 451.06 **[Cu(Mm)(PPh$_3$)]** and 469.20 **[Cu(Mm)(PCy$_3$)]** this is consistent with the fragmentation for **[Cu(Mmp)(PR$_3$)]**.

Table 3.11. Selected spectroscopic data for the ligand [Na(Mm)] and [Cu(Mm)(PR$_3$)] complexes. *NMR chemical shifts record as ppm and (h.h.w.) in Hz. Powder film IR data in cm^{-1}, (t)-terminal and (b)-bridging BH's*

Compound	$^{11}B\{^{1}H\}$ NMR	$^{31}P\{^{1}H\}$ NMR	$^{1}H\{^{11}B\}$ NMR BH_n	$^{13}C\{^{1}H\}$ NMR C=S	IR B–H
Na[Mm]	−19.00	-	-	162.4	2395, 2359, 2279(t)
[Cu(Mm)(PPh$_3$)]	−19.99 (88)	6.86	2.38	159.5	2434 (t) / 2091 (b)
[Cu(Mm)(PCy$_3$)]	−19.56 (81)	24.57	2.17	159.8	2450 (t) / 2067 (b)

X-ray quality crystals for **[Cu(Mm)(PCy$_3$)]** were grown from the slow evaporation of a concentrated methanol solution, the crystals gave good quality data and showed no disorder. The copper centre is coordinated to a single Mm ligand and a single PCy$_3$ ligand. The Mm ligand coordinates to the metal centre with a tridentate (κ^3-S,H,H) coordination mode, via an L-type interaction from the sulfur and two 3c-2e bonds originating from two of the BH bonds. The third BH unit from the ligand is not involved in coordination and is orientated away from the copper centre. This mode of coordination is consistent with the previously described copper complexes of Mmp, ^{R}Mmp and Mai ligands with a single phosphine donor. The Cu-P bond distance was found to be 2.1886(4) Å. This is consistent with the same distances in **[Cu(Mmp)(PCy$_3$)]** (2.1876(4) Å) and **[Cu(Mai)(PCy$_3$)]** (2.1835(3) Å) suggesting that there is little difference in the electron donating ability of each of the three ligands.

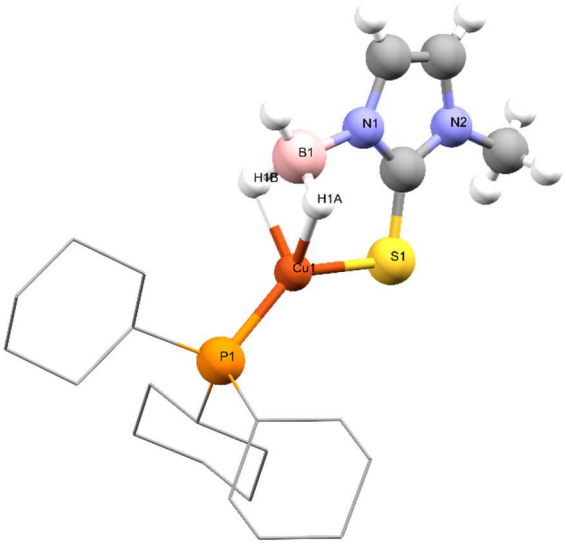

Figure 3.12. SC-XRD structure of **[Cu(Mm)(PCy$_3$)].** Hydrogens on Cy rings have been omitted for clarity.

Table 3.12. Selected crystallographic data for [Cu(Mm)(PCy_3)]

	[Cu(Mm)PCy_3]
Cu(1)-P(1)	2.1886(4)
Cu(1)-B(1)	2.208(2)
Cu(1)-S(1)	2.2515(3)
C(1)-S(1)	1.713(1)
B(1)-N(1)	1.541(2)
N(1)-C(1)	1.344(1)
B(1)-H(1A)	1.15(2)
B(1)-H(1B)	1.19(2)
B(1)-H(1B)	1.08(2)
Cu(1)-H(1A)	1.84(2)
Cu(1)-H(1B)	1.82(2)
S(1)-Cu(1)-P(1)	135.54(2)
S(1)-Cu(1)-B(1)	91.07(4)
P(1)-Cu(1)-B(1)	133.38(4)
$\Sigma_{\text{angles around Cu}}$	359.99
C(1)-S(1)-Cu(1)	96.45(4)
N(1)-B(1)-Cu(1)	103.74(9)

The C-S bond distance in **[Cu(Mm)(PCy_3)]** was recorded as 1.713(1) Å, this distance is similar to the reported distances in the complexes [Tc(Mm)$(CO)_3$] (1.717(2) Å) and [Re(Mm)$(CO)_3$] (1.71(1) Å) suggesting there is no deviation in thione/ thiolate tautomerism.[70] The Cu-B distance for **[Cu(Mm)(PCy_3)]** is 2.208(2) Å. This is longer than the corresponding distance in Mmp (2.153(16) Å) and shorter than in the Mai complex (2.334(1) Å). This data suggests that the Mmp ligand is best at bringing boron into close proximity with the metal, followed by Mm and finally Mai. The bridging BH bond distances 1.15(2) and 1.19(2) Å are slightly elongated in comparison to the terminal BH 1.08(2) Å this confirms that there is 3c-2e bonding between each of the bridging BH's and the metal. Each of the Cu-H distances are 1.84(2) and 1.82(2) Å this again is consistent with Mmp (1.75(2) and 1.81(2) Å) and slightly shorter than Mai (1.93(2) and 1.97(2) Å) PCy_3 complexes.

3.4.3 Synthesis of copper Bm complexes

The ligand Li[Bm] was synthesised according to the literature procedure outlined by Parkin.[146] Equimolar quantities of PR_3, CuCl and Li[Bm] were added into methanol and stirred over 24 hours after which a white precipitate was present. The resultant products were obtained in good yields, 71% for **[Cu(Bm)(PPh$_3$)]** and 55% for **[Cu(Bm)(PCy$_3$)]**. Both products were analysed by powder film IR spectroscopy these showed bands at 2381 and 2260 cm^{-1} for **[Cu(Bm)(PPh$_3$)]** and 2383 and 2288 cm^{-1} for **[Cu(Bm)(PCy$_3$)].** This again suggests both terminal and bridging BH's are present, in comparison to ^{Me}Bai complexes the bridging BH stretching frequency is higher suggesting a weaker B-H-Cu interaction.

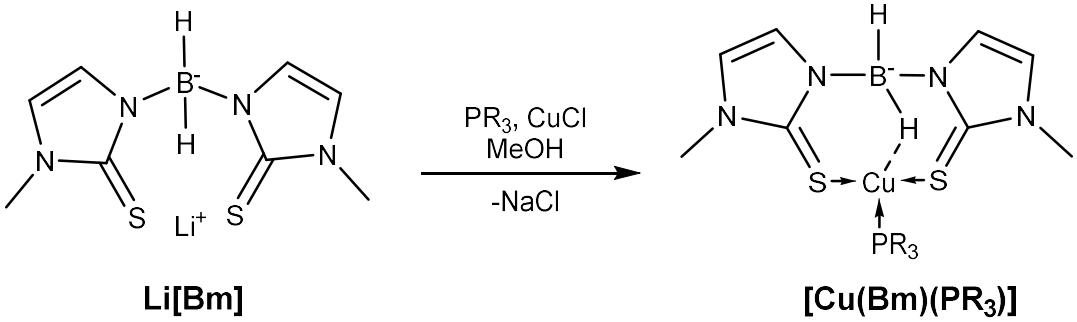

Scheme 3.22. Synthesis of **[Cu(Bm)(PR$_3$)]** complexes (PR_3 = PPh_3 and PCy_3)

^{1}H, ^{1}H{^{11}B}, ^{11}B, ^{11}B{^{1}H}, ^{13}C{^{1}H}, ^{31}P{^{1}H}, COSY, HSQC and HMBC NMR experiments were run in $CDCl_3$. ^{11}B NMR resonances for **[Cu(Bm)(PR$_3$)]** complexes were both triplets at −8.2 **[Cu(Bm)(PPh$_3$)]** and −8.6 ppm **[Cu(Bm)(PCy$_3$)]** . Further confirmation of the presence of hydrogen in both complexes was given by the ^{11}B{^{1}H} experiment in which each triplet resolved to a singlet. Further to this, there was a decrease in the half height widths. ^{31}P{^{1}H} NMR data indicates weakly coordinating phosphines with chemical shifts of −2.73 **[Cu(Bm)(PPh$_3$)]** and 13.9 ppm **[Cu(Bm)(PCy$_3$)]** this suggests that the Bm chelate is much better at relieving copper's electron deficiency than the Mm ligands. This trend is consistent with that observed for Mmp and Bmp complexes and Mai and ^{Me}Bai complexes. The ^{1}H spectra shows broad peaks that resolve to singlets in the ^{1}H{^{11}B} spectra at 3.44 **[Cu(Bm)(PPh$_3$)]** and

3.36 ppm **[Cu(Bm)(PCy$_3$)].** These are more protic in character than for the Mm BH_3 protons, this is consistent with the trends observed for Mmp and Bmp, and Mai and ^{Me}Bai.

Table 3.13. Selected spectroscopic data for **[Li(Bm)]** and **[Cu(Bm)(PR$_3$)]** complexes. *NMR chemical shifts record as ppm and (h.h.w.) in Hz. Powder film IR data in cm^{-1}, (t)-terminal and (b)-bridging BH's*

Compound	$^{11}B\{^1H\}$ NMR	$^{31}P\{^1H\}$ NMR	$^1H\{^{11}B\}$ NMR BH_n	$^{13}C\{^1H\}$ NMR C=S	IR B–H
[Li(Bm)]	-	-	3.19	163.3	2439
[Cu(Bm)(PPh$_3$)]	−8.23 (270)	−2.73	3.44	161.0	2381 (t) / 2260 (b)
[Cu(Bm)(PCy$_3$)]	−8.60 (286)	13.9	3.36	160.9	2383 (t) / 2288 (b)

X-ray quality crystals of **[Cu(Bm)(PPh$_3$)]** were grown from the slow evaporation of a concentrated methanol solution. The copper centre is host to one Bm and one PPh_3 ligand. The PPh_3 ligand coordinates via an L-type interaction and the Bm ligand has 2 L-type interactions via the sulfur donors and a single B-H-M 3c-2e bond, the second BH bond is not involved with bonding to the metal. The Cu-P bond distance was recorded as 2.223(1) Å this is similar the Cu-P distance for **[Cu(Bmp)(PPh$_3$)]** 2.216(3) Å and shorter than the distance for **[Cu(^{Me}Bai)(PPh$_3$)]** 2.1834(4) Å. This suggests the overall the Bm and Bmp ligands have a greater effect on reducing copper's electron deficiency than ^{Me}Bai. The Cu-S distances are 2.2936(9) and 2.2900(8) Å this is slightly longer when compared to the Cu-S distance for **[Cu(Mm)(PCy$_3$)]** 2.2515(3) Å.

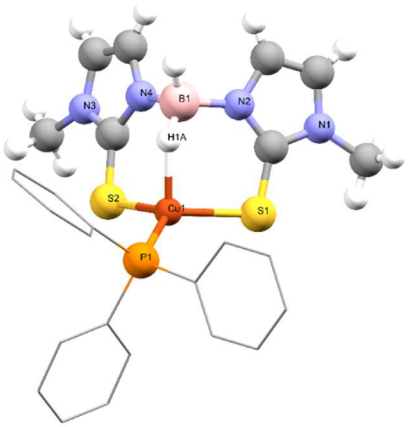

Figure 3.13. SC-XRD structure for **[Cu(Bm)(PPh$_3$)].** Hydrogens on Ph rings have been omitted for clarity.

The Cu-B distance in **[Cu(Bm)(PPh$_3$)]** is 2.745(3) Å. This represents an increase when compared to **[Cu(Mm)(PCy$_3$)]** in which the corresponding distance is 2.208(2) Å. The increase in Cu-B bond distance is consistent with the difference in coordination mode between the two complexes from two 3c-2e bond to one 3c-2e bond. The distance is in fact closer to that of **[Cu(Bmp)(PPh$_3$)]** 2.7479(15) Å which is consistent with its κ^3-S,S,H coordination mode. The BH bond lengths are of similar distances and fall within the region of uncertainty of each other. This is different to the **[Cu(Mm)(PCy$_3$)]** in which the terminal and bridging BH units have clearly distinguishable bond distances. This small difference between the BH distances is in line with the IR stretching frequencies as the bridging BH band in the spectrum for the complex **[Cu(Bmp)(PPh$_3$)]** is much higher than that of **[Cu(Mm)(PR$_3$)]** complexes. Despite this, the Cu-H bond distance remains largely consistent with that of the previous complexes 1.81 Å.

Table 3.14. Selected bond distances and angles for [Cu(Bm)(PPh$_3$)]

	[Cu(Bm)(PPh$_3$)]
Cu(1)-P(1)	2.223(1)
Cu(1)-B(1)	2.745(3)
Cu(1)-S(1)	2.2936(9)
Cu(1)-S(2)	2.2900(8)
C(1)-S(1)	1.716(2)
C(5)-S(2)	1.707(3)
B(1)-N(2)	1.550(3)
B(1)-N(4)	1.554(4)
N(2)-C(1)	1.346(3)
N(2)-C(5)	1.354(3)
B(1)-H(1A)	1.14(4)
B(1)-H(1B)	1.09(4)
Cu(1)-H(1A)	1.81
S(1)-Cu(1)-P(1)	117.94(3)
S(2)-Cu(1)-P(1)	116.50(3)
S(1)-Cu(1)-S(2)	117.15(3)
Cu(1)-H(1A)-B(1)	135(3)
Cu(1)-S(1)-C(1)	101.59(8)
C(1)-S(1)-Cu(1)	101.57(9)

3.5 Chapter summary/conclusions

In this chapter a wide range of copper centred complexes bearing mono- and bis substituted borohydride ligands were synthesised. Spectroscopic data was used to characterise and compare these complexes. The complexes synthesised in this chapter have demonstrated that, in addition to the metal centres outlined in chapter 2 of this thesis, mono-supported borohydride ligands can coordinate to copper centres. The previously unexplored copper complexes have demonstrated that the mono-supported borohydride ligands can bind to the metal via either a single 3c-2e bond or via a dihydroborate interaction. This is in addition to a L-type interaction from a sulfur or nitrogen donor. The complexes synthesised have also continued to demonstrate that the presence of additional ligands around the metal will influence the coordination of mono-substituted ligands. For example, in the complexes **[Cu(Mmp)(dppe)]** and **[Cu(Mai)(PPh_3)$_2$]**, the Cu-B distance is longer when compared to the complexes **[Cu(Mmp)(PPh_3)]** and **[Cu(Mai)(PCy_3)]**. This is because the presence of additional substituents around the copper centre limit the coordination of the $[BH_n]^-$ unit to a single 3c-2e bond. The difference in coordination mode of the $[BH_n]^-$ unit from κ^2-H,H to κ^1-H is therefore a factor in the Cu-B distance. A similar observation has also been found in unsupported tetrahydroborate complexes.[151] Adding additional substituents to the borohydride unit, such as, a phenyl or methyl group has been shown to influence the B-H-M interaction. The results in this chapter suggest that adding a methyl group to the Mmp ligand produces BH protons which are more hydridic in character. Dissimilarly, adding a phenyl group results in BH hydrogens that are less hydridic in character. We envisage that the insights provided by these experiments may have further influence on design and synthesis of complexes that undergo hydride migration. This is because BH hydrogens that are more hydridic in character may have a smaller energy barrier and greater susceptibility to undergo hydride migration at metal centres. Using a supported borohydride ligand with hydrogens that are more hydridic in character could therefore result in a faster process. Alternatively, where greater control is required a phenyl group could be added to allow for greater control or to inhibit the process.

Bis substituted complexes in this chapter coordinated to the metal through 2 L-type donors and a single B-H-M interaction with either a methyl group or a second BH unit not involved in coordination. Again, in comparison to the mono-supported ligands, the B-M bond distances are longer for these complexes. This is for two reasons, firstly mono ligands are more flexible and are capable bringing the boron in closer proximity to the metal in comparison to bis substituted ligand and secondly the coordination of a second donor atom increases the electron count of the metal centre and therefore decreases the number of potential 3c-2e bonds. This results in a single B-H-M interaction which is a comparative change in coordination mode of the $[BH_n]^-$ (from κ^2-H,H to κ^1-H) and this results in an increased M-B bond distance.

Throughout this chapter, copper complexes using the mercaptopyridyl, methimazoyl and azaindoyl scaffolds were synthesised. The three separate scaffolds gave varying degrees of interaction with the copper centre. The ligands Mm and Mmp which both contained sulfur donors, appeared to be most effective at bringing the $[BH_n]^-$ group into close proximity with the metal centre. The nitrogen-supported Mai ligand gave larger B-M distances. The reason for this can be attributed to the wider bond angles provided by the sp^2hybridised nitrogen donor atom, in which, the bond angles fall close to the idealised 120°. In comparison, the Mm and Mmp ligands have sulfur donors which accommodate C-S-Cu bond angles between 96° and 102° as measured in their corresponding X-ray structures. Comparing the three corresponding bis ligands (Bm, Bmp and ^{Me}Bai), again the sulfur based ligands bring the $[BH_n]^-$ unit into closer proximity with the metal centre however this difference is minor in comparison the mono ligands. This suggests that the conformational restrictions of multiple fused chelate rings gives less variation in the B-M distances.

Chapter 4: Synthesis and structure of silver and gold complexes containing a supported anionic borohydride ligand with a 3-atom bridge

4.1 Introduction

Chapter 3, of this thesis outlined the synthesis of copper complexes bearing monosubstituted borohydride ligands of which there were several existing higher substituted borohydride ligands available for comparison. In the case of silver and gold, there are less examples available for comparison. This chapter extends the investigation of these ligands down the coinage metal group for comparison with their lighter copper counterparts. Silver is one of the few elements that has examples of *mono-, bis-* and *tris-* supported borohydride complexes. Despite this, there are only a limited number of each case. As outlined in the literature review chapter of this thesis, there is just one example of a silver mono-substituted borohydride complex in the literature. The CF_3 functionalised pyrazole ligand **2.66** (Section 2.4) was added as the sodium salt to silver nitrate with two equivalents of phosphine in methanol thus forming [Ag{^{CF3}(pz{BH_3})(PR_3)$_2$}] (**2.67**).[68] The discovery of a silver complex bearing a bis-substituted borohydride ligand **[Ag(^{Ph}Bm^{Me})(PPh$_3$)]** was accidental (Scheme 4.1). This occurred when Reglinski and Spicer were exploring the synthesis of the ligand tri-methimazoyl ligand **Li[^{Ph}Tm^{Me}]**. They found that the reaction did not proceed to completion and resulted in the formation of a small amount of the corresponding bis-substituted version **Li[^{Ph}Bm^{Me}]**. The ligand impurity **Li[^{Ph}Bm^{Me}]** present in the mixture went on to form the silver compound **[Ag(^{Ph}Bm^{Me})(PPh$_3$)]**. The desired compound in this reaction was **[Ag(^{Ph}Tm^{Me})(PPh$_3$)]**, which, has a tetra substituted boron centre and therefore no possibility of B-H···M bond formation. **[Ag(^{Ph}Bm^{Me})(PPh$_3$)]** was separated by crystallisation of the complex from the **[Ag(^{Ph}Tm^{Me})(PPh$_3$)]** mixture. As a result of only small quantities of crystals produced, the complex was only assessed via SC-XRD and ESI techniques. Only structural analysis of a bis compound exists, the targeted synthesis and full characterisation of any silver complex containing a bis-substituted borohydride ligand has still yet to be reported. The crystal structure for **[Ag(^{Ph}Bm^{Me})(PPh$_3$)]** revealed a trigonal planar metal centre

which contained two thiourea donors and one phosphine donor where the sum of the bond angles is equal to 359.16°. The BH bond then coordinates to the metal from above the trigonal plane. The distances for the bonds are 1.109, 2.164 and 3.070(2) Å for B-H, Ag-H and Ag-B respectively.[152]

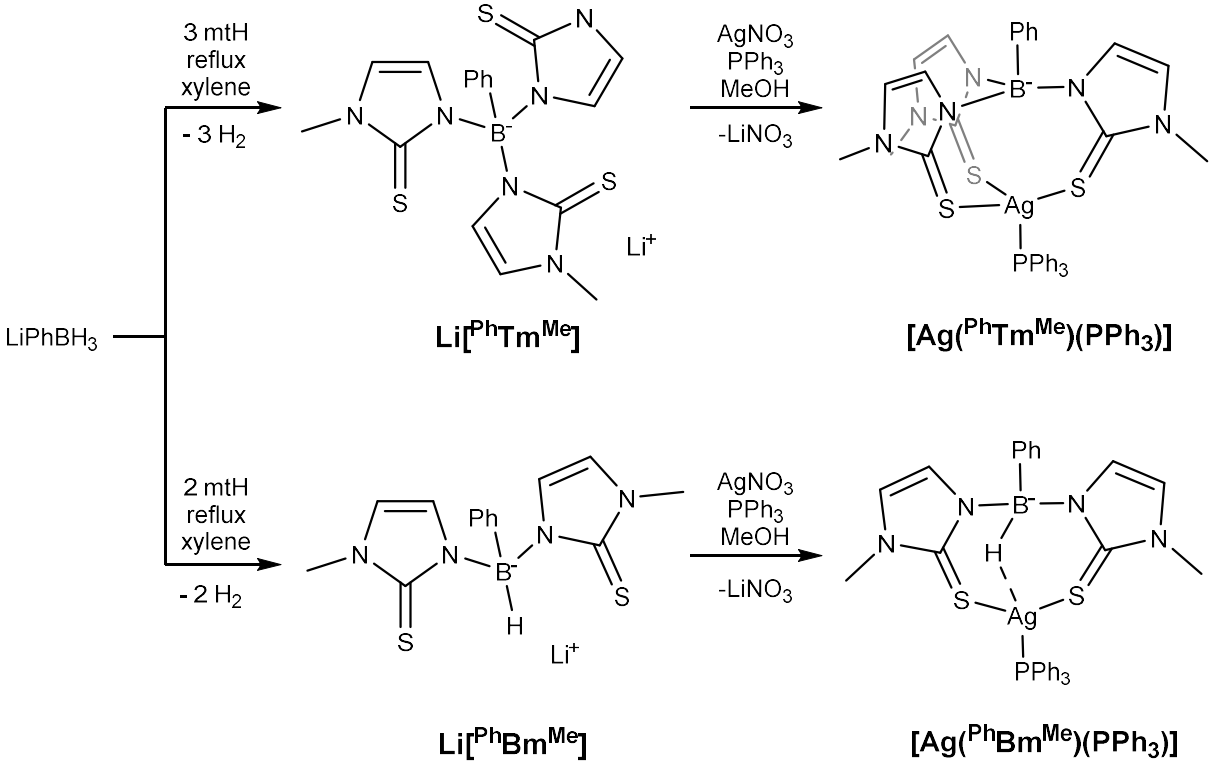

Scheme 4.1. Synthesis of silver complexes bearing both tris and bis supported borohydride ligands based on methimazole.

Further examples for silver scorpionate complexes centre around the Tm and Tp scaffolds (Figure 4.1) of which early work by Santini and co-workers synthesised several silver complexes. The synthesis of the phosphine compounds was achieved by either equimolar quantities of the ligand salt, phosphine and [Ag(NO_3)] in THF at −70 °C, or with [Ag(NO_3)] in MeOH at room temperature. For the Tm based complex, each of the three methimazole sulfur donors from the ligand Tm coordinate to the metal (κ^3-S,S,S), therefore, there is no interaction between the metal and the BH bond is observed in this case as the BH bond is orientated away from the metal centre (as indicated in Figure 4.1, middle).[153] Further studies showed that complexes could be synthesised without the need for additional phosphine, again the synthesis proceeds using silver nitrate as the metal precursor in methanol. The resultant dinuclear

complex $[Ag(Tm)]_2$ was fully characterised, SC-XRD studies gave a dimeric structure as shown in Figure 4.1. The ligand Tm coordinates in a κ^3-N,N,H,μ-N manor, the BH is orientated towards the metal centre and there is a Ag-H distance of 2.83(5) Å which is longer that reported for the $[Ag(^{Ph}Bm^{Me})(PPh_3)]$ complex at 2.1643 Å.[12,138,154]

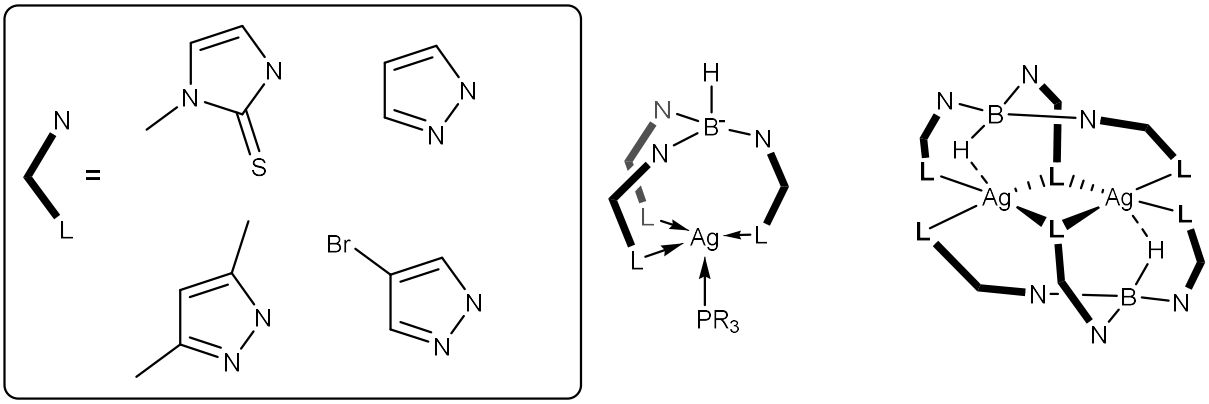

Figure 4.1. Left – Ligand scaffolds utilised in supported borohydride ligands Middle – Monomeric silver phosphine complex, Right – structure of a dimeric silver scorpionate compound.

Rabinovitch found that in the presence of PPh_3, the ligand salt **Na[Tm^{tBu}]** and silver nitrate in methanol formed complex **[Ag(Tm^{tBu})(PPh$_3$)]** (Scheme 4.2).[144] This complex was fully characterised and SC-XRD studies revealed a distorted tetrahedral arrangement around the metal centre. A similar reaction was also performed without the presence of phosphine leading to the formation of the complex **[Ag(Tm^{tBu})]$_2$**. Reactivity studies on this complex showed it was a suitable ligand transfer reagent (via transmetalation); this was demonstrated using $CoBr_2$. The distance between the Ag and H nuclei in **[Ag(Tm^{tBu})]$_2$** was reported to be 2.52(2) Å.

The silver complex **[Ag(Tm^{Et})(PPh$_3$)]** was synthesised from $AgBF_4$ and **[Na(Tm^{Et})]** in THF with excess phosphine (Scheme 4.2).[145] VT studies of the resultant complex show that one of the methimazole rings is hemilabile and that both three and four coordinate silver were present in solution (where the scorpionate ligand interchanges between κ^2-*S,S* and κ^3-*S,S,S* coordination modes). No crystal structure was reported for this complex and a single BH stretching frequency was reported in the solid

state IR spectrum at 2435 cm^{-1}.This suggests that there is no coordination of the BH bond to the metal centre since this is typical of a terminal B-H stretch.

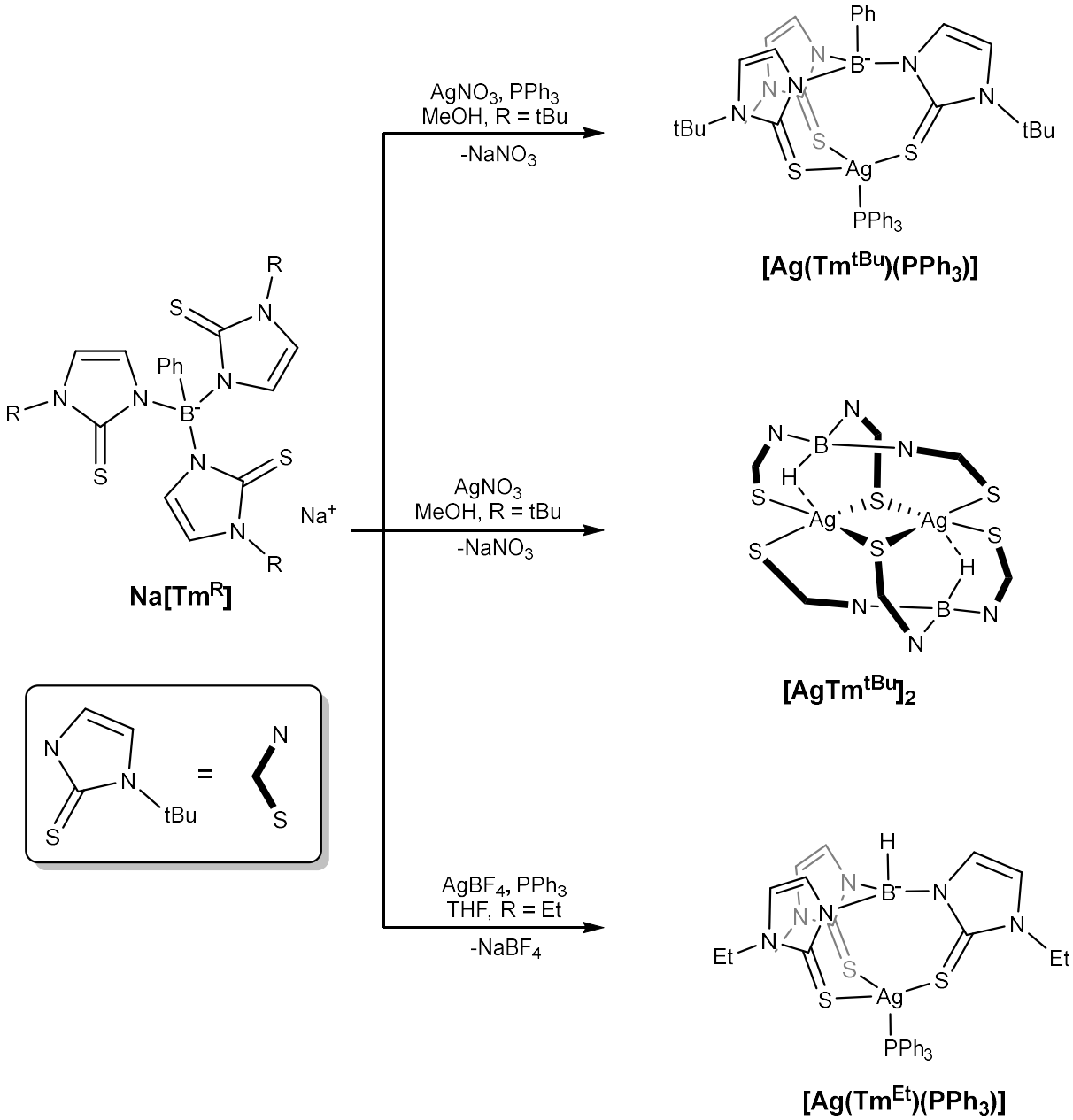

Scheme 4.2. Synthesis of silver complexes reported by Rabinovich bearing the ligand Tm^R

In 2013, our group demonstrated using the hybrid scorpionate ligand ^{mp}Bm that a BH bond could bind to silver in preference of a methimazole sulfur donor. The ligand salt **Na[^{mp}Bm]** was synthesised by the addition of mercaptopyridine to **Na[Bm]** in toluene under reflux. The respective PCy_3 and PMe_3 complexes were synthesised by addition of the ligand salt **Na[^{mp}Bm]**, PR_3 and $AgNO_3$ in THF. The

product, **[Ag(mpBm)(PR3)]**, was purified by uptake into a concentrated DCM solution and precipitation by addition of hexane. Crystals were obtained for the **[Ag(mpBm)(PCy3)]** complex and the structure was solved using SC-XRD analysis. This confirmed that a single mt unit was in fact pendant and that coordination of the BH moiety to the metal is preferred. M-H, B-H and M···B distances are 2.21(3), 1.12(2) and 3.110(2) Å respectively.[155]

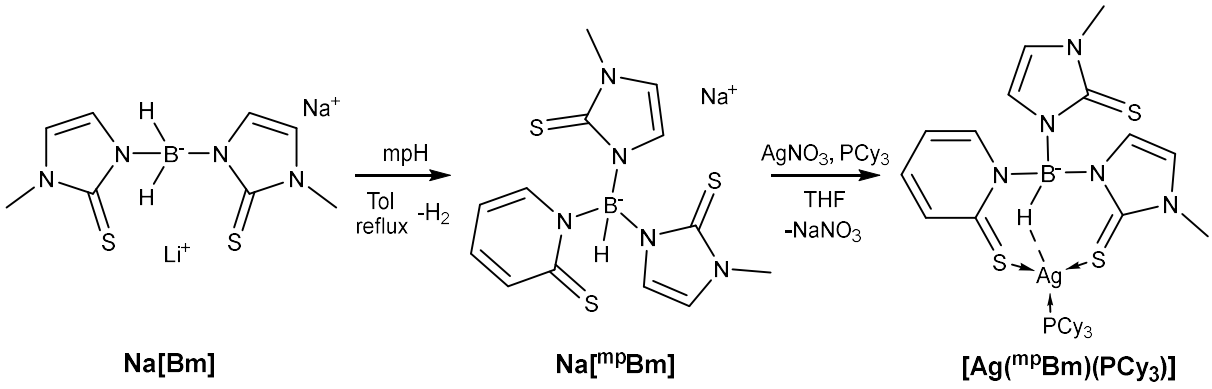

*Scheme 4.3. Synthesis of the flexible scorpionate **Na[mpBm]** from **Na[Bm]** and subsequent addition to silver to make complex **[Ag(mpBm)(PCy3)]** showing preference for κ3-S,S,H coordination over κ3-S,S,S.*

4.2 Synthesis of silver complexes

4.2.1 Introduction

Given the limited prevalence of silver complexes bearing mono-supported borohydride ligands in the literature, it was decided to extend our investigations into the coordination of such ligands to include silver centres. This chapter intends to continue the investigations of mercapto-pyridyl and azaindoyl scaffolds as supports for the $[BH_n]^-$ unit. This will be achieved by synthesising the isoleptic complexes of those synthesised in Chapter 3 of this thesis. Spectroscopic data from these complexes will continue to provide a useful insight into the coordination of these complexes and will aid in their comparison with examples from the literature and those which have already been synthesised in this thesis. Again, additional non coordinating substitutions have been made to the borohydride unit in the case of the Mmp scaffolds and the effect this has on the coordination of the $[BH_n]^-$ unit has been investigated.

Following the exploration of the silver complexes this chapter will extend the investigation to include gold complexes bearing monosubstituted borohydrides. This will therefore allow for comparisons to between all complexes in the coinage metal group.

4.2.2 Mmp complexes

In targeting the complexes **[Ag(Mmp)(PPh$_3$)]** and **[Ag(Mmp)(PCy$_3$)]**, silver(I) nitrate ($AgNO_3$) was selected as the metal precursor as it had been previously been used in the synthesis of tris-supported borohydride complexes which utilised methanol as a solvent.[138,144] The use of methanol as a solvent is particularly useful for the synthesis of copper complexes as the product is insoluble, and this trend continues with the generation of the complexes **[Ag(Mmp)(PPh$_3$)]** and **[Ag(Mmp)(PCy$_3$)]**. $AgNO_3$ was added to equimolar quantities of **Na[Mmp]** and either triphenyl phosphine (PPh_3) or tricyclohexyl phosphine (PCy_3) in methanol (Scheme 4.4). The reaction itself was shielded from light by covering the Schlenk flask completely in foil as a precautionary measure due to the documented light sensitivity of silver(I) complexes.[156] The synthesis in both cases gave black powders which were pure by NMR spectroscopy. Further purification of the complexes was achieved by extraction using a 3:1 pentane/DCM solution, removal of the solvent under vacuum gave the pure complexes as a white powder which again darkened over the course of a few days. The reaction gave yields of 71% and 48% for **[Ag(Mmp)(PPh$_3$)]** and **[Ag(Mmp)(PCy$_3$)],** respectively.

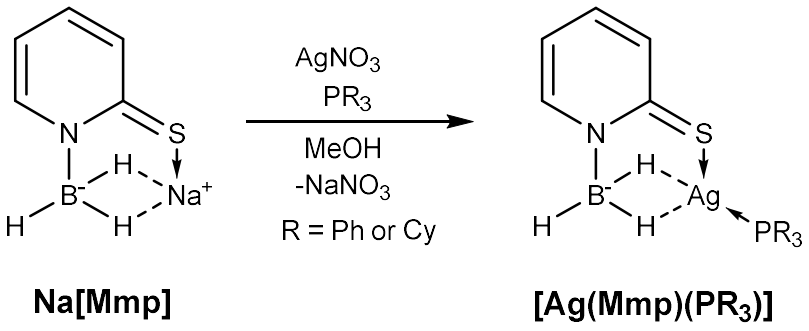

Scheme 4.4. Synthesis of silver Mmp complexes

For each of the complexes, a small amount of product was subsequently taken up into $CDCl_3$ for analysis by NMR spectroscopy. The ^1H spectra showed a clear shift for the mp protons from that of the free ligand salt which confirms the coordination of the ligand to silver. The resonances corresponding to the BH_3 protons were again present as a single broad peak which resolves to a sharp singlet in the $^1H\{^{11}B\}$ experiments at 3.23 **[Ag(Mmp)(PPh$_3$)]** and 3.31 ppm **[Ag(Mmp)(PCy$_3$)]** (Table

4.1). In comparison the $^{1}H\{^{11}B\}$ spectra for both **[Cu(Mmp)(PPh$_3$)]** and **[Cu(Mmp)(PCy$_3$)]** complexes have BH_3 resonances of 2.64 and 2.42 ppm respectively. This indicates that the BH protons are more protic in character when compared to the **[Cu(Mmp)(PR$_3$)]** complexes (Table 4.1). The NMR spectra confirmed that one equivalent of phosphine was present, with a relative integration of 15 H for **[Cu(Mmp)(PPh$_3$)]** and 33 H for **[Cu(Mmp)(PCy$_3$)]**. The $^{31}P\{^{1}H\}$ for the complexes show resonances that are more downfield than that of the Cu complexes, a singlet is present at 16.1 ppm **[Ag(Mmp)(PPh$_3$)]** and a doublet of doublets (dd) is present at 40.5 ppm for the complex **[Ag(Mmp)(PCy$_3$)]**. The apparent doublet of doublets signal in the spectra for **[Ag(Mmp)(PCy$_3$)]** consisted of a superposition of two doublets, which is a result of both coupling to Ag^{107} and Ag^{109} nuclei ($^{1}J_{PAg107}$ = 452 and $^{1}J_{PAg109}$ = 523 Hz) (Figure 4.2).

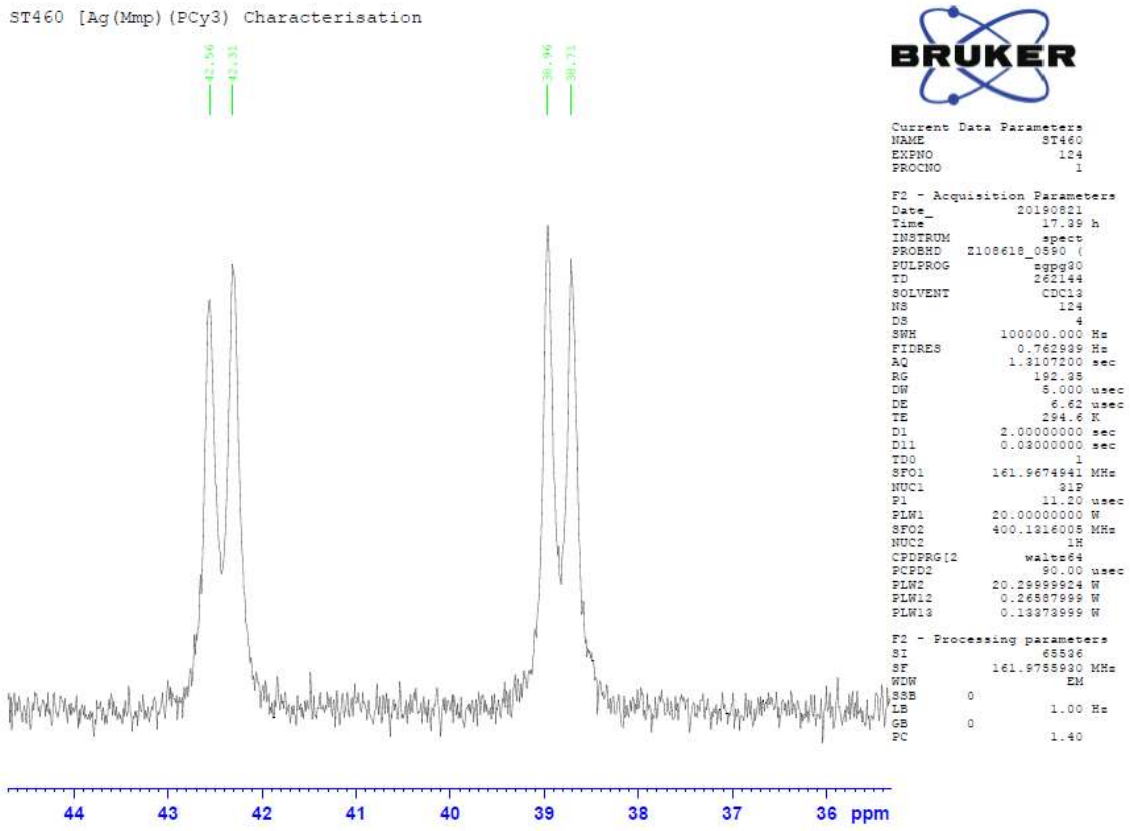

Figure 4.2. *$^{31}P\{^{1}H\}$ spectra of **[Ag(Mmp)(PCy$_3$)]** showing Ag^{107} and Ag^{109} splitting*

The $^{13}C\{^1H\}$ spectra was assigned with the assistance of both HSQC and HMBC experiments. The C=S resonances for both complexes is the same at 174.6 ppm representing a slightly more shielded carbon than in the **[Cu(Mmp)(PPh_3)]** complex. The ^{11}B spectra, again gives more shielded resonances at −16.3 and −15.7 ppm for the PPh_3 and PCy_3 complexes when compared to their copper analogues. Both carbon and boron nuclei possessing both more shielded resonances, this suggests that on comparison to the copper, the overall strength of coordination of the Mmp ligand to the silver metal centre is weaker. Further analysis of the metal complexes was carried out using an ATR spectrometer. Both terminal and bridging BH stretching bands were observed for the PPh_3 complex at 2391 and 2067 cm^{-1} respectively. Due to the weak nature of the peaks only a terminal BH band could be identified at 2401 cm^{-1} for **[Ag(Mmp)(PCy_3)]**. Both complexes were analysed by MS. The molecular ion in both cases could not be observed, however, fragmentation in both cases gave loss of the BH_2 fragment and the [M-BH_2] could clearly be observed with two peaks of approximately equal intensities for both complexes at m/z = 480.01/482.01 **[Ag(Mmp)(PPh_3)]** and m/z = 498.15/500.15 for **[Ag(Mmp)(PCy_3)]**. In both cases the isotopic distribution of silver leads to two molecular ion peaks of equal intensities, this is due to the natural abundance of both Ag^{107} and Ag^{109} being approximately equal. This fragmentation pattern is also consistent with that observed in the copper chapter as **[Cu(Mmp)(PPh_3)]** gave a $[M\text{-}BH_2]^+$ ion at m/z = 436.03 and **[Cu(Mmp)(PCy_3)]** gave an $[M]^+$ ion at m/z = 467.2.

Table 4.1. Spectroscopic data for [Ag(Mmp)(PR_3)] complexes synthesised and examples for comparison. NMR chemical shifts record as ppm and (h.h.w.) in Hz. Powder film IR data in cm^{-1}, (t)- terminal and (b)-bridging BH's.

Compound	$^{11}B\{^1H\}$ NMR	$^{31}P\{^1H\}$ NMR	$^{13}C\{^1H\}$ NMR ***C*=S**	$^1H\{^{11}B\}$ NMR BH_n	IR B–H
Na[Mmp]	−14.1 (44)	-	181.3	2.11	2307
[Cu(Mmp)(PPh_3)]	−13.9 (113)	4.8	175.9	2.64	2439 (t) / 2078 (b)
[Cu(Mmp)(PCy_3)]	−13.4 (90)	27.2	176.1	2.42	2448 (t) / 2085 (b)
[Ag(Mmp)(PPh_3)]	−16.3 (138)	16.1	174.6	3.23	2391 (t) / 2067 (b)
[Ag(Mmp)(PCy_3)]	− 15.7 (151)	40.6	174.6	3.31	2401 (t) / N. O. (b)

X-ray quality single crystals for the complex **[Ag(Mmp)(PCy_3)]** were obtained by slow evaporation of a concentrated solution of MeCN. The SC-XRD crystal structure confirmed the presence of the complex

and one equivalent of MeCN that was disordered. To the silver centre the ligand, Mmp coordinates κ^3-S,H,H in addition to the coordination of a single tricyclohexyl phosphine ligand. The structure is shown in Figure 4.3. The Mmp ligand was disordered over two positions in which the sulfur donor site and dihydroborate interaction were orientated 180° from each other and found to be in a ratio of 68:32. In the major component, considering the boron as the site of attachment for the dihydroborate interaction the sum of the bond angles is 359.68° indicating a trigonal planar arrangement. This, however, is distorted from the idealised geometry as a wide P-Ag-B bond angle is observed at 157.4(4)° which is a significant deviation in comparison to the expected 120°. In comparison the complex **[Cu(Mmp)(PCy_3)]** gave tighter bond angle in the major component 140.3(4)°. The B-H hydrogens were located in the difference map and refined with the riding model. This showed that two BH bonds coordinate to the metal, and subsequently the third hydrogen is orientated away from the metal centre.

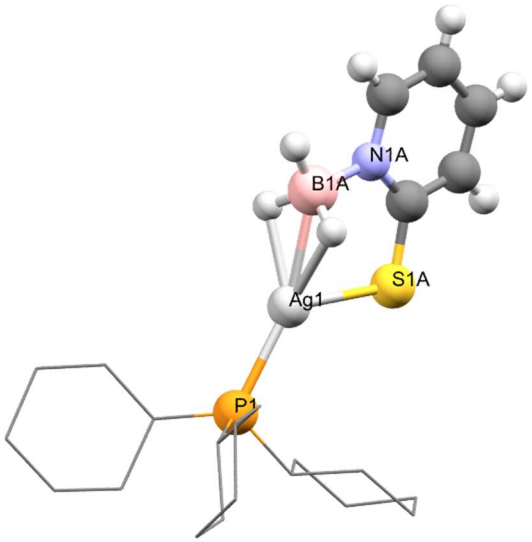

*Figure 4.3. SC-XRD structure for **[Ag(Mmp)(PCy_3)]** the disorder solvent, minor component and* Hydrogens on Cy rings have *been removed for clarity.*

The Ag-P bond distance was measured as 2.3674(7) Å. This is slightly shorter in comparison to the [Ag(^{mp}Bm)(PCy_3)] complex in which a distance of 2.3836(6) Å is reported and shorter again in comparison to the nitrogen donor complex [Ag(Mp^{CF3})(PPh_3)$_2$] complex **2.66** and [Ag(Tm^{tBu})(PPh_3)] which reports Ag-P bond lengths in a disordered structure of 2.428(1)/2.413(1) and 2.474(1)/2.455(1)

Å for [Ag(Mp^{CF3})(PPh_3)] and 2.424 Å for [Ag(Tm^{tBu})(PPh_3)]. Again when switching between mono-, bis- and tris- supported ligands a difference in P-Ag distance is expected as both these complexes are more saturated and the phosphine in this case is required for greater electron donation, which is consistent with ^{1}H NMR data.[68,144] The Ag-B distance is 2.42(2)/2.50(2) Å for both major and minor components despite the boron being negatively charged, this distance is consistent with the neutral unsupported $NMe_3{\cdot}BH_3$ ligand which binds in a similar manner to our ligand, in which Weller reports the Ag-B distance as 2.453(4) Å.[157] Weller described an asymmetric BH_2 bridging unit within their complex where the reported BH distances were 1.20(3), 1.07(3) and 1.06(5) Å. In comparison the BH bond distances for the major component in **[Ag(Mmp)(PCy_3)]** were 1.13(3), 1.20(3) and 1.10(3) Å. These are similar suggesting that the BH_2 unit of the Mmp ligand also binds asymmetrically to the silver centre. The C-S distances, 1.721(2)/1.735(3) Å, are consistent with the distances recorded for the copper complex **[Cu(Mmp)(PCy_3)]** (1.7244(17)/1.751(13) Å), the similarity between these isoleptic complexes indicates that the bonding description in terms of thione/thiolate tautomerism remains the same, hence, the C-S bond is more single bond in character when compared to the ligand **MpH** (bearing no $[BH_n]^-$ group).

*Table 4.2. Selected bond distances (Å) and angles (°) for the complex **[Ag(Mmp)(PCy_3)]***

	[Ag(Mmp)(PCy_3)]
Ag (1)-P(1)	2.3674(7)
Ag(1)-B(1)	2.42(2)/2.50(2)
Ag(1)-S(1)	2.546(2)/2.478(8)
C(1)-S(1)	1.721(2)/1735(6)
B(1)-N(1)	1.57(1)/1.57(2)
N(1)-C(1)	1.361(2)/1.361(2)
B(1)-H(1A)	1.13(3)*
B(1)-H(1B)	1.20(3)*
B(1)-H(1C)	1.10(3) *
Ag(1)-H(1A)	2.09(3)*
Ag(1)-H(1B)	2.05(3)*
S(1)-Ag(1)-P(1)	122.78(5)/152.7(2)
S(1)-Ag(1)-B(1)	79.5(4)/80.3(5)
P(1)-Ag(1)-B(1)	157.4(4)/126.8(5)
$\Sigma_{\text{angles around Ag}}{}^4$	359.68/359.8
C(1)-S(1)-Ag(1)	102.2(1)/102.3(3)
N(1)-B(1)-Ag(1)	111.0(8)/109(1)

*The hydrogens in the minor component could not be reliably located

4.2.3 ^{R}Mmp complexes

In addition to Mmp, both ^{Me}Mmp and ^{Ph}Mmp ligands were added to silver utilising the same procedure as used for the synthesis of **[Ag(Mmp)(PR$_3$)]** complexes. The ligand salts **Li[^{Me}Mmp]** and **Li[^{Ph}Mmp]** were both added to equimolar quantities of either tricyclohexyl phosphine or triphenyl phosphine and one equivalent of $AgNO_3$ in methanol (Scheme 4.5). The reactions were all left to stir between 24 and 72 hours. This led to the precipitation of a black powder which was separated from the reaction mixture by filtration. The reaction mixtures did also contain a small amount of product, as determined by NMR spectroscopy and so these were left to stand in attempt to obtain single crystals suitable for analysis. Unfortunately, due to the stability of these complexes, the complexes degraded and the clear solution again turned black. The black precipitates gave spectroscopically pure NMR spectra, however, it was apparent that they needed further purification. The complexes could indeed be further purified by extracting into a 3:1 pentane/DCM solution, removing volatiles in vacuum and subsequent washing of the resulting solids with methanol. These reactions gave comparably lower yields with yields of 38 – 64 % recorded. The workup gave white powders which would again turn to black over a few days. The colour black indicates the presence of silver(0) and suggests that the ligand reduces the metal to this oxidation state.

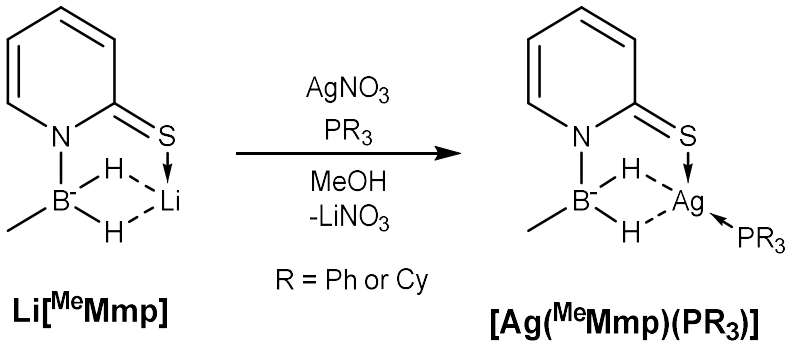

Scheme 4.5. Synthesis of the [Ag(^{Me}Mmp)(PR$_3$)] complexes

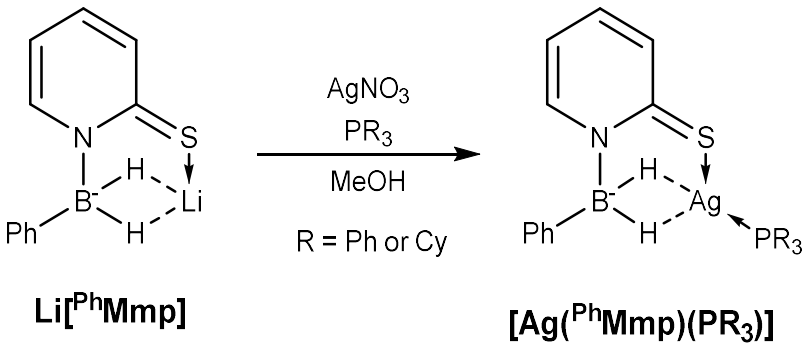

Scheme 4.6. Synthesis of the [Ag(^{Ph}Mmp)(PR_3)] complexes

All four complexes were all fully characterised by ^{1}H, $^{1}H\{^{11}B\}$, ^{11}B, $^{11}B\{^{1}H\}$, $^{13}C\{^{1}H\}$ and $^{31}P\{^{1}H\}$ NMR spectroscopy with the exception of the **[Ag(^{Me}Mmp)(PPh_3)]** complex. In the $^{13}C\{^{1}H\}$ experiment it was clear that the complex had degraded over the course of the experiment (10,000 scans/ 9 hours acquisition) reducing the reliability of the assignments. Selected spectroscopic data for these complexes is presented in Table 4.3. The proton NMR for all complexes showed a single resonance integrating to 2H for the BRH_2 environments and again the resonances for the methyl complexes **[Ag(^{Me}Mmp)(PPh_3)]** and **[Ag(^{Me}Mmp)(PCy_3)]** were more hydridic with their respective resonances appearing at 3.46 and 3.24 ppm in comparison to the **[Ag(^{Ph}Mmp)(PPh_3)]** and **[Ag(^{Ph}Mmp)(PCy_3)]** complexes at 4.23 and 4.03 ppm, respectively. On coordination to silver, in comparison to the ligand salts, the complexes exhibit slightly more shielded resonances at −10.62 ppm for **[Li(^{Me}Mmp)]**, when compared to **[Ag(^{Me}Mmp)(PPh_3)]** and **[Ag(^{Me}Mmp)(PCy_3)]** with resonances of −11.18 and −11.32 ppm respectively. **[Li(^{Ph}Mmp)]** has a resonance of −6.26 ppm which shifts to −7.26 and −7.00 ppm in the complexes **[Ag(^{Ph}Mmp)(PPh_3)]** and **[Ag(^{Ph}Mmp)(PCy_3)]**. Again, as observed with the copper ^{R}Mmp complexes no distinct splitting pattern to the adjacent hydrogen substituents is observed, the presence of the BH_2 group is therefore confirmed by the reduction in half height width from the ^{11}B to $^{11}B\{^{1}H\}$ experiments. $^{31}P\{^{1}H\}$ NMR experiments for the complexes bearing triphenyl phosphine (PPh_3) as a ligand gave singlets at 4.8 and 16.9 ppm for **[Ag(^{Me}Mmp)(PPh_3)]** and **[Ag(^{Ph}Mmp)(PPh_3)]** respectively. In contrast to this, the $^{31}P\{^{1}H\}$ NMR for complexes **[Ag(^{Me}Mmp)(PCy_3)]** and **[Ag(^{Ph}Mmp)(PCy_3)]** gave doublets at 40.5 and 39.9 ppm respectively. The presence of a doublet in

both cases is as a result of AgP coupling. However, these peaks are poorly resolved and do not display coupling for the individual Ag^{107} and Ag^{109} nuclei. The difference between complexes bearing triphenyl phosphine and tricyclohexyl phosphine may indicate that the triphenyl phosphine ligand is labile in solution on an NMR timescale and therefore no silver phosphorous coupling is observed. Tricyclohexyl phosphine as a ligand is more basic and therefore may not be as labile in comparison to triphenyl phosphine.

The mass spectra for both **[Ag(^{Ph}Mmp)(PR_3)]** and **[Ag(^{Me}Mmp)(PR_3)]** complexes were obtained using ESI mass spectrometry. The mass spectrum for **[Ag(^{Me}Mmp)(PPh_3)]**, gave two peaks of approximately equal intensities at m/z = 480.01 and 482.01 corresponding the [M-MeBH] fragment. This is a common fragmentation pattern also observed in the copper complexes. It appears that the BH_2R unit is unstable under ionisation conditions and readily leads to the fragmentation of this group. Again, the two separate peaks of equal intensity confirms that the ion retains the silver centre as silver 107 and 109 isotopes are approximately of the same natural abundance. This results in the same peak being observed for the **[Ag(^{Ph}Mmp)(PPh_3)]** complex again with gave two peaks of approximately equal intensities at m/z = 480.01 and 482.01 corresponding the $[M\text{-}PhBH]^+$ fragment. The **[Ag(^{Ph}Mmp)(PCy_3)]** complex continues the trend and again loses the $[M\text{-}PhBH]^+$ fragment giving two peaks of approximately equal intensities at m/z = 498.15 and 500.15.

Table 4.3. Spectroscopic data for silver complexes bearing the ligand ^{R}Mmp. NMR chemical shifts record as ppm and (h.h.w.) in Hz. Powder film IR data in cm^{-1}, (t)-terminal and (b)-bridging BH's

Compound	$^{11}B\{^1H\}$ NMR (h.h.w.)	$^{31}P\{^1H\}$ NMR	$^{13}C\{^1H\}$ NMR *C*=S	$^{1}H\{^{11}B\}$ NMR BH_n	IR B–H
[Li(^{Me}Mmp)]	−10.62 (70)	-	179.7	2.17	2226
[Li(^{Ph}Mmp)]	−6.26 (55)	-	182.4	3.22	2263
[Ag(^{Me}Mmp)(PPh_3)]	−11.18 (176)	4.8	N/A	3.46	2053 (b)
[Ag(^{Me}Mmp)(PCy_3)]	−11.32(236)	40.5	174.7	3.24	Not observed
[Ag(^{Ph}Mmp)(PPh_3)]	−7.26 (266)	16.0	174.3	4.23	-
[Ag(^{Ph}Mmp)(PCy_3)]	− 7.00 (263)	39.9	173.3	4.03	-

4.2.4 Mai complexes

The ligand **Na[Mai]·2MeCN** was obtained via the same synthetic procedures mentioned in Chapter 3. Addition of this ligand salt to silver was performed using a foil covered Schlenk flask in methanol with one equivalent of either tricyclohexyl phosphine or triphenyl phosphine and $AgNO_3$. Again, in both cases a black powder was formed even though it was found to be spectroscopically pure by NMR. Further purification by extraction into a DCM/pentane mixture gave a white powder which indicated that the black powder was due to the formation of silver black. The reduction of silver(I) to metallic silver is not unexpected given the reducing power of the $[BH_n]^-$ moiety. A small amount of complex was dissolved by $CDCl_3$ and assessed by ^1H NMR. The NMR spectra showed that the product that had precipitated out of solution in the reaction using triphenyl phosphine was **[Ag(Mai)(PPh_3)$_2$]**, the relative integration of the phenyl rings in the triphenyl phosphine ligand was 30H. In the reaction using the tricyclohexyl ligand, the complex formed gave a relative integration of 33H confirming that the complex which had precipitated from the reaction was **[Ag(Mai)(PCy_3)]**. The formation of the two contrasting complexes as observed with the copper complexes bearing the ligand Mai may also be attributed to the difference in steric and electronic effects of the respective phosphine ligands.

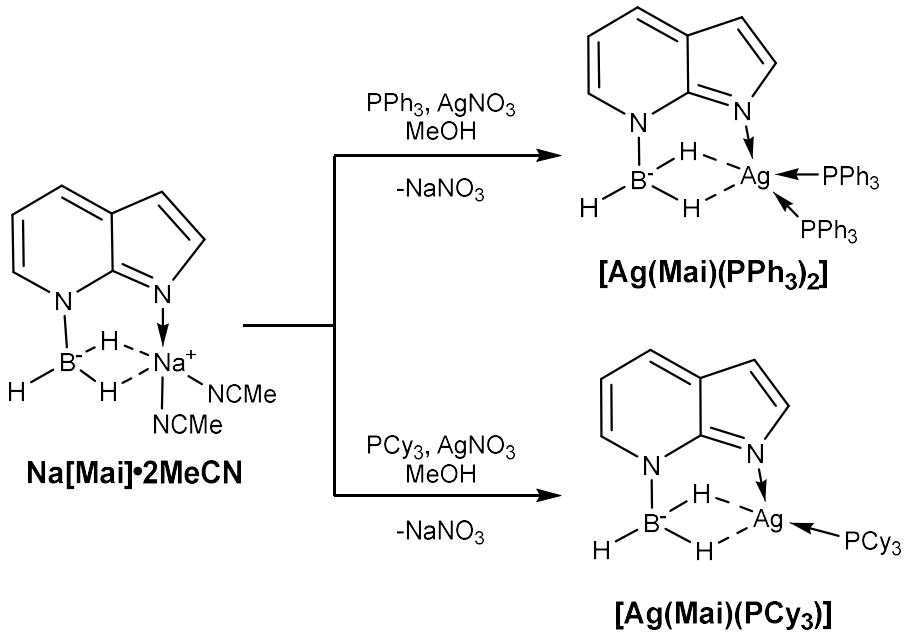

Scheme 4.7. Synthesis of complexes [Ag(Mai)(PPh_3)$_2$] and [Ag(Mai)(PCy_3)]

Further analysis of the ^{1}H NMR spectra revealed broad resonances for the BH_3 hydrogens which resolve to singlets in the $^{1}H\{^{11}B\}$ at 3.39 and 3.20 ppm for the complexes **[Ag(Mai)(PPh$_3$)$_2$]** (Figure 4.4) and **[Ag(Mai)(PCy$_3$)]** respectively. The ^{11}B NMR spectra gave one single resonance for each complex showing a broad quartet corresponding to the BH_3 environment that subsequently resolves into a singlet in experiments with ^{1}H decoupling. This confirms that the splitting is due to the presence of hydrogen around the boron nuclei. The resonances recorded for these environments were at −18.4 and −17.2 ppm which represents an upfield shift from their copper analogues.

Table 4.1. Spectroscopic data for the complex [Ag(Mai)(PPh$_3$)$_2$] and [Ag(Mai)(PCy$_3$)] and examples for comparison. NMR chemical shifts record as ppm and (h.h.w.) in Hz. Powder film IR data in cm−1, (t)- terminal and (b)-bridging BH's.

Compound	$^{11}B\{^{1}H\}$ NMR (h.h.w.)	$^{31}P\{^{1}H\}$ NMR	$^{1}H\{^{11}B\}$ NMR BH_n	IR B–H
[Na(Mai)]	−16.8	-	2.4	2320
[Ag(Mai)(PPh$_3$)$_2$]	−18.4 (182)	9.12	3.39	2373(t)/2174(b)
[Ag(Mai)(PCy$_3$)]	−17.2 (174)	41.8	3.20	2373(t)/ 2190(b)

The $^{31}P\{^{1}H\}$ resonances were shifted downfield in comparison to the **[Cu(Mai)(PR$_3$)$_n$]** complexes. The complex **[Ag(Mai)(PPh$_3$)$_2$]** also has a more upfield resonance at 9.12 ppm when compared to **[Ag(Mmp)(PPh$_3$)]** at 16.1 ppm. This is a consequence of the formation of the bis phosphine as each phosphine is not required to coordinate as strongly as a singly coordinating PPh_3 ligand. Another factor in determining the PPh_3 resonance is attributed to the strength of the Mai chelate which has a nitrogen donor in comparison to the Mmp chelates which have sulfur donors. This is more apparent in the PCy_3 complex. The ^{31}P resonance for PCy_3 in **[Ag(Mai)(PCy$_3$)]** is observed at 41.8 ppm exhibits the same splitting pattern in which two doublets are observed corresponding to splitting with ^{107}Ag and ^{109}Ag nuclei ($^{1}J_{PAg107}$ = 597 Hz, $^{1}J_{PAg109}$ = 686 Hz). In comparison to **[Ag(Mmp)(PCy$_3$)]** in which the $^{31}P\{^{1}H\}$ NMR resonance was recorded at 40.6 ppm ($^{1}J_{PAg107}$ = 452 Hz, $^{1}J_{PAg109}$ = 523 Hz) the complex **[Ag(Mai)(PCy$_3$)]** exhibits a less shielded resonance and higher coupling constants indicating a stronger silver-phosphorous bond. This again suggests that, as found in copper complexes, the Mai chelate is overall

a slightly weaker one. Powder film IR spectroscopy again shows the presence of both terminal and bridging hydrogens, confirming that the BH_3 unit does interact with the metal centre in the solid state.

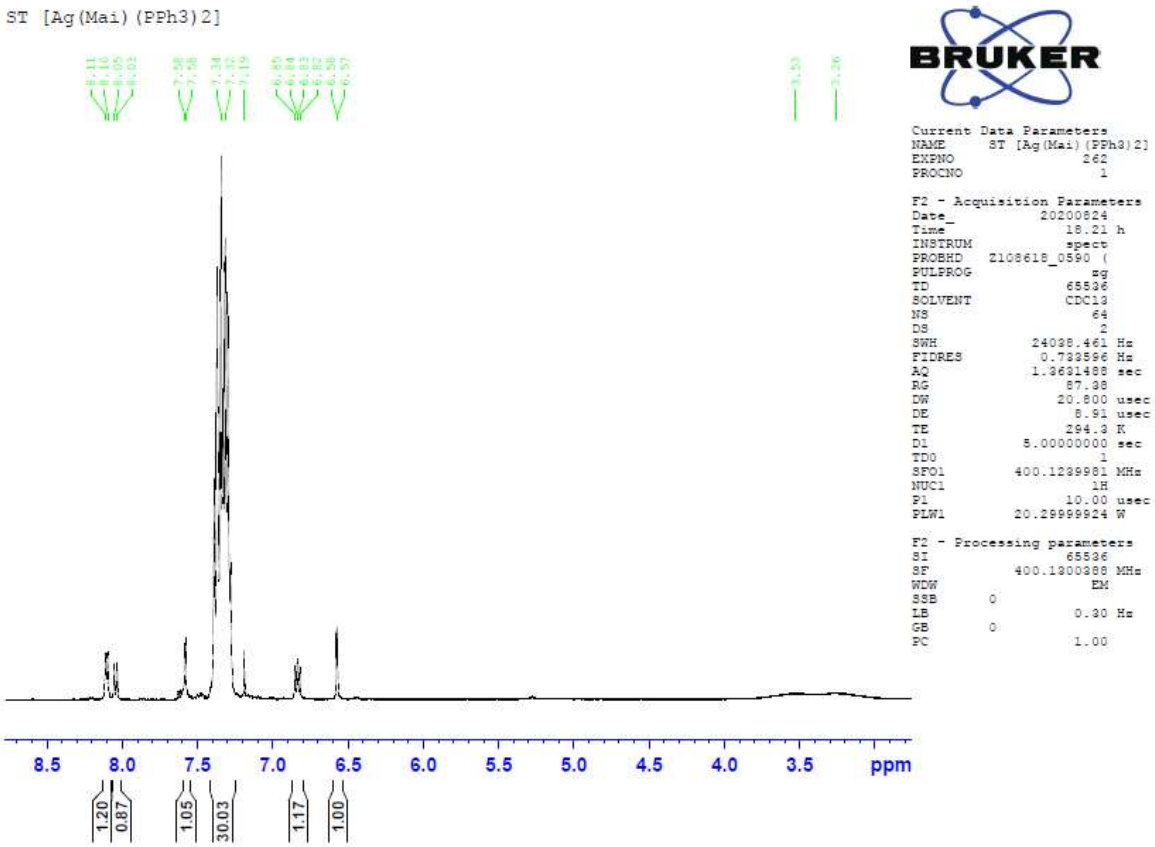

Figure 4.4. *^{1}H NMR spectra of* ***[Ag(Mai)(PPh$_3$)$_2$]***

X-ray quality crystals for the complexes **[Ag(Mai)(PPh$_3$)$_2$]** and **[Ag(Mai)(PCy$_3$)]** were grown from the slow evaporation of a concentrated methanol solution, after which their structures were obtained from diffraction studies (Figure 4.5). The structure for the complex **[Ag(Mai)(PCy$_3$)]** is very similar to that of **[Cu(Mai)(PCy$_3$)]** in which a single tricyclohexyl ligand coordinating to the silver centre and a Mai ligand which has a tridentate coordination mode (κ^3-N,H,H). Considering the boron as the point of attachment for the dihydroborate interaction, the geometry of the complex has a distorted trigonal planar arrangement in which the sum of the bond angles around the silver centre is 359.57° (Table 4.5). These bond angles, however, exhibit significant distortion from the idealised 120° for a trigonal planar geometry. This discrepancy appears to be dictated by the tight N-Ag-B angle of the Mai chelate

which is 73.38(4)° allowing for the much wider P-Ag-N and P-Ag-B bond angles of 151.48(3)° and 134.71(3)°, respectively. The crystal structure for **[Ag(Mai)(PPh$_3$)$_2$]** confirms the presence of two coordinating triphenyl phosphine ligands and a single Mai ligand which coordinates via a κ^2-N,H coordination mode (Figure 4.5). Again, as with the complex **[Cu(Mai)(PPh$_3$)$_2$]**, this results in a distortion of the N-Ag bond in which the bond does not extend along the same direction as the aromatic plane of the azaindoyl ring. The overall geometry of the complex gives a distorted trigonal pyramidal arrangement (ignoring the BH_3 unit) in which both triphenyl phosphine ligands and the nitrogen donor of the Mai ligand coordinate on the trigonal plane. The sum of these bond angles is 358.51°, the P-Ag-P bond angle is much closer to the idealised geometry at 120.85°. This is because the final coordination site in the axial position is occupied by the 3c-2e BH-M interaction originating from the Mai ligand which gives a slightly tighter than right angle N-Ag-H bond angle recorded as 82.9(7)°.

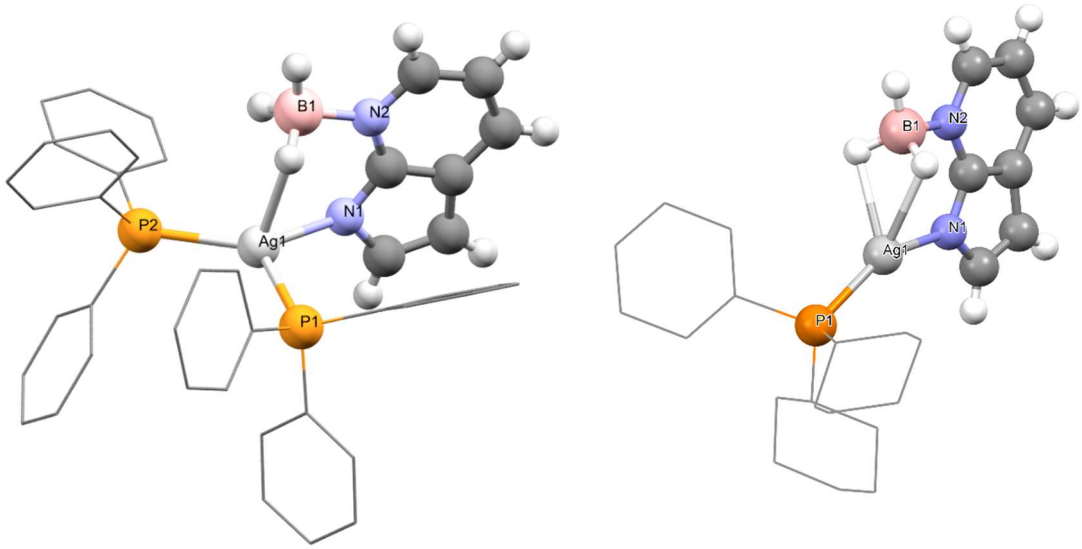

Figure 4.5. SC-XRD structures for [Ag(Mai)(PPh$_3$)$_2$] and [Ag(Mai)(PCy$_3$)]. Hydrogens on Cy and Ph rings have been omitted for clarity.

The Ag-P bond distance in the complex **[Ag(Mai)(PCy$_3$)]** was found to be 2.3410(3) Å (Table 4.5). In comparison to the Ag-P bond distance of 2.3674(7) Å in the complex **[Ag(Mmp)(PCy$_3$)]**, this Ag-P

distance is shorter. The increased requirement for election donation in the Mai complex may be associated with a decreased affinity for binding to the metal centre. This, along with the difference in steric and electronic properties of both the triphenyl and tricyclohexyl phosphine complexes, allows for the coordination of two triphenyl phosphine ligands in the **[Ag(Mai)(PPh$_3$)$_2$]** complex. The Ag-P bond distances in this complex were found to be 2.4698(7) and 2.4248(6) Å. Both distances are consistent with the Ag-P distances of 2.4285(10) and 2.4736(1) Å in the complex [Ag(Mp^{CF3})(PPh$_3$)$_2$] (**2.67**, Scheme 2.22**.**) reported by Santini in which the same number of triphenyl phosphine ligands coordinate and the mono supported borohydride ligand coordinates via a κ^2-N,H coordination mode. The complex **[Ag(Mai)(PPh$_3$)$_2$]** has a longer Ag-B distance of 2.882(3) Å when compared to **[Ag(Mai)(PCy$_3$)]** which has a distance of 2.684(1) Å. The 'off centre' coordination of the Mai ligand has an influence on the Ag-N bond distances in each complex. A longer distance of 2.264(2) Å was recorded in the complex **[Ag(Mai)(PPh$_3$)$_2$]** when compared to **[Ag(Mai)(PCy$_3$)]** which had an Ag-N bond distance of 2.157(1) Å. Both complexes are also shorter in comparison to the silver complex **2.67** reported by Santini in which the Ag-N distance was recorded as 2.335(3) Å. This is due to the conformational restrictions introduced by using only a two-atom supported borohydride ligand in comparison to the Mai ligand which is a three-atom supporting ligand.

Further inspection of the Ag-N bond in both cases, confirms the same trend observed for their corresponding copper complexes. The BN-NAg torsion angles in the complex **[Ag(Mai)(PCy$_3$)]** confirms that the N-Ag bond extends out at a near straight angle from the aromatic plane. The torsion angle is this case is 1.65(7)° (Table 4.5). In contrast to this, the complex **[Ag(Mai)(PPh$_3$)$_2$]** experiences a much greater deviation from 0° and demonstrates a significant distortion with a torsion angle of −23.2(1)° recorded (Figure 4.6). This is consistent with the distortion observed in the copper complexes in which a BN-NAg torsion angle of 23.08(8)° was found. Subsequent analysis of the crystal structures provided in the supporting information by Santini revealed that a similar distortion is indeed observed for the complex **2.67** (based on the pz scaffold) the BN-NAg torsion angles in the crystal structure were measured as -11.9(4)° and 16.1(4)°. Although these are tighter angles, these do again represent a

significant distortion from the expected mode of coordination and suggests that this may not be unique to the Mai ligand. As with the complex **[Cu(Mai)(PPh$_3$)$_2$]**, the distance from the closest point on the extended aromatic plane was calculated giving a longer distance of 0.914 Å for **[Ag(Mai)(PPh$_3$)$_2$]** when compared to the former in which a distance of 0.776 Å was measured. Given that the M-N bond distance is longer in the silver complex this larger difference is to be expected.

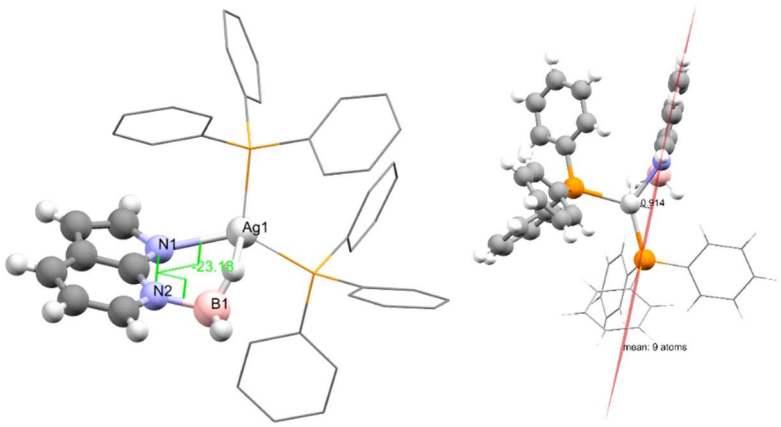

*Figure 4.6. SC-XRD structures of **[Ag(Mai)(PPh$_3$)$_2$]** showing the torsion angles and extended 7-azaindole plane.*

The hydrogen substituents within the $[BH_3]^-$ unit were located within the certainty associated with SC-XRD. In the complex **[Ag(Mai)(PPh$_3$)$_2$]**, a single BH bond is elongated to 1.16(3) Å in comparison to the terminal BH bond which have been measured as 1.11(3) and 1.11(2) Å. Again, this is consistent with the coordination mode (κ^2-N,H) observed for the ligand. This is also consistent with the observations made in the copper complex **[Cu(Mai)(PPh$_3$)$_2$]**, in which, BH bond distances of 1.21(2), 1.12(2) and 1.13(2) Å which were recorded for the bridging and both terminal BH bonds, respectively. The BH bond distances in the complex **[Ag(Mai)(PCy$_3$)]** again remain consistent with the coordination mode of the ligand and were recoded as 1.14(2), 1.15(2) and 1.09(2) Å. Further comparisons of the BH-Ag interactions in the silver complexes bearing the ligand Mai reveal that the single BH-Ag interaction in **[Ag(Mai)(PPh$_3$)$_2$]** is more κ^1-H in character with a B-H-Ag bond angle of 116(2)°, whilst the dihydroborate interaction in **[Ag(Mai)(PCy$_3$)]** has greater 3c-2e bond characteristics reporting tighter B-H-Ag bond angles of 97.4(9)° and 97.0(9)°. The Ag-H bond distances in **[Ag(Mai)(PCy$_3$)]** which are

2.29(2) and 2.29(2) Å, are longer in comparison to the distances reported in the silver complex **[Ag(Mai)(PCy$_3$)]** in which Ag-H bond distances of 2.09(3) and 2.05(3) Å were recorded. This continues to illustrate that the Mai ligand is less effective as a ligand at bringing the BH bonds into close proximity with the metal centre. In the complex **[Ag(Mai)(PPh$_3$)$_2$]**, the Ag-H bond is slightly shorter at 2.18(2) Å when compared to the Ag-H bonds in **[Ag(Mai)(PCy$_3$)]**. This shows that the 'off centre' coordination of the Ag-N bond assist in facilitating a closer BH-Ag interaction. Again, it appears that the Mai ligand has a weak affinity for binding to both copper and silver centres in comparison to the Mmp ligand. This therefore results in the flexible coordination of the Mai ligand to the silver centre which allows for the coordination of the additional phosphine in which the insolubility of the complex is a factor in driving the equilibrium towards the complex **[Ag(Mai)(PPh$_3$)$_2$]**.

*Table 4.2. Selected bond distances (Å) and angles (°) for the complexes **[Ag(Mai)(PPh$_3$)$_2$]** and **[Ag(Mmp)(PCy$_3$)]***

	[Na(Mai)]·0.5dioxane	**[Ag(Mai)(PPh$_3$)$_2$]**	**[Ag(Mai)(PCy$_3$)]**
Ag(1)-P(1)	-	2.4698(7)	2.3410(3)
Ag(1)-P(2)	-	2.4248(6)	-
Ag(1)-B(1)	-	2.882(3)	2.684(1)
Ag(1)-N(1)	-	2.264(2)	2.157(1)
C(7)-N(1)	1.353(3)	1.350(3)	1.342(1)
N(2)-B(1)	1.580(3)	1.574(3)	1.575(2)
C(7)-N(2)	1.366(2)	1.357(3)	1.354(2)
B(1)-H(1A)	1.16(2)	1.16(3)	1.14(2)
B(1)-H(1B)	1.13(2)	1.11(3)	1.15(2)
B(1)-H(1C)	1.15(2)	1.11(2)	1.09(2)
Ag(1)-H(1A)	-	2.18(2)	2.29(2)
Ag(1)-H(1B)	-	-	2.29(2)
Ag(1)-^{aza}plane		0.914	0.015
P(1)-Ag(1)-N(1)	-	107.61(5)	151.48(3)
P(2)-Ag(1)-N(1)	-	130.05(5)	-
P(1)-Ag(1)-P(2)	-	120.85(2)	-
N(1)-Ag(1)-B(1)	-	69.00(7)	73.38(4)
P(1)-Ag(1)-B(1)	-	113.57(6)	134.71(3)
$\Sigma_{angles\ around\ Ag}$	-	358.51	359.57
Ag(1)-N(1)-C(7)	-	119.8(1)	121.92(7)
Ag(1)-B(1)-N(2)	-	96.5(1)	99.68(7)
B(1)-N(2)-N(1)-Ag(1)	-	-23.2(1)	1.65(7)

Overall, in comparison to the Mmp ligands, as with the copper complexes, the Mai scaffold does not bring the borohydride unit into the same proximity with the metal centre as the Mmp support. This is due to the difference in the coordinating group of the donor scaffold where the Mai ligand is supported by a nitrogen donor and the Mmp ligand is supported by a sulfur donor. For example, the Ag-N-C bond angles are 119.8(1)° and 121.92(7)° for **[Ag(Mai)(PPh_3)$_2$]** and **[Ag(Mai)(PCy_3)]** respectively, and the Ag-S-C angle in **[Ag(Mmp)(PCy_3)]** shows a tighter angle of 102.2(1)/102.3(3)°. This then allows the BH_3 unit to come closer to the metal centre and subsequently explains the difference between the two ligands. This difference is due to the hybridisation of each of the respective donor atoms where the nitrogen donor is sp^2 hybridised which would result in an idealised angle of 120°, sulfur compounds are however capable of supporting tighter bond angles, for example the C-S-C bond angle in dimethyl sulfide has been previously measured by Iijima as 99.05(4)°.[158]

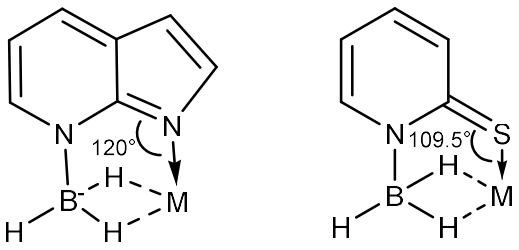

4.1 **4.2**

Figure 4.7. Idealised bond angles in Mmp and Mai chelates

4.3 Synthesis of gold complexes

4.3.1 Examples of bis and tris complexes of gold

Again, as with silver there are a limited number of examples of scorpionate ligands coordinating to gold metal centres (Figure 4.8). The ligand framework Tp has been functionalised in 3 separate positions on the pyrazole ring leading to a whole host of known and potential scorpionate ligands.[91,92,159,160] Examples in which linear gold centres are present include the synthesis of complexes such as $[Au_3(o\text{-}C_6BrF_4)_3(Tp)]$ **4.3** a trinuclear gold(I) complex which was reported by Echeverria.[161] The complex **4.3** is synthesised by the addition of the ligand salt K[Tp] with three equivalents of [Au(*o*-C_6BrF_4)(tht)] and one equivalent of $[NuBu_4]Br$ in THF. The complex **4.3** was used to encapsulate the lead complex [Pb(Tp)] thus generating the complex $\{[Pb(Tp)][Au_3(o\text{-}C_6BrF_4)_3(Tp)]\}$ which features a rare gold(I) lead(II) interaction. In a study by Mendoza-Espinosa and Salazar-Pereda the ligand Tp^{R_2} (R = Me or H) was added to a single equivalent of [(NHC)AuCl] in THF.[162] This reaction again results in a complex with a linear gold centre is observed, in which, only a single pyrazole ligand binds to the metal centre trans to the NHC ligand **4.4** (Figure 4.8). This allows the two pendant 'pz^{R_2}' groups in **4.4** to react with several different metal precursors allowing the ligand to host an additional metal centre such as platinum, nickel, and copper in addition to gold. The bis carbene ligand Bis^R was also added to the metal precursor $[AuCl(PPh_3)]$ resulting in the bis gold compound **4.5** which allows for a linear geometry at both gold centres. Me, Et and ^{i}Pr groups at the R group on the respective carbene ligands all gave the gold linear compounds which was confirmed by SC-XRD studies which also showed no BH-M interactions.[163]

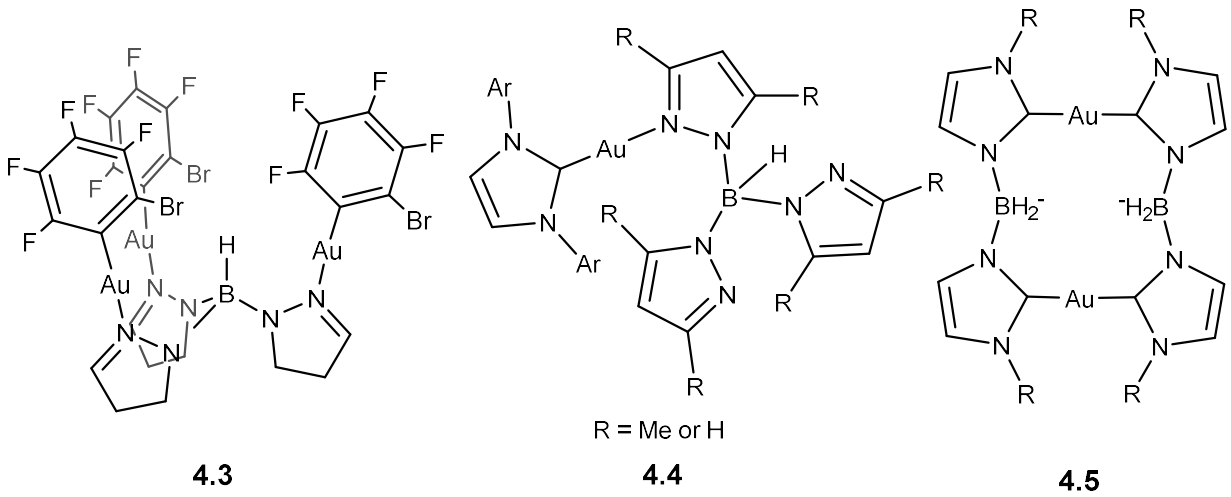

4.3 4.4 4.5

Figure 4.8. Selected examples of linear gold scorpionate compounds Left – [Au_3(o-$C_6F_4Br)_3$(Tp)], Middle – [Au(NHC)(Tp)] showing κ^1-N coordination of Tp, Right – [$Au_2(Bis^R)_2$]

Another example in which the gold forms a linear geometry was that reported by Hill in 2010 (Figure 4.9).[94,164] In this case, the ligand Bm was added through the addition of the ligand salt Na[Bm] to [AuBr(PEt_3)]. The ligand adopted a monodentate κ^1-S coordination mode leaving a single methimazole pendant. The P-Au-C bond angle was reported to be 174.99(9)° which is close to the idealised linear geometry. On stirring the complex **[Au(Bm)(PEt_3)]** with [$Mo(CO)_3(NCMe_3)$], an unusual metal salt was generated [Mo_2(Bm)$(CO)_7$]**[Au_2(Bm)($PEt_3)_2$]**. In the anionic component **[Au_2(Bm)($PEt_3)_2$]**$^-$ each methimazole unit coordinates to a separate gold centre allowing for the Au centres adopt a near linear geometry, in which both Au centres form an aurophilic interaction between each other with a recorded distance of 3.0420(5) Å (Figure 4.10).[165–167] The measured distance between Au and the H nuclei of the BH bond express long Au H distances of 3.12(8) Å in **[Au(Bm)(PEt_3)]** and a comparably shorter distance of 2.73(6) Å in the [Au_2(Bm)$(PEt_3)_2$] portion of the salt, this in comparison to previously reported Au-H bond distances originating from a BH bond is outside the scope of what is has been previously reported for such an interaction (1.71 - 2.06 Å).[164,168–175] This distance is again, longer however than Rabinovitch's complex **[Au(Bm)(PPh_3)]** in which an Au-H distance of 2.556 Å was reported where their complex give a slightly distorted T-shaped complex. A PPh_3 ligand is coordinated trans to a sulfur donor, perpendicular to which is the second sulfur donor. The second sulfur donor has a longer Au-S distance of 2.815(1) Å when compared to the trans PPh_3 methimazole at 2.351(1) Å

which is closer to the sum of the covalent radii of 2.41 Å for gold and sulfur.[33] This shows that the additional Au-S interaction is weak so that the P-Au-S bond angle can as far as possibly maintain a linear geometry. The resultant Au···H interaction is achieved from the BH bond that orientates towards the gold centre from above the plane of the T-shaped complex.[176]

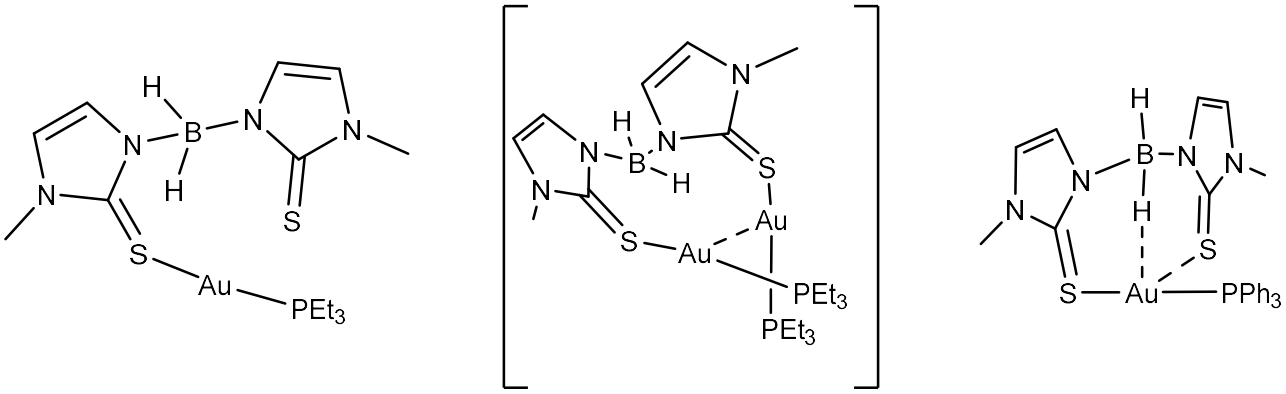

Figure 4.9. Selected examples of gold sulfur scorpionate complexes Left - ***[Au(Bm)(PEt$_3$)],*** *Middle – the* ***[Au$_2$(Bm)(PEt$_2$)]*** *anion of molybdenum salt and Right –* ***[Au(Bm)(PPh$_3$)]***

Dias and co-workers used the Tp variants, $Tp^{(CF_3)_2}$ and $Tp^{(CF_3)Ph}$ as ligands for gold (Figure 4.10). Treatment of the ligand salts with gold chloride under an ethylene atmosphere resulted in the respective $[Au(Tp^{R_2})(C_2H_4)]$ (**4.6** and **4.7**) complexes. Both complexes adopt a trigonal planar geometry where the sum of the angles around the gold centre are 359.4° and 359.8°, respectively. In both cases the BH bond is orientated away from the metal showing that there is no BH interaction.[177] Earlier work by Dias using the $Tp^{(CF_3)_2}$ ligand gave different coordination modes depending on the ancillary ligand coordinated trans to the Tp chelate.[178] In the case of the complex **[Au(Tp)$^{(CF_3)_2}$CO]**, the ligand was bound to the metal κ^3-N,N,N. On addition of N^tBu_3 to the complex the CO ligand is exchanged resulting in the complex **[Au(Tp)$^{(CF_3)_2}$(N^{t}Bu$_3$)]** in which the ligand $Tp^{(CF_3)_2}$ coordinates to the metal in a κ^2-N,N fashion. Increased π back bonding in the CO complex in comparison to the ethylene complex allows the gold centre to support a greater number of nitrogen donors.

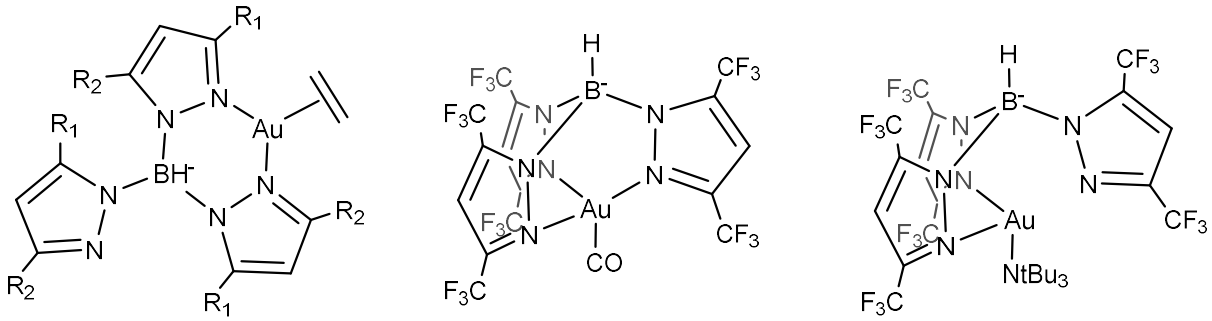

*Figure 4.10. Examples of κ¹, κ² and κ³ coordination to gold from the Tp scaffold Left – [Au(Tp^{R2})(C$_2$H$_4$)] (**4.6** and **4.7**), middle **[Au(Tp$^{(CF_3)_2}$)(CO)]** and Right – **[Au(Tp$^{(CF_3)_2}$)(N^{t}Bu$_3$)]***

One final example using the ligand scaffold Tp exhibits κ^3-N,N,N coordination to the gold centre. Santini used both ligands Tp and Tp*, the ligand Tp* has two methyl groups in the 3- and 5- positions of the pyrazole scaffold. The complex [Au(Tp*)(PPh$_3$)] was characterised by SC-XRD and showed that again the BH bond was indeed orientated away from the gold centre and confirmed the κ^3-N,N,N coordination mode of the ligand.[179]

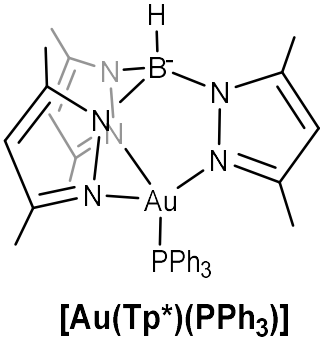

*Figure 4.11. Example of a κ^3-N,N,N complex **[Au(Tp*)(PPh$_3$)]***

As a summary of the known complexes, the denticity of the scorpionate ligands on coordination to gold appears to be dictated by gold's preference for low saturation and linear geometry. Despite this preference, the gold centre has been fine-tuned to adapt to higher coordination numbers, in particular, where the ancillary ligand is weakly coordinating. This effect is clear when looking at the differences in coordination mode of complexes **[Au(Bm)(PEt$_3$)]**, **[Au(Bm)(PPh$_3$)]**, **[Au(Tp$^{(CF3)2}$)(CO)]** and **[Au(Tp$^{(CF3)2}$)(N^{t}Bu$_3$)]**. This demonstrates that more strongly donating ancillary ligands promote the

formation of linear compounds. As a result of this, [AuCl(PPh_3)] was selected as the metal precursor for the synthesis of mono gold complexes. Gold scorpionate complexes bearing the ligand PPh_3 have been shown to allow for higher coordination modes up to κ^3 (e.g. **[Au(Tp*)(PPh_3)]** coordinates κ^3-N,N,N). Therefore is hoped that the use of the PPh_3 ligand this will result in the previously unobserved gold dihydroborate interaction. Again, as with copper, no complexes bearing a mono-substituted borohydride ligand have been reported on gold centres to date. The following work will therefore describe the synthesis and characterisation of such compounds in order to further extend our knowledge of group 11 compounds bearing mono supported borohydride ligands.

4.3.2 Synthesis of mono gold complexes

The synthesis of the complex **[Au(Mmp)(PPh_3)]** was achieved by the addition of the ligand **Na[Mmp]** to a methanol solution of [Au(Cl)(PPh_3)]. On stirring, a brick red precipitate began to form. The solution was stirred for 2 hours to ensure completion. The resultant brick red precipitate gave only a single broad BH stretching band at 2297 cm^{-1} in the infrared spectrum. This is close to the previously reported stretching frequency for the ligand salt at 2307 cm^{-1}, This may be an indication that the BH_3 group remains pendant. The broad nature of the peak, however, could indicate overlapping IR bands from both terminal and bridging B-H's. This suggests that there is, indeed, a weak interaction between the gold centre and the B-H bonds. Previously reported examples containing the PPh_3 ligand and gold allow for multiple donor sites in coordinating scorpionate ligands (e.g. **[Au(Tp*)(PPh_3)]** and **[Au(Bm)(PPh_3)]**) which would mean that coordination of BH bonds to the gold centre would be more likely in our case. The $^{1}H\{^{11}B\}$ NMR spectrum revealed a resonance at 4.01 ppm corresponding to the three hydrogens on the BH_3 unit. This is more protic in character when compared to the free ligand **Na[Mmp]** in which a $^{1}H\{^{11}B\}$ NMR resonance of 2.11 ppm was observed, again pointing to a pendant BH_3 group. The $^{11}B\{^{1}H\}$ NMR spectrum shows a resonance at −9.74 ppm which is shifted downfield in comparison to the sodium salt, copper complexes and silver complexes (c.f. −14.1, −13.9, and −16.3 ppm). The $^{13}C\{^{1}H\}$ NMR spectra again gave a more significant upfield shift at 169.2 ppm in comparison to the ligand salt **Na[Mmp]** at 181.3 ppm and the copper and silver salts respectively at 175.6 and 174.6 ppm. The chemical shift is consistent with the C=S resonance in the gold complex [Au(mpH)$_2$] 166.3 ppm.[180] In the mass spectrum obtained for the complex the parent ion for the complex **[Au(Mmp)(PPh_3)]** is present as an [M-H] peak at *m/z* = 582.09.

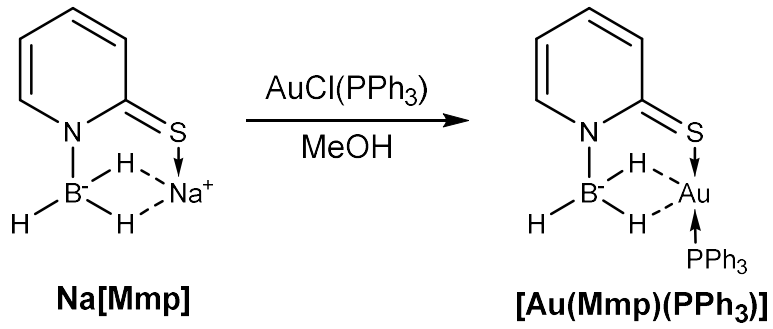

*Scheme 4.8. Synthesis of the complex **[Au(Mmp)(PPh$_3$)]***

The synthesis of the complex **[Au(Mai)(PPh$_3$)]** proceeded via a similar synthesis to **[Au(Mmp)(PPh$_3$)]** (Scheme 4.8). The synthesis involved the addition of a single equivalent of the ligand salt **Na[Mai]·2MeCN** into a solution of [AuCl(PPh$_3$)] which was subsequently stirred for 24 hours. Filtration of the reaction mixture resulted in a pale brown solid which was confirmed as **[Au(Mai)(PPh$_3$)]** by ^{1}H NMR spectroscopy (Figure 4.12). In the ^{1}H NMR spectrum it was confirmed that a single equivalent of phosphine was present in the complex, as the relative integration of the PPh$_3$ phenyl rings remained at 15 H. The use of the 'pre-coordinated' PPh$_3$ ligand in the [AuCl(PPh$_3$)] precursor allows for the gold centre to retain its linear geometry and the reaction does not result in the formation of the bis phosphine complex as seen the silver and copper complexes. Multiple BH stretching bands are present between 2232 and 2321 cm^{-1} which suggests that the BH does interact with the metal centre. The ^{1}H{^{11}B} resonance attributed the BH$_3$ group at 3.86 ppm is slightly more hydridic when compared to the resonance associated with **[Au(Mmp)(PPh$_3$)]** and the ^{11}B{^{1}H} resonance at −13.33 ppm is closer to that of the free ligand as seen with Cu and Ag complexes that interact with the metal.

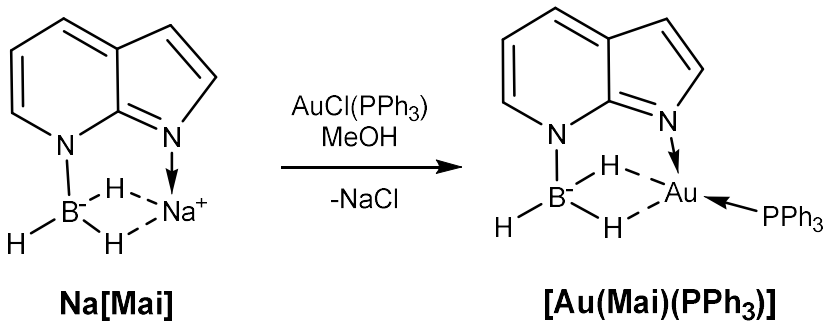

Scheme 4.9. Synthesis of the complex [Au(Mai)(PPh$_3$)]

Table 4.3. Spectroscopic data for gold complexes bearing mono-supported borohydride ligands and free ligand salts for comparison. NMR chemical shifts record as ppm and (h.h.w.) in Hz. Powder film IR data in cm^{-1}, (t)-terminal and (b)-bridging BH's.

Compound	$^{11}B\{^{1}H\}$ NMR	$^{31}P\{^{1}H\}$ NMR	$^{13}C\{^{1}H\}$ NMR *C*=S	$^{1}H\{^{11}B\}$ NMR BH_n	IR B–H
Na[Mmp]	−14.1 (44)	-	181.3	2.11	2307
Na[Mai]	−16.8	-	-	2.40	2320
[Au(Mmp)(PPh_3)]	−9.74 (558)	34.5	169.2	4.01	2297
[Au(Mai)(PPh_3)]	−13.33 (138)	31.3	-	3.86	2321(t)/ 2232(b)

Attempts to obtain single crystals for analysis of these compounds so far have proved difficult, this is because in solution these complexes are air and heat sensitive and over time the complex deposits a layer of metallic gold on the crystallisation vessel. Supported borohydride ligands such as the ligand Tai have previously been reported to reduce metals such as Pt^{II}, Pd^{II} and Ag^{I}. This is due to the reducing power of the ligand, showing that the stability of these compounds can be an issue when synthesising their respective lower group 10 and 11 complexes.[76]

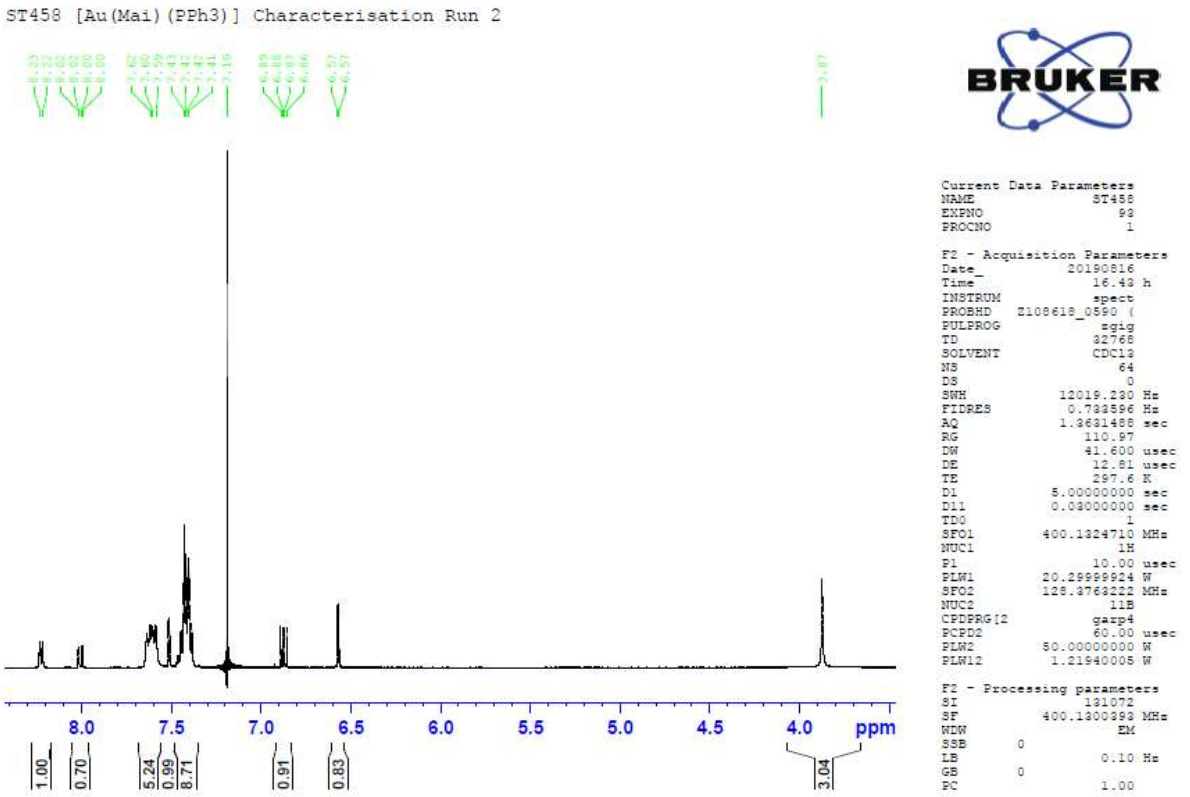

*Figure 4.12. $^{1}H\{^{11}B\}$ spectra of **[Au(Mai)(PPh_3)]***

The synthesis of both the ^{Me}Mmp and ^{Ph}Mmp gold complexes were also attempted, however, no product could be isolated from the reaction mixtures which had turned black over the course of 24 hours. NMR spectroscopic studies of the reaction suggested that the product does form in the reaction mixture but is not stable in solution at room temperature and eventually decays. This result was surprising as the [Au(Mmp)(PPh_3)] complex appeared to be more stable and was easily synthesised and gold complexes bearing sulfur ligands are typically more stable.[181–183] The introduction of an R group to the borohydride moiety clearly has an effect on the stability of the compound and therefore its isolation is more difficult to achieve.

4.4 Summary, discussion and comparisons of complexes synthesised in chapter 3 and 4

The synthesis of mono and bis complexes of coinage metals is one which is easily reproducible across a range of supporting scaffolds. Both chapters 3 and 4 have shown that despite the lack of prevalence in the literature the complexes of mono supported borohydrides are easily accessible through a simple reproducible procedure. The use of methanol as a solvent, in which, the product of these reactions has poor solubility, results in the precipitation of the desired complex in good purities. The products from the reaction can be stored in air as powders, although in the case of silver, whilst remaining spectroscopically pure by NMR, the complexes will darken over time. In most cases the complexes were synthesised without the need for further purification, principally in the case of the copper complexes. With regards to the silver complexes, on occasion, extraction into a DCM/pentane mixture and subsequent work up gave the pure product.

In comparison of the supporting scaffolds, a wide range of copper complexes were synthesised, therefore it is appropriate to use the copper complexes to compare the effect of the supporting scaffolds. Comparison of the $[BH_n]^-$ environments in the $^1H\{^{11}B\}$ NMR spectra (Table 4.7) showed that the copper complexes bearing the ligand Mm gave the more hydridic environments, followed closely by the Mmp complexes and the least hydridic in character were the Mai complexes. The hydricity of the $[BH_n]^-$ hydrogens in the ^1H NMR spectra may be an indication of the ease at which hydride migration may occur in other metal complexes. Complexes which bear $[BH_n]^-$ hydrogens that are more hydridic in character may have the lowest energy barrier for hydride migration from ligand to metal to occur. Therefore, this insight is an important indication into which ligands may or may not undergo hydride migration. This data is supported by SC-XRD diffraction bond length data which shows that boron is in closer proximity when the Mmp and Mm ligand scaffolds are used and the distance between copper and boron is much greater when compared with the Mai ligand. This was shown to be due to the method of attachment in which the comparatively narrower bond angles of the sulfur donor accommodate a closer B-H-M interaction.

Table 4.4. Combined spectroscopic data for all complexes synthesised in chapters 3 and 4

Compound	$^{11}B\{^1H\}$ NMR	$^{31}P\{^1H\}$ NMR	$^{13}C\{^1H\}$ NMR *C*=S	$^1H\{^{11}B\}$ NMR B*H*$_n$	IR B–H
[Cu(Mmp)(PPh$_3$)]	−13.9	4.8	175.9	2.64	2439 (t) / 2078 (b)
[Cu(Mmp)(PCy$_3$)]	−13.4	27.2	176.1	2.42	2448 (t) / 2085 (b)
[Cu(Mmp)(dppe)]	−14.54	−5.4	176.2	2.69	2378 (t) / 2081 (b)
[Cu(^{Ph}Mmp)(PPh$_3$)]	−5.74	10.1	175.6	3.32	2039 (b, w)
[Cu(^{Ph}Mmp)(PCy$_3$)]	−5.43	28.8	173.3	3.06	2068 (b, w)
[Cu(^{Me}Mmp)(PPh$_3$)]	−8.87	8.8	175.8	2.46	2016 (b, vw)
[Cu(^{Me}Mmp)(PCy$_3$)]	−8.59	28.0	174.4	2.17	2032 (b, w)
[Cu(Mai)(PPh$_3$)$_2$]	−15.9	2.4	-	3.72	2375 (t) / 2104 (b)
[Cu(Mai)(PCy$_3$)]	−15.4	23.0	-	3.93	2368 (t) / 2115 (b)
[Cu(^{Me}Bai)(PPh$_3$)]	−7.64	1.26	-	4.99	2095 (b)
[Cu(^{Me}Bai)(PCy$_3$)]	−8.39	23.9	-	4.29	2091 (b)
[Cu(Mm)(PPh$_3$)]	−19.99	6.86	159.5	2.38	2434 (t) / 2091 (b)
[Cu(Mm)(PCy$_3$)]	−19.56	24.5	159.8	2.17	2450 (t) / 2067 (b)
[Cu(Bm)(PPh$_3$)]	−8.23	−2.73	161.0	3.44	2381 (t) / 2260 (b)
[Cu(Bm)(PCy$_3$)]	−8.60	13.9	160.9	3.36	2383 (t) / 2288 (b)
[Ag(Mmp)(PPh$_3$)]	−16.3	16.1	174.6	3.23	2391 (t) / 2067 (b)
[Ag(Mmp)(PCy$_3$)]	−15.7	40.6	174.6	3.31	2401 (t)
[Ag(^{Me}Mmp)(PPh$_3$)]	−11.18	3.95	n.o.	3.46	2053 (b)
[Ag(^{Me}Mmp)(PCy$_3$)]	−11.32	40.5	174.7	3.24	n.o.
[Ag(^{Ph}Mmp)(PPh$_3$)]	−7.26	16.0	174.3	4.23	n.o.
[Ag(^{Ph}Mmp)(PCy$_3$)]	−7.00	39.9	173.3	4.03	n.o.
[Ag(Mai)(PPh$_3$)$_2$]	−18.4	9.12	-	3.39	2373 (t) / 2174 (b)
[Ag(Mai)(PCy$_3$)]	−17.2	41.8	-	3.20	2373 (t) / 2190 (b)
[Au(Mmp)(PPh$_3$)]	−9.74	34.5	169.2	4.01	2297
[Au(Mai)(PPh$_3$)]	−13.33	31.3	-	3.86	2321(t) / 2232(b)

The consequence of the use of different scaffolds is most apparent when looking at crystal structures for complexes bearing the ligand Mai. Notably, when using triphenylphosphine as an ancillary ligand in both copper and silver complexes, the reaction generates the unexpected product **[M(Mai)(PPh$_3$)$_2$]** (where M = Cu or Ag) this product is in direct contrast to all other mono complexes synthesised in which only a single phosphine coordinates to the metal centre. The analogous reaction only consumes a single equivalent of tricyclohexyl phosphine. This difference is attributed to both the larger cone angle of PCy_3 and its increased basicity in comparison to PPh_3. This means that the PCy_3 ligand is therefore able to satisfy the electron deficiency of the metal centre. However, the consequence of the

coordination of two equivalents of PPh_3 in the complex **[Cu(Mai)(PPh_3)$_2$]** results in an unforeseen structure in which the Mai chelate demonstrates an unusual mode of coordination to the metal. This deviance from the expected mode of coordination was measured by the distance of the copper centre from the extended aromatic plane and as the BN-NCu torsion angle which both deviated from their expected values of 0°. This flexible coordination is again demonstrated in the isoleptic silver complex, thus cementing the ligand Mai's ability to adapt depending on the saturation of the metal centre.

Table 4.5. Selected SC-XRD bond lengths for complexes in chapters 3 and 4

Compound	M-B	M-P	B-H (b)	B-H (t)
[Cu(Mmp)(PPh_3)]	2.113(17)	2.1789(4)	1.17(2) / 1.16(2)	1.17(2)
[Cu(Mmp)(PCy_3)]	2.153(16)	2.1876(4)	1.16(2) / 1.17(2)	1.14(2)
[Cu(^{Ph}Mmp)(PPh_3)]	2.185(2)	2.1748(8)	1.17(2) / 1.18(2)	-
[Cu(^{Ph}Mmp)(PCy_3)]	2.230(3)	2.1867(7)	1.18(2) / 1.18(2)	-
[Cu(^{Me}Mmp)(PPh_3)]	2.194(1)	2.1829(3)	1.17(2) / 1.18(2)	-
[Cu(Mai)(PPh_3)$_2$]	2.657(2)	2.2772(6) / 2.2493(4)	1.21(2)	1.12(2) / 1.13(2)
[Cu(Mai)(PCy_3)]	2.334(1)	2.1835(3)	1.17(2) / 1.17(2)	1.09(2)
[Cu(^{Me}Bai)(PPh_3)]	2.776(2)	2.1834(4)	1.18(2)	-
[Cu(^{Me}Bai)(PCy_3)]	2.763(2)	2.1802(6)	1.23(2)	-
[Cu(^{Me}Bai)$_2$]	2.944	-	1.18(3)	-
[Cu(Mm)(PCy_3)]	2.208(2)	2.1886(4)	1.15(2) / 1.19(2)	1.08(2)
[Cu(Bm)(PPh_3)]	2.745(3)	2.223(1)	1.14(4)	1.09(4)
[Ag(Mmp)(PCy_3)]	2.42(2)	2.3674(7)	1.13(3) / 1.20(3)	1.10(3)
[Ag(Mai)(PPh_3)$_2$]	2.882(3)	2.4698(7) / 2.4248(6)	1.16(3)	1.11(3) / 1.11(2)
[Ag(Mai)(PCy_3)]	2.684(1)	2.3410(3)	1.14(2) / 1.15(2)	1.09(2)

The coordination of the $[BH_n]^-$ group to the metal was also shown to be affected by the introduction of additional non-coordinating functional groups to the borohydride moiety. The $^1H\{^{11}B\}$ NMR data for the phenyl and methyl substituted Mmp ligands, reveal a more protic resonance in the case of the phenyl ligand and a more hydridic resonance in the case of the methyl ligand. Again, this provides an important insight into the tunability of these ligands. Moreover, this pattern is replicated within the silver complexes in which, again, the methyl complexes give more shielded resonance when compared to the silver complexes of the ligand ^{Ph}Mmp. The addition of a functional group to the $[BH_n]^-$ also prevents the free rotation of the BH_n interaction.

Looking at the complexes [M(Mmp)(PPh_3)] where M = Cu, Ag or Au. As you move down the group the BH_3 resonance in the $^1H\{^1B\}$ NMR shifts to a more protic resonance. This can be attributed to two potential reasons, the first is that as you move down the group each metal centre prefers a lower coordination number therefore the dihydroborate interaction will become less favoured. The second is due to the classification of the BH_3^- under HSAB theory, given the fact that the BH_3^- group is anionic giving it an ionic component it is reasonable to assume that the BH_3^- group tends towards being a hard base. This is in contrast to the silver and gold which are soft acids which would give them poor affinity for bonding with the BH_3^- group. Comparisons of the SC-XRD bond length data between the isoleptic complexes can be made by comparing the M-B distances to the sum of the covalent radii. In [M(Mmp)(PCy_3)] (M = Cu or Ag) complexes, the M-B distance for the copper complex was measured as 2.153(16) Å. This bond distance is slightly shorter in comparison to the sum of the covalent radii for copper and boron which was calculated as 2.16 Å. In the complex **[Ag(Mmp)(PCy_3)]** the Ag-B distance of 2.42(2) is noticeably larger than the sum of the covalent radii for silver and boron (2.29 Å). The [M(Mai)(PCy_3)] (M = Cu or Ag) complexes also show greater deviation in the silver complex in comparison to the sum of covalent radii. The copper complex **[Cu(Mai)(PCy_3)]** M-B distance was recorded as 2.334(1) which represents an 8% increase from the sum of covalent radii. In comparison the M-B distance of 2.684(1) recorded for the complex **[Ag(Mai)(PCy_3)]** represents a 17% increase. This data shows that as you move down from copper to silver the M-B interaction becomes weaker.

In comparison to bis- and tris- ligands, the mono- ligands have shown to be most effective in bringing the $[BH_n]^-$ into close proximity with the metal centre. The reasons for this again are two-fold, firstly as described in the introduction as the denticity of then BH_n unit increases from κ^1-H through to κ^3-H,H,H the M-B bond length decreases so this result is therefore consistent with what has been observed in unsupported BH_4^- ligands. Secondly when using singly supporting borohydrides, there is greater flexibility when compared to bis or tris complexes. This is due to the conformational restrictions of multiple fused chelate rings that form rigid chelates in which less flexibility is afforded to the $[BH_n]^-$ unit.

4.5 Chapter conclusions

This chapter has sought to complete the family of isoleptic complexes of coinage metals. Whilst copper complexes are prevalent, the corresponding silver and gold are rare. In doing so this chapter has demonstrated the ability of the mono substituted borohydride ligands to coordinate to both silver and gold. As discussed in Chapter 2, the coordination of these ligands to metal centres is not well documented, the synthesis of these complexes has helped develop our understanding of these ligands and has provided a unique insight into the ability to modify these ligands. Sulfur donor scaffolds have again demonstrated their ability to coordinate and bring the BH bonds in close proximity to the metal centre. Azaindole scaffolds have also demonstrated a varying degree of flexibility to allow for coordination of the BH bond to the metal centre, in which the M-N bond resulting from the pyrrole unit distorts resulting in an unusual bonding mode for the complex. The Mai ligand demonstrates both κ^3-N,H,H and κ^2-N,H coordination confirming that these ligands are indeed flexible and will coordinate depending on the saturation of metal complexes. Further evidence for the flexibility of these ligands is attributed to the free rotation of the BH_3 group at the metal centre which is supported by a single environment for all BH's. As you move down group 11 the B-H···M bond appears to get weaker which is supported by spectroscopic data. This change in bonding is because metal centres lower down in the group are less likely to support highly saturated compounds.

Chapter 5: Towards the synthesis of novel supported borane and borohydride-based ligands

5.1 Introduction

As set out in the introduction of this thesis, many ligand frameworks have been adapted to support either borane or borohydride ligands.[184] These have provided a useful toolkit in the synthesis of such compounds. Carbene ligands have been used as two atom supports in scorpionate systems,[185] however these two atom supports do not provide a suitable framework in which hydride migration might occur.[3] It is for this reason we decided to pursue the synthesis of a carbene ligand as a three atom supports (Figure 5.1). Carbenes were chosen as a supporting unit because they are notorious for their electron donating properties,[186,187] and a three atom bridge may facilitate hydride migration as this reactivity is one of the key-focuses of the Owen research group at the University of South Wales.[14,126,127,188]

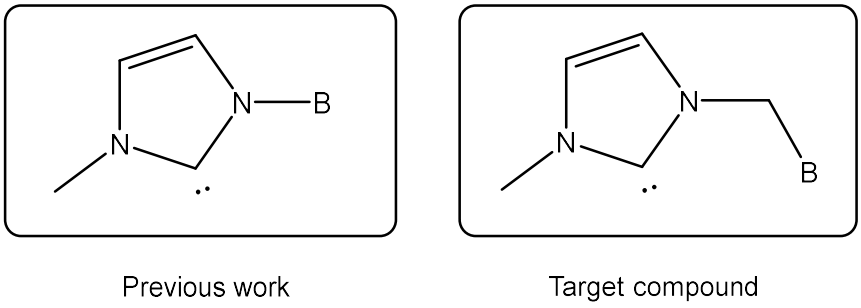

Figure 5.1. Structure of two (left) and three (right) atom bridged carbenes

Carbenes are neutral divalent carbon atoms which have two electrons available for bonding.[189–193] There are two main classifications of carbene; the first is the Fischer carbene, otherwise known as a singlet carbene. In Fischer carbenes the two electrons available for bonding reside in a single orbital. These two electrons are available for bonding with Lewis acidic species and will form a dative bond. The remaining vacant orbital on the carbene is then free to accept electrons via back bonding from the metal centre (Figure 5.2). Fischer carbenes arise from a large energy barrier between the two orbitals on carbon resulting in the preferential filling of a single orbital. In contrast to Fischer carbenes,

Schrock carbenes arise when the orbitals are closer or equal in energy. In this case, the electrons are unpaired, and a single electron is present in each orbital. These can also be referred to as triplet carbenes. Schrock carbenes will form X_2-type interactions with a metal centre with both σ and π bonding components.[194–197]

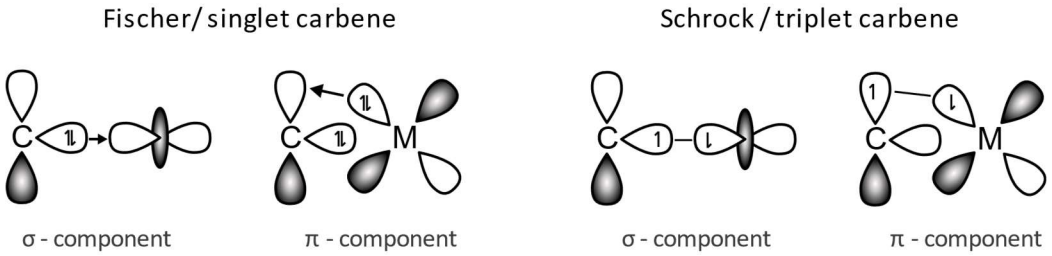

Figure 5.2. MO diagrams showing both Fischer and Schrock type carbenes

Further classification of singlet carbenes introduces a subsection of carbenes known as Wanzlick-Ardeungo carbenes or *N*-heterocyclic carbenes (NHC's). In NHC's, the two substituents adjacent the carbene unit are nitrogen groups which form part of a cyclic diimine. The lone pairs on the nitrogen provide electronic support to the vacant p-orbital of the carbene and increases the carbene's stability as a free ligand. In addition to this, the electron donation into the empty p orbital reduces the back bonding from the π-component resulting in a greater net electron donation of the carbene to the metal (Figure 5.3). Since their discovery, NHC's have been widely used in carbene chemistry, this is due to their robust nature and ease of functionalisation.[198]

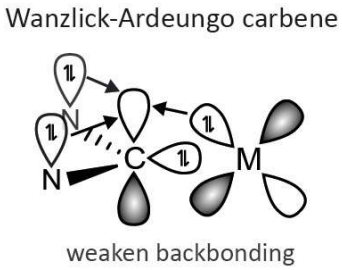

Figure 5.3. A MO diagram showing both σ and π components in Wanzlick Ardeungo carbenes

NHC's are synthesised from their pro-ligand, imidazolium salts. Imidazolium salts are easily synthesised from imidazole or functionalised imidazoles, and their deprotonation will lead to the

formation of a carbene. Typical examples of reagents used for deprotonation are the use of bases such as NaOAc, NaH, KOtBu or M[HMDS] basic ligands can also be used to generate the ligand 'on metal' such as $Pd(OAc)_2$.[190]

5.1.1 Hydroboration of vinyl phosphine ligands

In 2014 Crossley reported the synthesis of the singly bridged phosphane-borane **5.2**. The synthesis of **5.2** was achieved by the hydroboration of the vinylic phosphine **5.1** (Scheme 5.1). The ligand **5.2** was synthesised in refluxing THF for 3 hours, concentration and subsequent cooling to −20 °C for 12 hours results in the formation of colourless crystals of the product **5.2** in good yield (75%). The synthesis of the rhodium complex **5.3** was achieved by the direct addition of a solution of $[RhCl(cod)]_2$ to a stirred solution **5.2** after an hour stirring removal of solvent in vacuo gives the product in high yield.[199,200]

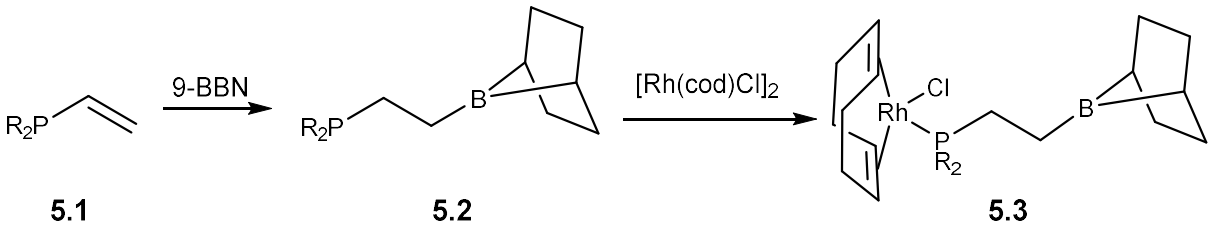

Scheme 5.1. Hydroboration of vinyl phosphine using 9-BBN and subsequent addition to $[Rh(cod)Cl]_2$ (R = Fu and Ph)

This research paper provided the inspiration for the synthesis of an analogous carbene ligand in which a potentially similar route could be investigated. Carbenes are readily functionalised and the vinyl group can easily be introduced during the synthesis of carbenes. Vinyl imidazole is a cheap commercially available reagent that can easily react with alkyl halides in an N-quaternarisation reaction to form their respective imidazolium salts.[201–203]

Hydroboration chemistry was first pioneered by Nobel laureate Herbert C. Brown in 1956. Brown was able to generate borane by the addition of aluminium chloride to sodium borohydride. Reactivity studies of borane with alkenes showed that borane reacts with three molar equivalents of alkene, in which the BH bond is added across the double bond resulting in the synthesis an organoboron alkane. The addition of borane to alkenes favourably proceeds in an anti-Markovnikov fashion adding to the least substituted carbon, this is due to the electrophilic nature of borane. The least substituted carbon has a partial negative charge as higher substituted carbon atoms can generate the most stable

carbocations (Scheme 5.2).[204] Therefore, the partial charges align and the reaction will favourably proceed as shown in Scheme 5.2.

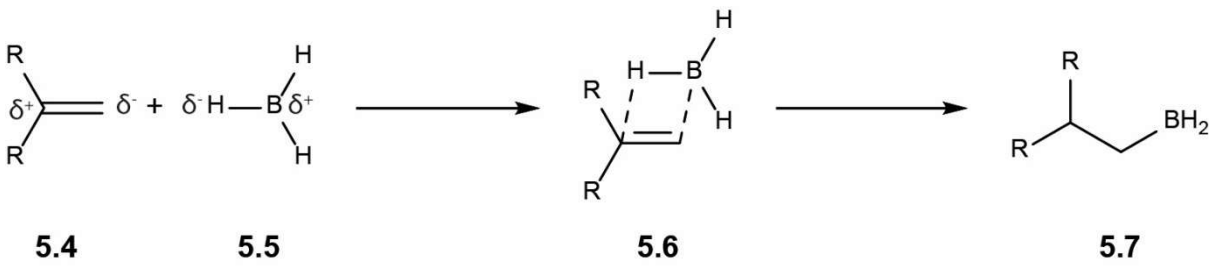

Scheme 5.2. Anti-Markovnikov addition of a BH bond to an alkene.

5.2 The hydroboration route

5.2.1 Reactions of borane with vinyl imidazole

Initial attempts at the synthesis of a carbene supported borane ligand via hydroboration started with testing the reactivity of a series of boranes with vinyl imidazole (Scheme 5.3). The reaction was tested using equimolar quantities of a 1 M BH_3·THF solution and vinyl imidazole in THF under nitrogen. Analysis of the reaction mixture by ^{11}B NMR spectroscopy revealed that the quartet observed at −1.1 ppm corresponding to BH_3·THF had shifted upfield to −19.2 ppm, this suggests that a new adduct had formed. A second experiment run with proton decoupling ($^{11}B\{^1H\}$ NMR) results in the resolution of the quartet into a singlet, this confirms that the quartet is indeed due to coupling with hydrogen. After 20 minutes of stirring the volatiles were removed in vacuo and the solid white product was taken up into $CDCl_3$ and analysed by ^1H, ^{13}C and ^{11}B NMR techniques. The BH_3 protons were present as a broad quartet between 1.8 and 2.6 ppm and the integrations and splitting for the vinyl imidazole protons were consistent with that of the starting material vinyl imidazole, with their chemical shift values shifted downfield. The compound **5.9** has previously been reported by Zhang and the synthesis is the same as described in the literature.[205] Comparison of the ^1H and ^{13}C NMR data confirms that the white solid synthesised is the vinyl imidazole borane adduct **5.9**. In this case it appeared that hydroboration does not occur here because the free Lewis basic nitrogen in the imidazole ring forms a stable adduct with the Lewis acidic borane. Zhang also reports the synthesis of the allyl imidazole adducts, in which hydroboration is not observed.

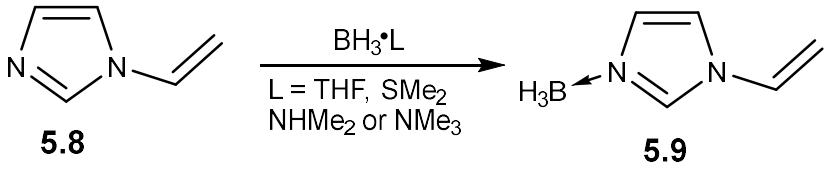

*Scheme 5.3. Synthesis of **5.9** using a series of borane precursors*

This synthesis was replicated by testing a variety of boranes on an NMR scale and monitoring the ^{11}B NMR spectra which revealed that the same reactivity occurred when using different boranes such as

$BH_3{\cdot}SMe_2$, $BH_3{\cdot}NHMe_2$ and $BH_3{\cdot}NMe_3$. The molar ratio was then increased to 2:1 with respect to the borane in a further attempt to observe hydroboration, the reaction conditions were kept the same and stirred at room temperature in THF. The vinyl protons were monitored in the proton spectra for any indication of hydroboration, but this was not observed. Adduct formation was once again observed with a quartet present at −19.2 ppm in the boron NMR spectrum confirming that the product of the reaction was **5.9**. If the desired hydroboration reactivity had been observed, the splitting pattern would give a triplet representing a BH_2 group and a chemical shift value between 20 and 25 ppm for a pendant RBH_2 moiety nitrogen based adduct would give an expected chemical shift value of between −7.5 and +2.5 ppm as has been reported for similar compounds.[206–211] As no hydroboration was observed at room temperature the temperature of the reaction in THF was increased to refluxing temperature. Again, only adduct formation was observed in the reaction. A further test reaction using toluene under reflux was also trialled, in which only adduct formation was observed. As the temperature increased it was also observed that there was a greater formation of boric acid in the reaction mixture, this was present in the NMR spectra as singlet at approximately 18 ppm (figure 5.4).

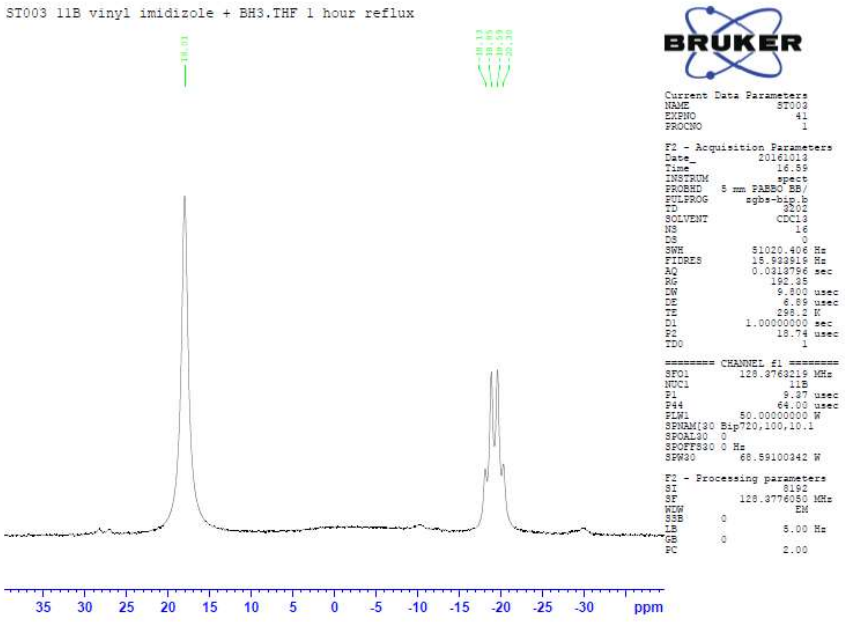

Figure 5.4. *^{11}B spectra of the reaction between vinyl imidazole and borane showing formation of both boric acid and the vinyl imidazole adduct*

Wilkinson's catalyst has previously been utilised in hydroboration chemistry as a catalyst which facilitates hydroboration (Scheme 5.4). The use of the catalyst allows for the use of much milder conditions. The activation of Wilkinson's catalyst occurs via ligand dissociation of a single triphenylphosphine ligand, the BH bond then undergoes oxidative addition at the metal centre followed by ligand association of the olefin. The complex then undergoes migratory insertion to form the alkyl rhodium complex that subsequently undergoes reductive elimination to form the hydroborated species. The reaction between vinyl imidazole and borane was tested at both room temperature and under reflux using THF at 1% mol catalyst loading. Only adduct formation between the BH_3 and vinyl imidazole was observed and no change in the protons for the double bond in the ^1H NMR spectra which confirms that no reactivity occurred.

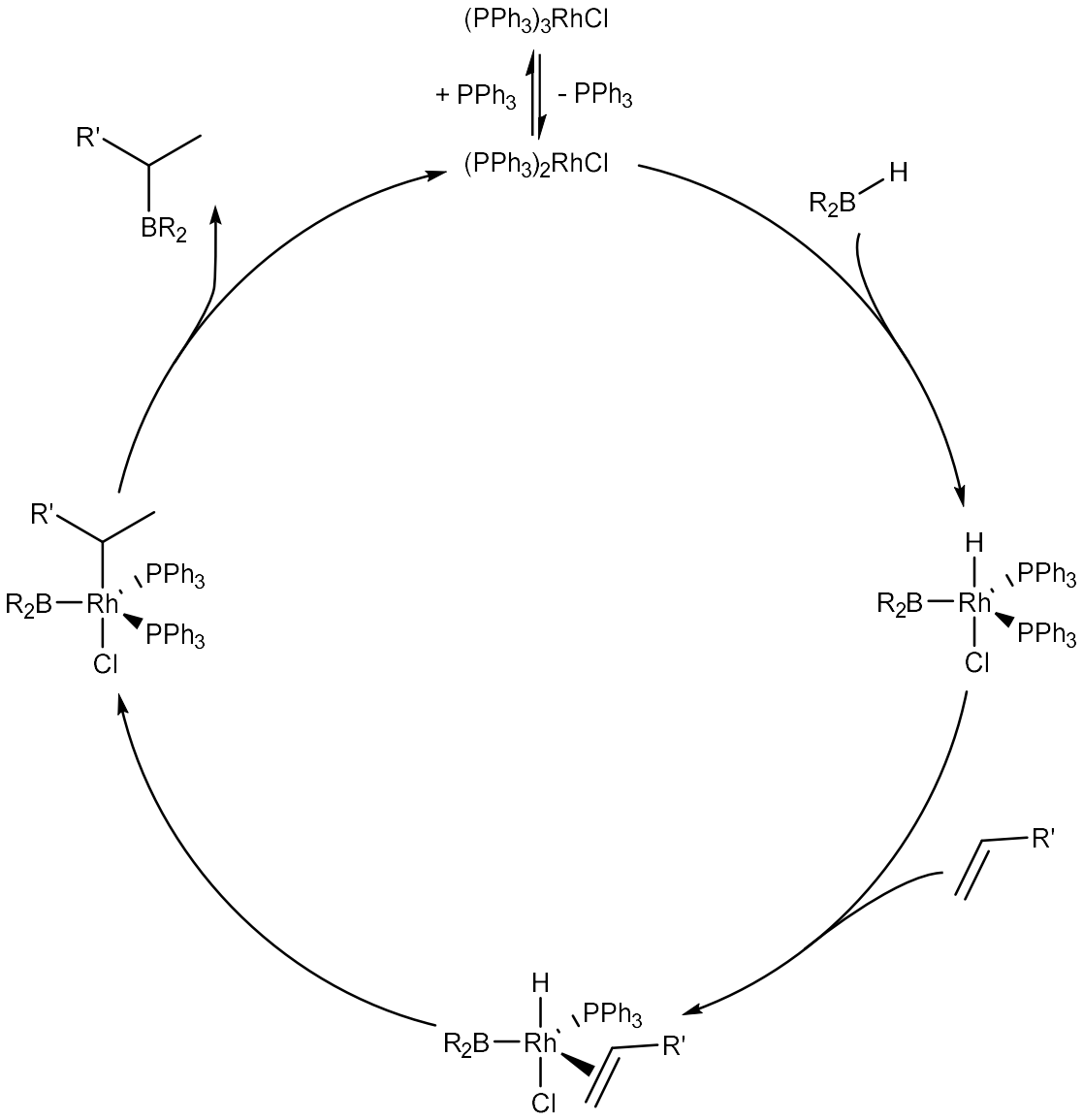

Scheme 5.4. Catalytic cycle for hydroboration using Wilkinson's catalyst

Functionalised boranes have also been used as hydroboration reagents and vary in both stability and reactivity. Catechol borane is a commercially available hydroboration reagent and is sold as a solution in THF. Catechol borane was again added in a 1:1 and 2:1 molar ratio with respects to vinyl imidazole and the reaction was carried out at both room temperature and reflux. In both cases no hydroboration was observed. This reaction was also tested using Wilkinson's catalyst and hydroboration again was not observed.

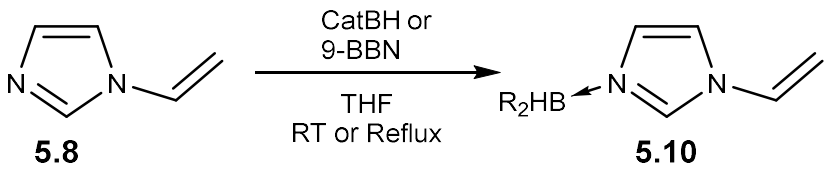

Scheme 5.5. Reactivity of CatBH and 9-BBN with vinyl imidazole

The hydroboration reagent 9-BBN was synthesised following a previously reported procedure. Cyclooctadiene (cod) was slowly added to a solution of 1 M borane in THF cooled in an ice bath. Following the addition of cod, the reaction was refluxed for three hours, after which time the product was crystallised out of solution at –40 °C forming white tree shaped crystals in good yield. The formation of 9-BBN was confirmed by a sharp doublet in the ^{11}B NMR spectra at 28.0 ppm which is the same value which has been reported in previous literature examples.[212,213] 9-BBN was tested in both 1 and 2 molar ratios with respect to vinyl imidazole and at room temperature. Again, no hydroboration of the vinyl group was observed. This is in contrast to the reactivity observed by Crossley where the vinyl moiety of a phosphine undergoes hydroboration to form **5.2** (Scheme 5.1). The vinyl group of vinyl imidazole is most likely more stubborn to hydroboration due to the formation of an extended π-system that includes the double bonds of the imidazole rings, the nitrogen lone pairs and the vinyl group. It is clear that under the conditions described hydroboration of vinyl imidazole did not occur and other avenues had to be explored.

5.2.2 Synthesis of vinyl imidazolium salts

After testing for hydroboration, it was decided to proceed with the synthesis of a vinyl imidazole based carbene and to test whether it was possible to hydroborate or add boron at any point in the synthesis of vinyl imidazole based carbenes. The N-quaternarisation of vinyl imidazole is a known reaction and has been performed in a solvent free synthesis as described by Morvan et al.[214] Due to the exothermic nature of the reaction, it was decided to use a solvent as N-quaternarisation reactions proceed slower in solvent systems to allow greater control of its reactivity and exothermic nature. The reaction was tested in both THF and toluene, in THF the product precipitated out as an oil and was washed with excess THF and dried in vacuo, which was difficult and required several hours and dynamic vacuum to complete. Using toluene as a solvent presented a more straightforward workup as the product precipitated out as a white solid in excellent yield (99%).

The presence of 3-methyl-1-vinylimidazolium iodide was confirmed by uptake of a small amount of product in DMSO-d_6 and subsequent analysis by ^{1}H NMR. The presence of the methyl group in the product was confirmed by a singlet at 3.98 ppm with a relative integration of 3H. With respect to the vinyl protons, the splitting pattern in the proton NMR remained the same. In comparison to the vinyl imidazole, the chemical shift values for the imidazole and vinyl protons in **5.11** were shifted downfield. The NCHN proton in particular experienced the greatest shift to 9.58 ppm (from 7.63 ppm) which is indicative of an acidic imidazolium proton. The NMR data is also agreement with the published data confirming that the product is indeed 3-methyl-1-vinylimidazolium iodide.

Para-xylene bromide was also used to functionalise vinyl imidazole in a reaction that was left to stir for 24 hours in toluene. The product precipitated out of solution as a pale yellow solid and was present in excellent yield 91%. A small portion of the product was dissolved in $CDCl_3$ and assessed by ^{1}H NMR, as observed in the synthesis of methyl-vinyl-imidazolium. The imidazole protons experience a downfield shift this is most apparent in the NCHN proton again which is present at 10.76 ppm representing a possible site for deprotonation and formation of a carbene. The presence of the para-

xylyl functionality was also confirmed in the NMR studies as two doublets each integrating to 2H in the aromatic region, and two singlets with integrations of 2H and 3H in the aliphatic region representing both CH_3 and CH_2 groups. Further confirmation that the product was the expected product came from MS data which gave the $[M\text{-}Br]^+$ ion at m/z = 199.12.

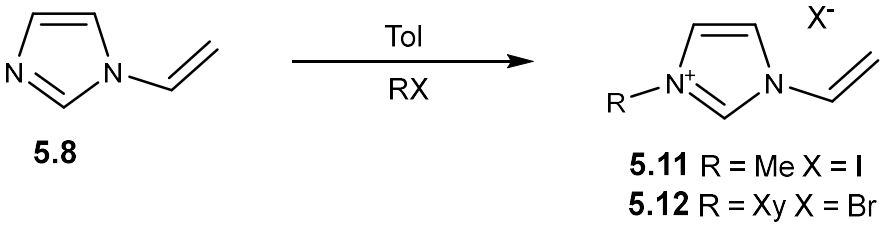

Scheme 5.6. Synthesis of vinyl imidazolium salts

In addition to the N-quaternarisation reactions using xylyl bromide and methyl iodide, 4-iodotoluene was also tested on a 1 mmol scale. The reaction between 4-iodotoluene and vinyl imidazole was tested at both room temperature and reflux, after a few hours of reflux the reaction mixture was analysed by ^1H NMR spectroscopy and no quarterisation was observed. This is because the iodine is attached to a sp^2 hybridised carbon, this transformation requires more energy in comparison to the sp^3 hybridised centre which require the support of a catalyst in order to undergo a N-quaternarisation reaction.[215]

5.2.3 Reactions of borane with vinyl imidazolium salts

Testing the propensity for vinyl imidazolium salts to undergo hydroboration was followed using the same procedure outlined for vinyl imidazole with the exception of the variation of molar ratios. The nitrogen on the imidazole ring was now functionalised and could no longer form adducts with the borane, therefore, only a single equivalent was needed. Again, as with vinyl imidazole no hydroboration of the double bond is observed this is clearly apparent in the ^{1}H NMR spectra of the reaction mixture which shows no change in the double bond protons or in ^{11}B environment of BH_3·THF.

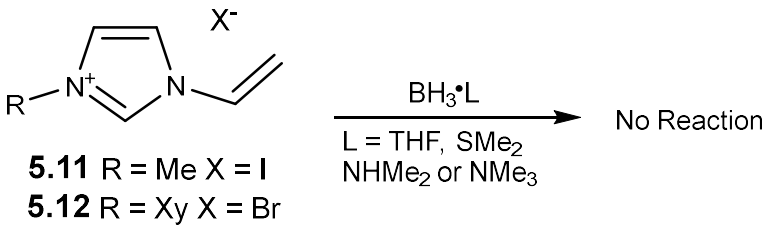

Scheme 5.7. Attempted hydroboration of vinyl imidazolium salts

Extending the scope of the test reactions to use catechol borane and 9-BBN also presented no reactivity associated with hydroboration of the vinyl group. The reactivity was tested over a temperature range of –94 °C to refluxing THF. This reinforces the possibility that the vinyl group forms part of an extended π system that increases its stability and therefore decreases its reactivity and the possibility of hydroboration. This stubbornness to react is maintained even in the imidazolium salts.

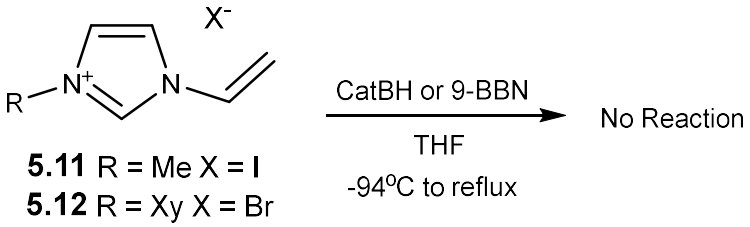

Scheme 5.8. Attempted hydroboration of vinyl imidazolium salts using CatBH and 9-BBN

5.2.4 Synthesis vinyl functionalised carbenes

Initial attempts to deprotonate the vinyl imidazolium salts **5.11** and **5.12** were carried out using copper (I) oxide and copper (I) acetate. Copper (I) salts have previously been utilised in the direct synthesis of copper NHC complexes. In this case the reaction was carried out under a nitrogen atmosphere in acetonitrile. Whilst monitoring the reaction there was no observable change in the colour of the solution for Cu_2O which was a red powder. Monitoring the reaction mixture using proton NMR spectroscopy for both copper (I) salts, at room temperature, for over a week did not show that any reactivity had occurred. This did not change after increasing the temperature of the solution which eventually reached reflux. NEt_3 was also employed to attempt to deprotonate the imidazolium salt but again deprotonation did not occur even after $[RhCl(cod)]_2$ was added to the mixture.

Silver oxide activation and subsequent transmetalation has been touted as a robust activation method for the generation of silver (I) carbene complexes as described by Lin and Wang in 1997.[216] Lin and Wang demonstrated that silver oxide was capable of deprotonating imidazolium salts to generate their respective silver carbene complexes. The reaction involves two equivalents of imidazolium salt to one equivalent of Ag_2O and the resultant carbene complex is generated via the release of water. The product from this reaction is typically a white solid that is sensitive to light. The advantage of generating silver (I) carbene complexes is that the complex can be added to a series of metal precursors in order to undergo transmetalation of the ligand to a new metal centre. Thus, leading to the synthesis of many metal complexes bearing the same carbene ligand.

The reaction of both **5.11** and **5.12** with Ag_2O proceeded over 74 hours in MeCN and was monitored by ^1H NMR spectroscopy. The disappearance of the NCHN acidic proton suggested that the product was the corresponding carbene in both cases. The resultant product was collected by filtration of the reaction solution and removing MeCN under vacuum gave a brown solid **5.14** and a white solid **5.13**. Both products once removed from solution were very insoluble in most solvents, analysis by NMR was carried out in DMSO-d_6 by slightly warming a suspension of product and subsequent filtering directly

into an NMR tube. In complex **5.13**, the first indication of carbene formation is again the absence of the acidic imidazolium proton in the ^{1}H NMR spectra which, suggests that carbene formation has occurred. The environments for the methyl, imidazole backbone and vinyl all remain albeit with different chemical shift values indicting that the groups remain the same but are in different chemical environments. The change in chemical shift is due to the influence of the newly formed silver carbene bond. The ^{13}C{^{1}H} spectra confirmed the presence of a silver carbene bond with a downfield peak of 184.2 ppm. The fragmentation in the mass spectra shows that a singular iodide is lost to give the molecular peak at m/z = 558 which suggests the product is present as dimeric species **5.13**.

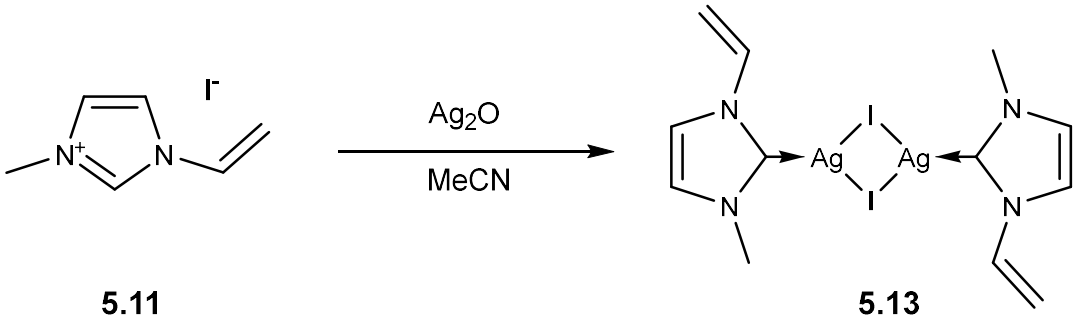

5.11 **5.13**

*Scheme 5.9. Synthesis of the dimeric silver iodide carbene complex **5.13***

Again, as in **5.13**, **5.14** was first indicated by the absence of the acidic imidazolium proton located on the NCN carbon of the former imidazolium ring in the ^{1}H NMR spectra. When compared to the spectra of **5.12**, the chemical environments with the exception of the acidic imidazolium proton are all present in the spectra further confirming that a silver carbene complex has indeed been formed. In the ^{13}C{^{1}H} NMR studies of **5.12**, the resonance corresponding to the carbene was located at 180.7 ppm, which is in the same region as **5.12** confirming that carbene formation has occurred. In contrast to **5.13**, mass spectrometry on **5.14** shows loss of silver dibromide suggesting that the silver complex is present as a bis carbene-bis silver complex m/z = 503.14 [M-$AgBr_2$] with silver(I) dibromide readily lost as the counterion. It is not uncommon for the structures of such silver carbene complexes to differ based on the substituents on the imidazolium unit.[189,216–222] Heating this complex in MeCN resulted in degradation of the compound leaving a black precipitate in the reaction flask. This showed that the

complex was both heat sensitive and insoluble. Unfortunately, despite a number of attempts it was not possible to obtain single crystals of either complex suitable for analysis.

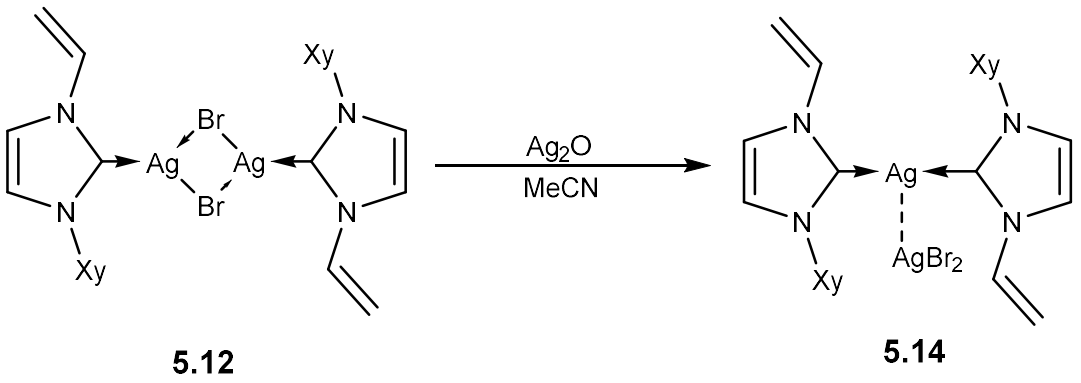

5.12 **5.14**

*Scheme 5.10. Synthesis of the dicarbene complex **5.14***

5.2.5 Synthesis of a rhodium carbene complex

As stated previously, the silver oxide method for activation of carbenes by Lin and Wang utilises silver's ability to be used as a transmetalation reagent, in which the silver complexes are added to a metal precursor and the carbene ligand preferentially binds to the new metal centre. $[RhCl(cod)]_2$ was selected as the metal precursor as rhodium catalysts are prevalent in hydrogenation chemistry and supported borohydride complexes are well studied by our group.[98,223–225] The synthesis of $[RhCl(cod)]_2$ was carried out in accordance with previously reported procedures.[226] After refluxing two equivalents of $RhCl_3 \cdot 6H_2O$ in the presence of two equivalents of cod in a degassed 5:1 ethanol water mixture and orange powder formed in the flask. The orange powder was collected by filtration and presence of $[RhCl(cod)]_2$ is confirmed using ^1H NMR spectroscopy.

The silver complex **5.13** was added in equimolar quantities to $[RhCl(cod)]_2$ in DCM. On addition, the solution immediately turned yellow and a white precipitate (silver halide salt) had formed, the solution was filtered after one hour of stirring and the DCM was removed under vacuum to give a yellow powder. ^1H NMR analysis of the product was performed in $CDCl_3$ showed that both the vinyl and imidazole protons remain present in the spectra with the same integration and splitting patters albeit with slightly shifted resonances. The presence of the cod ligand is also confirmed with environments that have shifted downfield from that of the $[RhCl(cod)]_2$ precursor. $^{13}C\{^1H\}$ NMR experiments unambiguously confirmed the presence of a rhodium carbene bond with a characteristic doublet as a result of Rh-C coupling at 186.0 ppm and a coupling constant of 51.8 Hz (Figure 5.5). Further confirmation of the presence of the desired product came from an ESI parent ion of m/z = 319.06 indicating loss of the chloride ion.

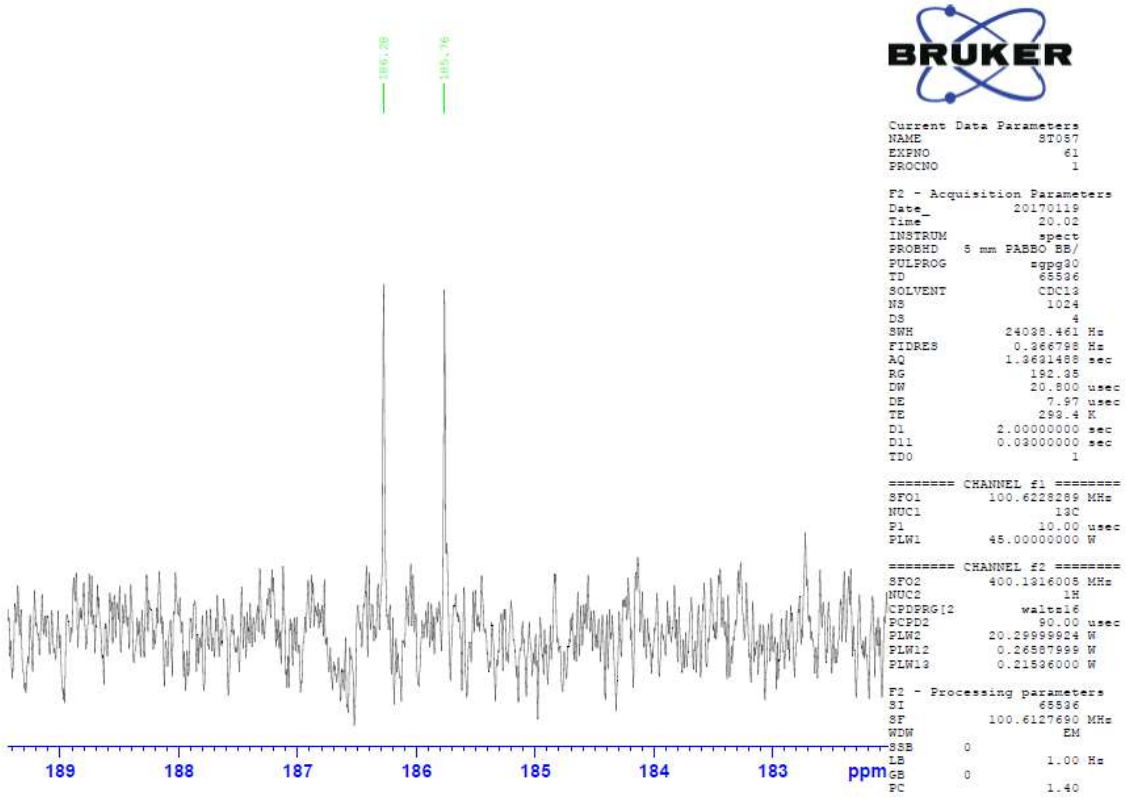

Figure 5.5. $^{13}C\{^{1}H\}$ *NMR spectra showing C-Rh coupling in* ***5.15***

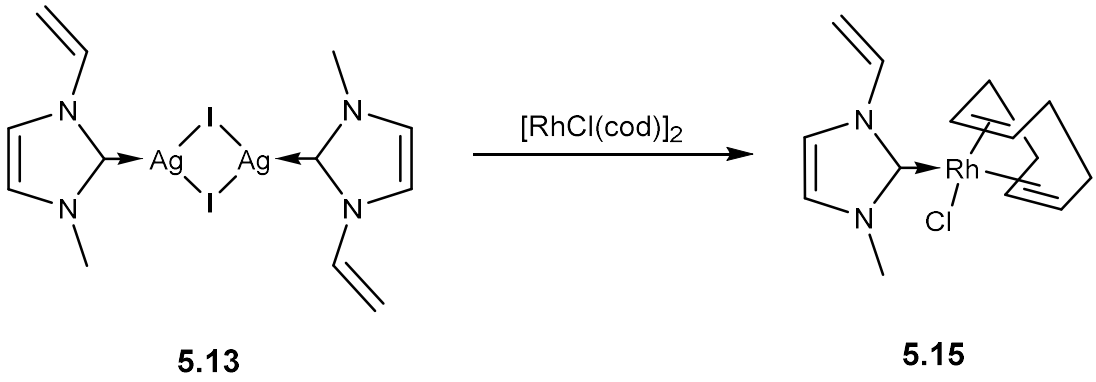

5.13 **5.15**

Scheme 5.11. Use of the silver carbene complex ***5.13*** *as a transmetalation reagent for the synthesis of the rhodium carbene complex* ***5.15***

Following on from the synthesis of complex **5.15** further hydroboration attempts were studied to investigate whether coordination of carbene to rhodium has any effect on the propensity of the vinyl group to undergo hydroboration at the rhodium centre. On addition of one equivalent of a 1 M

BH_3·THF solution at room temperature to the complex**,** the reaction mixture gradually turned black and ^{11}B NMR analysis reveals several products in solution. Lowering the temperature and cooling the reaction in an ice bath also resulted in the solution turning black. The black colour indicates the presence of rhodium in the oxidation state 0 and therefore suggests that the reactivity that has taken place at the metal centre is a reduction from the rhodium (I) centre in **5.15**.

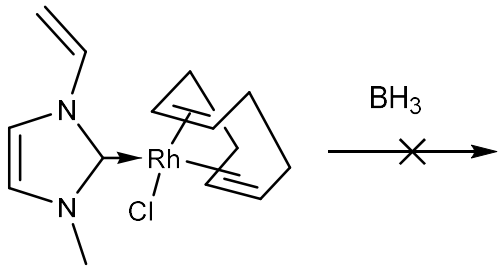

5.15

Scheme 5.12. Hydroboration attempts of a rhodium vinyl-carbene complex

From these studies, it was clear that the prospects of hydroboration were not improved by addition of the vinyl carbene ligand to a rhodium centre and that the pattern of stubbornness to hydroboration extends across all compounds. This is because the vinyl group attached to the imidazole ring most likely forms part of an extended π-system this grants the vinyl group greater stability than if it was attached to an allyl substituent, which is not broken by coordination of the ligand to rhodium and the vinyl groups stability remains consistent. This was apparent in the $^{13}C\{^1H\}$ studies which on coordination of a double bond would observe Rh-C coupling as seen in the cod ligand, however this is not the case.

5.3 An alternative method involving boron-containing alkylating reagents

As it was clear hydroboration was not a viable option for the stubborn vinyl imidazole-based ligands attention was turned to adding an imidazole through a 'pre functionalised' boron containing alkylating reagent. Previous work completed by Brown had shown olefinic halides can undergo hydroboration. An example of this reactivity is the hydroboration of 1-chloro-2-methyl-propene **5.16.** This has been performed by the addition of equimolar quantities to a borane solution as shown in Scheme 5.13.[227] Further reactivity can take place at the BH_2 moiety, in which, it has been oxidised to an aldehyde or converted into a boronic acid by the addition of water. The presence of 2 methyl groups on the second carbon allows for the selective addition of the boron to the carbon in the 1 position which is less substituted. This reaction could then be employed as an alkylating reagent in the functionalisation of imidazolium salts. When further reacted into a carbene complex this could potentially create a 3-atom bridge supporting the borane unit in a Z-type interaction with the metal centre.

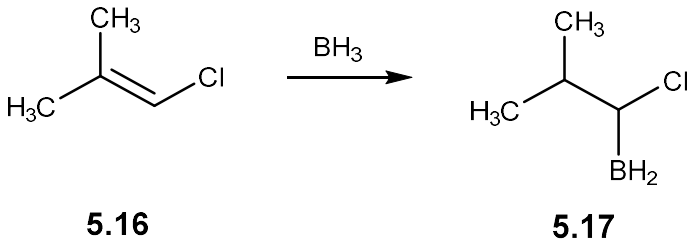

5.16 **5.17**

Scheme 5.13. Hydroboration of a chloroalkene as reported in the literature.

Hydroboration of 1-bromo-2-methyl-propene was also reported using catechol borane under reflux or with Wilkinson's catalyst at room temperature. Using Wilkinson's catalyst, it was reported that after 28 hours a 98% yield was obtained following purification and isolation by distillation. However, our attempts at this reaction did not proceed in the manner reported. After 18 hours at room temperature in toluene in the presence of Wilkinson's catalyst no reactivity was observed in solution state NMR studies. After heating the reaction to 90°C for a few hours, an aliquot of the reaction mixture was taken, and a white solid remained after removal of the solvent in vacuum. The white precipitate was dissolved in chloroform and ^{1}H NMR studies indicated the presence of both hydroboration isomers in

the ^{1}H NMR this is because of several different peaks observed in the upfield region of the spectra and in the ^{11}B NMR new singlets emerged at 29.6, 32.2, 35.3 and 66.8 ppm. As the hydroboration did not proceed as expected, it was decided to try a different approach.

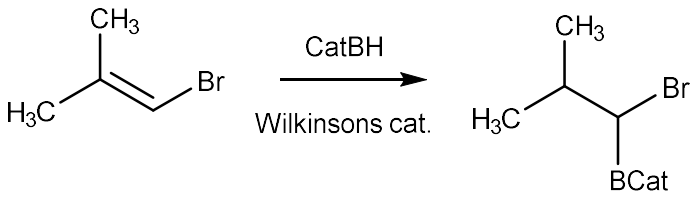

5.18 **5.19**

Scheme 5.14. Expected reactivity for the hydroboration of a bromoalkene using Wilkinson's catalyst

The proposed compound **5.22** was also targeted as a potential starting material for supported borane/ borohydride ligands. Bromo benzene boronic acid **5.20** can be synthesised via the lithiation of dibromo benzene, subsequent addition of $B(OMe)_3$. An acidic work up followed by a recrystallisation from water results a white solid in good yields 66%.[20] Pinacol was added to resulting bromo benzene boronic acid in an equimolar ratio in ether. After stirring for 24 hours a TCL was run of the reaction mixture using silica plates and ether as the mobile phase. The TLC plate showed that the reaction had gone to completion. Fresh ether was added, and the organic layer was washed with water and subsequently dried using $MgSO_4$, removal of solvent under vacuum gave the product bromobenzene pinacol borane in a 95% yield. The NMR was in good agreement with literature data for the compound.[228] BPin functionality was added as a precautionary measure as the next planned step in the reaction was an coupling step, cross coupling reactions involving copper are a well-studied and well known area of chemistry in particular C-N bond formation.[229] The reaction will typically involve a copper salt in the presence of a ligand, base and an aryl halide or boronic acid.[230] In the first attempt we decided to use available reagents as it appeared that the ligand choice was not crucial, this is because of the large variety of ligands reported for this reaction.[231] The test reaction was carried out in MeCN as this has also found use as a ligand in catalytically active copper (I) complexes. The copper

salt used was copper iodide in conjunction with the base K_2CO_3. This reaction was monitored by both ^{11}B and ^{1}H NMR in which no coupling was observed and only the imidazole BBBA adduct was observed.

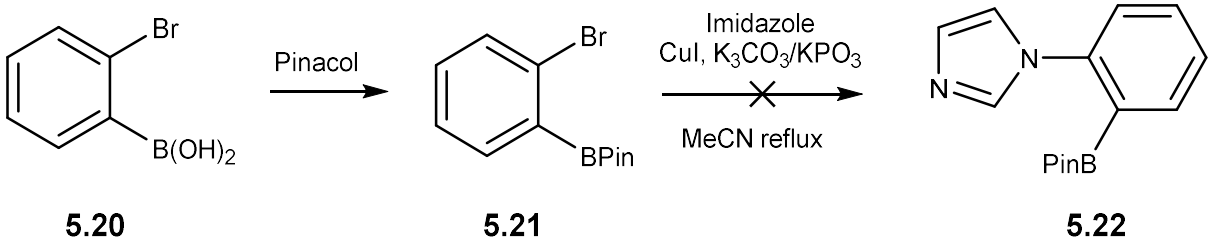

5.20 **5.21** **5.22**

Scheme 5.15. Synthesis and attempted further reactivity of bromo benzene boronic acid pinacol ester

One example of a copper coupling catalysed reaction that has previously been reported in good yields uses the ligand **5.24**. The ligand **5.24** is synthesised by the procedure outlined by Kim (Scheme 5.16).[232] Hydrazine was added to a methanol solution of salicylic aldehyde (**5.23**), the product **5.24** precipitates out of solution and is purified by Buchner filtration and subsequent washing with hexanes. The ligand **5.24** formed part of a study by Cristau in which they tested a series of ligands for copper cross coupling reactions in order to identify the best systems using aryl bromides and iodides.[233]

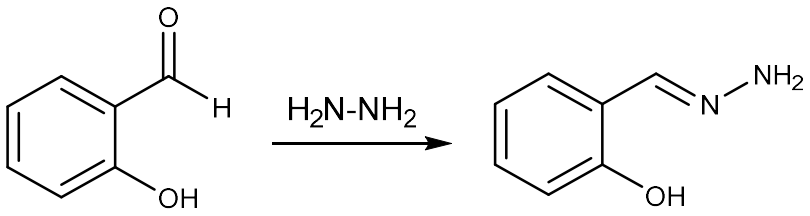

5.23 **5.24**

*Scheme 5.16. Synthesis of ligand **5.24** from salicylic aldehyde*

The study, which tested 12 potential ligands and found that using 5% mol equivalent of Cu_2O in combination with 20 mol% of **5.24** reached completion for the coupling of phenyl bromide to imidazole after 100 hours of reflux (Scheme 5.15). The same reaction was therefore set up to test for coupling of **5.23** to imidazole. Following the same conditions as reported the reaction mixture was heated to reflux for 100 hours and aliquots were taken at 8, 24, 32 and 100 hours which were assessed

by ^{1}H and ^{11}B NMR spectroscopy, after which time again only the imidazole BPin adduct was observed. This suggests that the catalytic activity does not extend to this compound.

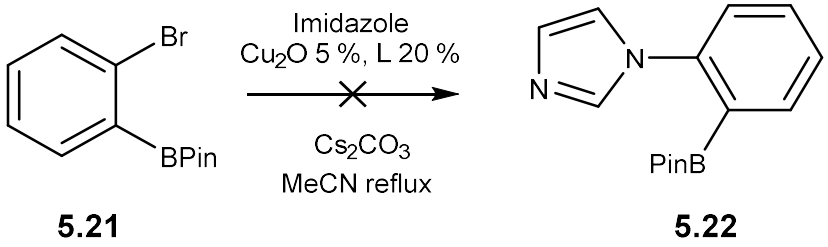

5.21 **5.22**

*Scheme 5.17. Attempted copper cross coupling between **5.21** and imidazole*

Chuzel and Parrain, reported the synthesis of carbene complexes containing a pendant Lewis acidic boronic ester moiety (Scheme 5.18). Their carbene complexes containing the BPin moiety tethered to the N-heterocyclic carbene via a propyl chain, the use of a propyl chain in this case does not lead to any kind of interaction between the metal and the boron. They synthesised ligands **5.26** and **5.27** by the addition of a pre-functionalised alkylation reagent **5.25**. This was carried out under reflux in order to prevent adduct formation. The pendant BPin moiety was confirmed by a single resonance at 34.0 (for **5.26**) and 33.3 ppm (for 5**.27**) in the ^{11}B NMR spectra. Both compounds showed the presence of the acidic imidazolium proton at 11.00 and 10.72 ppm.[234]

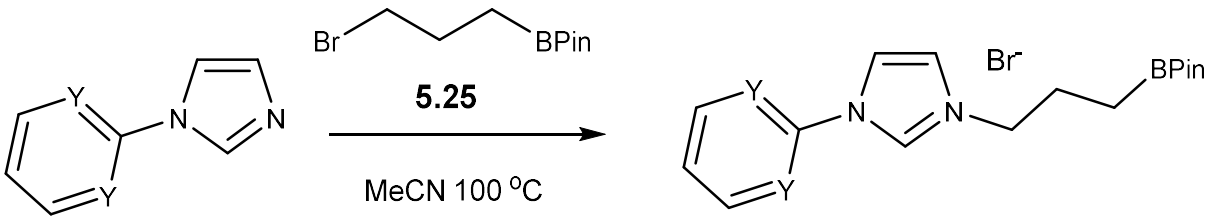

5.23 Y = CH
5.24 Y = N

5.26 Y = CH
5.27 Y = N

*Scheme 5.18. N-quaternarisation reactions involving **5.25***

Carbene formation was achieved in quantitative yields for both **5.26** and **5.27**, resulting in the formation of complexes **5.28** and **5.29** the resultant bis carbene silver complex was similar in structure to that observed for **5.14** as it results in the formation of a bis silver complex with a silver dibromide

anion. The first indication of carbene formation comes from the disappearance of the acidic imidazolium protons and then subsequently significant downfield shift of the attached carbon in the $^{13}C\{^{1}H\}$ spectra to 179.7 and 183.5 ppm. The parent ions for these complexes give ions at m/z = 731.4 and 735.1 for **5.28** and **5.29** respectively which represents loss of the silver dibromide anion in both cases which again suggests the presence of the silver bis carbene cationic complexes. Again, the BPin moiety remains pendant with ^{11}B NMR resonances of 33.3 and 33.7 ppm.

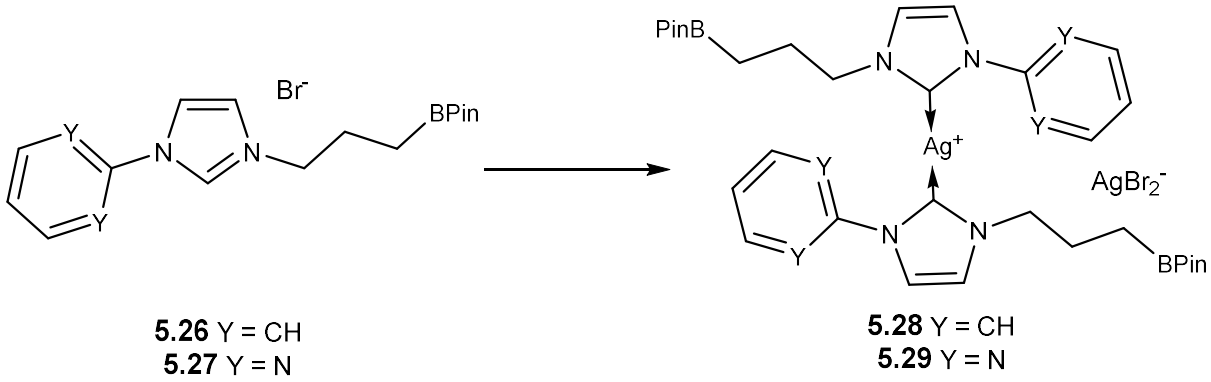

Scheme 5.19. Formation of silver carbene complexes bearing a pendant BPin moiety

Both ligands were utilised in the synthesis of rhodium, palladium, and gold complexes, demonstrating the versatile nature of silver oxide as a transmetalation agent for carbenes. One such example of this reactivity is presented with the addition of the ligand **5.29** to the rhodium cod dimer this occurs in equimolar quantities and proceeds in DCM whilst stirring for 1 hour. The resultant product was a yellow solid and indication that a rhodium carbene bond has formed is apparent from the $^{13}C\{^{1}H\}$ NMR spectra in which a doublet at 182.2 ppm with a coupling constant of 51.3 Hz. In this complex the BPin moiety remains pendant this is confirmed initially by ^{11}B NMR which remains a singlet at 33.4 ppm if any interaction between the rhodium had occurred you would expect an upfield shift and or coupling with the rhodium would be observed. This is confirmed in the published crystal structure which clearly shows the BPin Group as pendant. Using a propyl tether does not result in a favourable ring size so there is no driving force to form any interaction with the metal.

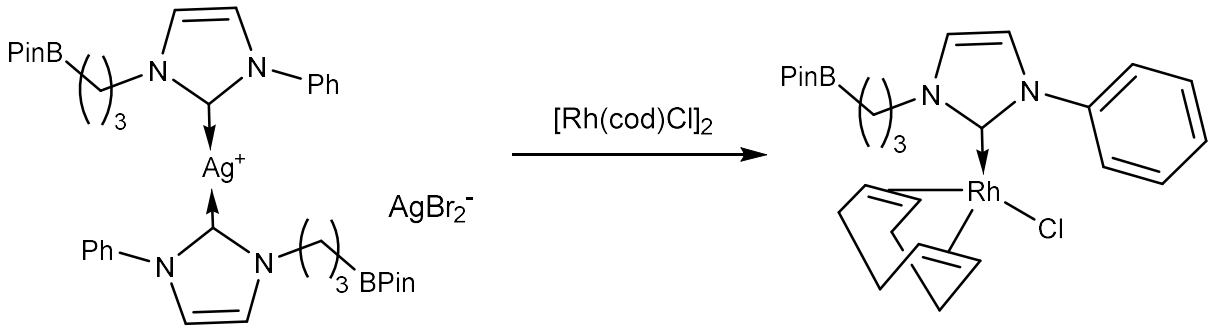

5.28 **5.30**

Scheme 5.20. Synthesis of a rhodium (I) complex bearing a pendant BPin Moiety

5.3.1 Synthesis MeBPin imidazolium salts

Whilst Chuzel and Parrain were successful in synthesising carbene complexes with a boron containing functional group, their methods did not observe any rhodium boron Z-type interaction. One such reason for this can be attributed to the length of the carbon chain to which the BPin moiety is attached. This results in a potential ring size of seven atoms which is two atoms greater than the more favourable stable five membered ring. For this reason, our research looked at reducing the chain length and attempted to synthesise the respective carbene with the potential to form a rhodium Z-type interaction. Our strategies to achieve this are outlined in the following sections.

The compound bromo methyl boronic acid pinacol ester ($BrCH_2BPin$) can be synthesised by the lithiation of dibromo methane and subsequent addition to the boronic ester or it can be obtained from commercial sources. The addition of $BrCH_2BPin$ to methyl imidazole occurs at room temperature in toluene and results in the formation of a white powder (Scheme 5.21). Subsequent uptake of the product in $CDCl_3$ and analysis by NMR reveals an upfield shift to 7.7 ppm this suggests that adduct formation had occurred. The ^1H NMR also suggested that the N-quaternarisation reaction had occurred resulting in the formation of an imidazolium salt which was identified by the imidazolium salt acidic proton at 9.37 ppm in addition to which there was also additional methyl imidazole present in the ^1H NMR spectra suggesting that the adduct had formed with an additional equivalent of methyl imidazole. $^{13}C\{^1H\}$ studies of the complex showed all the expected environments and was assigned with the aid of HSQC and HMBC experiments. The HSQC experiment was essential in the observation of the BCH_2 carbon peak as this is present as a very broad peak which is not distinguishable as a peak without HSQC experiments. Integration of the baseline further confirmed that the peak was indeed due to a single carbon. ESI studies of the compound revealed the parent ion to be the pendant $MeImCH_2BPin$ cation without the adducted methyl imidazole, however, elemental analysis further confirmed that the product was indeed **5.34**.

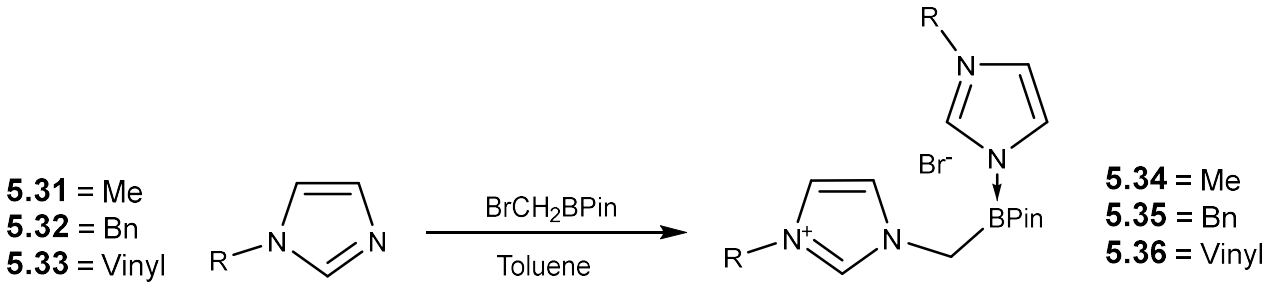

Scheme 5.21. N-quaternarisation reactions of functionalised imidazoles using $BrCH_2BPin$

In addition to the methyl derivative **5.31**, both benzyl **5.32** and vinyl **5.33** derivatives were employed. These compounds were also obtained in good yields 99% (for **5.32**) and 86% (for **5.33**). In both cases adduct formation was observed giving ^{11}B NMR resonances of 8.1 and 14.7 ppm for **5.32** and **5.33,** respectively. ^{1}H NMR spectroscopy again showed that the NCHN proton has become more acidic as a result of this reaction with resonances shifted downfield to 9.61 and 10.23 ppm (Figure 5.6).

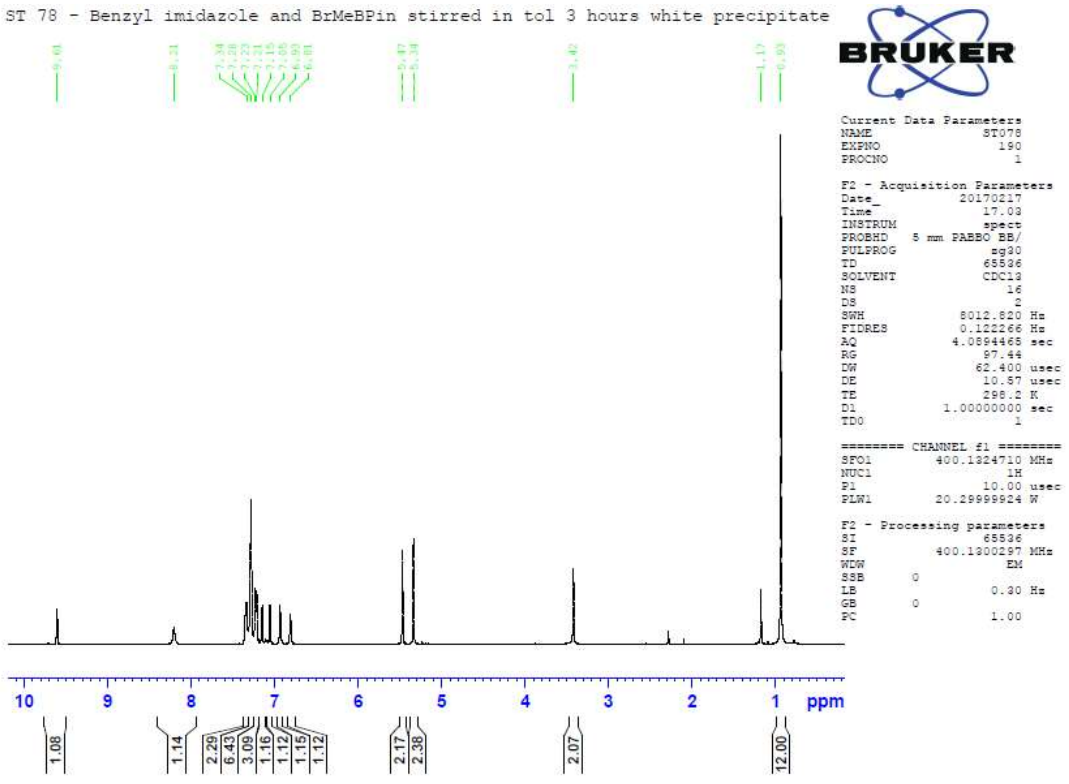

*Figure 5.6. ^{1}H NMR spectra of **5.35***

In addition to the synthesis of the products **5.34**, **5.35** and **5.36** which contained an additional equivalent of imidazole. We also targeted the synthesis of imidazolium salts in which the BPin moiety

remained pendant. Our room temperature reactions with toluene with a single equivalent of imidazole, again favoured the adducted imidazolium salt. However, Chuzel and Parrain's synthesis utilised refluxing acetonitrile to combat the formation of the adducted product. Our initial attempt with equimolar quantities of methyl imidazole and bromo methyl boronic acid pinacol ester whilst refluxing in acetonitrile, did indeed generate the respective imidazolium salt with the BPin moiety remaining pendant as the favoured product. However, this reaction also generated the adducted product **5.34** which could not be separated from the mixture. The use of more bulky substituents on the functionalised imidazole such as benzyl, vinyl and phenyl groups were more successful in that the respective spectroscopically pure non-adducted products **5.38**, **5.39** and **5.40** were obtained (Scheme 5.22). The synthesis of **5.32** was achieved by adding equimolar quantities of benzyl imidazole and $BrCH_2BPin$ in acetonitrile under reflux for 2 hours. Following this the volume of the solvent was reduced under vacuum until the solution was very concentrated and the product precipitated out of solution by cooling to −40 °C, this gave the product as a white solid that was present in a yield of 57%. Again, addition of the CH_2BPin moiety to the nitrogen of the imidazole gave rise to a more acidic NCHN proton. This proton was present in the ^{1}H NMR spectra at 9.43 ppm. The ^{11}B NMR spectra confirmed that the BPin moiety was pendant with a singlet present at 31.5 ppm which is a clear difference from the benzyl imidazole adduct **5.35** at 8.1 ppm and closer to **5.26** and **5.27**. The $^{13}C\{^{1}H\}$ spectra again has a very broad peak of which the presence is confirmed by HSCQ experiments at approximately 36.5 ppm. Both vinyl and phenyl products undergo N-quaternarisation without adduct formation after reflux in acetonitrile which is confirmed by the free BPin resonances in the ^{11}B spectra at 30.7 (**5.39**) and 28.6 (**5.40**) ppm respectively.

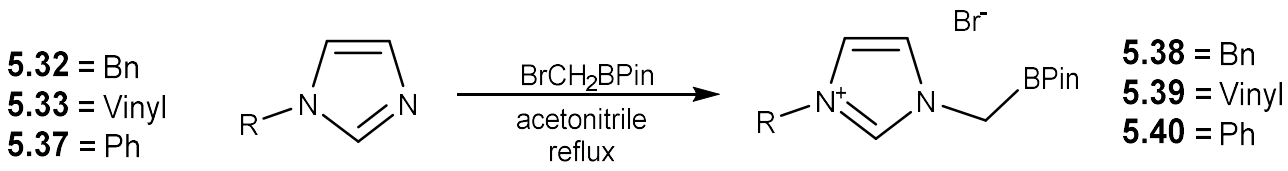

*Scheme 5.22. Synthesis of pendant BPin imidazolium salts **5.38**, **5.39** and **5.40**.*

In addition to the bromide salts in the phenyl derivative **5.40** the Br^- ion was exchanged for a PF_6^- anion. The counter ion exchange reaction was carried out in acetonitrile and on the addition of KPF_6 a white precipitate immediately crashed out of solution. The precipitate was tested using powder film IR and found to be KBr and the product identified by solution NMR experiments was present in solution, isolation of which was achieved by removal of MeCN under vacuum. The NMR of the product clearly showed the presence of the PF_6^- anion in solution with a doublet in the ^{19}F NMR spectra at −70.2 ppm ($^1J_{PF}$ = 710 Hz) and a septet in the ^{31}P NMR at −144.2 ppm ($^1J_{FP}$ = 710 Hz). The ^{11}B NMR experiences a slight upfield shift to 28.6 ppm and the imidazolium proton becomes slightly less acidic with a ^1H resonance corresponding to a single proton at 9.68 ppm.

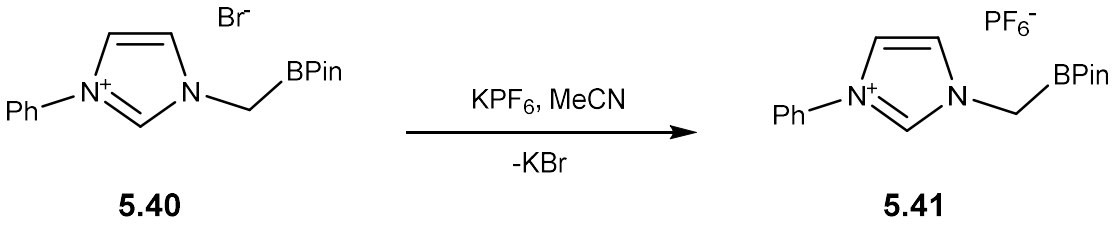

5.40 **5.41**

*Scheme 5.23. Counter ion exchange of Br^- for PF_6^- in **5.40***

5.3.2 Activation attempts

Following Lin and Wang's silver oxide method previously utilised by Perrain and Chauvin in their synthesis of carbenes containing the BPin moiety. **5.34**, **5.35**, **5.36**, **5.38**, **5.39** and **5.40** were all added to silver oxide in acetonitrile (Scheme 5.24). The reaction solution was monitored by taking small aliquots and analysing by ^{1}H NMR however no evidence of carbene formation was observed. If carbene formation was observed the acidic NCHN proton would have disappeared. The reactions were left for a few weeks after which final aliquots were taken and analysed by both ^{1}H and $^{13}C\{^{1}H\}$ experiments again no disappearance of the imidazolium peak was observed or carbene peak formation observed in the carbon. This was repeated for the silver oxide precipitate in which the same was observed. This result was surprising as the silver oxide method has previously been touted as a robust method for generating carbenes and was utilised by Perrain and Chauvin.

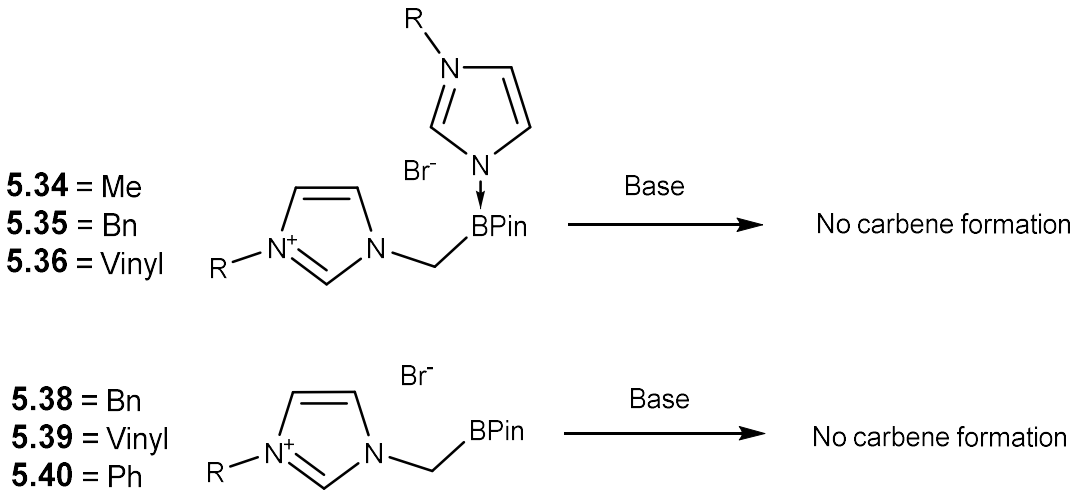

Scheme 5.24. Addition of a base to imidazolium salts bearing both adducted and non-adducted BPin moiety's

The reaction with silver oxide was also tested in the presence of $[RhCl(cod)]_2$, in this reaction the imidazolium salt still remained after several days of stirring. In the $^{13}C\{^{1}H\}$ NMR spectrum there was a slight indication of a doublet being formed in the carbene region which would be consistent with a rhodium carbene bond. Any attempt to separate this minor product from the reaction mixture proved unsuccessful this reactivity is not favoured as there are still large amounts of starting material available

after several days. Further basic metal salts such as Cu_2O and $Pd(OAc)_2$ were tested for activation but again no carbene formation was observed. As rhodium carbene bonds had been observed but the Ag_2O method was ineffective at generating the desired complexes it was decided to synthesise some rhodium complexes that contained internal bases to see if this was an effective method of generating the carbene complex.

Previous literature examples show that the chloride in the complex **[RhCl(cod)]$_2$** can be readily substituted for either an acetate or an methoxy group, these groups have previously been used as bases in alkali metals to generate carbene ligand.[235,236] The complex **[Rh(OAc)(cod)]$_2$** was synthesised from the addition of KOAc to **[RhCl(cod)]** in acetone (Scheme 5.25). The reaction was heated to reflux for 18 hours and followed by a filtration and removal of acetone under vacuum to give the crude product as a dark orange solid. This is subsequently recrystalised from ethyl acetate to give "blood orange" crystals. Subsequent NMR, IR and MS analysis of this compound matched with the previously reported spectra.[237] The complex **[Rh(OMe)(cod)]$_2$** again is a known compound and the previously reported procedure for its synthesis was followed. The resultant yellow product is crystalized from DCM hexane and is again consistent with previously reported NMR data.[238,239] A test reaction on an NMR scale was used to confirm the expected reactivity of **[Rh(OAc)(cod)]$_2$** as a basic metal salt that is capable of generating a carbene. The test reaction utilised the imidazolium salt **5.11** in which the imidazolium is functionalised with both a vinyl and methyl group. The imidazolium salt **5.11** was previously demonstrated to deprotonate and form the respective silver complex **5.13** (Scheme 5.9) and subsequently form the rhodium complex on addition of **[RhCl(cod)]$_2$** to a solution of **5.13** in DCM. Since we have confirmed that **5.11** may undergo deprotonation to subsequently form a rhodium carbene complex it was selected for the test reaction. Half an equivalent of **[Rh(OAc)(cod)]$_2$** was added to a solution of **5.11** in $CDCl_3$ in an NMR tube in which the reaction solution was monitored by NMR spectroscopy. Over the course of a few hours, the ^{1}H NMR spectra observed the gradual disappearance of the acidic imidazolium peak at 9.56 ppm. Once the reaction had reached completion a further $^{13}C\{^1H\}$ experiment clearly indicated the presence of a rhodium carbene bond in the spectra

with a doublet at 185.5 ppm ($^1J_{CRh}$ = 49.4 Hz) in $CDCl_3$. This confirms that a rhodium carbene complex had clearly been formed in the reaction and that the [Rh(OR)(cod)] complexes were suitable reagents for carbene activation.

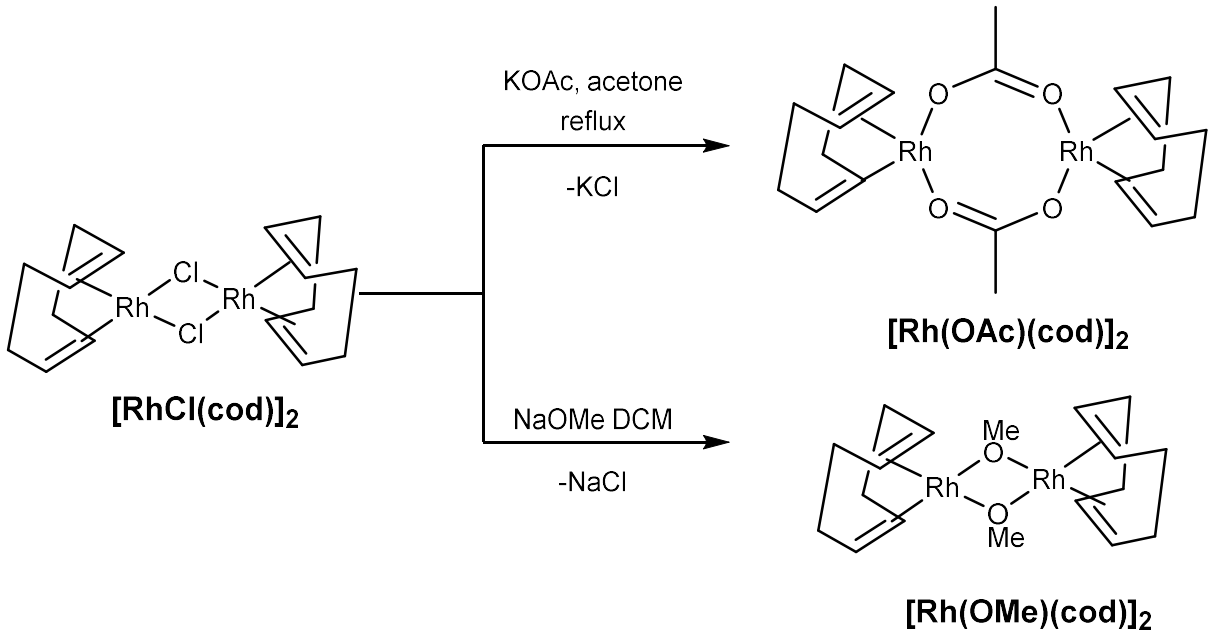

Scheme 5.25. Synthesis of the complexes [Rh(OAc)(cod)] and [Rh(OMe)(cod)]

The rhodium (I) methoxy and acetate complexes **[Rh(OAc)(cod)]$_2$** and **[Rh(OMe)(cod)]$_2$** were both tested on NMR scale test reactions for the deprotonation of imidazolium salts **5.34**, **5.35**, **5.36**, **5.38**, **5.39** and **5.40** in DCM-d_2. The imidazolium precursors when added did not give any sign of reactivity associated with the formation of a rhodium carbene bond. It was therefore decided to try some stronger bases such as NaH, LiHMDS, KHMDS and LDA, no deprotonations were observed again using these bases. Another reaction that was attempted was the addition of a metal hydride species such as $[CoH\{P(OPh)_3\}_3]$[240] in attempt to generate a carbene and release hydrogen this was attempted by heating DCM to reflux and stirring overnight, however no reactivity was observed. Further attention was drawn to the HMDS ligand which has been touted as a non-nucleophilic basic ligand which could be used for the activation of these imidazolium salts. The complex **[Cu(HMDS)]$_4$** was generated *in situ* by the addition of a **LiHMDS** solution toluene to suspension of copper(I) iodide (CuI) in THF (Scheme 5.26). Once the CuI was no longer present as a suspension the respective imidazolium salts were added

with no observed reactivity.[241] **[Zn(HMDS)$_2$]** can also be generated by the addition of **LiHMDS** to $ZnCl_2$, this again was synthesised according to a previous procedure set out by Power in 1991.[242] The complex **[Zn(HMDS)$_2$]** again showed no signs of activating the imidazolium salts to form a carbene ligand.

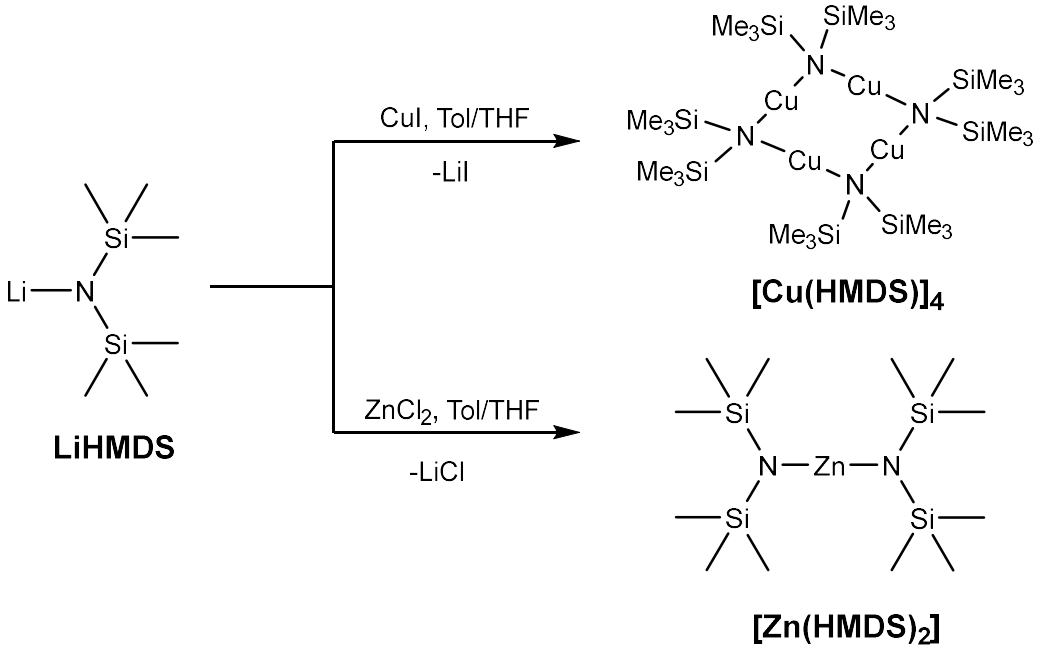

*Scheme 5.26. Synthesis of the complexes **[Cu(HMDS)]$_4$** and **[Zn(HMDS)$_2$]***

Organolithium reagents are important tools in synthetic chemistry as they allow for the nucleophilic addition of both alkyl and aryl substituents.[243–245] This includes the synthesis of organoboron compounds from boronic acid or boronic esters.[246] In addition to the former, organolithium compounds have been previously used to generate carbenes.[247] The reagents phenyl lithium (PhLi) and *n*-butyl lithium (*n*-BuLi) were both reacted with **2.40** in attempt to generate a carbene species (Scheme 5.27). However, the reactivity observed was not consistent with the generation of a carbene. The solution state NMR of the reaction between PhLi and **2.40** gave clear indication of the formation of a 4-coordinate boron giving a singlet at 6.0 ppm in the ^{11}B NMR spectra. This suggested that the phenyl group had undergone nucleophilic addition at the boron generating the proposed species **5.41A**. Whilst PhLi has preference for nucleophilic substitution at the boron, it was decided to add further equivalents of PhLi in order to probe whether deprotonation will occur. On the addition of three equivalents of PhLi, the resonance corresponding to the acidic imidazolium proton at 10.69 ppm

in the ^{1}H NMR spectra had disappeared. Confirmation of the formation of a carbene in solution was obtained by the presence of a new singlet in the $^{13}C\{^{1}H\}$ NMR spectra at 195.7 ppm. Further reactivity at the boron was indicated by a shift to 7.8 ppm in the ^{11}B NMR spectra. The *in situ* NMR observations suggest the formation of **5.41B** in solution. This observed species, however, could not be isolated from the reaction mixture. Acidic workup using 1M HCl in ether results in the loss of the carbene functionality. The product of this reaction could not be identified and isolated from the reaction mixture. This reactivity, however, gives an indication that a 4-coordinate, negatively charged boron species may be more prone to deprotonation and this should be investigated further.

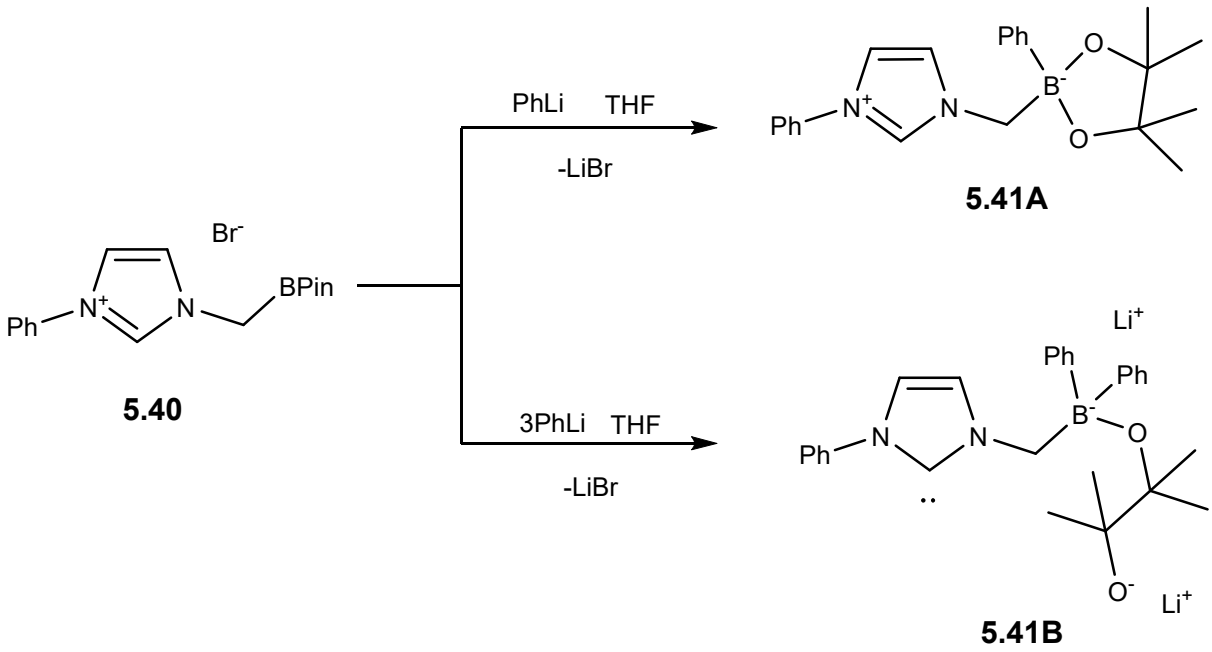

*Scheme 5.27. Addition and reactivity of **5.40** with different quantities of PhLi generating the proposed products **5.41A** and **5.41B***

5.3.3 Reduction using $LiAlH_4$

Whilst a BPin moiety forming a Z-type interaction with a metal centre would provide for an interesting compound, the main aim of this research involves the coordination and subsequent reactivity at metal centres. Lithium aluminium hydride ($LiAlH_4$) is a strong reducing agent that has been utilised in a variety of reductions, in particular, the reduction of boronic esters to borohydrides such as outlined in chapter 2 of this thesis. It is also possible that the presence of a BH_3^- moiety could lead to deprotonation and subsequent carbene formation as seen with the proposed reactivity of **5.40** in Scheme 5.27. The reduction of functionalised boronic esters to borohydrides is well known and was explored by Brown in 1984.[120] Following a similar procedure, the compounds **5.34**, **5.35**, **5.36**, **5.38**, **5.39** and **5.40** all undergo reduction in THF with 1.6 equivalents of $LiAlH_4$ (Scheme 5.29). Each reaction was able to demonstrate the formation of the respective products **5.42**, **5.43**, **5.44** and **5.45** *in situ*.

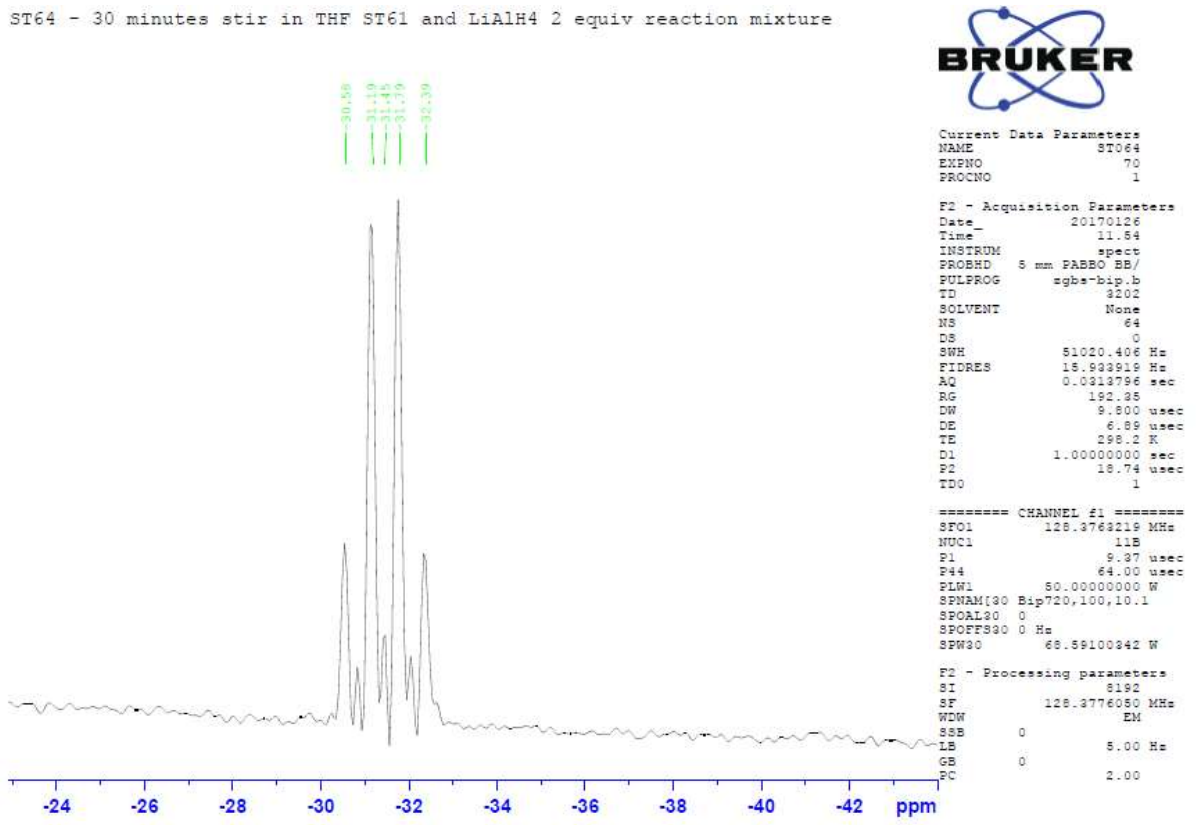

Figure 5.7. *^{11}B spectra indicating the formation of **5.42** in situ*

In the reaction of **5.35** with $LiAlH_4$, ^{11}B and $^{11}B\{^1H\}$ NMR spectroscopy were used to monitor the reaction mixture over the course of six hours. The reaction appeared to have reached completion after 20 minutes in which full conversion of the starting material **5.35** to the major product of the reaction (**5.43**) was observed. The product **5.35** was indicated as a quartet in the ^{11}B experiments at -31.4 ppm (figure 5.7), which resolves to a singlet in the $^{11}B\{^1H\}$ experiment. This represents a significantly more shielded resonance in comparison to the precursor **5.35** at 8.1 ppm. The splitting pattern in the ^{11}B NMR spectra confirms the presence of three hydrogen nuclei around the boron representing a BH_3^- group in solution. Following the formation of **5.35**, the reaction was continuously monitored by ^{11}B NMR spectroscopy. This showed the gradual formation of a new peak at -13.3 ppm. The peak was broad and poorly resolved on proton decoupling the half height width (h.h.w.) of the peak decreases from 621 Hz to 239 Hz. This indicates the presence of hydrogen around the boron centre. Following this another smaller quartet representing a BH_3^- moiety at −30.0 ppm is formed. This peak also overlaps the peak at -31.4 ppm corresponding to **5.35** but gives a distinct peak in the $^{11}B\{^1H\}$ NMR spectra. After 6 hours the ratio of the peaks is 12:3:5 for the peaks at -13.3, -30.0 and 31.4 ppm respectively and new smaller peaks at -6.2, -8.5, -33.5 and -41.2 ppm were also observed. This shows that continued reactivity of the BH_3 group occurs after 20 minutes and multiple side products are generated.

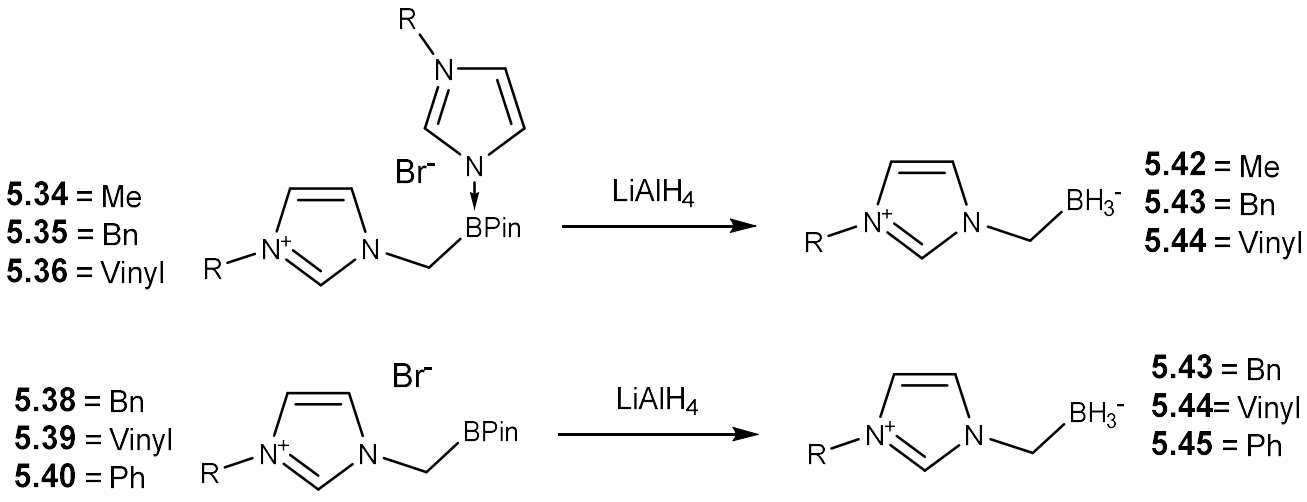

Scheme 5.29. Reduction of the BPin groups to BH_3^- using $LiAlH_4$

A repeat reaction was carried out, and after confirmation of successful conversion of **5.34** to **5.42**. The reaction was filtered to remove excess $LiAlH_4$ and lithium products and the THF was removed under vacuum to yield a viscous oil. To which, the addition of $CDCl_3$ resulted in the formation of an insoluble precipitate accompanied by effervescence. The spectrum of the filtrate was recorded. This gave a triplet at −8.3 ppm was observed which again resolved to a singlet in the $^{11}B\{^1H\}$ spectra, this chemical shift and splitting pattern suggests that there is a BH_2 group with adduct formation. This peak disappears after further precipitation and no new signals are formed. In the ^1H NMR spectra the resulting white precipitate could not be analysed by ^1H NMR spectroscopy as it was insoluble, this result suggests the possibility of polymer formation **4.46** (Scheme 5.30). In comparison after removal of solvents in vacuum and dissolving the viscous oil back into THF, the product **4.43** remained. This suggests that the addition of the NMR solvent $CDCl_3$ to the complex promotes release of H_2 and subsequent polymer formation. Similar observations were made on uptake into MeCN-d_3, DCM-d_2, benzene-d_6 and DMSO-d_6. Attempts to isolate and fully characterise **5.42** – **5.45** proved unsuccessful.

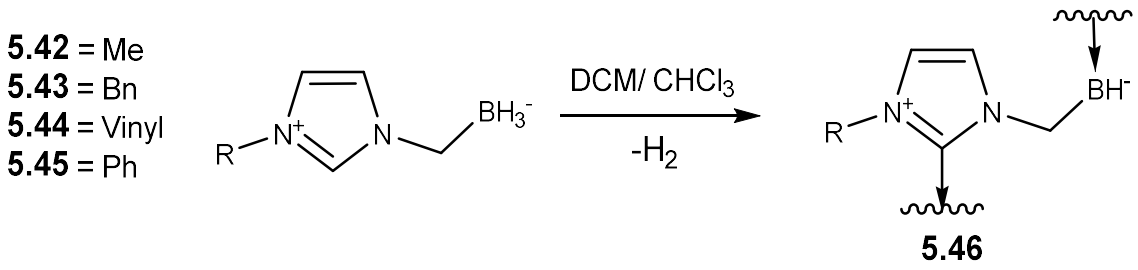

Scheme 5.30. Addition of DCM and $CHCl_3$ to zwitterionic imidazolium BH_3^+ compounds

Despite not isolating the BH_3^- zwitterionic compounds, the ^{11}B NMR data after 20 minutes of stirring the product had been fully converted and was of reasonable purity. The reaction mixtures of **5.43**, **5.44**, **5.45** were therefore employed in an attempt to synthesise a respective carbene complex given that we suspect that the loss of the acidic proton can easily be promoted. The addition of solutions of **5.42** – **5.45** to silver oxide did not result in carbene formation. In addition to this, when adding to a cooled solution of [Rh(OR)(cod)] complexes the solution turned black indicating the presence of rhodium black and therefore suggesting the reduction of the metal centre. As the release of H_2 gas

has also been observed on addition of chlorinated solvents (Scheme 5.30) more stable non-basic metal salts such as [AuCl(PPh_3)] were added in attempt to 'trap' the monomer before it formed a polymer, again as with the rhodium metal salts the solution turned black again indicating that the metal had been reduced.

5.3.4 Synthesis of iminium salts bearing a pendant BPin moiety

Cyclic alkyl amino carbenes (CAACs) are a new type of NHC developed by the Bertrand group.[248] One of the two nitrogen units from the NHC is replaced with an sp^3 carbon atom. This change results in a narrower HOMO-LUMO band gap when compared with traditional Wanzlick-Ardeungo NHC's. This in turn, results in a stronger σ-donating and stronger π-accepting ligand. A paper by Bertrand in 2016 outlined a procedure in which CAAC pro-ligands have been functionalised with the same simplicity that functionalised imidazole compounds have been modified to form their respective imidazolium.[249] Given the contrast in electronic properties of the CAAC ligand to that of NHC ligands. We contemplated the effect of utilising CAACs as supports for the BH_3^-/BPin moiety. Bertrand demonstrated using their procedure that the formation of CAACs using KHMDS was tolerant to a range of different functional groups, such as ethers, alkenes, amines, imines, and phosphines. This led us to anticipate that an iminium salt bearing the BPin moiety may be able to greater facilitate the generation of the respective carbene ligand.

Using the procedure outlined by Bertrand, we decided to target the synthesis of the cyclic iminium salt bearing the BPin group **5.54** (Scheme 5.31). The first stage of the multi-step synthesis replicates Bertrand's procedure in which propanal **5.48** is added in excess to diisopropyl amine **5.47.** The addition releases one equivalent of water, which is absorbed by an equimolar quantity of magnesium sulfate. This resultant imine **5.49**, was isolated by filtration and removal of volatiles under vacuum. ^1H and $^{13}C\{^1H\}$ NMR spectra gave values which were consistent with the observations made by Bertrand and showed that the product was present in good purity. Uptake of **5.49** into THF was followed by the slow addition of ^{n}BuLi and subsequent inclusion of 3-chloro-2-methylpropene **5.50** into the reaction mixture resulted in the formation of **5.51**. Bertrand's procedure continues by the addition HCl in ether and heating in pressure tube to 110°. Our attempts to carry out the synthesis in different solvent such as toluene or dioxane to mitigate the need for pressure apparatus did not yield the desired product **5.52**. Therefore, ring closure was achieved by the addition of HCl in diethyl ether heated in a sealed

pressure tube to 110 ˚C and subsequent addition of ammonium hydroxide solution generates the cyclic imine **5.52**. Bertrand uses enamine **5.52** to generate a series of iminium salts by adding reagents such as Me_2NCH_2Cl, N-diisopropylphenylpivalimidoyl chloride and CH_2I_2. successful deprotonation in each case, was achieved by the addition of KHMDS to generate the free carbenes which were found to persist in solution between a few hours and indefinitely.

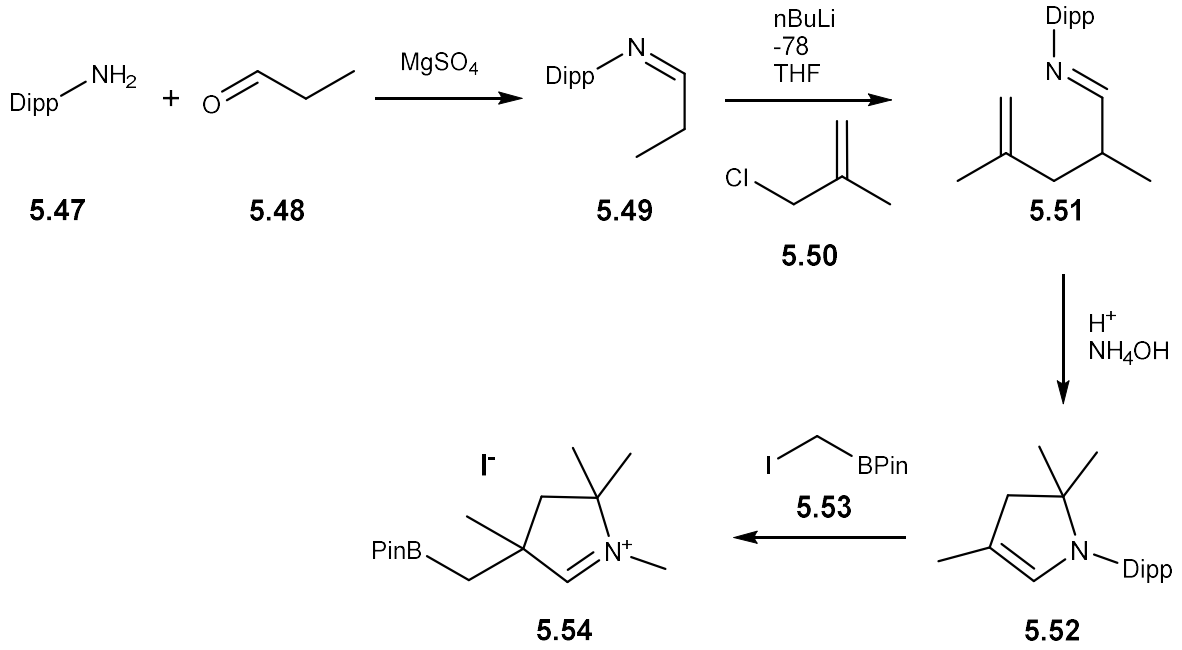

Scheme 5.31. Synthesis of an iminium salt containing the BPin moiety

For the purposes of adding a boron based functionality, we aimed to add ICH_2BPin to **5.52** in place of $BrCH_2BPin$ as Bertrand's procedure did not report the addition of organobromide compounds to 5.52. Prior to this $BrCH_2BPin$ was converted to ICH_2BPin. This was achieved by halide exchange. $BrCH_2BPin$ was added to a solution of sodium iodine in acetone and sodium bromide immediately precipitated out of solution. The solution was filtered, and the spectra was in agreement with that which has already been published for the compound **5.53**. This compound was added to **5.52** in a solvent free synthesis to generate the iminium salt **5.54**. **5.54** was purified by uptake into DCM and subsequent precipitation by addition of hexane resulting in a pale-yellow powder in good yield. The presence of the pendant CH_2BPin group was observed by the presence of a singlet at 31.9 ppm in the $^{13}C\{^1H\}$ NMR spectrum. This is in the same region as the non-adducted imidazolium salts **5.38**, **5.39**, and **5.40** in

which ^{11}B resonances were recorded at 31.5, 30.7 and 31.1 ppm in $CDCl_3$ respectively. In the 13C{^{1}H} NMR experiments the carbon adjacent to the boron, again as observed in the imidazolium salt, cannot be unambiguously confirmed in the $^{13}C\{^1H\}$ NMR without the assistance of HSQC experiments. This experiment confirms a resonance which was attributed to the carbon adjacent to the boron at 23.2 ppm. This represents a more upfield shift when compared to the imidazolium salts. Looking at the iminium carbon this is shifted to a significantly more downfield resonance of 192.4 ppm. This is in contrast to the imidazolium salts **5.38**, **5.39** and **5.40** in which the imidazolium carbons are present at 137.1, 135.8 and 134.2 ppm respectively. This however, is consistent with the iminium salts generated by Bertrand in which the $^{13}C\{^1H\}$ resonance was recorded between 183.7 and 192.7 ppm.[249] The ^1H NMR spectra (figure 5.8) was assigned using the assistance of COSY, HSQC and HMBC, of particular note the ^1H NMR spectra gave an acidic NCH proton at 10.41 which represents a potential site for deprotonation.

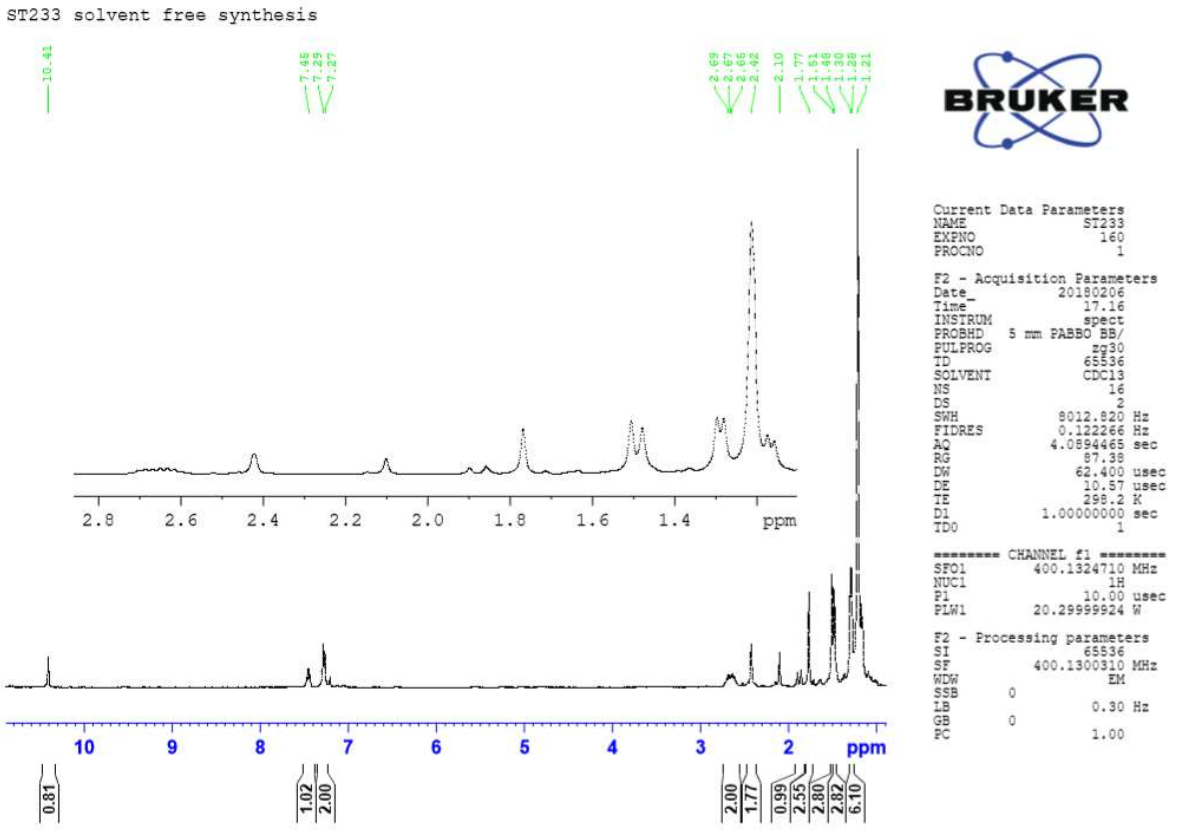

*Figure 5.8. ^1H NMR spectra of **5.54** in $CDCl_3$*

As with Bertrand's iminium precursors, we set out to deprotonate the iminium salt **5.54** using KHMDS in the manner described by Bertrand. As with the imidazolium salts the addition of a solution of KHMDS in toluene did not result in the formation of a carbene. No disappearance of the acidic imidazolium hydrogen peak in the proton NMR spectra was observed. KHMDS was also paired in two *in situ* reactions with half an equivalent of $[RhCl(cod)]_2$ and a single equivalent of $AuCl(PPh_3)$. Bertrand has documented the possibility that these carbenes may not persist as independent species for an extended period.[250] So, both these reactions were trialled to promote complex formation. The reaction of **5.54** with Ag_2O or AgOAc in both cases generated an insoluble white or grey precipitate that would not dissolve in in C_6D_6, $CDCl_3$, MeCN-d_3 or DMSO-d_6. The EI mass spectrum for the precipitate in the Ag_2O reaction was obtained using a direct insertion probe (DIP). In the mass spectrum a m/z peak at 286.2 was observed which indicates the presence of a free methyl CAAC ligand. The loss of the BPin group might have occurred under the vaporisation and ionisation conditions of the DIP EI mass spectrometer. An insoluble precipitate in this reaction accompanied by the presence of the CAAC scaffold in the MS might be an indication of either the formation of the respective silver complex (which is highly insoluble) or the formation of a polymeric species. The formation of an insoluble silver complex would be consistent with the poor solubility observed for the vinyl-based silver carbene complexes **5.13** and **5.14**. If a silver carbene complex had formed, it may be possible to still utilise the white precipitate in the as a transmetalation complex. Therefore, subsequent to the addition of **5.54** to Ag_2O and the precipitation of a white precipitate, to the reaction vessel was added half an equivalent of **$[RhCl(cod)]_2$** with respects to **5.54**. The reaction mixture was carefully monitored by ^1H NMR spectroscopy but no change to the **$[RhCl(cod)]_2$** complex was observed. A wide $^{13}C\{^1H\}$ NMR experiment was also run at a high number of scans (n = 10000) to check for the presence of a rhodium carbene bond (expected as a doublet resonance) however this was not observed. If the silver complex had formed, the results of this experiment suggest that this would be a poor transmetalation agent so other methods should be explored. If a polymer had formed, it may have been possible to 'trap' the carbene before polymerisation had occurred. In order to investigate

this possibility, the reaction between Ag_2O and **5.54** was re-run on an NMR scale with half an equivalent of $[RhCl(cod)]_2$ added before the addition of THF. This did not lead to any observations of CAAC rhodium bond formation. Further reactions using different bases were trialled, copper(I) oxide (Cu_2O) and copper(I) acetate were both employed in an attempt to deprotonate the **5.54**, this was tested in THF first at room temperature and subsequently to reflux, after which no deprotonation of the iminium salt was observed. Two test reactions using palladium(II) acetate and **$[Rh(OAc)(cod)]_2$** did not give rise to the formation of CAAC complexes bearing a BPin moiety.

Again, as with the imidazolium salts the cyclic iminium was shown to undergo a reduction using $LiAlH_4$ to generate the respective zwitterionic BH_3 compound **5.55** (Scheme 5.32). The ^{11}B and $^{11}B\{^1H\}$ NMR spectroscopic analysis confirmed the presence of the BH_3^- group in solution at -32.2 ppm. After removal of volatiles, attempts to characterise the compound in $CDCl_3$ lead to the spontaneous release of hydrogen, although it was noted that this reaction was less vigorous and the proportion of BH_3^- remaining in solution was higher in comparison with the same timescales for the imidazolium salts. The use of other NMR solvents such as benzene-d_6, MeCN-d_3 and DMSO again resulted in the disappearance of the BH_3 peak. The resultant precipitate from the reaction was thought to be a polymeric species due to its insolubility. Again, the addition of metal salts as demonstrated with the imidazolium salts did not 'trap' the observed ligand.

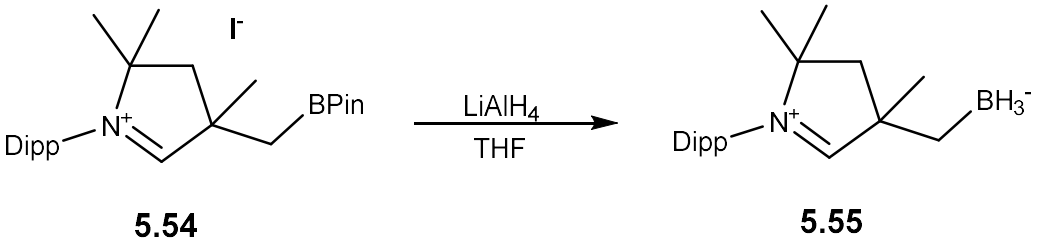

5.54 **5.55**

*Scheme 5.32. Reduction of the iminium salt **5.54** using $LiAlH_4$*

5.4 Chapter conclusions

This chapter set out to explore the synthesis of new previously unreported borohydride and borane ligands for their coordination to metal centres. The focus of this investigation was, in particular, directed towards the synthesis of carbene ligands. Carbene ligands are ubiquitous in organometallic chemistry and their prevalence in the literature is due to their strong electron donation properties. Carbenes have indeed been previously utilised as supports for boron functional groups. Their use however has yet to result in the elusive Z-type interaction between boron and metal. This, we postulated was due to the number of atoms in the supporting bridge being either too long or too short. Our research has previously shown that 3-atom bridges have been sufficient in mono supported borohydride complexes in facilitating hydride migration and subsequently supporting a Z-type interaction.

Initial investigations focused on the hydroboration of the vinyl group in vinyl imidazole. A series of reagents known to hydroborate alkenes were employed in attempts to hydroborate vinyl imidazole. No hydroboration of the vinyl group was observed and therefore we decided to test for hydroboration using both imidazolium salts and carbene complexes bearing the vinyl group. Unfortunately, this did not appear to be an efficient route to obtaining carbene supported borane ligands. Further hydroboration was attempted using halo-alkenes in view to hydroborate and subsequently use in the N-quaternarisation of functionalised imidazole's. This method also did not prove an effective route.

Attention was then turned to the use of reagents containing the BPin functional group that could be used in the N-quaternarisation of imidazole. We initially attempted a copper cross coupling reaction between imidazole and bromo benzene boronic acid pinacol ester which unfortunately did not couple. The commercially available $BrCH_2BPin$ was instead used and was effective in the quaternarisation of functionalised imidazole's. The reaction in toluene at room temperature precipitated out of solution the adducted product and when refluxed in MeCN gave the free pendant BPin group.

The imidazolium salts were reacted with a series of bases known to activate carbenes however carbene activation was not observed. In some reactions there were slight indications of carbene formation, but this could not be unambiguously confirmed. Further investigations looked into the possibility of using metals with a precoordinated basic ligand that could abstract the acidic imidazolium proton but again in these cases no carbene formation was observed. Reduction of the imidazolium salts using $LiAlH_4$ yielded a zwitterionic compound containing both protic and hydridic hydrogens which appeared to release hydrogen on the addition of DCM or chloroform. We postulated that the resultant product was indeed a carbene however this could not be isolated or further reacted in order to fully characterise the ligand.

Moving from imidazolium to iminium salts a multi-step synthesis for an iminium salt was investigated to attempt to see if the prospects of carbene activation would change on substitution of a nitrogen to a carbon. CAAC's generated from iminium salts have stronger electron donating properties than their NHC counter parts due to a smaller HOMO LUMO band gap. This, however, did not translate into a greater ease of activation of the carbene and using the same methods no deprotonation of the iminium salt was observed. Again, reduction using $LiAlH_4$ results in a zwitterionic compound which releases hydrogen on a comparably longer timescale when placed into DCM or chloroform.

Having successfully synthesised a range of precursors containing a boron functional group, capable of further functionalisation, this chapter lays down the groundwork for the further future development of supported borohydride complexes. The complexes prepared are of particular interest as very few examples of NHC ligands in which silver oxide is not an appropriate base have been reported. It is anticipated that further development and refinement of these compounds is possible in order to achieve the synthesis of the target complexes.

Chapter 6: Experimental

6.1 General experimental remarks

All manipulations were carried out using standard Schlenk techniques unless otherwise stated. Solvents were supplied extra dry from "*Acros Organics*" and were stored over 4 Å or 3 Å molecular sieves. The NMR solvents were stored in Young's ampules under N_2, over 4 Å molecular sieves and were degassed through three freeze–thaw cycles prior to use. All reagents were used as purchased from commercial sources unless otherwise stated. **Na[Mmp],**[251] **[LiBH$_3$Me], [LiBH$_3$Ph],**[120] **Li[^{Ph}Mmp], Li[^{Me}Mmp],**[121] **Na[Mai],**[74] **Li[^{Me}Bai]·2MeCN,**[98] **Na[Mm],**[70] **Li[Bm],**[146] **9-BBN,**[213] **[RhCl(cod)]$_2$,**[226] **5.21,**[16] **5.24,**[232] **[Rh(OAc)(cod)]$_2$,**[238] **[Rh(OMe)(cod)]$_2$,**[239] **[Cu(HMDS)],**[241] **[Zn(HMDS)$_2$],**[242] **5.49, 5.51 and 5.52**[249,252] were all synthesized according to standard literature procedures. All NMR experiments were conducted on a Bruker 400 MHz Ascend^{TM} 400 spectrometer. Spectra were referenced internally to the residual protic solvent (^{1}H) or the signals of the solvent (^{13}C). Proton (^{1}H) and carbon (^{13}C) assignments were supported by HSQC, HMBC and COSY NMR experiments. All coupling constants are measured in hertz (Hz) and chemical shift values (δ) are recorded in ppm. The symbol 'τ' is used to represent an apparent triplet where the resonance is expected to be a 'dd'. In these cases, the apparent coupling constant has been provided. Infrared spectra were recorded on a PerkinElmer Spectrum Two ATR FT-IR spectrometer and the intensity or characteristics of the peak is denoted by w = weak, vw = very weak and br. = broad. Mass spectrometry was conducted on a Thermoscientific ISQ Single quad with direct insertion probe or by the EPSRC NMSF at Swansea University using a LTQ Orbitrap XL 1 or at Cardiff University's mass spectrometry facility using a Waters MALDI-TOF micro mx. Elemental analysis was performed at London Metropolitan University by their elemental analysis service. Single crystal X-ray diffraction studies were performed by the EPSRC X-ray crystallography service at Southampton University.

6.2 Synthesis and structure of copper complexes containing a supported anionic borohydride ligand with a 3-atom bridge

Synthesis of [Cu(Mmp)(PPh$_3$)]

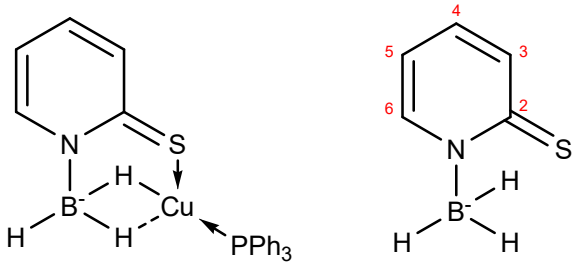

To a Schlenk flask containing CuCl (24 mg, 0.24 mmol), PPh_3 (117 mg, 0.45 mmol) and **Na[Mmp]** (33 mg, 0.22 mmol) was added to methanol (5 mL). The stirred solution gradually turned yellow and a precipitate formed. The reaction was left stirring for 36 hours after which the flask was cooled to – 40 °C and left overnight to further precipitate the product out of solution. The solution was removed via cannula filtration and the resultant solid dried under vacuum to give **[Cu(Mmp)(PPh$_3$)]** as a pale-yellow powder (68 mg, 0.15 mmol, 68%). X-ray quality crystals were grown from the slow evaporation of a 50:50 methanol: diethyl ether solution.

^{1}H NMR (δ, $CDCl_3$): 6.76 [1H, τ, J_{HH} = 6.5 Hz, ^{mp}CH-(4)], 7.17-7.44 [16H, m, P(C_6H_5)$_3$ + ^{mp}CH-(5)], 7.80 [1H, d, $^3J_{HH}$ = 8.5 Hz, ^{mp}CH-(6)], 8.51 [1H, d, $^3J_{HH}$ = 5.8 Hz ^{mp}CH-(3)]. ^{1}H{^{11}B} (δ, $CDCl_3$): 2.64 (3H, s br, BH_3). ^{13}C{^{1}H} (δ, $CDCl_3$): 115.6 [^{mp}CH-(4)], 128.6 [d, $^2J_{CP}$ = 9.6 Hz, P^{ortho}(C_6H_5)$_3$], 130.0 [d, $^4J_{CP}$ = 1.5 Hz, P^{para}(C_6H_5)$_3$], 131.5 [^{mp}CH-(6)], 132.9 [d, $^1J_{CP}$ = 32 Hz, P^{ipso}(C_6H_5)$_3$], 133.8 [d, $^3J_{CP}$ = 16 Hz, P^{meta}(C_6H_5)$_3$], 135.0 [^{mp}CH-(5)], 146.5 [^{mp}CH-(5)], 175.9 [^{mp}C=S-(2)]. ^{31}P{^{1}H} NMR (δ, $CDCl_3$): 4.8 [s, h.h.w. = 392 Hz]. ^{11}B NMR (δ, $CDCl_3$): −13.9 [q, $^1J_{BH}$ = 75 Hz, BH_3]. ^{11}B{^{1}H} NMR (δ, $CDCl_3$): −13.9 [s, h.h.w. = 113 Hz]. MS APCI (ASAP+) m/z = 436.03 (M – BH_3 + H). IR (cm^{-1}, powder film) 2322 w (B-H), 1614 s, 1568 s. Elemental analysis (%): Calc: for $CuSNPC_{23}H_{22}B$: C 61.41 H 4.93 N 3.11 Found: C 61.56 H 4.80 N 3.15

Synthesis of **[Cu(Mmp)(PCy$_3$)]**

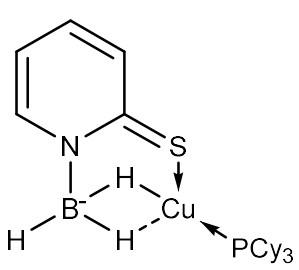

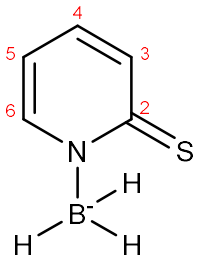

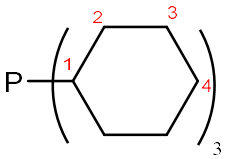

To a Schlenk flask containing CuCl (22 mg, 0.22 mmol), PCy_3 (123 mg, 0.44 mmol) and **Na[Mmp]** (30 mg, 0.20 mmol) was added methanol (5 mL). The stirred solution gradually turned yellow and a precipitate formed. The reaction was left stirring for 36 hours after which the flask was cooled to –40 °C and left overnight to further precipitate the product out of solution. The solution was removed via cannula filtration and the resultant solid dried under vacuum to give **[Cu(Mmp)(PCy$_3$)]** as an off-white powder (62 mg, 0.13 mmol, 65%). X-ray quality crystals were grown from the slow evaporation of a 50:50 methanol: diethyl ether solution.

^{1}H NMR (δ, $CDCl_3$): 1.19-1.87 [33H, m, PCy_3], 2.43 [3H, d vb, $^1J_{BH}$ = 106 Hz, BH_3], 6.71 [1H, τ, J_{HH} = 6.6 Hz, ^{mp}CH-(3)], 7.29 [1H, τ, J_{HH} = 7.6 Hz, ^{mp}CH-(4)], 7.75 [1H, d, J = 8.3 Hz, ^{mp}CH-(5)], 8.48 [1H, d, J = 6.3 Hz, ^{mp}CH-(2)]. ^{1}H{^{11}B} (δ, $CDCl_3$): 2.4 (3H, s br, BH_3). ^{13}C{^{1}H} (δ, $CDCl_3$): 26.2 [PCy_3-(4)], 27.4 [d, $^3J_{CP}$ = 11.0 Hz, PCy_3-(3)], 30.6 [d, $^2J_{CP}$ = 4.0 Hz, PCy_3-(2)], 31.8 [d, $^1J_{CP}$ = 18 Hz, PCy_3-(1)], 115.3 [^{mp}CH-(4)], 131 [^{mp}CH-(6)], 134.8 [^{mp}CH-(5)], 146.3 [^{mp}CH-(3)], 176.1 [^{mp}C=S-(2)].^{31}P{^{1}H} NMR (δ, $CDCl_3$): 27.2 (s br, h.h.w. = 111 Hz). ^{11}B NMR (δ, $CDCl_3$): −13.4 (q, $^1J_{BH}$ = 82 Hz, BH_3). ^{11}B{^{1}H} NMR (δ, $CDCl_3$) −13.4 (s, h.h.w. = 90 Hz). IR (cm^{-1}, powder film) 2448 w (B-H), 1606 s, 1540 s. MS APCI (ASAP+) m/z = 467.2 (M^+). Elemental analysis (%): Calc for $C_{23}H_{40}BCuSNP$: C 59.03 H 8.62 N 2.99, Found: C 59.21 H 8.48 N 2.90.

Synthesis of [Cu(Mmp)(dppe)]

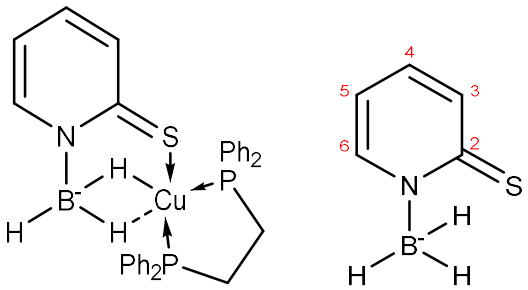

A clean dry Schlenk flask was charged with **[Na(Mmp)]** (123 mg, 0.84 mmol), CuCl (84 mg, 0.84 mmol) and dppe (334 mg, 0.84 mmol).Methanol (5 mL) was added and the reaction was stirred for 24 hours after which a yellow precipitate had formed in the reaction vessel. The solution was removed by filtration to give **[Cu(Mmp)(dppe)]** as a pale yellow powder (360 mg, 0.61 mmol, 73%).

^{1}H NMR (δ, $CDCl_3$): 2.21 [4H, τ, $^{2}J_{CP}$ = 2.9 Hz, $^{dppe}CH_2$], 2.70 [3H, d (vb), $^{1}J_{HB}$ = 96 Hz, BH_3], 6.74 [1H, ddd (τd), $^{3}J_{HH}$ = 6.1 Hz, $^{3}J_{HH}$ = 7.4 Hz, $^{4}J_{HH}$ = 1.2 Hz, ^{mp}CH-(4)], 7.25 – 7.46 [20H, m, $^{dppe}P(C_6H_5)$], 7.30 [1H, ddd (τd), $^{3}J_{HH}$ = 6.8 Hz, $^{3}J_{HH}$ = 7.4 Hz, $^{4}J_{HH}$ = 1.7 Hz, ^{mp}CH-(5)], 7.79 [1H, d, $^{3}J_{HH}$ = 8.2 Hz, ^{mp}CH-(6)], 8.50 [1H, d, $^{3}J_{HH}$ = 6.1 Hz, ^{mp}CH-(3)]. $^{1}H\{^{11}B\}$ (δ, $CDCl_3$): 2.70 [3H, s, BH_3] $^{13}C\{^{1}H\}$ (δ, $CDCl_3$): 24.0 [t, $^{1}J_{CP}$ = 10.2 Hz, $^{dppe}CH_2$], 115.4 [^{mp}CH-(4)], 128.7 [τ, $^{2}J_{CP}$ = 4.4 Hz, $P^{ortho}(C_6H_5)$], 129.6 [$P^{para}(C_6H_5)$], 131.6 [^{mp}CH-(6)], 132.9 [τ, $^{3}J_{CP}$ = 8.5 Hz, $P^{meta}(C_6H_5)$], 134.8 [τ, $^{1}J_{CP}$ = 10.2 Hz, $P^{ipso}(C_6H_5)$], 135.0 [^{mp}CH-(5)], 146.6 [^{mp}CH-(3)], 176.2 [^{mp}C=S]. $^{31}P\{^{1}H\}$ NMR (δ, $CDCl_3$): −5.42 [Cu(dppe)]. ^{11}B NMR (δ, $CDCl_3$): −14.76 [q, $^{1}J_{BH}$ = 52 Hz, h.h.w. = 332 Hz, BH_3]. $^{11}B\{^{1}H\}$ NMR (δ, $CDCl_3$): −14.76 [s, h.h.w. = 158 Hz, BH_3]. MS APCI (ASAP+) m/z = 584.09 [M-H]. IR (cm^{-1}, powder film): 2378, 2081.

Synthesis of [Cu(^{Ph}Mmp)(PPh_3)]

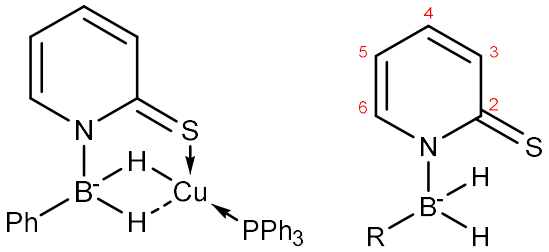

A clean dry Schlenk flask was charged with **[Li(^{Ph}Mmp)]** (44 mg, 0.21 mmol), CuCl (26 mg, 26 mmol) and PPh_3 (62 mg, 24 mmol). Methanol (5 mL) was added and the reaction was stirred for 24 hours after which, a pale yellow solid had precipitated, the solution was removed by filtration to give **[Cu(^{Ph}Mmp)(PPh_3)]** as a pale yellow solid (85 mg, 0.16 mmol, 76%). X-ray quality crystals were grown from the slow evaporation of a methanol ether solution.

^{1}H NMR (δ, $CDCl_3$): 6.67 [1H, τd, J_{HH} = 6.8, $^4J_{HH}$ = 1.4 Hz, ^{mp}CH-(4)], 7.21 - 7.74 [21H, m, $P(C_6H_5)_3$ + $B(C_6H_5)$ + ^{mp}CH-(5)*], 7.86 [1H, ddd, $^3J_{HH}$ = 6.2, $^4J_{HH}$ = 1.4, J_{HH} = 0.8 Hz, ^{mp}CH-(6)], 7.94 [1H, dd, $^3J_{HH}$ = 6.4, $^4J_{HH}$ = 0.9, ^{mp}CH-(3)]. ^{1}H{^{11}B} (δ, $CDCl_3$): 3.33 [2H, s, BH_2^-]. ^{13}C{^{1}H} (δ, $CDCl_3$): 115.5 [^{mp}CH(4)], 126.3 [$B^{para}(C_6H_5)$], 127.9 [$B^{ortho}(C_6H_5)$], 128.7 [d, $^2J_{CP}$ = 9.9 Hz, $P^{ortho}(C_6H_5)_3$], 130.2 [d, $^4J_{CP}$ = 1.9 Hz, $P^{para}(C_6H_5)_3$], 132.1 [^{mp}CH-(6)], 132.3 [d, $^1J_{CP}$ = 34 Hz, $P^{ipso}(C_6H_5)_3$], 133.9 [d, $^3J_{CP}$ = 15.9 Hz, $P^{meta}(C_6H_5)_3$], 134.2 [^{mp}CH-(5)], 136.7 [$B^{meta}(C_6H_5)$], 145.0 [^{mp}CH-(3)], 175.6 [^{mp}C=S],[$B^{ipso}(C_6H_5)$], not observed]. ^{31}P{^{1}H} NMR (δ, $CDCl_3$): 10.1 [$CuPPh_3$]. ^{11}B NMR (δ, $CDCl_3$): −5.7 [BH_2^-, h.h.w. = 317 Hz]. ^{11}B{^{1}H} NMR (δ, $CDCl_3$): −5.7 [BH_2^-, h.h.w. = 203 Hz]. MS APCI (ASAP+) m/z = 524.08 $[M-H]^+$. IR (cm^{-1}, powder film): 2039, 1987. Elemental analysis (%): Calc for $CuC_{29}H_{26}BCuNPS$: C 66.23, H 4.98, N 2.66. Found: C 66.31, H 5.06, N 2.68. *Assignment confirmed by COSY.

Synthesis of [Cu(^{Ph}Mmp)(PCy_3)]

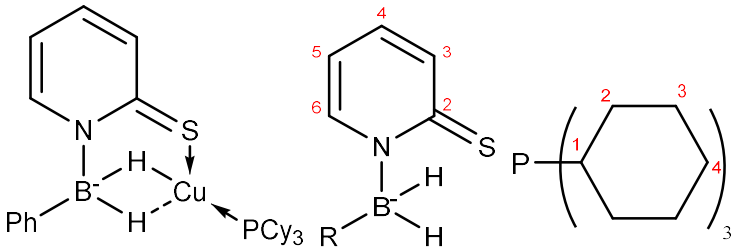

A clean dry Schlenk flask was charged with **[Li(^{Ph}Mmp)]** (75 mg, 0.36 mmol), CuCl (40 mg, 40 mmol) and PCy_3 (110 mg, 39 mmol). Methanol (5 mL) was added and the reaction was stirred for 24 hours after which a precipitate had formed in the reaction vessel. The solution was removed by filtration to give **[Cu(^{Ph}Mmp)(PCy_3)]** as a pale yellow solid (162 mg, 0.30 mmol, 83%). X-ray quality crystals were grown from the slow evaporation of a 50:50 methanol: diethyl ether solution.

^{1}H NMR (δ, $CDCl_3$): 0.95 – 1.90 [33H, m, PCy_3], 3.06 [2H, d (vb), $^1J_{HB}$ = 55 Hz, BH_2], 6.64 [1H, τ, J_{HH} = 6.2 Hz, ^{mp}CH-(4)], 7.17[1H, t, $^3J_{HH}$ = 7.3 Hz, $B^{para}(C_6H_5)$], 7.27 [3H, m, ^{mp}CH-(5) + $B^{meta}(C_6H_5)$], 7.42 [2H, d, $^3J_{HH}$ = 6.9 Hz, $B^{ortho}(C_6H_5)$], 7.84 [1H, d, $^3J_{HH}$ = 8.3 Hz, ^{mp}CH-(6)], 7.88 [1H, d, $^3J_{HH}$ = 6.2, ^{mp}CH-(3)]. ^{1}H{^{11}B} (δ, $CDCl_3$): 3.06 [2H, s, BH_2]. ^{13}C{^{1}H} (δ, $CDCl_3$): 24.0 [PCy_3-(4)], 25.3 [d, $^3J_{CP}$ = 11.4 Hz, PCy_3-(3)], 28.6 [d, $^2J_{CP}$ = 3.7 Hz, PCy_3-(2)], 29.6 [d, $^1J_{CP}$ = 19.4 Hz, PCy_3-(1)], 113.5 [^{mp}CH-(4)], 124.1 [$B^{para}(C_6H_5)$], 125.8 [$B^{ortho}(C_6H_5)$], 130.2 [^{mp}CH-(6)], 132.1 [^{mp}CH-(5)], 134.7 ($B^{meta}(C_6H_5)$], 142.9 [^{mp}CH-(3)], 173.5 [^{mp}C=S], [$B^{ipso}(C_6H_5)$, not observed]. ^{31}P{^{1}H} NMR (δ, $CDCl_3$): 28.8 [$CuPCy_3$]. ^{11}B NMR (δ, $CDCl_3$): 5.26 [s, h.h.w = 1144 Hz]. ^{11}B{^{1}H} NMR (δ, $CDCl_3$): 5.26 [s, h.h.w = 526 Hz]. MS APCI (ASAP+) m/z = 542.2248 [M-H]. IR (cm^{-1}, powder film): 2068. Elemental analysis (%): Calc for $C_{29}H_{44}BCuNPS$: C 64.02, H 8.15, N 2.57. Found: C 63.93, H 8.24, N 2.66.

Synthesis of [Cu(^{Me}Mmp)(PPh_3)]

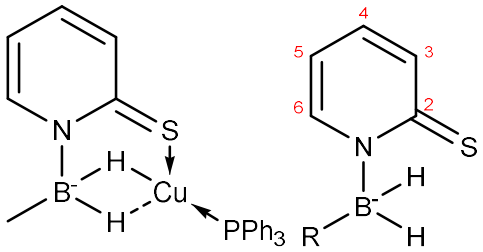

A clean dry Schlenk flask was charged with **[Li(^{Me}Mmp)]** (20 mg, 0.14 mmol), CuCl (20 mg, 0.20 mmol) and PPh_3 (40 mg, 0.15 mmol). Methanol (5 mL) was added and the reaction was stirred for 24 hours after which a precipitate had formed and the solution was removed by filtration to give **[Cu(^{Me}Mmp)(PPh_3)]** as a pale yellow solid (30 mg, 0.06 mmol, 40%). X-ray quality crystals were grown from the slow evaporation of a methanol ether solution.

^{1}H NMR (δ, $CDCl_3$): 0.37 [3H, t, $^3J_{HH}$ = 6.1 Hz, B(CH_3)], 2.46 [2H, d (vb), $^1J_{HB}$ = 72 Hz, BH_2], 6.87 [1H, t, $^3J_{HH}$ = 6.7 Hz, ^{mp}CH-(4)], 7.23 – 7.48 [16H, m, P(C_6H_5) + ^{mp}CH-(5)*], 7.86 [1H, d, $^3J_{HH}$ = 8.4 Hz, ^{mp}CH-(6)], 8.21 [1H, d, $^3J_{HH}$ = 6.1 Hz, ^{mp}CH-(3)]. ^{1}H{^{11}B} (δ, CDCl3): 2.46 [2H, q, $^3J_{HH}$ = 4.7 Hz, BH_2]. ^{13}C{^{1}H} (δ, $CDCl_3$): 2.8 [s (b), B(CH_3)], 115.7 [^{mp}CH-(4)], 128.7 [d, $^2J_{CP}$ = 9.0 Hz, $P^{ortho}(C_6H_5)_3$], 130.1 [$P^{para}(C_6H_5)_3$], 132.1 [^{mp}CH-(5)], 132.4 [d, $^1J_{CP}$ = 36.7 Hz, $P^{ipso}(C_6H_5)_3$],133.8 [^{mp}CH-(6)], 133.9 [d, $^3J_{HH}$ = 14.9 Hz, $P^{meta}(C_6H_5)_3$], 143.5 [^{mp}CH-(3)], 175.8 [^{mp}C=S]. ^{31}P{^{1}H} NMR (δ, $CDCl_3$): 8.8 [s, $CuPPh_3$]. ^{11}B NMR (δ, $CDCl_3$): −8.87 [s, h.h.w. = 284 Hz, BH_2]. ^{11}B{^{1}H} NMR (δ, $CDCl_3$): −8.87 [s, h.h.w. = 165 Hz, BH_2]. MS APCI (ASAP+) m/z = 462.06 [M-H]. IR (cm^{-1}, powder film): 2016 (vw) (B-H).

Synthesis of [Cu(^{Me}Mmp)(PCy_3)]

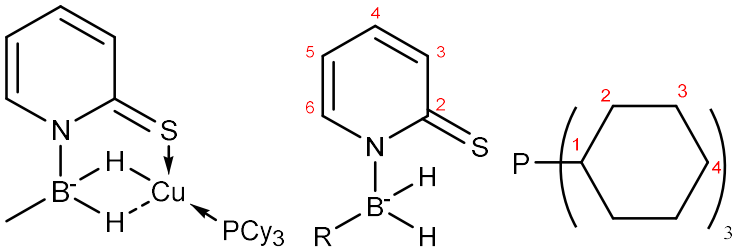

A clean dry Schlenk flask was charged with **[Li(^{Me}Mmp)]** (25 mg, 0.17 mmol), CuCl (20 mg, 0.20 mmol) and PCy_3 (60 mg, 0.21 mmol). Methanol (5 mL) was added and the reaction was stirred for 24 hours. A precipitate had formed in the reaction vessel and the solution was removed by filtration to give **[Cu(^{Me}Mmp)(PCy_3)]** as a pale yellow solid (53 mg, 0.11 mmol, 65%). X-ray quality crystals were grown from the slow evaporation of a methanol ether solution.

^{1}H NMR (δ, $CDCl_3$): 0.34 [3H, t, $^{3}J_{HH}$ = 4.7 Hz, B(CH_3)], 1.1- 1.9 [33H, m, PCy_3], 2.17 [2H, d (vb), BH_2], 6.82 [1H, td, $^{3}J_{HH}$ = 6.7 Hz, $^{4}J_{HH}$ = 1.3 Hz, ^{mp}CH-(4)], 7.29 [1H, τ, $^{3}J_{HH}$ = 7.3 Hz, ^{mp}CH-(5)], 7.81 [1H, d, $^{3}J_{HH}$ = 8.3 Hz, ^{mp}CH-(6)], 8.18 [1H, d, $^{3}J_{HH}$ = 6.3 Hz, ^{mp}CH-(3)]. ^{1}H{^{11}B} (δ, $CDCl_3$): 2.17 [2H, q, $^{3}J_{HH}$ = 4.7 Hz, BH_2]. ^{13}C{^{1}H} (δ, $CDCl_3$): 0.7 [vb, B(CH_3)], 24.3 [PCy_3-(4)], 25.5 [d, $^{3}J_{CP}$ = 9.0 Hz, PCy_3-(3)], 28.6 [PCy_3-(2)], 29.8 [d, $^{1}J_{CP}$ = 16 Hz, PCy_3-(1)], 113.4 [^{mp}CH-(4)], 130.0 [^{mp}CH-(6)], 131.5 [^{mp}CH-(5)], 141.2 [^{mp}CH-(3)], 174.4 [^{mp}C=S]. ^{31}P{^{1}H} NMR (δ, $CDCl_3$): 28.0 [Cu(PCy_3)]. ^{11}B NMR (δ, $CDCl_3$): −8.59 [h.h.w. = 285.8 Hz]. ^{11}B{^{1}H} NMR (δ, $CDCl_3$): −8.59 [h.h.w. = 165.7 Hz]. MS APCI (ASAP+) m/z = 480.2091 $[M-H]^+$. IR (cm^{-1}, powder film): 2032 (w) (B-H).

Synthesis of **[Cu(Mai)(PPh$_3$)$_2$]**

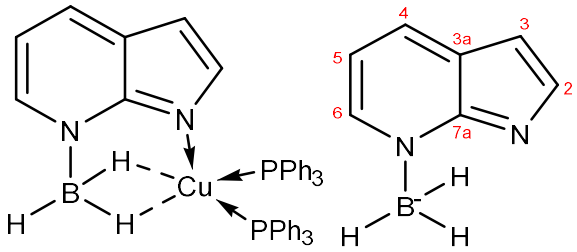

A clean dry Schlenk flask was charged with **[Na(Mai)]** (76 mg, 0.32 mmol), CuCl (40 mg, 0.40 mmol) and PPh_3 (85 mg, 0.32 mmol). Methanol (5 mL) was added and the reaction was stirred for 24 hours. After which the solution had turned a pale green colour and a precipitate was present in the reaction vessel. The precipitate was removed by filtration to give **[Cu(Mai)(PPh$_3$)$_2$]** as a pale green solid (119 mg, 0.16 mmol, 99%). X-ray quality crystals were grown from slow evaporation of methanol.

^{1}H NMR (δ, C_6D_6): 3.93 [3H, d (vb), $^1J_{HB}$ = 114 Hz, BH_3], 6.52 [1H, dd, $^3J_{HH}$ = 7.4 Hz $^3J_{HH}$ = 7.4 Hz, ^{aza}CH-(5)], 6.77 [1H, d, $^3J_{HH}$ = 2.7 Hz, ^{aza}CH-(3)], 7.02 [18H, m, $P^{meta}(C_6H_5)_3$ + $P^{para}(C_6H_5)_3$], 7.51 [12H, m, $P^{ortho}(C_6H_5)_3$], 7.81 [1H, d, $^3J_{HH}$ = 7.4 Hz, ^{aza}CH-(4)], 7.84 [1H, d, $^3J_{HH}$ = 2.7 Hz, ^{aza}CH-(2)], 8.08 [1H, d, $^3J_{HH}$ = 5.7 Hz]. ^{1}H{^{11}B} (δ, C_6D_6): 3.93 [3H, s, BH_3]. ^{13}C{^{1}H} (δ, C_6D_6): 101.2 [^{aza}CH-(3)], 111.1 [^{aza}CH-(5)], 125.6 [^{aza}C-(3a)], 128.5 [d, $^2J_{CP}$ = 8.8 Hz, $P^{ortho}(C_6H_5)_3$], 129.4 [d, $^4J_{CP}$ = 1.0 Hz, $P^{para}(C_6H_5)_3$], 130.1 [^{aza}CH-(4)], 133.8 [d, $^3J_{CP}$ = 16.6 Hz, $P^{meta}(C_6H_5)_3$], 134.5 [d, $^1J_{CP}$ = 21.2 Hz, $P^{ipso}(C_6H_5)_3$], 136.3 [^{aza}CH-(6)], 140.3 [^{aza}CH-(2)], 152.9 [^{aza}C-(7a)]. ^{31}P{^{1}H} NMR (δ, C_6D_6): 2.4667 [Cu(PPh_3)]. ^{11}B NMR (δ, C_6D_6): −15.9 [q, $^1J_{BH}$ = 73 Hz, h.h.w. = 317 Hz]. ^{11}B{^{1}H} NMR (δ, C_6D_6): −15.9 [s, h.h.w. = 131 Hz]. MS APCI (ASAP+) m/z = 455.09 [M-H]. IR (cm^{-1}, powder film): 2375, 2104.

Synthesis of **[Cu(Mai)(PCy$_3$)]**

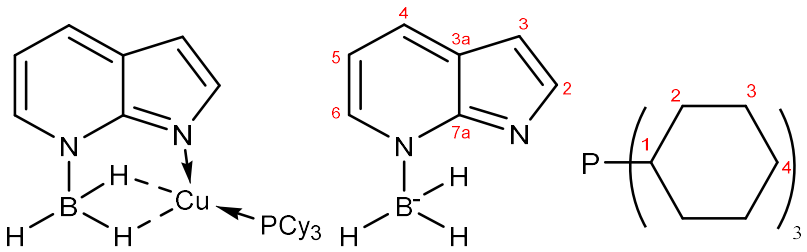

A clean dry Schlenk flask was charged with **[Na(Mai)]** (80 mg, 0.34 mmol), CuCl (38 mg, 0.38 mmol) and PCy_3 (98 mg, 0.35 mmol). Methanol (5 mL) was added and the reaction was stirred for 24 hours. after which a precipitate had formed in the reaction mix and the solution was removed by filtration to give **[Cu(Mai)(PCy$_3$)]** as a pale green solid (104 mg, 0.22 mmol, 65%). X-ray quality crystals were grown from slow evaporation of methanol.

^{1}H NMR (δ, $CDCl_3$): 1.0-1.9 [33H, m, PCy_3], 3.72 [3H, d (vb), $^{1}J_{HB}$ = 108 Hz, BH_3], [1H, dd, $^{3}J_{HH}$ = 5.8 Hz $^{3}J_{HH}$ = 7.5 Hz, ^{aza}CH-(5)], 6.79 [1H, d, $^{3}J_{HH}$ = 2.5 Hz, ^{aza}CH-(3)], 7.77 [1H, d, $^{3}J_{HH}$ = 7.9 Hz, ^{aza}CH-(4)], 7.94 [1H, d, $^{3}J_{HH}$ = 2.5 Hz, ^{aza}CH-(2)], 8.07 [1H, d, $^{3}J_{HH}$ = 5.8 Hz, ^{aza}CH-(6)]. ^{1}H{^{11}B} (δ, CDCl3): 3.72 [3H, s, BH_3]. ^{13}C{^{1}H} (δ, $CDCl_3$): 26.2 [d, $^{4}J_{CP}$ = 0.7 Hz, PCy_3-(4)], 27.3 [d, $^{3}J_{CP}$ = 10.7 Hz, PCy_3-(3)], 30.8 [d, $^{2}J_{CP}$ = 5.9 Hz, PCy_3-(2)], 31.9 [d, $^{1}J_{CP}$ = 11.1 Hz, PCy_3-(1)], 101.0 [^{aza}CH-(3)], 111.0 [^{aza}CH-(5)], 125.5 [^{aza}C-(3a)], 129.9 [^{aza}CH-(4)], 136.2 [^{aza}CH-(6)], 140.3 [^{aza}CH-(2)], 152.9 [^{aza}C-(7a)]. ^{31}P{^{1}H} NMR (δ, $CDCl_3$): 23.0 [Cu(PCy_3)]. ^{11}B NMR (δ, $CDCl_3$): −15.4 [q, $^{1}J_{BH}$ = 80 Hz, h.h.w. = 305 Hz, BH_3]. ^{11}B{^{1}H} NMR (δ, $CDCl_3$): −15.4 [s, h.h.w. = 118 Hz, BH_3]. MS APCI (ASAP+) m/z = 473.23 [M-H]. IR (cm^{-1}, powder film): 2368, 2115.

Synthesis of **[Cu(^{Me}Bai)(PPh$_3$)]**

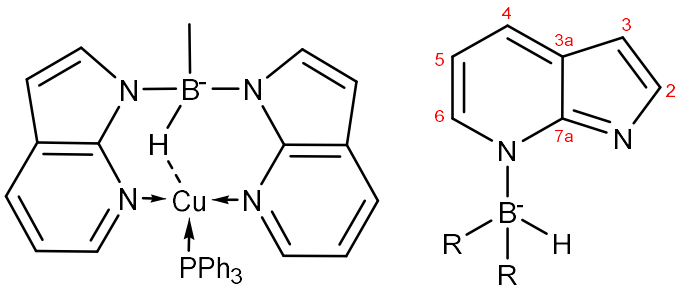

A clean dry Schlenk flask was charged with **[Li(^{Me}Bai)]** (100 mg, 0.29 mmol), CuCl (29 mg, 0.29 mmol) and PPh_3 (76 mg, 0.29 mmol). Methanol (5 mL) was added and the reaction was stirred for 24 hours after which the product had precipitated out of solution. The solution was subsequently removed by filtration to give **[Cu(^{Me}Bai)(PCy$_3$)]** as a pale green powder (94 mg, 0.16 mmol, 55%). X-ray quality crystals were grown directly from the reaction mixture.

^{1}H NMR (δ, $CDCl_3$): 0.63 [3H, vb, BCH_3], 4.99 [1H, q(vb), $^1J_{HB}$ = 89 Hz, BH], 6.63 [2H, d, $^3J_{HH}$ = 3.3 Hz, ^{aza}CH-(3)], 6.66 [2H, dd, $^3J_{HH}$ = 5.0 Hz, $^3J_{HH}$ = 7.7 Hz, ^{aza}CH-(5)], 7.26 – 7.49 [15H, PPh_3], 7.62 [2H, d, $^3J_{HH}$ = 3.3 Hz, ^{aza}CH-(2)], 7.71 [2H, dd, $^3J_{HH}$ = 7.7 Hz, $^4J_{HH}$ = 1.4 Hz, ^{aza}CH-(4)], 7.77 [2H, dd, $^3J_{HH}$ = 5.0 Hz, $^4J_{HH}$ = 1.4 Hz, ^{aza}CH-(6)]. ^{1}H{^{11}B} (δ, CDCl3): 0.63 [3H, d, $^3J_{HH}$ = 4.1 Hz, BCH_3], 4.99 [1H, q, $^3J_{HH}$ = 4.1, BH]. ^{13}C{^{1}H} (δ, $CDCl_3$): 2.95* [vb, BCH_3], 98.4 [^{aza}CH-(3)], 112.6 [^{aza}CH-(5)], 122.6 [^{aza}C-(3a)], 127.4 [^{aza}CH-(4)], 127.7 [d, $^2J_{CP}$ = 9.6 Hz, $P^{ortho}(C_6H_5)$], 128.9 [d, $^4J_{CP}$ = 6.1 Hz, $P^{para}(C_6H_5)$], 130.3 [^{aza}CH-(2)], 132.8 [d, $^3J_{CP}$ = 15.5 Hz, $P^{meta}(C_6H_5)$], 132.9 [d, $^1J_{CP}$ = 42.4 Hz, $P^{ipso}(C_6H_5)$], 139.5 [^{aza}CH-(6)], 149.4 [^{aza}C-N-(7a)]. ^{31}P{^{1}H} NMR (δ, $CDCl_3$): 1.26 [Cu(PPh_3)]. ^{11}B NMR (δ, $CDCl_3$): −7.64 [d, $^1J_{BH}$ = 50.0 Hz, h.h.w. = 210 Hz, BH]. ^{11}B{^{1}H} NMR (δ, $CDCl_3$): − 7.64 [s, h.h.w. = 134 Hz, BH]. MS APCI (ASAP+) m/z = 560.12 [M-^{Me}BH]. IR (cm^{-1}, powder film) 2166, 2095. *Very broad, Assignment confirmed by HSQC and COSY experiments.

Synthesis of [Cu(^{Me}Bai)(PCy_3)]

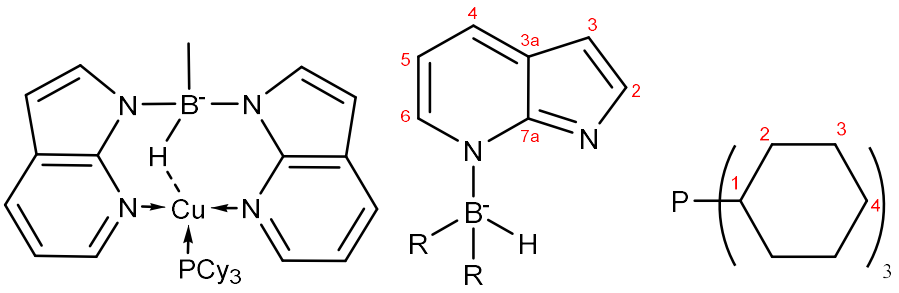

A clean dry Schlenk flask was charged with **[Li(^{Me}Bai)]** (100 mg, 0.29 mmol), CuCl (29 mg, 0.29 mmol) and PCy_3 (81 mg, 0.29 mmol). Methanol (5 mL) was added and the reaction was stirred for 24 hours after which the solution was removed by filtration to give the precipitate **[Cu(^{Me}Bai)(PCy_3)]** as a pale green powder (103 mg, 0.17 mmol, 59%) X-ray quality crystals were grown from the reaction mixture.

^{1}H NMR (δ, $CDCl_3$): 0.58 [3H, d, $^{3}J_{HH}$ = 4.2 Hz, BCH_3], 1.07 – 1.86 [33H, m, PCy_3], 4.92 [1H, vb, BH], 6.27 [2H, d, $^{3}J_{HH}$ = 3.2 Hz, ^{aza}CH-(3)], 6.77 [2H, dd, $^{3}J_{HH}$ = 5.1 Hz, $^{3}J_{HH}$ = 7.7 Hz, ^{aza}CH-(5)], 7.57 [2H, d, $^{3}J_{HH}$ = 3.2 Hz, ^{aza}CH-(2)], 7.72 [2H, dd, $^{3}J_{HH}$ = 7.7 Hz, $^{4}J_{HH}$ = 1.4 Hz, ^{aza}CH-(4)], 8.04 [2H, dd, $^{3}J_{HH}$ = 5.1 Hz, $^{4}J_{HH}$ = 1.4 Hz, ^{aza}CH-(6)]. ^{1}H{^{11}B} (δ, CDCl3): 0.58 [3H, d, $^{3}J_{HH}$ = 4.2 Hz, BCH_3], 4.29 [1H, s, BH]. ^{13}C{^{1}H} (δ, $CDCl_3$): 1.05* [BCH_3], 20 -35 [33H, PCy_3], 98.0 [^{aza}CH-(3)], 112.5 [^{aza}CH-(5)], 122.7 [^{aza}C-(3a)], 126.9 [^{aza}CH-(4)], 130.3 [^{aza}CH-(2)], 139.2 [^{aza}CH-(6)], 149.4 [^{aza}C-(7a)]. ^{31}P{^{1}H} NMR (δ, $CDCl_3$): 23.99 [$CuPCy_3$]. ^{11}B NMR (δ, $CDCl_3$): −8.39 [d, $^{1}J_{HB}$ = 47.7 Hz, h.h.w. = 254 Hz, BH]. ^{11}B{^{1}H} NMR (δ, $CDCl_3$): −8.39 [s, h.h.w. = 165 Hz]. MS APCI (ASAP+) m/z = 461.21 [M-^{Me}BHaza]. IR (cm^{-1}, powder film) 2091.

Synthesis of **[Cu(Mm)(PPh$_3$)]**

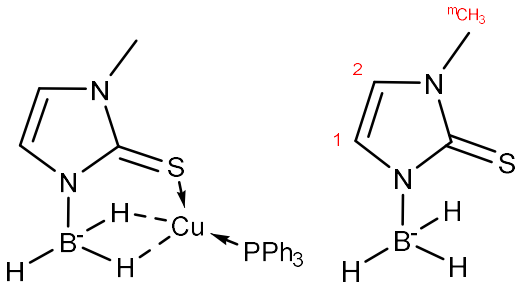

A clean dry Schlenk flask was charged with **[Na(Mm)]** (42 mg, 0.28 mmol), CuCl (28 mg, 0.28 mmol) and PPh_3 (74 mg, 0.28 mmol). Methanol (5 mL) was added and the reaction was stirred for 24 hours after which an off-white precipitate had formed in the reaction vessel. The solution was removed by filtration to give **[Cu(Mm)(PPh$_3$)]** as an off-white powder (81 mg, 0.18 mmol, 64%).

^{1}H NMR (δ, $CDCl_3$): 2.38 [3H, d (vb), $^1J_{HB}$ = 106 Hz, BH_3], 3.56 [3H, s, $^mCH_3$], 6.66 [1H, d, $^3J_{HH}$ = 2.0 Hz, ^mCH-(2)], 6.69 [1H, d, $^3J_{HH}$ = 2.0 Hz, ^mCH-(1)], 7.28 – 7.48 [15H, m, PPh_3]. $^1H\{^{11}B\}$ (δ, CDCl3): 2.38 [3H, s, BH_3]. $^{13}C\{^1H\}$ (δ, $CDCl_3$): 33.9 [$^mCH_3$], 118.0, [^mCH-(2)], 121.6 [^mCH-(1)], 127.8 [d, $^2J_{CP}$ = 10.3 Hz, $P^{ortho}(C_6H_5)$], 129.2 [$P^{para}(C_6H_5)$], 131.7 [d, $^1J_{CP}$ = 37.9 Hz, $P^{ipso}(C_6H_5)$], 132.9 [d, $^3J_{CP}$ = 15.5 Hz, $P^{meta}(C_6H_5)$, 159.5 [^mC=S]. $^{31}P\{^1H\}$ NMR (δ, $CDCl_3$): 6.86 [$CuPPh_3$]. ^{11}B NMR (δ, $CDCl_3$): −19.99 [q, $^1J_{BH}$ = 85 Hz, h.h.w. = 240 Hz]. $^{11}B\{^1H\}$ NMR (δ, $CDCl_3$): −19.99 [s, h.h.w. = 88 Hz]. MS APCI (ASAP+) m/z = 451.06 [M-H]. IR (cm^{-1}, powder film): 2434, 2081.

Synthesis of **[Cu(Mm)(PCy$_3$)]**

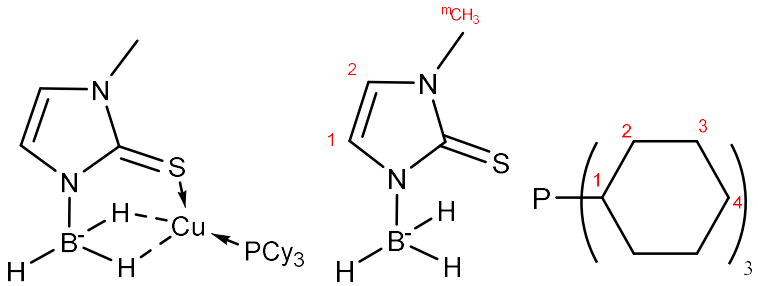

A clean dry Schlenk flask was charged with **[Na(Mm)]** (47 mg, 0.31 mmol), CuCl (31 mg, 0.31 mmol) and PCy_3 (90 mg, 0.31 mmol). Methanol (5 mL) was added and the reaction was stirred for 24 hours after which the solution was removed by filtration to give the resultant product **[Cu(Mm)(PCy$_3$)]** as an off white powder (79 mg, 0.17 mmol, 55%) X-ray quality crystals were grown from a concentrated methanol solution.

^{1}H NMR (δ, $CDCl_3$): 1.12 – 1.87 [33H, m, PCy_3], 2.17 [3H, vb, BH_3], 3.55 [3H, s, $^{m}CH_3$], 6.64 [1H, d, $^{3}J_{HH}$ = 2.0 Hz, ^{m}CH-(2)], 6.91 [1H, d, $^{3}J_{HH}$ = 2.0 Hz, ^{m}CH-(1)]. ^{1}H{^{11}B} (δ, CDCl3): 2.17 [3H, s, BH_3]. ^{13}C{^{1}H} (δ, $CDCl_3$): 25.2 [PCy_3-(4)], 26.4 [d, $^{3}J_{CP}$ = 11.1 Hz, PCy_3-(3)], 29.6 [d, $^{2}J_{CP}$ = 3.8 Hz, PCy_3-(2)], 30.8 [d, $^{1}J_{CP}$ = 17.5 Hz, PCy_3-(1)], 33.8 [$^{m}CH_3$], 117.8 [^{m}CH-(2)], 121.4 [^{m}CH-(1)], 159.8 [^{m}C=S]. ^{31}P{^{1}H} NMR (δ, $CDCl_3$): 24.57 [$CuPCy_3$]. ^{11}B NMR (δ, $CDCl_3$): −19.56 [q, $^{1}J_{BH}$ = 81 Hz, h.h.w. = 255 Hz, BH_3]. ^{11}B{^{1}H} NMR (δ, $CDCl_3$): −19.56 [s, h.h.w. = 94 Hz, BH_3]. MS APCI (ASAP+) m/z = 469.2043 [M-H]. IR (cm^{-1}, powder film): 2450, 2067.

Synthesis of **[Cu(Bm)(PPh$_3$)]**

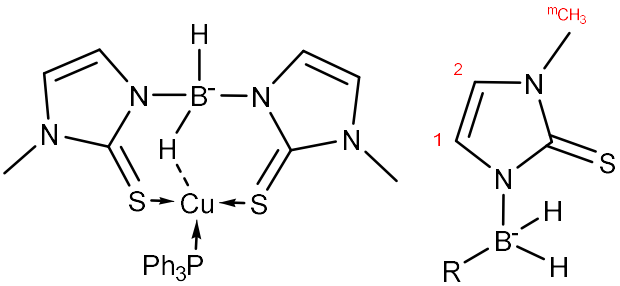

A clean dry Schlenk flask was charged with **[Na(Bm)]** (100 mg, 0.38 mmol), CuCl (43 mg, 0.43 mmol) and PCy_3 (113 mg, 0.43 mmol). Methanol (5 mL) was added and the reaction was stirred for 24 hours after which a precipitate had formed in the reaction vessel and the solution was removed by filtration to give **[Cu(Bm)(PPh$_3$)]** as a pale yellow solid (151 mg, 0.27 mmol, 71%) X-ray quality crystals were grown from a concentrated methanol solution.

^{1}H NMR (δ, $CDCl_3$): 3.44 [2H, vb, BH_2], 3.46 [3H, s, CH_3], 6.52 [2H, d, $^3J_{HH}$ = 2.0 Hz, ^{m}CH-(2)], 6.76 [2H, d, $^3J_{HH}$ = 2.0 Hz, ^{m}CH-(1)] 7.24 – 7.49 [15H, m, PPh_3]. ^{1}H{^{11}B} (δ, CDCl3): 3.44 [2H, s, BH_2]. ^{13}C{^{1}H} (δ, $CDCl_3$): 35.1 [CH_3], 118.6 [^{m}CH-(2)], 122.3 [^{m}CH-(1)], 128.5 [d, $^2J_{CP}$ = 9.3 Hz, $P^{ortho}(C_6H_5)$], 129.5 [d, $^4J_{CP}$ = 1.6 Hz, $P^{para}(C_6H_5)$], 134.0 [d, $^3J_{CP}$ = 15.2 Hz, $P^{meta}(C_6H_5)$], 134.1 [d, $^1J_{CP}$ = 29.5 Hz, $P^{ipso}(C_6H_5)$], 161 [^{m}C=S]. ^{31}P{^{1}H} NMR (δ, $CDCl_3$): −2.73 [Cu(PPh_3)]. ^{11}B NMR (δ, $CDCl_3$): −8.23 [t, $^1J_{BH}$ = 82 Hz, h.h.w. = 270 Hz, BH_2]. ^{11}B{^{1}H} NMR (δ, $CDCl_3$): −8.23 [s, h.h.w. = 126 Hz, BH_2]. MS APCI (ASAP+) m/z = 300.99 [M-$HPPh_3$]. IR (cm^{-1}, powder film): 2381, 2260.

Synthesis of **[Cu(Bm)(PCy$_3$)]**

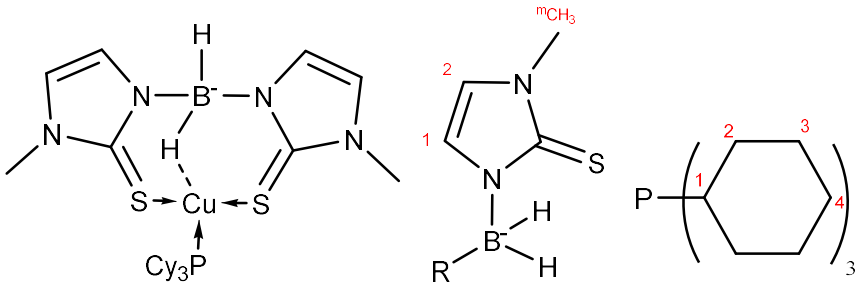

A clean dry Schlenk flask was charged with **[Na(Bm)]** (100 mg, 0.38 mmol), CuCl (43 mg, 0.43 mmol) and PCy_3 (123 mg, 0.44 mmol). Methanol (5 mL) was added and the reaction was stirred for 24 hours after which an off-wite precipitate had formed in the reaction mixture. The solution was removed by filtration to give **[Cu(Bm)(PCy$_3$)]** as an off-white powder (122 mg, 0.21 mmol, 55%).

^{1}H NMR (δ, $CDCl_3$): 0.76 – 1.93 [33H, m, PCy_3], 3.36 [2H, vb, BH_2], 3.52 [3H, s, CH_3], 6.54 [2H, s, ^{m}CH-(2)], 6.67 [2H, s, ^{m}CH-(1)]. ^{1}H{^{11}B} (δ, $CDCl_3$): 3.36 [2H, s, BH_2]. ^{13}C{^{1}H} (δ, $CDCl_3$): 25.4 [PCy_3-(4)], 26.6 [d, $^3J_{CP}$ = 10.7 Hz, PCy_3-(3)], 29.2 [d, $^2J_{CP}$ = 3.9 Hz, PCy_3-(2)], 31.2 [d, $^1J_{CP}$ = 12.9 Hz, PCy_3-(1)], 34.3 [$^mCH_3$], 117.2 [^{m}CH-(2)], 121.5 [^{m}CH-(1)], 160.9 [w, ^{m}C=S]. ^{31}P{^{1}H} NMR (δ, $CDCl_3$): 13.9 [PCy_3]. ^{11}B NMR (δ, $CDCl_3$): −8.60 [h.h.w. = 481 Hz, BH_2]. ^{11}B{^{1}H} NMR (δ, $CDCl_3$): −8.60 [h.h.w. = 286 Hz, BH_2]. MS APCI (ASAP+) m/z = 581.21 [M-H]. IR (cm^{-1}, powder film) = 2383, 2288.

6.3 Synthesis of silver and gold complexes

Synthesis of [Ag(Mmp)(PPh$_3$)]

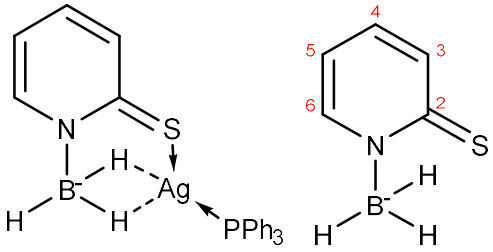

A clean dry Schlenk flask was charged with **[Na(Mmp)]** (52 mg, 0.35 mmol), $AgNO_3$ (60 mg, 0.35 mmol) and PPh_3 (92 mg, 0.35 mmol). Methanol (5 mL) was added and the reaction was stirred for 24 hours after which the solution had turned black. The solution was removed by filtration to give **[Ag(Mmp)(PPh$_3$)]** as a black powder (123 mg, 0.25 mmol, 71%).

^{1}H NMR (δ, $CDCl_3$): 3.23 [3H, q (vb), $^1J_{HB}$ = 111.6 Hz, BH_3], 6.72 [1H, τ, J_{HH} = 7.0 Hz, ^{mp}CH-(4)], 7.28 [1H, τ, J_{HH} = 8.1 Hz, ^{mp}CH-(5)], 7.31 - 7.45 [15H, m, PPh_3], 7.77 [1H, d, $^3J_{HH}$ = 8.4, ^{mp}CH-(6)], 8.52 [1H, d, $^3J_{HH}$ = 6.3 Hz, ^{mp}CH-(3)]. ^{1}H{^{11}B} (δ, $CDCl_3$): 3.23 [3H, s, BH_3]. ^{13}C{^{1}H} (δ, $CDCl_3$): 115.8 [^{mp}CH-(4)], 129.0 [d, $^3J_{HH}$ = 10.1 Hz, $P^{meta}(C_6H_5)$], 130.5 [$P^{para}(C_6H_5)$], 132.0 [d, $^1J_{CP}$ = 32.6 Hz, $P^{ipso}(C_6H_5)$], 133.1 [^{mp}CH-(6)], 133.9 [d, $^2J_{CP}$ = 16.9 Hz, $P^{ortho}(C_6H_5)$], 135.2 [^{mp}CH-(5)], 147.9 [^{mp}CH-(3)], 174.6 [^{mp}CH-(2)]. ^{31}P{^{1}H} NMR (δ, $CDCl_3$): 16.12 [Ag(PPh_3)]. ^{11}B NMR (δ, $CDCl_3$): −16.3 [q, $^1J_{BH}$ = 16.3 Hz, h.h.w. = 323 Hz]. ^{11}B{^{1}H} NMR (δ, $CDCl_3$): −16.3 [s, h.h.w. = 138 Hz]. MS APCI (ASAP+) m/z = 480.1 [M-BH_2]. IR (cm^{-1}, powder film): 2391, 2326, 2160, 2067.

Synthesis of [Ag(Mmp)(PCy_3)]

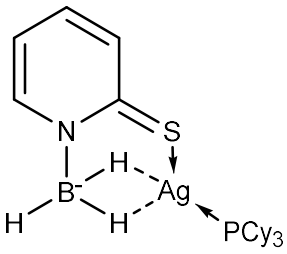

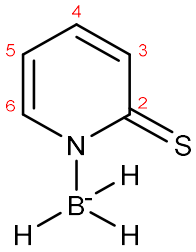

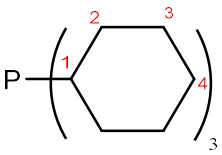

A clean dry Schlenk flask was charged with **[Na(Mmp)]** (89 mg, 0.61 mmol), $AgNO_3$ (103 mg, 0.61 mmol) and PCy_3 (171 mg, 0.61 mmol). Methanol (5 mL) was added and the reaction vessel was covered in foil. This was left to stir for 24 hours after which a black powder remained. The solution was removed by filtration to give **[Ag(Mmp)(PCy_3)]** as a black powder (150 mg, 0.29 mmol, 48%) X-ray quality crystals were grown from a concentrated methanol solution.

^{1}H NMR (δ, $CDCl_3$): 1.03 – 1.94 [33H, m, PCy_3], 3.31 [3H, q (vb), $^{1}J_{HB}$ = 102.5 Hz, BH_3], 6.68 [1H, ddd, $^{3}J_{HH}$ = 6.4 Hz, $^{3}J_{HH}$ = 7.1 Hz, $^{4}J_{HH}$ = 1.4 Hz, ^{mp}CH-(4)], 7.25 [1H, ddd, $^{3}J_{HH}$ = 7.1 Hz, $^{3}J_{HH}$ = 8.7 Hz, $^{4}J_{HH}$ = 1.8 Hz, ^{mp}CH-(5)], 7.72 [1H, dd, $^{3}J_{HH}$ = 8.4 Hz, $^{4}J_{HH}$ = 1.4 Hz, ^{mp}CH-(6)], 8.49 [1H, dd, $^{3}J_{HH}$ = 6.3 Hz, $^{4}J_{HH}$ = 1.1 Hz, ^{mp}CH-(3)]. $^{1}H\{^{11}B\}$ (δ, $CDCl_3$): 3.31 [3H, s, BH_3]. $^{13}C\{^{1}H\}$ (δ, $CDCl_3$): 26.0 [d, $^{4}J_{CP}$ = 0.9 Hz, PCy_3-(4)], 27.3 [d, $^{3}J_{CP}$ = 11.7 Hz, PCy_3-(3)], 31.0 [d, $^{2}J_{CP}$ = 3.9 Hz, PCy_3-(2)], 31.7[dd, $^{1}J_{CP}$ = 14.8, J = 3.3 Hz, PCy_3-(1)], 115.8 [^{mp}CH-(4)], 133.0 [^{mp}CH-(6)], 147.7 [^{mp}CH-(3)], 174.6 [^{mp}C=S]. $^{31}P\{^{1}H\}$ NMR (δ, $CDCl_3$): 40.6 [dd, $^{1}J_{PAg107}$ = 452 Hz, $^{1}J_{PAg109}$ = 523 Hz, PCy_3]. ^{11}B NMR (δ, $CDCl_3$): −15.7 [q, $^{1}J_{BH}$ = 78.7 Hz, h.h.w. = 338 Hz, BH_3]. $^{11}B\{^{1}H\}$ NMR (δ, $CDCl_3$): − 15.7 [s, h.h.w. = 151 Hz, BH_3]. MS APCI (ASAP+) m/z = 498 / 500.15 [B-BH_2]. IR (cm^{-1}, powder film) 2401 cm^{-1}.

Synthesis of [Ag(^{Me}Mmp)(PPh_3)]

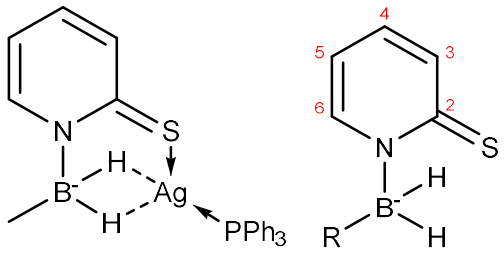

A clean dry Schlenk flask was charged with **[Li(^{Me}Mmp)]** (89 mg, 0.61 mmol), $AgNO_3$ (104 mg, 0.61 mmol) and PPh_3 (160 mg, 0.61 mmol). Methanol (5 mL) was added and the reaction vessel was covered in foil. The reaction was stirred for 24 hours after which the solution was removed by filtration to give **[Ag(^{Me}Mmp)(PPh_3)]** as a dark grey powder (120 mg, 0.23 mmol, 38%).

^{1}H NMR (δ, $CDCl_3$): 3.46 [2H, vb, BH_2], 6.12 [1H, τ, J_{HH} = 8.2 Hz, ^{mp}CH-(4)], 6.55 [1H, t, $^3J_{HH}$ = 7.7 Hz, ^{mp}CH-(5)], 6.95 – 7.45 [15H, m, PPh_3] 7.98 [1H, d, $^3J_{HH}$ = 8.2 Hz, ^{mp}CH-(3)], 8.18 [1H, d, $^3J_{HH}$ = 6.2 Hz, ^{mp}CH-(6)]. H{^{11}B} (δ, $CDCl_3$): 3.46 [2H, q, $^3J_{HH}$ = 5.2 Hz, BH_2]. ^{31}P{^{1}H} NMR (δ, $CDCl_3$): 4.8 [PPh_3]. ^{11}B NMR (δ, $CDCl_3$): − 11.18 [s, h.h.w. = 678 Hz]. ^{11}B{^{1}H} NMR (δ, $CDCl_3$): − 11.18 [s, h.h.w. = 176 Hz]. MS APCI (ASAP+) m/z = 482.01/480.01 [M – BHMe]. IR (cm^{-1}, powder film) ; 2340 and 2053. A clean ^{13}C{^{1}H} NMR of **[Ag(^{Me}Mmp)(PPh_3)]** was not obtained as the complex was not stable in solution.

Synthesis of [Ag(^{Me}Mmp)(PCy_3)]

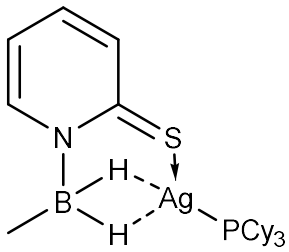

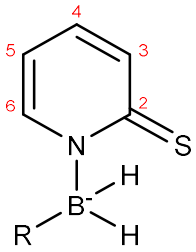

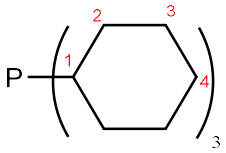

To a clean dry Schlenk flask was charged **[Li(^{Me}Mmp)]** (35 mg, 0.24 mmol), $AgNO_3$ (41 mg, 0.24 mmol) and PCy_3 (68 mg, 0.24 mmol). The Schlenk flask was covered in foil and methanol (5 mL) was added. The reaction was left to sir for 72 hours after which a black precipitate was formed **[Ag(^{Me}Mmp)(PCy_3)]** the powder was isolated by filtration and subsequent dying under vacuum to afford the product as a dark powder (58 mg, 0.11 mmol, 46%).

^{1}H NMR (δ, $CDCl_3$): 0.20 [3H, t, $^3J_{HH}$ = 5.3 Hz, BCH_3], 1.11 – 1.87 [33H, m, PCy_3], 3.24 [2H, vb, BH_2], 6.79 [1H, τd, J_{HH} = 6.7 Hz, $^4J_{HH}$ = 1.5 Hz, ^{mp}CH-(4)], 7.25 [1H, ddd, $^3J_{HH}$ = 8.5 Hz, $^3J_{HH}$ = 7.1 Hz, $^4J_{HH}$ = 1.7 Hz, ^{mp}CH-(5)], 7.77 [1H, ddd, $^3J_{HH}$ = 8.4 Hz, $^4J_{HH}$ = 1.4 Hz, $^5J_{HH}$ = 0.5 Hz, ^{mp}CH-(6)], 7.98 [1H, dd, $^3J_{HH}$ = 6.4 Hz, $^4J_{HH}$ = 1.4 Hz, ^{mp}CH-(3)]. ^{1}H{^{11}B} (δ, $CDCl_3$): 3.24 [2H, q, $^3J_{HH}$ = 5.3 Hz, BH_2]. ^{13}C NMR (δ, $CDCl_3$): 1.4 [BCH_3], 26.0 [PCy_3-(4)], 27.2 [d, $^3J_{CP}$ = 11.7 Hz, PCy_3–(3)], 31.1 [d, $^2J_{CP}$ = 4.0 Hz, PCy_3-(2)], 35.0 [d, $^1J_{CP}$ = 61.8 Hz, PCy_3-(1)], 133.4 [^{mp}CH-(6)], 133.7 [^{mp}CH-(5)], 144.1 [^{mp}CH-(3)], 155.8 [^{mp}CH-(4)], 174.7 [^{mp}C=S]. ^{31}P{^{1}H} NMR (δ, $CDCl_3$): 40.5 [d, $^1J_{PAg}$ = 570 Hz, PCy_3]. ^{11}B NMR (δ, $CDCl_3$): −11.32 [s, h.h.w. = 414.7 Hz, BH_2]. ^{11}B NMR (δ, $CDCl_3$): −11.32 [s, h.h.w. = 263.1 Hz, BH_2]. TOF MS ES+ m/z = 498.15/500.15 $[M\text{-}MeBH]^+$.

Synthesis of [Ag(^{Ph}Mmp)(PPh_3)]

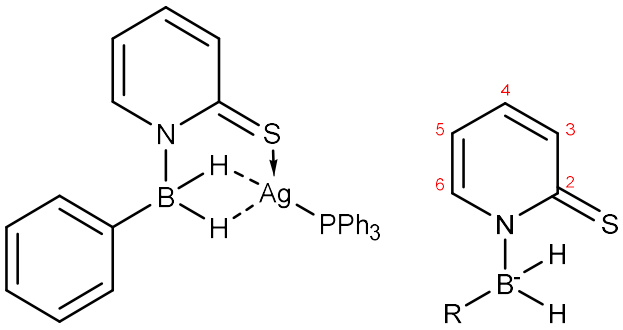

To a clean dry Schlenk flask was added **Li[^{Ph}Mmp]** (53 mg, 0.26 mmol), $AgNO_3$ (44 mg, 0.26 mmol) and PPh_3 (68 mg, 0.26 mmol). The Schlenk flask was covered in foil and subsequently charged with methanol (5mL) and left to stir for 72 hours after which the solution had turned black. Removal of volatiles under vacuum resulted in a black precipitate from which the product was extracted with a 3:1 pentane/DCM mixture. Removal of volatile gave a white powder which was then washed with methanol to give the pure product **[Ag(^{Ph}Mmp)(PPh_3)]** as a white powder (56 mg, 0.10 mmol, 38%).

^{1}H NMR (δ: $CDCl_3$): 4.23 [2H, vb, BH_2], 6.67 [1H, τ, $^3J_{HH}$ 6.5 Hz, ^{mp}CH-(4)], 7.05-7.37 [21H,m*, B(C_6H_5), PPh_3 and ^{mp}CH-(5)], 7.82 [1H, d, $^3J_{HH}$ = 8.3 Hz, ^{mp}CH-(6)], 8.05 [1H,d, $^3J_{HH}$ = 6.2 Hz, ^{mp}CH-(3)]. ^{13}C{^{1}H} (δ, $CDCl_3$): 116.0 [^{mp}CH-(4)], 125.5 [^{mp}CH-(5)], 127.6 [$B^{ortho}(C_6H_5)$], 128.0 [$B^{ipso}(C_6H_5)$], 128.8 [d, $^3J_{CP}$ = 9.9 Hz, $P^{meta}(C_6H_5)$], 130.3 [s, $P^{para}(C_6H_5)$], 132.1 [br, $P^{ipso}(C_6H_5)$], 133.6 [^{mp}CH-6], 133.9 [d, $^3J_{CP}$ = 17.0 Hz, $P^{ortho}(C_6H_5)$], 134.0 [$B^{meta}(C_6H_5)$], 134.8 [$B^{para}(C_6H_5)$], 145.8 [^{mp}CH-(3)], 174.3 [^{mp}C=S]. ^{11}B (δ, $CDCl_3$): −7.26 [s, h.h.w. = 381.6 Hz]. ^{11}B{^{1}H} (δ, $CDCl_3$): −7.26 [s, h.h.w. = 266.5 Hz]. TOF MS ES+ m/z = 480.01/482.01 [M-HBPh]. *Overlapping peaks assignments confirmed by COSY, HSQC and HMBC experiments

Synthesis of [Ag(^{Ph}Mmp)(PCy_3)]

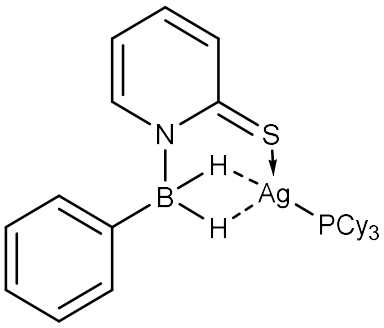

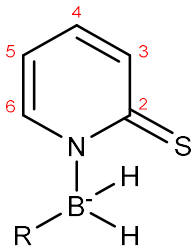

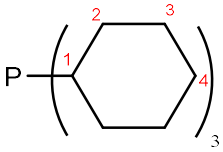

To a clean dry Schlenk flask was added **[Na^{Ph}Mmp]** (81 mg, 0.39 mmol), $AgNO_3$ (67 mg, 0.39 mmol) and PCy_3 (109 mg, 0.39 mmol). The Schlenk flask was covered in foil and subsequently charged with Methanol (5mL). After stirring for 24 hours a precipitate had formed and subsequent filtration and removals of volatiles under vacuum gave the product as a black powder **[Ag(^{Ph}Mmp)(PCy_3)]** (120 mg, 0.25 mmol, 64%).

^{1}H NMR (δ, $CDCl_3$): 1.01 – 1.85 (33H, m, PCy_3), 4.03 (2H, vb, BH_2), 6.62 (1H, τd, J_{HH} = 6.5 Hz, $^4J_{HH}$ = 1.5 Hz, ^{mp}CH-(4)], 7.08[1H, tt, $^3J_{HH}$ = 7.3 Hz, $^4J_{HH}$ = 1.5 Hz, B^{para}(C_6H_5)], 7.18 [2H, t, $^3J_{HH}$ = 7.3 Hz, B^{ortho}(C_6H_5)], 7.24 [1H, ddd, $^3J_{HH}$ = 7.1 Hz, $^3J_{HH}$ = 8.6 Hz, $^4J_{HH}$ = 1.8 Hz, ^{mp}CH-(5)], 7.31 [2H, dd, $^3J_{HH}$ = 7.7 Hz, $^4J_{HH}$ = 1.4 Hz, B^{meta}(C_6H_5)], 7.79 [1H, ddd, $^3J_{HH}$ = 8.4 Hz, $^4J_{HH}$ = 1.4 Hz, $^5J_{HH}$ = 0.5 Hz, mpCH-(6)], 7.98 [1H, dd, $^3J_{HH}$ = 6.4 Hz, $^4J_{HH}$ = 1.4 Hz, ^{mp}CH-(3)]. ^{13}C NMR (δ, $CDCl_3$): 24.8 [PCy_3-(4)], 26.1 [d, $^3J_{CP}$ = 11.6 Hz, PCy_3–(3)], 29.9 [d, $^2J_{CP}$ = 3.7 Hz, PCy_3-(2)], 30.6 [d, $^1J_{CP}$ = 15.1 Hz, PCy_3-(1)], 114.8 [^{mp}CH-(4)], 124.4 [B^{para}(C_6H_5)], 126.4 [B^{ortho}(C_6H_5)], 128.5 [B^{ipso}(C_6H_5)], 132.4 [^{mp}CH-(6)], 133.4 [^{mp}CH-(5)], 134.8 [B^{meta}(C_6H_5)], 145.3 [^{mp}CH-(3)], 173.3[^{mp}C=S]. ^{31}P{^{1}H} NMR (δ, $CDCl_3$): 39.9 [d, $^1J_{PAg}$ = 591 Hz, PCy_3]. ^{11}B NMR (δ, $CDCl_3$): −7.00 [s, h.h.w. = 414.7 Hz, BH_2]. ^{11}B NMR (δ, $CDCl_3$): −7.00 [s, h.h.w. = 263.1 Hz, BH_2]. TOF MS ES+ m/z = 498.15/500.15 $[M\text{-}PhBH]^+$

Synthesis of **[Ag(Mai)(PPh$_3$)$_2$]**

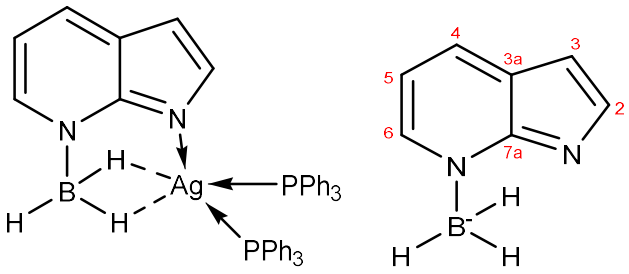

A clean dry Schlenk flask was charged with **[Na(Mai)]** (89 mg, 0.38 mmol), $AgNO_3$ (64 mg, 0.38 mmol) and PPh_3 (100 mg, 0.38 mmol). Methanol (5 mL) was added and the reaction was stirred for 24 hours after which the solution was removed by filtration to give **[Ag(Mai)(PPh$_3$)$_2$]** as a black powder (92 mg, 0.12 mmol, 63%) X-ray quality crystals were grown from the slow evaporation of a concentrated methanol solution.

^{1}H NMR (δ, $CDCl_3$): 3.39 [3H, q(vb), $^1J_{HB}$ = 85 Hz], 6.57 [1H, d, $^3J_{HH}$ = 2.5 Hz, ^{ai}CH-(5)], 6.84 [1H, s (br), ^{ai}CH-(3)], 7.20 – 7.39 [30H, m, PPh_3], 7.57 [1H, s (br), ^{ai}CH-(4)], 8.03 [1H, d, $^3J_{HH}$ = 7.57 Hz, ^{ai}CH-(2)], 8.11 ppm [1H, d, $^3J_{HH}$ = 4.5 Hz, ^{ai}CH-(6)]. ^{1}H{^{11}B} (δ, $CDCl_3$): 3.39 [3H, s, BH_3]. ^{13}C{^{1}H} (δ, $CDCl_3$): 100.6 [^{ai}CH-(5)], 111.1 [^{ai}CH-(3)], 125.7 [^{ai}C-(3a)], 128.8 [d, $^2J_{CP}$ = 9.6 Hz, P^{ortho}(C_6H_5)], 130.1 [P^{para}(C_6H_5)], 130.6 [^{ai}CH-(2)], 132.9 [d, $^1J_{CP}$ = 24.0 Hz, P^{ipso}(C_6H_5)], 134.0 [d, $^3J_{CP}$ = 16.9 Hz, P^{meta}(C_6H_5)], 138.3 [^{ai}CH-(6)], 140.7 [^{ai}CH-(4)], 150.1 [^{ai}C-(7a)]. ^{31}P{^{1}H} NMR (δ, $CDCl_3$): 9.12 [PPh_3]. ^{11}B NMR (δ, $CDCl_3$): −18.4 [q, $^1J_{BH}$ = 60 Hz, h.h.w. = 334 Hz, BH_3]. ^{11}B{^{1}H} NMR (δ, $CDCl_3$): −18.4 [s, h.h.w. = 182, BH_3]. MS APCI (ASAP+) m/z =501.08/ 503.08 [M-PPh_3+H]. IR (cm^{-1}, powder film) 2373, 2175.

Synthesis of **[Ag(Mai)(PCy$_3$)]**

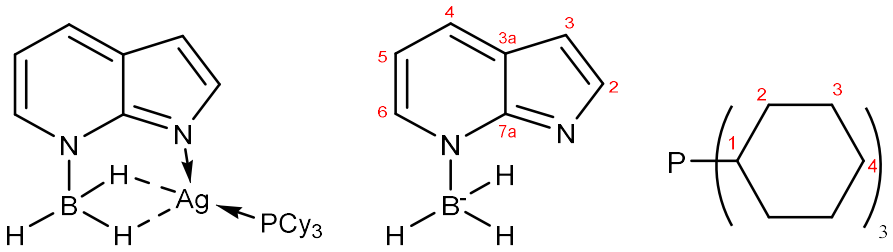

A clean dry Schlenk flask was charged with **Na[Mai]·2MeCN** (84 mg, 0.36 mmol), $AgNO_3$ (60 mg, 0.36 mmol) and PCy_3 (101 mg, 0.36 mmol). Methanol (5 mL) was added and the reaction was stirred for 24 hours after which the solution was removed by filtration to give **[Ag(Mai)(PCy$_3$)]** as a black powder (60 mg, 0.12 mmol, 33%). X-ray quality crystals were grown directly from the slow evaporation of the reaction solution.

^{1}H NMR (δ, $CDCl_3$): 1.10 – 1.95 [33H, m, PCy_3], 3.20 [3H, s (vb), BH_3], 6.56 [1H, s, ^{ai}CH-(5)]. 6.82 [1H, s, ^{ai}CH-(3)], 7.51 [1H, s, ^{ai}CH-(4)], 8.03 [1H, s, ^{ai}CH-(2)], 8.09 [1H, s, ^{ai}CH-(6)]. ^{1}H{^{11}B} (δ, CDCl3): 3.20 [3H, s, BH_3]. ^{13}C{^{1}H} (δ, $CDCl_3$): 26.2 [PCy_3-(4)], 27.4 [d, $^3J_{CP}$ = 8.5 Hz, PCy_3-(3)], 31.0 [PCy_3-(2)], 31.8 [PCy_3-(1)], 100.3 [^{ai}CH-(5)], 110.8 [^{ai}CH-(3)], 125.6 [^{ai}C-(3a)], 130.3 [^{ai}CH-(2)], 138.0 [^{ai}CH-(6)], 140.6 [^{ai}CH-(4)], 153.4 [^{ai}C-(7a)]. ^{31}P{^{1}H} NMR (δ, $CDCl_3$): 41.8 ppm [dd, $^1J_{PAg107}$ = 597 Hz, $^1J_{PAg109}$ = 686 Hz, PCy_3]. ^{11}B NMR (δ, $CDCl_3$): −17.18 [q, $^1J_{BH}$ = 79 Hz, h.h.w. = 374 Hz, BH_3]. ^{11}B{^{1}H} NMR (δ, $CDCl_3$): −17.18 [s, h.h.w. = 174 Hz]. MS APCI (ASAP+) m/z = 519 .22 $[M+H]^+$. IR (cm^{-1}, powder film): 2373, 2190.

Synthesis of **[Au(Mmp)(PPh$_3$)]**

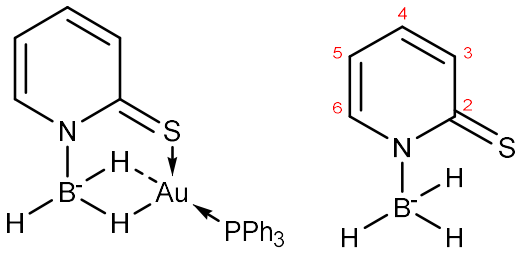

A clean dry Schlenk flask was charged with **[Na(Mmp)]** (23 mg, 0.16 mmol) and [AuCl(PPh$_3$)] (78 mg, 0.16 mmol). Methanol (5 mL) was added and the mixture was stirred, a red-brown precipitate was immediately formed. The solution was stirred for an additional 2 hours to ensure completion after which the resulting solution was filtered via cannula filtration and dried in vacuous to give a red-brown powder **[Au(Mmp)(PPh$_3$)]** (57 mg, 0.10 mmol, 63%).

^{1}H NMR (δ, CDCl$_3$): 4.01 [3H, q (vb), $^1J_{HB}$ = 108 Hz, BH$_3$], 6.79 [1H, dd, $^3J_{HH}$ = 6.3 Hz, $^4J_{HH}$ = 1.4 Hz, ^{mp}CH-(4)], 7.37 - 7.52 [15 H, m, PPh$_3$], 7.60 [1H, dd, $^3J_{HH}$ = 12.0 Hz, $^4J_{HH}$ = 1.5 Hz, ^{mp}CH-(5)], 7.79 [1H, d, $^3J_{HH}$ = 8.0 Hz, ^{mp}CH-(6)], 8.63 [1H, dd, $^3J_{HH}$ = 6.3 Hz, $^4J_{HH}$ = 1.5 Hz]. ^{1}H{^{11}B} (δ, CDCl3): 4.01 [3H, s, BH$_3$]. ^{13}C{^{1}H} (δ, CDCl$_3$): 116.5 [^{mp}CH-(4)], 128.1 [d, $^3J_{CP}$ = 11.2 Hz, P^{meta}(C$_6$H$_5$)$_3$], 129.3 [d, $^1J_{CP}$ = 51.0 Hz, P^{ipso}(C$_6$H$_5$)$_3$], 130.3 [d, $^4J_{CP}$ = 2.2 Hz, P^{para}(C$_6$H$_5$)$_3$], 131.2 [^{mp}CH-(6)], 131.2 [^{mp}CH-(5)], 133.2 [d, $^2J_{CP}$ = 14.3 Hz, P^{ortho}(C$_6$H$_5$)$_3$], 147.6 [^{mp}CH-(3)], 169.2 [^{mp}CH-(2)]. ^{31}P{^{1}H} NMR (δ, CDCl$_3$): 34.5 [AuPPh$_3$]. ^{11}B NMR (δ, CDCl$_3$): −9.74 [q, h.h.w. = 646 Hz]. ^{11}B{^{1}H} NMR (δ, CDCl$_3$): −9.74 [s, h.h.w. = 558 Hz]. MS APCI (ASAP+) m/z = 582.09 [M-H]. IR (cm^{-1}, powder film) 2297 cm^{-1}.

Synthesis of **[Au(Mai)(PPh$_3$)]**

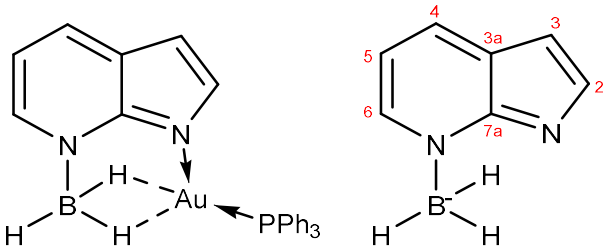

A clean dry Schlenk flask was charged with **[Na(Mai)]** (52 mg, 0.22 mmol) and [AuCl(PPh$_3$)] (109 mg, 0.22 mmol), Methanol (5 mL) was added and the reaction was stirred for 24 hours. After which a precipitate had formed. The solution was removed by filtration to give **[Au(Mai)(PPh$_3$)]** as a pale brown powder (81 mg, 0.20 mmol, 91%).

^{1}H NMR (δ, CDCl$_3$): 3.86 [3H, q (vb), $^1J_{HB}$ = 98.6 Hz, BH$_3$], 6.57 [1H, d, $^3J_{HH}$ = 3.0 Hz, ^{ai}CH-(3)], 6.87 [1H, d, $^3J_{HH}$ = 5.8 Hz, $^4J_{HH}$ = 1.3 Hz, ^{ai}CH-(5)], 7.42 – 7.62 [15H, m, PPh$_3$], 7.52 [1H, d, $^3J_{HH}$ = 3.0 Hz, ^{ai}CH-(2)], 8.01 [1H, dd, $^3J_{HH}$ = 7.7 Hz, $^4J_{HH}$ = 1.3 Hz, ^{ai}CH-(4)], 8.23 [1H, d, $^3J_{HH}$ = 5.7 Hz]. ^{1}H{^{11}B} (δ, CDCl3): 3.86 [3H, s, BH$_3$]. ^{13}C{^{1}H} (δ, CDCl$_3$): 100.9 [^{ai}CH-(3)], 112.3 [^{ai}CH-(5)], 125.9 [^{ai}C-(3a)], 129.1 [d, $^3J_{CP}$ = 13.7 Hz, P^{meta}(C$_6$H$_5$)$_3$], 130.2 [d, $^1J_{CP}$ = 61.0 Hz, P^{ipso}(C$_6$H$_5$)$_3$], 130.6 [^{ai}CH-(4)], 131.5 [P^{para}(C$_6$H$_5$)$_3$], 134.3 [d, $^2J_{CP}$ = 13.7 Hz, P^{ortho}(C$_6$H$_5$)$_3$], 139.9 [^{ai}CH-(3)], 140.0 [^{ai}CH-(6)], 150.6 [^{ai}C-(7a)]. ^{31}P{^{1}H} NMR (δ, CDCl$_3$): 31.3 [Au(PPh$_3$)]. ^{11}B NMR (δ, CDCl$_3$): −13.33 [q, $^1J_{BH}$ = 58 Hz, h.h.w. = 433 Hz]. ^{11}B{^{1}H} NMR (δ, CDCl$_3$): −13.33 [s, h.h.w. = 209 Hz]. MS APCI (ASAP+) m/z = 591.14 [M + H]. IR (cm^{-1}, powder film): 2387, 2344, 2321, 2274, 2232.

6.4 Synthesis of pro-ligands for carbene supported borohydride complexes

Synthesis of **5.12**

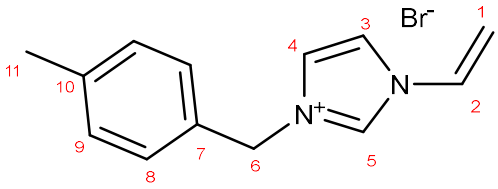

In a reaction vessel open to air, vinyl imidazole (2.5 mL, 27.6 mmol) was dissolved in THF (10 mL) and para-xylyl bromide (4.5 g, 24.3 mmol) was added and reacted vigorously with the solution. The mixture was left to stir for 24 hours to ensure the reaction had gone to completion. The product precipitated out as a pale-yellow powder. Excess toluene was removed by filtration and the product was washed with fresh toluene to afford **5.12** a pale-yellow solid (6.10 g, 21.8 mmol, 91%).

^{1}H NMR (δ, $CDCl_3$): 2.20 [3H, s, CH_3-(11)], 5.22 [1H, dd, $^{3}J_{HH}$ = 2.9 Hz, $^{3}J_{HH}$ = 8.7 Hz, C=CH-(1)], 5.53 [2H, s, NCH_2Ph-(6)], 5.97 [1H, dd, $^{3}J_{HH}$ = 2.9 Hz, $^{3}J_{HH}$ = 15.6 Hz, C=CH-(1)], 7.03 [2H, d, $^{3}J_{HH}$ = 7.7 Hz, 2H, ^{xy}CH-(8)], 7.29 [1H, dd, $^{3}J_{HH}$ = 8.7 Hz, $^{3}J_{HH}$ = 15.7 Hz, CH=C-(2)], 7.36 [2H, d, $^{3}J_{HH}$ = 7.9 Hz, CH-(9)], 7.62 [1H, s, CH-(4)], 8.03 [1H, s, CH-(3)], 10.74[1H, s, NCH=N-(5)]. ^{13}C{^{1}H} (δ, $CDCl_3$): 21.1 [CH_3-(11)], 52.9 [CH_2-(6)], 109.8 [=CH-(1)], 120.0 [CH-(3)], 122.6 [CH-(4)], 128.0 [CH=(2)], 128.8 [^{xy}CH-(8)], 129.8 [^{xy}CH-(9)], 129.9 [^{xy}C-(7)], 134.8 [^{xy}C-(5)], 139.3 [NCH=N-(5)]. IR (cm^{-1}, powder film): 3422, 3086, 3060, 3042, 2857, 1648, 1565, 1547. Mass Spec: MS $(ESI)^{+}$: 199.12 [M-Br].

Synthesis of **5.13**

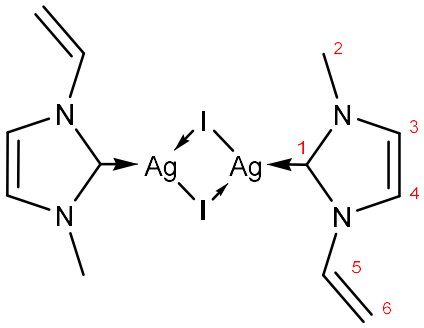

Ag_2O (1.05 g, 4.53 mmol) was added to a clean oven dried Schlenk flask, this was followed by the addition of **5.11** (2.02 g, 8.56 mmol). The Schlenk flask was covered in foil. Acetonitrile (20 mL) was added and the reaction was left to stir for 74 hours whilst monitoring aliquots using ^{1}H NMR spectroscopy. Once the reaction had reached completion by ^{1}H NMR the acetonitrile was removed *in vacuo* to afford **5.13** as a white powder which was washed with hexanes (2.77 g, 4.04 mmol, 95%).

^{1}H NMR (δ, DMSO-d_6): 3.87 [6H, s, NCH_3-(2)], 5.08 [2H, d, $^3J_{HH}$ = 8.7 Hz, C=CH-(6)], 5.71 [2H, d, $^3J_{HH}$ = 15.8 Hz, C=CH-(6)], 7.50 [2H, dd, $^3J_{HH}$ = 15.7 Hz, $^3J_{HH}$ = 8.9 Hz, NCH=C-(5)], 7.58 [2H, s, CH-(4)], 7.98 [s, 2H, CH-(3)]. ^{13}C{^{1}H} (δ, DMSO-d_6): 39.0 [NCH_3-(2)], 103.8 [=CH_2-(6)], 118.0 [CH-(4)], 124.6 [CH-(3)], 134.5 [=CH-(5)], 184.2 [NC:N-(1)]. IR (cm^{-1}, powder film): 1654, 1453, 1416, 1232, 945, 878, 746, 730. MS (ESI)$^+$: 558 [M-I].

Synthesis of **5.14**

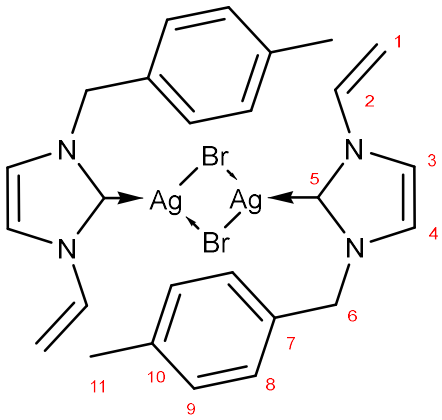

Ag_2O (1.07 g, 4.62 mmol) was added to a clean oven dried Schlenk flask, this was followed by **5.12** (2.38 g, 8.53 mmol). The Schenk flask was covered in foil and charged with 20 mL of acetonitrile. The reaction was stirred for 74 hours whist monitoring aliquots using ^{1}H NMR spectroscopy, once the reaction had reached completion by ^{1}H NMR the acetonitrile was removed *in vacuo* to afford a brown solid which was extracted into DCM to give a pale brown powder after removal of volatiles under vacuum **5.14** (2.72g, 3.52 mmol, 76%).

^{1}H NMR (δ, DMSO-d_6): 2.26 [6H, s, (CH_3-(11))], 5.10 [2H, d, $^{3}J_{HH}$ = 8.8 Hz, =CH-(1)], 5.30 [4H, s, CH_2-(6)], 5.73 [2H, d, $^{3}J_{HH}$ = 15.7 Hz, =CH-(1)], 7.16 [4H, d, $^{3}J_{HH}$ = 7.6 Hz, ^{xy}CH-(8)], 7.23 [4H, d, $^{3}J_{HH}$ = 7.8 Hz, 4H, , ^{xy}CH-(9)], 7.35 [2H, dd, $^{3}J_{HH}$ = 8.9 Hz, $^{3}J_{HH}$ = 15.7 Hz, HC=C-(2)], 7.69 [2H, s, CH-(4)], 8.01 [2H, s, CH-(3)]. $^{13}C\{^{1}H\}$ (δ, DMSO-d_6): 19.0 [CH_3-(11)], 52.4 [CH_2-(6)], 102.1 [=CH_2-(1)], 116.3 [CH-(3)], 121.7 [CH-(4)], 126.1 [^{xy}CH-(8)], 127.6 [^{xy}CH-(9)], 132.2 [^{xy}C-(7)], 132.3 [^{xy}C-(10)], 135.7 [CH=(2)], 180.7 [N:CN-(5)]. IR (cm^{-1}, powder film): 1647, 1420, 1231, 735, 475. MS $(ESI)^{+}$: 503.14 [M-$AgBr_2$].

Synthesis of **5.15**

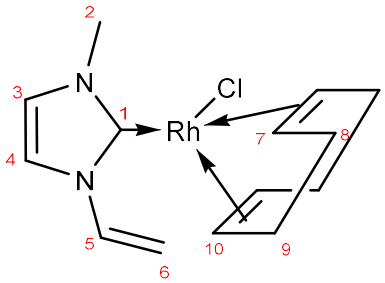

$[RhCl(cod)]_2$ (52 mg, 0.1 mmol) was dissolved with **5.13** (74 mg, 0.1 mmol) in 4 mL of DCM. On the addition of DCM, a white precipitate started to form, and the solution turned yellow. This was then left to stir at room temperature for 1 hour. After one hour the resultant solution was filtered via cannula and the solvent was then removed under vacuum to afford **5.15** as a solid yellow product (29 mg, 0.08 mmol, 40%).

^{1}H NMR (δ, $CDCl_3$): 1.88 – 1.90 [4H, m, COD-(8/9)], 2.33 – 2.35 [4H, m, COD-(8/9)], 3.21 [2H, s, COD-(7)], 4.06 [3H, s, NCH_3-(2)], 4.95 [1H, d, $^3J_{HH}$ = 9.1 Hz, =CH-(6)], 4.99 [2H, s, COD-(10)], 5.25 [1H, d, $^3J_{HH}$ = 15.8 Hz, C=CH-(6)], 6.79 [1H, s, NCH=C-(4)], 7.09 [1H, s, NCH=C-(3)], 8.07 [1H, dd, $^3J_{HH}$ = 9.0 Hz, $^3J_{HH}$ = 16.0 Hz, NCH=C-(5)]. $^{13}C\{^1H\}$ (δ, $CDCl_3$): 28.9 [d, $^1J_{CRh}$ = 3.5 Hz, COD-(9)], 32.9 [d,$^1J_{CRh}$ = 10.8 Hz, COD-(6)], 38.3 (C_2), 68.1 [d, $^1J_{CRh}$ = 14.2, COD-(7)], 68.9 [d, $^1J_{Rh}$ = 14.7 Hz, COD-(7)], 99.3 [τ, $^1J_{CRh}$ = 6.9 Hz, COD-(10)], 101.2 [$=CH_2$-(6)], 116.7 [CH-(3)], 122.7 [CH-(4)], 134.2 [CH=(5)], 186.0 [d, $^1J_{CRh}$ = 51.8 Hz, C:Rh-(1)]. MS $(ESI)^+$: 319.06 $[M - Cl]^+$. Elemental analysis (%): Calc. for $RhClC_{14}H_{20}N_2$: C 47.41, H 5.68, N,7.90. Found: C 47.30, H 5.81, 7.84.

Synthesis of **5.34**

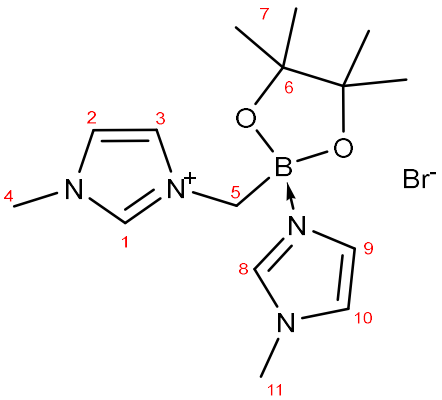

BrMeBPin (1.00 g, 4.53 mmol) was added to a round bottomed flask containing 10 mL of toluene and stirred for 1 minute. Methyl imidazole (821 mg, 10.0 mmol) was then added, after a further minute of stirring a white precipitate began to form and the reaction generated heat. This was then left to stir for 48 h to ensure completion. The solvent was subsequently removed via cannula filtration and the precipitate was washed with 2 × 10 mL portions of fresh ice-cold toluene to afford **5.34** as a white powder which was dried in vacuo (1.73 g, 4.49 mmol, 99%).

^{1}H NMR (δ, $CDCl_3$): 0.99 [12H, s, CH_3-(7)], 3.43 [2H, s, NCH_2B-(5)], 3.88 [3H, s, NCH_3-(11)], 3.99 [3H, s, NCH_3-(4)], 6.90 [1H, s, CH-(9)], 7.01 [1H, s, CH-(10)], 7.11 [1H, s, CH-(3)], 7.21 [1H, s, CH-(2)], 8.21 [1H, s, CH-(8)], 9.37 [1H, s, NCH=N(1)]. $^{13}C\{^{1}H\}$ (δ, $CDCl_3$): 25.6 [CH_3-(7)], 35.7 [CH_3-(11)], 36.6 [CH_3-(4)], 46 - 49 [CH_2-(5)]*, 80.9 [C-(6)], 121.5 [CH-(9)], 121.9 [CH-(3)], 123.2 [CH-(10)], 123.5 [CH-(2)], 136.1 [NCH=N-(8)], 136.3 [NCH=N-(1)]. * -C_5 observed by HSQC and integration of $^{13}C\{^{1}H\}$ baseline. ^{11}B (δ, $CDCl_3$): 7.77 [s, L·BPin]. IR (cm^{-1}, powder film): 3099, 3044, 2988, 1082. MS $(ESI)^+$: 223.16 [M-MeIm], Elemental analysis (%): Calc for $C_{15}H_{26}N_4BBrO_2$: 46.68, H 6.81, N 14.55. Found: C 46.65, H 6.90, N 14.38.

Synthesis of **5.35**

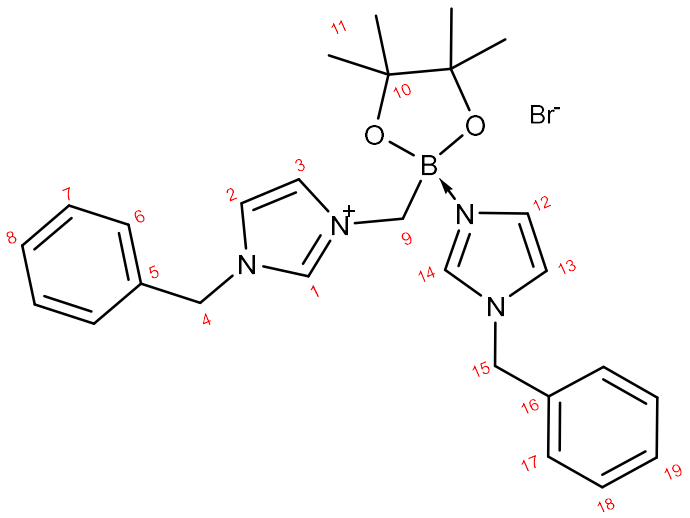

BrMeBPin (1.00 g, 4.53 mmol) was added to a round bottomed flask containing 10 mL of toluene and stirred for 1 minute. Benzyl imidazole (1.58 g, 10.0 mmol) was then added, after a further minute of stirring a white precipitate began to form, this was then left to stir for 48 hours to ensure completion. The solvent was then removed via cannula and the precipitate was washed with 2 × 15 mL portions of ice-cold THF to afford a white powder **5.35** which was dried in vacuo (2.43 g, 4.23 mmol, 93%)

^{1}H NMR (δ, $CDCl_3$): 0.93 [12H, s, CH_3-(11)], 3.41 [2H, s, NCH_2B-(9)], 5.34 [2H, s, CH_2-(15)], 5.47 [2H, s, CH_2-(4)], 6.81 [1H, s, CH-(13)], 6.93 [1H, s, CH-(12)], 7.05 [1H, s, CH-(3)], 7.14 [1H, s, CH-(2)], 7.21-7.34 [10H, m, $^{Bn}(C_6H_4)$-(6-8, 17-19)], 8.20 [1H, s, NCH=N-(14)], 9.61 [1H, s, NCH=N-(1)]. $^{13}C\{^{1}H\}$ (δ, $CDCl_3$): 25.5 [CH_3-(11)] , 46 - 49 [CH_2-(9)]*, 52.5 [CH_2-(15)], 53.1 [CH_2-(4)], 80.9 [C-(10)], 120.3 [CH-(13)], 120.5 [CH-(3)], 123.5 [CH-(2)], 123.7 [CH-(12)], 128.2-134.5 [C_6H_5)-(5-8, 16-19)], 135.7 [NCH=N-(14)], 135.8 [NCH=N-(11)]. * C_5 observed by HSQC and integration of $^{13}C\{^{1}H\}$ baseline. ^{11}B (δ, $CDCl_3$), 8.10 ppm [s, L·BPin]. IR (cm^{-1}, powder film): 3151, 2974, 1547, 1086, 711.

Synthesis of **5.36**

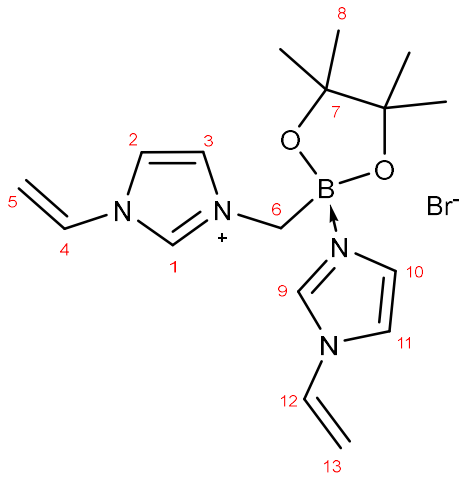

BrMeBPin (500 mg, 2.27 mmol) was added to a round bottomed flask containing 5 mL of toluene and stirred for 2 minutes. vinyl imidazole (420 mg, 4.46 mmol) was then added to the mix instantly a white precipitate began to form, this was then left to stir over the weekend to ensure completion. The solvent was then removed via cannula and the precipitate was washed with 3 × 5 mL portions of fresh ice-cold toluene to afford **5.36** a white powder which was dried in vacuo (800 mg, 1.96 mmol 86%).

^{1}H NMR (δ, $CDCl_3$): 1.04 [12H, s, CH_3-(8)], 3.73 [2H, s, NCH_2B-(9)], 5.04 [1H, d, $^{3}J_{HH}$ = 8.8 Hz, [C=CH-(13)], 5.22 [1H, d, $^{3}J_{HH}$ = 8.6 Hz, C=CH-(5)], 5.43 [1H, d, $^{3}J_{HH}$ = 15.7 Hz, C=CH-(13)], 5.77 [1H, d, $^{3}J_{HH}$ = 15.7 Hz, C=CH-(5)], 7.10 [1H, s, CH-(10)], 7.14 [1H, dd, $^{3}J_{HH}$ = 8.8 Hz, $^{3}J_{HH}$ = 16.1 Hz, HC=C-(12)], 7.20 [1H, s, CH-(11)], 7.37 [1H, dd, $^{3}J_{HH}$ = 8.9 Hz, $^{3}J_{HH}$ = 15.7 Hz, HC=C-(4)], 7.38 [1H, s, CH-(3)], 7.56 [1H, CH-(2)], 8.38 [1H, s, NCH=N-(9)], 10.23 [1H, s, NCH=N-(1)]. $^{13}C\{^{1}H\}$ (δ, $CDCl_3$): 25.5 [CH_3-(8), 43 - 45 [CH_2-6]*, 82.2 [C-(7)], 105.2 [=CH_2-(13)], 108.6 [=CH_2-(5)], 116.7 [CH-(11)], 117.8 [CH-(2)], 124.1 [CH-(3)], 125.7 [CH-(10)], 128.6 [CH=(4)], 129.3 [CH=(12)], 135.83 [NCH=N-(9)], 135.5 [NCH=N-(1)]. * C_6 observed by HSQC and integration of $^{13}C\{^{1}H\}$ baseline. ^{11}B (δ, $CDCl_3$), 14.7 ppm [s, L·BPin]. IR (cm^{-1}, powder film): 3099, 3043, 2965, 1527, 1096, 659.

Synthesis of **5.38**

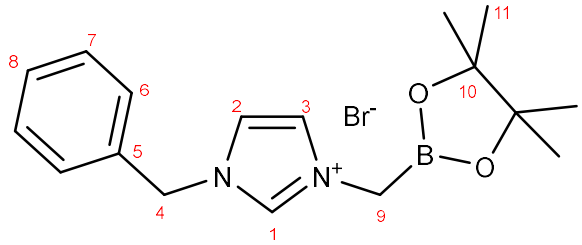

A clean oven dried round bottomed flask was charged with benzyl imidazole (1.55 g, 10 mmol), approximately 15 mL of acetonitrile and BrMeBPin (1.8 mL, 10.5 mmol). The round bottomed flask was attached to a condenser and the reaction was heated to reflux for 2 hours. After 2 hours the solvent was reduced and the product crystallised out of solution as a white solid by the addition of toluene and cooling to −40 °C, the solution was then removed and the product dried in vacuo to give **5.38** as a white powder (2.15 g, 5.7 mmol, 57%).

^{1}H NMR (δ, CD_3CN): 1.18 [12H, s, CH_3-(8)], 3.97 [2H, s, CH_2-(9)], 5.47 [2H, s, CH_2-(4)], 7.31 [3H, m $^{meta/para}(C_6H_5)$-(8-7)], 7.42 [3H, m*, CH-(2)/$^{ortho}(C_6H_5)$-(6)], 7.56 [1H, s, CH-(C_3)], 9.43 [1H, s, NCH=N-(1)] *overlapping peaks. $^{13}C\{^{1}H\}$ (δ, CD_3CN): 25.6 [CH_3-(11)], 36.5** [CH_2-(9)], 52.9 [CH_2(4)], 85.8 [C-(10)], 122.3 [CH-(3)], 124.8 [CH-(2)], 129.1 [$^{meta}(C_6H_5)$-(7)], 129.5 [$^{ortho}(C_6H_5)$-(6)], 129.6 [$^{para}(C_6H_5)$-(8)], 135.0 [$^{ipso}(C_6H_5)$-(5)], 137.1 [NCH=N-(1)].** very broad confirmed by HSQC. ^{11}B (CD_3CN, 128 MHz), 31.5. [s, BPin].

Synthesis of 5.39

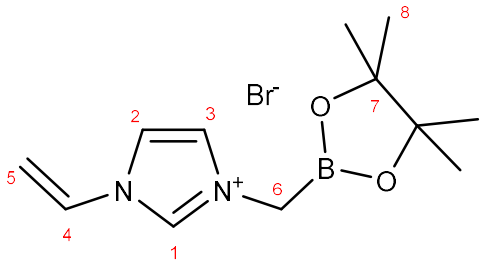

To a clean, dry round bottomed flask was added Vinyl imidazole (94 mg, 1.00 mmol) and acetonitrile (2mL). The mixture was stirred and $BrCH_2BPin$ was added to the flask. A condenser was attached to the round bottomed flask and the solution was then heated to reflux for 3 hours. Removal of the acetonitrile under reduced pressure afforded a white powder which was subsequently washed with hexanes. This gave the product **5.39** a white solid (290 mg, 0.92 mmol, 92.0%).

^{1}H NMR (δ, DMSO-d_6): 1.28 [12H, s, CH_3-(8)], 4.06 [2H, s, CH_2-(6)], 5.45 [1H, d, $^3J_{HH}$ = 8.4 Hz, =CH-(4)], 6.00 [1H, d, $^3J_{HH}$ = 15.5 Hz, =CH-(C4)], 7.44 [1H, dd, $^3J_{HH}$ = 8.4 Hz, $^3J_{HH}$ = 15.5 Hz, HC=(5)], 7.85 [1H, s, CH-(3)], 8.27 [1H, s, CH-(2)], 9.47 [1H, s, CH-(1)]. $^{13}C\{^1H\}$ (δ, DMSO-d_6): 25.2 [CH_3-(8)], 37* [CH_2-(6)], 84.7 [C-(7)], 108.8 [HC=(5)], 119.0 [=CH-(4)], 125.3 [CH-(2)], 129.3 [CH-(3)], 135.8 [1H, s, CH-(1)]. ^{11}B (δ, DMSO-d_6): 30.7 [s, BPin]. *Very broad, assignment confirmed by HSQC experiments.

Synthesis of **5.40**

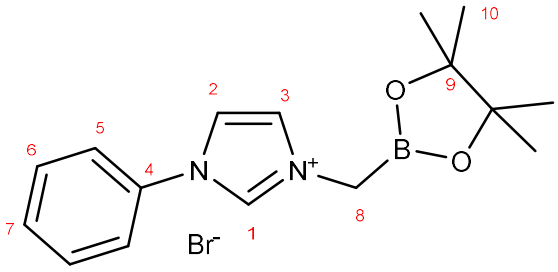

In a clean dry 50 mL round bottomed flask phenyl imidazole (770 mg, 5.34 mmol) was added to 35 mL of toluene, this was followed by BrMeBpin (1.2 g, 5.45 mmol). The round bottomed flask was attached to a condenser and the reaction mix was heated to reflux for 2 hours. After the reaction had cooled the solvent was removed in vacuo and the product was washed with hexane and dried in vacuo to give a white powder (1.84 g, 5.0 mmol, 97%).

^{1}H NMR (δ, $CDCl_3$): 1.23 [12H, s, CH_3-(10)], 4.36 [2H, s, CH_2-(8)], 7.4-7.5 [3H, m, $^{meta/para}(C_6H_5)$-(6-7)], 7.60 [1H, s, CH-(3)], 7.75 [1H, d, $^{3}J_{HH}$ = 7.6 Hz, $^{ortho}(C_6H_5)$-(5)], 7.84 [1H, s, CH-(2)], 10.69 [1H, s, NCH=N-(1)]. $^{13}C\{^{1}H\}$ (δ, $CDCl_3$): 22.9 [CH_3-(10)], 34.7* [CH_2-(8)], 83.7 [C-(9)], 118.4 [CH-(2)], 119.8 [$^{ortho}(C_6H_5)$-(5)], 122.7 [CH-(3)], 128.0 [$^{para}(C_6H_5)$-(7)], 128.5 [$^{meta}(C_6H_5)$-(6)], 132.6 [$^{ipso}(C_6H_5)$-(4)], 134.2 [NCH=N-(1)]. *Very broad, confirmed by HSQC. ^{11}B ($CDCl_3$, 128 MHz), 31.1 [s, BPin]. *Very broad, assignment confirmed by HSQC experiments.

Synthesis of **5.41**

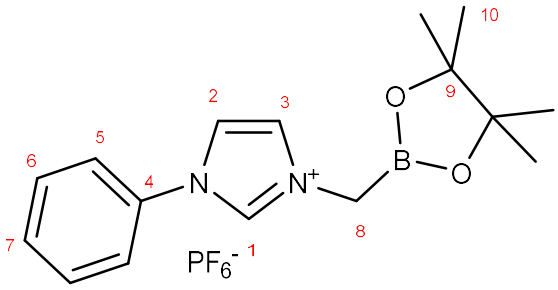

5.40 (502 mg, 1.38 mmol) was added to 30 mL acetonitrile contained in a round bottomed flask. The solution was stirred for 5 minutes then KPF_6 (253 mg, 1.38 mmol) was added whilst stirring and a white precipitate formed in the flask after 10 minutes the reaction was filtered to give a white powder which was dried in vacuo to give **5.41** (473 mg, 1.10 mmol, 80%).

^{1}H NMR (δ, DMSO-d_6): 1.29 [12H, s, CH_3-(10)], 4.08 [2H, s, CH_2-(8)], 7.65 [1H, t, $^{3}J_{HH}$ = 7.5 Hz, $^{para}(C_6H_5)$-(7)], 7.73 [1H, τ, $^{3}J_{HH}$ = 7.8 Hz, $^{meta}(C_6H_5)$-(6)], 7.81 [1H, d, $^{3}J_{HH}$ = 7.6 Hz, $^{ortho}(C_6H_5)$-(5)], 7.92 [1H, s, CH-(3)], 8.31 [1H, s, CH-(2)], 9.68 [1H, s, NCH=N-(1)]. $^{13}C\{^{1}H\}$ (δ, DMSO-d_6): 25.1 [CH_3-(10)], 37* [CH_2-(8)],C 84.7 [C-(9)], 121.1 [CH-(2)], 122.3 [$^{ortho}(C_6H_5)$-(5)], 125.2 [CH-(3)], 130.2 [$^{para}(C_6H_5)$-(7)], 130.7 [$^{meta}(C_6H_5)$-(6)], 135.2 [$^{ipso}(C_6H_5)$-(4)], 135.7 [NCH=N-(1)]. ^{11}B (δ, DMSO-d_6): 28.6 [s, BPin]. $^{31}P\{^{1}H\}$ (δ, DMSO-d_6): −69.2 [d, $^{1}J_{PF}$ = 711 Hz, PF_6]. *Very broad, assignment confirmed by HSQC experiments.

Synthesis of **5.54**

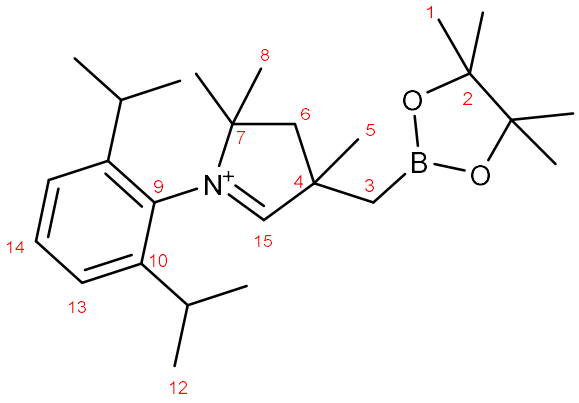

In a clean dry Schlenk flask IMeBPin (**5.53**) (1.08 g, 4.03 mmol) was added followed by the direct addition of the cyclic imine **5.52** (850 mg, 3.13 mmol). The reaction was left to proceed whist stirring and without the addition of any solvent. After 24 hours a yellow solid had formed and the crude product was present as a yellow solid which was quickly dissolved in the minimum amount of DCM and precipitated out by the addition of hexane resulting in a fine yellow powder that was separated by cannula filtration and dried in vacuo to give **5.54** (1.23 g, 2.28 mmol, 72.8%).

^{1}H NMR (δ, $CDCl_3$): 1.17 [6H, d, $^{3}J_{HH}$ = 6.8 Hz, CH_3-(12)], 1.21 [12H, s, CH_3-(1)], 1.29 [6H, d, $^{3}J_{HH}$ = 6.5 Hz, CH_3-(12)], 1.47 [3H, s, CH_3-(8)], 1.50 [4H, s, CH_3-(8) + CH_2-(3)] , 1.76 [3H, s, CH_3-(5)], 1.88 [1H, d, $^{2}J_{HH}$ = 16.2 Hz, CH_2-(3)], 2.42 [2H, s, CH_2-(6)], 2.66 [2H, m, CH-(11)], 7.28 [2H, d, $^{3}J_{HH}$ = 7.7 Hz, ^{dipp}CH-(13)], 7.45 [1H, t, $^{3}J_{HH}$ = 7.7 Hz, ^{dipp}CH-(14)], 10.40 [1H, s, N=CHC-(15)]. ^{13}C{^{1}H} (δ, $CDCl_3$): 22.0 [CH_3-(12)], 22.1 [CH_3-(12)], 23.2* [CH_2-(3)], 24.90 [CH_3-(1)], 24.94 [CH_3-(2)], 26.7 [CH_3-(5)], 26.9 [CH_3-(12)], 27.0 [CH_3-(12)], 28.3 [CH_3-(8)], 28.4 [CH_3-(8)], 29.6 [CH-(11)], 29.8 [CH-11)], 49.1 [CH_2-6], 49.4 [C-(4)], 82.9 [C-(7)], 84.1 [C-(2)], 84.2 [C-(2)], 125.3 [^{dipp}CH-(13)], 125.4 [^{dipp}CH-(13)], 128.6 [^{dipp}C-(9)], 131.9 [^{dipp}CH-(14)], 144.6 [^{dipp}CH-(10)], 192.4 [CH-(15)]. *Not observed but confirmed though HSQC experiments. ^{11}B (δ, $CDCl_3$): 31.9 [s, BPin].

6.5 X-ray data tables

Complex	**[Cu(Mmp)(PPh$_3$)]**	**[Cu(Mmp)(PCy$_3$)]**	**[Cu(^{Ph}Mmp)(PPh$_3$)]**
Formula	$C_{23}H_{22}BCuNPS$	$C_{23}H_{40}BCuNPS$	$C_{29}H_{26}BNPSCu$
$D_{calc.}$/ g cm^{-3}	1.427	1.296	1.413
μ/mm^{-1}	3.175	2.773	1.051
Formula Weight	449.79	467.94	525.89
Colour	light yellow	colourless	colourless
Shape	block	block	(cut) bock
Size/mm^3	0.13×0.09×0.07	0.18×0.12×0.04	0.10×0.10×0.10
T/K	100(2)	100(2)	100(2)
Crystal System	monoclinic	triclinic	orthorhombic
Space Group	$C2/c$	P-1	$Fdd2$
a/Å	11.90994(6)	8.16720(10)	11.49410(10)
b/Å	13.21619(7)	9.38370(10)	66.6424(8)
c/Å	26.83905(13)	17.2612(2)	12.9084(2)
α/°	90	96.9390(10)	90
β/°	97.6274(4)	95.6170(10)	90
γ/°	90	112.3730(10)	90
V/Å^3	4187.20(4)	1199.33(3)	9887.8(2)
Z	8	2	16
Z'	1	1	1
Wavelength/Å	1.54178	1.54178	0.71075
Radiation type	CuK_α	CuK_α	MoK_α
Θ_{min}/°	3.323	2.611	2.392
Θ_{max}/°	70.065	70.033	32.605
Measured Refl.	38239	30937	34426
Independent Refl.	3963	4471	7423
Reflections with I > 2(I)	3908	4402	7237
R_{int}	0.0259	0.0278	0.0187
Parameters	290	285	313
Restraints	68	37	2
Largest Peak	0.316	0.330	0.256
Deepest Hole	−0.349	−0.364	−0.282
GooF	1.065	1.052	1.019
wR_2 (all data)	0.0661	0.0628	0.0473
wR_2	0.0659	0.0625	0.0470
R_1 (all data)	0.0246	0.0239	0.0200
R_1	0.0244	0.0236	0.0190

Complex	**[Cu(^{Ph}Mmp)(PCy$_3$)]**	**[Cu(^{Me}Mmp)(PPh$_3$)]**	**[Cu(Mai)(PPh$_3$)$_2$]**
Formula	$C_{29}H_{44}BNPSCu$	$C_{24}H_{24}BNPSCu$	$C_{43}H_{38}BCuN_2P_2$
$D_{calc.}$/ g cm^{-3}	1.291	1.392	1.339
μ/mm^{-1}	0.930	1.164	0.736
Formula Weight	544.03	463.82	719.04
Colour	colourless	colourless	colourless
Shape	shard (cut block)	block	(cut) block
Size/mm^3	0.19×0.16×0.04	0.11×0.10×0.09	0.10×0.09×0.07
T/K	100(2)	100(2)	100(2)
Crystal System	triclinic	triclinic	monoclinic
Space Group	P-1	P-1	$P2_1/c$
a/Å	9.5148(2)	9.04710(10)	12.58080(10)
b/Å	11.8527(3)	10.76880(10)	12.53910(10)
c/Å	13.5154(3)	12.08960(10)	22.9341(3)
α/°	101.979(2)	108.9040(10)	90
β/°	103.778(2)	92.6300(10)	99.5410(10)
γ/°	101.286(2)	95.0430(10)	90
V/Å^3	1399.08(6)	1106.54(2)	3567.85(6)
Z	2	2	4
Z'	1	1	1
Wavelength/Å	0.71075	0.71075	0.71075
Radiation type	MoKα	Mo Kα	MoKα
Θ_{min}/°	1.610	2.011	2.227
Θ_{max}/°	28.693	30.507	28.700
Measured Refl.	30274	60042	87633
Independent Refl.	6983	6699	9178
Reflections with I > 2(I)	5768	6244	8508
R_{int}	0.0518	0.0307	0.0367
Parameters	368	269	451
Restraints	44	0	0
Largest Peak	0.643	0.428	0.410
Deepest Hole	−0.537	−0.248	−0.303
GooF	1.065	0.919	1.071
wR_2 (all data)	0.0894	0.1057	0.0725
wR_2	0.0834	0.1022	0.0708
R_1 (all data)	0.0549	0.0281	0.0338
R_1	0.0401	0.0251	0.0300

Complex	**[Cu(Mai)(PCy_3)]**	**[Cu(^{Me}Bai)(PPh_3)]**	**[Cu(^{Me}Bai)(PCy_3)]**
Formula	$C_{25}H_{41}BN_2PCu$	$C_{33}H_{29}BN_4PCu$	$C_{33}H_{47}BCuN_4P$
$D_{calc.}$/ g cm^{-3}	1.271	1.366	1.292
μ/mm^{-1}	0.959	0.851	0.782
Formula Weight	474.92	586.92	605.06
Colour	colourless	colourless	colourless
Shape	(cut) block	prism	block (cut)
Size/mm^3	0.20×0.10×0.10	0.20×0.14×0.09	0.07×0.06×0.05
T/K	100(2)	100(2)	100(2)
Crystal System	monoclinic	monoclinic	triclinic
Space Group	$P2_1/c$	$P2_1/c$	P-1
a/Å	9.33090(10)	11.00910(10)	9.5265(2)
b/Å	10.43520(10)	18.1167(2)	10.1703(3)
c/Å	25.5280(2)	14.7128(2)	16.5786(5)
α/°	90	90	78.203(2)
β/°	93.1340(10)	103.4210(10)	81.587(2)
γ/°	90	90	88.993(2)
V/Å^3	2481.94(4)	2854.31(6)	1555.28(7)
Z	4	4	2
Z'	1	1	1
Wavelength/Å	0.71075	0.71073	0.71075
Radiation type	MoKα	MoKα	Mo Kα
Θ_{min}/°	2.523	1.813	2.046
Θ_{max}/°	28.699	30.505	30.507
Measured Refl.	120860	120931	28133
Independent Refl.	6398	8676	9476
Reflections with I > 2(I)	6259	8046	6984
R_{int}	0.0302	0.0427	0.0585
Parameters	280	365	474
Restraints	0	0	582
Largest Peak	0.422	0.506	0.511
Deepest Hole	−0.229	−0.546	−0.497
GooF	1.099	1.084	1.021
wR_2 (all data)	0.0600	0.0776	0.1105
wR_2	0.0596	0.0759	0.0981
R_1 (all data)	0.0251	0.0375	0.0728
R_1	0.0242	0.0329	0.0454

Complex	**[Cu(^{Me}Bai)$_2$]**	**[Cu(Mm)(PCy$_3$)]**	**[Cu(Bm)(PPh$_3$)]**
Formula	$C_{30}H_{28}B_2CuN_8$	$C_{22}H_{41}BN_2PSCu$	$C_{26}H_{27}BCuN_4PS_2$
$D_{calc.}$/ g cm^{-3}	1.487	1.300	1.453
μ/mm^{-1}	0.873	1.071	1.093
Formula Weight	585.76	470.95	564.95
Colour	brown	colourless	colourless
Shape	prism	block (cut)	block
Size/mm^3	0.12×0.08×0.04	0.12×0.11×0.08	0.22×0.12×0.08
T/K	100(2)	100(2)	100(2)
Crystal System	monoclinic	triclinic	orthorhombic
Space Group	$P2_1/c$	P-1	$Aea2$
a/Å	9.4133(3)	7.98870(10)	38.4815(6)
b/Å	16.7930(3)	9.6645(2)	18.4485(4)
c/Å	8.8715(2)	16.9278(3)	7.27410(10)
α/°	90	98.2330(10)	90
β/°	111.085(3)	95.6490(10)	90
γ/°	90	109.595(2)	90
V/Å^3	1308.49(6)	1203.43(4)	5164.07(16)
Z	2	2	8
Z'	0.5	1	1
Wavelength/Å	0.71075	0.71075	0.71073
Radiation type	Mo Kα	MoKα	Mo Kα
Θ_{min}/°	2.319	2.278	2.208
Θ_{max}/°	30.533	30.500	33.111
Measured Refl.	8906	55693	79549
Independent Refl.	8906	6953	9172
Reflections with I > 2(I)	7016	6230	8878
R_{int}	.	0.0414	0.0410
Parameters	192	263	324
Restraints	0	0	1
Largest Peak	0.739	0.479	0.801
Deepest Hole	−0.551	−0.485	−0.453
GooF	1.076	1.048	1.140
wR_2 (all data)	0.1355	0.0695	0.0797
wR_2	0.1304	0.0662	0.0789
R_1 (all data)	0.0614	0.0340	0.0377
R_1	0.0477	0.0276	0.0356

Complex	**[Ag(Mmp)(PCy$_3$)]**	**[Ag(Mai)(PPh$_3$)$_2$]**	**[Ag(Mai)(PCy$_3$)]**
Formula	$C_{24}H_{41.5}AgBN_{1.5}PS$	$C_{43}H_{38}AgBN_2P_2$	$C_{25}H_{41}AgBN_2P$
$D_{calc.}$/ g cm^{-3}	1.403	1.400	1.374
μ/mm^{-1}	0.958	0.679	0.881
Formula Weight	532.79	763.37	519.25
Colour	colourless	colourless	colourless
Shape	block	plate	block
Size/mm^3	0.10×0.07×0.05	0.08×0.05×0.01	0.14×0.06×0.05
T/K	100(2)	100(2)	100(2)
Crystal System	monoclinic	monoclinic	monoclinic
Space Group	$C2/c$	$P2_1/c$	$P2_1/c$
a/Å	20.2195(3)	12.7911(4)	9.34600(10)
b/Å	10.87150(10)	12.7944(3)	10.6736(2)
c/Å	23.9564(3)	22.5573(6)	25.1802(4)
α/°	90	90	90
β/°	106.653(2)	101.242(3)	92.4680(10)
γ/°	90	90	90
V/Å^3	5045.14(12)	3620.77(18)	2509.53(7)
Z	8	4	4
Z'	1	1	1
Wavelength/Å	0.71073	0.71075	0.71075
Radiation type	Mo Kα	Mo Kα	Mo Kα
Θ_{min}/°	2.331	2.331	2.503
Θ_{max}/°	30.508	28.699	30.508
Measured Refl.	39784	43756	34628
Independent Refl.	7693	9277	7402
Reflections with I > 2(I)	7152	7724	6828
R_{int}	0.0180	0.0657	0.0212
Parameters	310	451	280
Restraints	17	0	0
Largest Peak	0.428	0.477	0.457
Deepest Hole	−0.676	−0.578	−0.251
GooF	1.042	1.049	1.052
wR_2 (all data)	0.0477	0.0700	0.0465
wR_2	0.0463	0.0658	0.0453
R_1 (all data)	0.0218	0.0546	0.0221
R_1	0.0193	0.0386	0.0186

7. References

1 G. N. Lewis, *Valence and the structure of atoms and molecules*, 1923.

2 M. Grätz, A. Bäcker, L. Vondung, L. Maser, A. Reincke and R. Langer, *Chem. Commun.*, 2017, **53**, 7230–7233.

3 G. R. Owen, *Chem. Soc. Rev.*, 2012, **41**, 3535.

4 G. R. Owen, *Chem. Commun.*, 2016, **52**, 10712–10726.

5 G. Bouhadir and D. Bourissou, *Chem. Soc. Rev.*, 2016, **45**, 1065–1079.

6 S. H. Bauer, *J. Am. Chem. Soc.*, 1937, **59**, 1096–1103.

7 K. Hedberg and V. Schomaker, *J. Am. Chem. Soc.*, 1951, **73**, 1482–1487.

8 C. Pettinari, R. Pettinari and F. Marchetti, *Adv. Organomet. Chem.*, 2016, **65**, 175–260.

9 S. Trofimenko, *Chem. Rev.*, 1993, **93**, 943–980.

10 N. Kitajima and W. B. Tolman, *Prog. Inorg. Chem.*, 2007, **43**, 419–531.

11 J. M. Smith, *Comments Inorg. Chem.*, 2008, **29**, 189–233.

12 M. D. Spicer and J. Reglinski, *Eur. J. Inorg. Chem.*, 2009, 1553–1574.

13 D. C. Cummins, G. P. A. Yap and K. H. Theopold, *Eur. J. Inorg. Chem.*, 2016, **2016**, 2349–2356.

14 A. Iannetelli, G. Tizzard, S. J. Coles and G. R. Owen, *Inorg. Chem.*, 2018, **57**, 446–456.

15 H. I. Schlesinger, H. C. Brown, A. E. Finholt, J. R. Gilbreath, H. R. Hoekstra and E. K. Hyde, *J. Am. Chem. Soc.*, 1953, **75**, 215–219.

16 H. I. Schlesinger, H. C. Brown, H. R. Hoekstra and L. R. Rapp, *J. Am. Chem. Soc.*, 1953, **75**, 199–204.

17 H. I. Schlesinger, R. T. Sanderson and A. B. Burg, *J. Am. Chem. Soc.*, 1940, **62**, 3421–3425.

18 A. B. Burg and H. I. Schlesinger, *J. Am. Chem. Soc.*, 1940, **62**, 3425–3429.

19 H. I. Schlesinger and H. C. Brown, *J. Am. Chem. Soc.*, 1940, **62**, 3429–3435.

20 H. I. Schlesinger and H. C. Brown, *J. Am. Chem. Soc.*, 1953, **75**, 219–221.

21 M. Paskevicius, L. H. Jepsen, P. Schouwink, R. Černý, D. B. Ravnsbæk, Y. Filinchuk, M. Dornheim, F. Besenbacher and T. R. Jensen, *Chem. Soc. Rev.*, 2017, **46**, 1565–1634.

22 F. Takusagawa, A. Fumagalli, T. F. Koetzle, S. G. Shore, T. Schmitkons, A. V. Fratini, K. W. Morse, C. Y. Wei and R. Ban, *J. Am. Chem. Soc.*, 1981, **103**, 5165–5171.

23 J. L. Atwood, R. D. Rogers, C. Kutal and P. A. Grutsch, *J. Chem. Soc. Chem. Commun.*, 1977, 593–594.

24 C. Kutal, P. Grutsch, J. L. Atwood and R. D. Rogers, *Inorg. Chem.*, 1978, **17**, 3558–3562.

25 M. Shimoi, S. Nagai, M. Ichikawa, Y. Kawano, K. Katoh, M. Uruichi and H. Ogino, *J. Am. Chem. Soc.*, 1999, **121**, 11704–11712.

26 T. Yasue, Y. Kawano and M. Shimoi, *Angew. Chem., Int. Ed.*, 2003, **42**, 1727–1730.

27 J. C. Green, M. L. H. Green and G. Parkin, *Chem. Commun.*, 2012, **48**, 11481.

28 J. F. Van der Maelen, J. Brugos, P. García-Álvarez and J. A. Cabeza, *J. Mol. Struct.*, 2020, **1201**, 127217.

29 J. Brugos, J. A. Cabeza, P. García-Álvarez, E. Pérez-Carreño and J. F. Van Der Maelen, *Dalton Trans.*, 2017, **46**, 4009–4017.

30 A. Jarid, A. Lledos, Y. Jean and F. Volatron, *Inorg. Chem.*, 1993, **32**, 4695–4699.

31 A. Lledos, M. Duran, Y. Jean and F. Volatron, *Inorg. Chem.*, 1993, **32**, 4695–4699.

32 T. J. Marks and J. R. Kolb, *Chem. Rev.*, 1977, **77**, 263–293.

33 B. Cordero, V. Gómez, A. E. Platero-Prats, M. Revés, J. Echeverría, E. Cremades, F. Barragán and S. Alvarez, *J. Chem. Soc., Dalton Trans.*, 2008, 2832–2838.

34 H. Braunschweig and M. Colling, *Coord. Chem. Rev.*, 2001, **223**, 1–51.

35 H. Braunschweig, C. Kollann and D. Rais, *Angew. Chem., Int. Ed.*, 2006, **45**, 5254–5274.

36 H. Braunschweig, R. D. Dewhurst and A. Schneider, *Chem. Rev.*, 2010, **110**, 3924–3957.

37 S. Bontemps, M. Sircoglou, G. Bouhadir, H. Puschmann, J. A. K. Howard, P. W. Dyer, K. Miqueu and D. Bourissou, *Chem. - Eur. J.*, 2008, **14**, 731–740.

38 G. Bouhadir, A. Amgoune and D. Bourissou, *Adv. Organomet. Chem.*, 2010, **58**, 1–107.

39 M. Besora and A. Lledós, in *Contemporary Metal Boron Chemistry I*, Springer Berlin Heidelberg, Berlin, Heidelberg, 2008, vol. 130, pp. 149–202.

40 H.-W. Li, Y. Yan, S. Orimo, A. Züttel and C. M. Jensen, *Energies*, 2011, **4**, 185–214.

41 G. Alcaraz, M. Grellier and S. Sabo-Etienne, *Acc. Chem. Res.*, 2009, **42**, 1640–1649.

42 G. Alcaraz and S. Sabo-Etienne, *Angew. Chem., Int. Ed.*, 2010, **49**, 7170–7179.

43 A. Staubitz, A. P. M. Robertson, M. E. Sloan and I. Manners, *Chem. Rev.*, 2010, **110**, 4023–4078.

44 G. Dell'Amico, F. Marchetti and C. Floriani, *J. Chem. Soc., Dalt. Trans.*, 1982, 2197–2202.

45 D. V Khasnis, N. Pirio, D. Touchard, L. Toupet and P. H. Dixneuf, *Inorg. Chim. Acta*, 1992, **198**–**200**, 193–201.

46 Y. Huang and D. W. Stephan, *Organometallics*, 1995, **14**, 2835–2842.

47 D. G. Gusev, F. M. Dolgushin and M. Y. Antipin, *Organometallics*, 2000, **19**, 3429–3434.

48 J. Hooz, S. Akiyama, F. J. Cedar, M. J. Bennett and R. M. Tuggle, *J. Am. Chem. Soc.*, 1974, **96**, 274–276.

49 N. Lalaoui, T. Woods, T. B. Rauchfuss and G. Zampella, *Organometallics*, 2017, **36**, 2054–2057.

50 K. Saha, U. Kaur, S. Kar, B. Mondal, B. Joseph, P. K. S. Antharjanam and S. Ghosh, *Inorg. Chem.*, 2019, **58**, 2346–2353.

51 W. Diamantikos, H. Heinzelmann, E. Rath and H. Binder, *Zeitschrift f*r Anorg. und Allg. Chemie*, 1984, **517**, 111–117.

52 Z. Bajko, J. Daniels, D. Gudat, S. Häp and M. Nieger, *Organometallics*, 2002, **21**, 5182–5189.

53 D. H. Nguyen, J. Bayardon, C. Salomon-Bertrand, S. Jugé, P. Kalck, J.-C. Daran, M. Urrutigoity and M. Gouygou, *Organometallics*, 2012, **31**, 857–869.

54 D. H. Nguyen, H. Lauréano, S. Jugé, P. Kalck, J.-C. Daran, Y. Coppel, M. Urrutigoity and M. Gouygou, *Organometallics*, 2009, **28**, 6288–6292.

55 A. Weiss, H. Pritzkow and W. Siebert, *Eur. J. Inorg. Chem.*, 2002, **2002**, 1607–1614.

56 J. Brugos, J. A. Cabeza, P. García-Álvarez, A. R. Kennedy, E. Pérez-Carreño and J. F. Van der Maelen, *Inorg. Chem.*, 2016, **55**, 8905–8912.

57 D. J. Elliot, C. J. Levy, R. J. Puddephatt, D. G. Holah, A. N. Hughes, V. R. Magnuson and I. M. Moser, *Inorg. Chem.*, 1990, **29**, 5014–5015.

58 J. Feilong, T. P. Fehlner and A. L. Rheingold, *J. Organomet. Chem.*, 1988, **348**, C22–C26.

59 R. Macías, N. P. Rath and L. Barton, *Angew. Chem., Int. Ed.*, 1999, **38**, 162–164.

60 M. Ingleson, N. J. Patmore, G. D. Ruggiero, C. G. Frost, M. F. Mahon, M. C. Willis and A. S. Weller, *Organometallics*, 2001, **20**, 4434–4436.

61 N. Merle, G. Koicok-Köhn, M. F. Mahon, C. G. Frost, G. D. Ruggerio, A. S. Weller and M. C. Willis, *Dalton Trans.*, 2004, 3883–3892.

62 N. Merle, C. G. Frost, G. Kociok-Köhn, M. C. Willis and A. S. Weller, *Eur. J. Inorg. Chem.*, 2006, **3**, 4068–4073.

63 N. Frank, K. Hanau, K. Flosdorf and R. Langer, *Dalton Trans.*, 2013, **42**, 11252–11261.

64 C. A. Ghilardi, P. Innocenti, S. Midollini and A. Orlandini, *J. Organomet. Chem.*, 1982, **231**, C78–C80.

65 C. A. Ghilardi, P. Innocenti, S. Midollini and A. Orlandini, *J. Chem. Soc., Dalton Trans.*, 1985, 605.

66 M. Koutmos and D. Coucouvanis, *Inorg. Chem.*, 2004, **43**, 6508–6510.

67 M. Koutmos, I. P. Georgakaki and D. Coucouvanis, *Inorg. Chem.*, 2006, **45**, 3648–56.

68 H. V. R. Dias, S. Alidori, G. G. Lobbia, G. Papini, M. Pellei and C. Santini, *Inorg. Chem.*, 2007, **46**, 9708–9714.

69 T. F. Van Dijkman, H. M. De Bruijn, M. A. Siegler and E. Bouwman, *Eur. J. Inorg. Chem.*, 2015, **2015**, 5387–5394.

70 L. Maria, A. Paulo, I. C. Santos, I. C. Santos, P. Kurz, B. Spingler and R. Alberto, *J. Am. Chem. Soc.*, 2006, **128**, 14590–14598.

71 R. Garcia, A. Paulo, Â. Domingos, I. Santos, K. Ortner and R. Alberto, *J. Am. Chem. Soc.*, 2000, **122**, 11240–11241.

72 X. Y. Liu, S. Bouherour, H. Jacobsen, H. W. Schmalle and H. Berke, *Inorg. Chim. Acta*, 2002, **330**, 250–267.

73 M. Videira, L. Maria, A. Paulo, I. C. Santos, I. Santos, P. D. Vaz and M. J. Calhorda, *Organometallics*, 2008, **27**, 1334–1337.

74 J. Wagler and A. F. Hill, *Organometallics*, 2008, **27**, 2350–2353.

75 N. Tsoureas, T. Bevis, C. P. Butts, A. Hamilton and G. R. Owen, *Organometallics*, 2009, **28**, 5222–5232.

76 D. Song, W. L. Jia, G. Wu and S. Wang, *Dalton Trans.*, 2005, 433–438.

77 O. Volkov, R. Macías, N. P. Rath and L. Barton, *Inorg. Chem.*, 2002, **41**, 5837–5843.

78 K. Saha, R. Ramalakshmi, S. Gomosta, K. Pathak, V. Dorcet, T. Roisnel, J.-F. F. Halet and S. Ghosh, *Chem. - Eur. J.*, 2017, **23**, 9812–9820.

79 D. K. Roy, R. Borthakur, A. De, B. Varghese, A. K. Phukan and S. Ghosh, *ChemistrySelect*, 2016, **1**, 3757–3761.

80 A. F. Hill, G. R. Owen, A. J. White and D. J. Williams, *Angew. Chem., Int. Ed.*, 1999, **38**, 2759–2761.

81 C. Y. Tang, W. Smith, A. L. Thompson, D. Vidovic and S. Aldridge, *Angew. Chem., Int. Ed.*, 2011, **50**, 1359–1362.

82 J. C. Bommer and K. W. Morse, *Inorg. Chem.*, 1978, **17**, 3708–3710.

83 F. M. A. M. Aqra, *Transition Met. Chem.* , 2004, **29**, 921–924.

84 I. E. Golub, O. A. Filippov, E. I. Gutsul, N. V Belkova, L. M. Epstein, A. Rossin, M. Peruzzini and E. S. Shubina, *Inorg. Chem.*, 2012, **51**, 6486–6497.

85 Z. Xu and Z. Lin, *Coord. Chem. Rev.*, 1996, **156**, 139–162.

86 A. Lledos, M. Duran, Y. Jean and F. Volatron, *Inorg. Chem.*, 1991, **30**, 4440–4445.

87 H. V Rasika Dias and H.-L. Lu, *Inorg. Chem.*, 2000, **39**, 2246–2248.

88 T. Saito, S. Kuwata and T. Ikariya, *Chem. Lett.*, 2006, **35**, 1224–1225.

89 C. Lenczyk, D. K. Roy, B. Ghosh, J. Schwarzmann, A. K. Phukan and H. Braunschweig, *Chem. - Eur. J.*, 2019, **25**, 8585–8589.

90 G. R. Owen, *Chem. Commun.*, 2016, **52**, 10712–10726.

91 S. Trofimenko, *Scorpionates: The Coordination Chemistry of Polypyrazolylborate Ligands*, Imperial College Press, 1999.

92 S. Trofimenko, *J. Am. Chem. Soc.*, 1966, **88**, 1842–1844.

93 G. Dyson, A. Hamilton, B. Mitchell and G. R. Owen, *Dalton Trans.*, 2009, 6120–6126.

94 I. R. Crossley, A. F. Hill and A. C. Willis, *Organometallics*, 2010, **29**, 326–336.

95 S. L. Kuan, W. K. Leong, L. Y. Goh and R. D. Webster, *J. Organomet. Chem.*, 2006, **691**, 907–915.

96 I. R. Crossley and A. F. Hill, *Dalton Trans.*, 2008, 201–203.

97 A. Neshat, H. R. Shahsavari, P. Mastrorilli, S. Todisco, M. G. Haghighi and B. Notash, *Inorg. Chem.*, 2018, **57**, 1398–1407.

98 R. C. Da Costa, B. W. Rawe, N. Tsoureas, M. F. Haddow, H. A. Sparkes, G. J. Tizzard, S. J. Coles and G. R. Owen, *Dalton Trans.*, 2018, **47**, 11047–11057.

99 T.-P. Lin and J. C. Peters, *J. Am. Chem. Soc.*, 2013, **135**, 15310–15313.

100 W. H. Harman and J. C. Peters, *J. Am. Chem. Soc.*, 2012, **134**, 5080–5082.

101 R. C. Da Costa, B. W. Rawe, A. Iannetelli, G. J. Tizzard, S. J. Coles, A. J. Guwy and G. R. Owen, *Inorg. Chem.*, 2019, **58**, 359–367.

102 A. Iannetelli, G. Tizzard, S. J. Coles and G. R. Owen, *Organometallics*, 2018, **37**, 2177–2187.

103 G. Dyson, A. Zech, B. W. Rawe, M. F. Haddow, A. Hamilton and G. R. Owen, *Organometallics*, 2011, **30**, 5844–5850.

104 A. Zech, M. F. Haddow, H. Othman and G. R. Owen, *Organometallics*, 2012, **31**, 6753–6760.

105 K. Naktode, T. D. N. Reddy, H. P. Nayek, B. S. Mallik and T. K. Panda, *RSC Adv.*, 2015, **5**, 51413–51420.

106 K. Saha, R. Ramalakshmi, R. Borthakur, S. Gomosta, K. Pathak, V. Dorcet, T. Roisnel, J.-F. Halet and S. Ghosh, *Chem. - Eur. J.*, 2017, **23**, 18264–18275.

107 A. Iannetelli, G. Tizzard, S. J. Coles and G. R. Owen, *Inorg. Chem.*, 2018, **57**, 446–456.

108 K. Saha, B. Joseph, R. Borthakur, R. Ramalakshmi, T. Roisnel and S. Ghosh, *Polyhedron*, 2017, **125**, 246–252.

109 A. E. Nako, A. J. P. White and M. R. Crimmin, *Dalton Trans.*, 2015, **44**, 12530–12534.

110 S. C. Kokkou, S. Fortier, P. J. Rentzeperis and P. Karagiannidis, *Acta Crystallogr., Sect. C: Cryst. Struct. Commun.*, 1983, **39**, 178–180.

111 S. C. Davies, M. C. Durrant, D. L. Hughes, K. Leidenberger, C. Stapper and R. L. Richards, *J. Chem. Soc., Dalton Trans.*, 1997, **2**, 2409–2418.

112 T. S. Lobana, S. Paul and A. Castineiras, *Polyhedron*, 1997, **16**, 4023–4031.

113 T. S. Lobana, P. K. Bhatia and E. R. T. Tiekink, *J. Chem. Soc., Dalton Trans.*, 1989, 749.

114 S. K. Hadjikakou, P. Aslanidis, P. Karagiannidis, D. Mentzafos and A. Terzis, *Inorg. Chim. Acta*, 1991, **186**, 199–204.

115 S. K. Hadjikakou, P. Aslanidis, P. Karagiannidis, A. Aubry and S. Skoulika, *Inorg. Chim. Acta*, 1992, **193**, 129–135.

116 P. Aslanidis, P. J. Cox and P. Tsaliki, *Polyhedron*, 2008, **27**, 3029–3035.

117 O. P. Anderson, C. M. Perkins and K. K. Brito, *Inorg. Chem.*, 1983, **22**, 1267–1273.

118 S. R. Acott, C. D. Garner, J. R. Nicholson and W. Clegg, *J. Chem. Soc., Dalt. Trans.*, 1983, **8**, 713–719.

119 C. D. Garner, J. R. Nicholson and W. Clegg, *Inorg. Chem.*, 1984, **23**, 2148–2150.

120 B. Singaram, T. E. Cole and H. C. Brown, *Organometallics*, 1984, **3**, 774–777.

121 A. Iannetelli, University of South Wales, 2020.

122 B. E. Green, C. H. L. Kennard, G. Smith, M. M. Elcombe, F. H. Moore, B. D. James and A. H. White, *Inorg. Chim. Acta*, 1984, **83**, 177–189.

123 B. E. Green, C. H. L. Kennard, G. Smith, B. D. James, P. C. Healy and A. H. White, *Inorg. Chim. Acta*, 1984, **81**, 147–150.

124 V. D. Makhaev, A. P. Borisov, E. B. Lobkovskii, V. B. Polyakova and K. N. Semenenko, *Bull. Acad. Sci. USSR, Div. Chem. Sci.*, 1985, **34**, 1731–1736.

125 B. E. Green, C. H. L. Kennard, C. J. Hawkins, G. Smith, B. D. James and A. H. White, *Acta Crystallogr., Sect. B: Struct. Crystallogr. Cryst. Chem.*, 1980, **36**, 2407–2409.

126 N. Tsoureas, G. R. Owen, A. Hamilton and A. G. Orpen, *Dalton Trans.*, 2008, 6039–6044.

127 N. Tsoureas, Y. Y. Kuo, M. F. Haddow and G. R. Owen, *Chem. Commun.*, 2011, **47**, 484–486.

128 N. Tsoureas, J. Nunn, T. Bevis, M. F. Haddow, A. Hamilton and G. R. Owen, *Dalton Trans.*, 2011,

40, 951–958.

129 G. R. Owen, N. Tsoureas, R. F. Hope, Y. Y. Kuo and M. F. Haddow, *Dalton Trans.*, 2011, **40**, 5906–5915.

130 N. Tsoureas, R. F. Hope, M. F. Haddow and G. R. Owen, *Eur. J. Inorg. Chem.*, 2011, 5233–5241.

131 T. L. Brown and K. J. Lee, *Coord. Chem. Rev.*, 1993, **128**, 89–116.

132 D. J. Durand and N. Fey, *Chem. Rev.*, 2019, **119**, 6561–6594.

133 J. Reglinski, M. Garner, I. D. Cassidy, P. A. Slavin, M. D. Spicer and D. R. Armstrong, *J. Chem. Soc., Dalton Trans.*, 1999, 2119–2126.

134 I. Cassidy, M. Garner, A. R. Kennedy, G. B. S. Potts, J. Reglinski, P. A. Slavin and M. D. Spicer, *Eur. J. Inorg. Chem.*, 2002, **12**, 1235–1239.

135 M. R. S. J. Foreman, A. F. Hill, G. R. Owen, A. J. P. White and D. J. Williams, *Organometallics*, 2003, **22**, 4446–4450.

136 H. Baba and M. Nakano, *Polyhedron*, 2011, **30**, 3182–3185.

137 C. A. Dodds, A. R. Kennedy, J. Reglinski and M. D. Spicer, *Inorg. Chem.*, 2004, **43**, 394–395.

138 C. A. Dodds, J. Reglinski and M. D. Spicer, *Chem. - Eur. J.*, 2006, **12**, 931–939.

139 D. Wallace, K. Chalmers, C. A. Dodds, I. A. Stepek, D. R. Armstrong, L. E. A. Berlouis, J. Reglinski and M. D. Spicer, *Eur. J. Inorg. Chem.*, 2014, 2569–2575.

140 M. R. S. J. Foreman, C. Ma, A. F. Hill, N. E. Otten, M. Sharma, N. Tshabang and J. S. Ward, *Dalton Trans.*, 2017, **46**, 14957–14972.

141 G. C. Welch, R. R. S. Juan, J. D. Masuda and D. W. Stephan, *Science (80-.).*, 2006, **314**, 1124–1126.

142 S. Senda, Y. Ohki, T. Hirayama, D. Toda, J. Chen, T. Matsumoto, H. Kawaguchi and K. Tatsumi, *Inorg. Chem.*, 2006, **45**, 9914–9925.

143 P. A. Slavin, J. Reglinski, M. D. Spicer and A. R. Kennedy, *J. Chem. Soc., Dalton Trans.*, 2000, 239–240.

144 D. V. Patel, D. J. Mihalcik, K. A. Kreisel, G. P. A. Yap, L. N. Zakharov, W. S. KasselPermanent address: Department, A. L. Rheingold and D. Rabinovich, *Dalton Trans.*, 2005, 2410.

145 P. J. Bailey, A. Dawson, C. McCormack, S. A. Moggach, I. D. H. Oswald, S. Parsons, D. W. H. Rankin and A. Turner, *Inorg. Chem.*, 2005, **44**, 8884–8898.

146 C. Kimblin, B. M. Bridgewater, T. Hascall and G. Parkin, *J. Chem. Soc., Dalton Trans.*, 2000, 891–897.

147 R. Garcia, Â. Domingos, A. Paulo, I. Santos and R. Alberto, *Inorg. Chem.*, 2002, **41**, 2422–2428.

148 K. Yurkerwich, F. Coleman and G. Parkin, *Dalton Trans.*, 2010, **39**, 6939–6942.

149 X. Y. Wang, Q. Ma, T. Duan, Q. Chen and Q. F. Zhang, *Inorg. Chim. Acta*, 2012, **384**, 281–286.

150 S. L. Kuan, W. K. Leong, R. D. Webster and L. Y. Goh, *Organometallics*, 2012, **31**, 273–281.

151 A. Ariafard and M. M. Amini, *J. Organomet. Chem.*, 2005, **690**, 84–95.

152 C. A. Dodds, M. Garner, J. Reglinski and M. D. Spicer, *Inorg. Chem.*, 2006, **45**, 2733–2741.

153 C. Santini, G. Gioia Lobbia, C. Pettinari, M. Pellei, G. Valle and S. Calogero, *Inorg. Chem.*, 1998, **37**, 890–900.

154 Effendy, G. G. Lobbia, C. Pettinari, C. Santini, B. W. Skelton and A. H. White, *Inorg. Chim. Acta*, 2000, **308**, 65–72.

155 G. R. Owen, P. H. Gould, A. Moore, G. Dyson, M. F. Haddow and A. Hamilton, *Dalton Trans.*, 2013, **42**, 11074–11081.

156 F. G. Brickwedde, *J. Opt. Soc. Am.*, 1927, **14**, 312.

157 A. Johnson, A. J. Martínez-Martínez, S. A. Macgregor and A. S. Weller, *Dalton Trans.*, 2019, **48**, 9776–9781.

158 T. Iijima, S. Tsuchiya and M. Kimura, *Bull. Chem. Soc. Jpn.*, 1977, **50**, 2564–2567.

159 S. Trofimenko, *Polyhedron*, 2004, **23**, 197–203.

160 T. C. Higgs and C. J. Carrano, *Inorg. Chem.*, 1997, **36**, 298–306.

161 R. Echeverría, J. M. López-de-Luzuriaga, M. Monge, S. Moreno, M. E. Olmos and M. Rodríguez-Castillo, *Chem. Commun.*, 2018, **54**, 295–298.

162 C. Ángel-Jijón, D. Rendón-Nava, J. M. Vazques-Pérez, A. Álvarez-Hernández, D. Mendoza-Espinosa and V. Salazar-Pereda, *Dalton Trans.*, 2020, **49**, 6199–6204.

163 R. Fränkel, J. Kniczek, W. Ponikwar, H. Nöth, K. Polborn and W. P. Fehlhammer, *Inorg. Chim. Acta*, 2001, **312**, 23–39.

164 A. F. Hill, M. K. Smith, N. Tshabang and A. C. Willis, *Organometallics*, 2010, **29**, 473–477.

165 H. Schmidbaur, *Gold Bull.*, 2000, **33**, 3–10.

166 P. Pyykkö, *Angew. Chem., Int. Ed.*, 2004, **43**, 4412–4456.

167 H. Schmidbaur and A. Schier, *Chem. Soc. Rev.*, 2008, **37**, 1931–1951.

168 N. Carr, M. C. Gimeno, J. E. Goldberg, M. U. Pilotti, F. G. A. Stone and I. Topaloğlu, *J. Chem. Soc., Dalton Trans.*, 1990, 2253–2261.

169 J. C. Jeffery, P. A. Jelliss and F. G. A. Stone, *J. Chem. Soc., Dalton Trans.*, 1994, 25–32.

170 J. C. Jeffery, P. A. Jelliss and F. G. A. Stone, *Organometallics*, 1994, **13**, 2651–2661.

171 M. Hata, J. A. Kautz, X. L. Lu, T. D. McGrath and F. G. A. Stone, *Organometallics*, 2004, **23**, 3590–3602.

172 B. E. Hodson, T. D. McGrath and F. G. A. Stone, *Organometallics*, 2005, **24**, 3386–3394.

173 T. D. McGrath, S. Du, B. E. Hodson and F. G. A. Stone, *Organometallics*, 2006, **25**, 4452–4461.

174 M. J. Carr, T. D. McGrath and F. G. A. Stone, *Inorg. Chem.*, 2008, **47**, 713–722.

175 S. P. Fisher, S. G. McArthur, V. Tej, S. E. Lee, A. L. Chan, I. Banda, A. Gregory, K. Berkley, C. Tsay, A. L. Rheingold, G. Guisado-Barrios and V. Lavallo, *J. Am. Chem. Soc.*, 2020, **142**, 251–256.

176 A. A. Mohamed, D. Rabinovich and J. P. Fackler, *Acta Crystallogr., Sect. E: Struct. Rep. Online*, 2002, **58**, m726–m727.

177 H. V. R. Dias and J. Wu, *Angew. Chem., Int. Ed.*, 2007, **46**, 7814–7816.

178 H. V. R. Dias and W. Jin, *Inorg. Chem.*, 1996, **35**, 3687–3694.

179 G. Gioia Lobbia, J. V. Hanna, M. Pellei, C. Pettinari, C. Santini, B. W. Skelton and A. H. White, *Dalton Trans.*, 2004, **6**, 951.

180 M. T. Räisänen, N. Runeberg, M. Klinga, M. Nieger, M. Bolte, P. Pyykkö, M. Leskelä and T. Repo, *Inorg. Chem.*, 2007, **46**, 9954–9960.

181 H. Häkkinen, *Nat. Chem.*, 2012, **4**, 443–455.

182 M. Grandbois, *Science (80-.).*, 1999, **283**, 1727–1730.

183 H. Schmidbaur, *Chem. Soc. Rev.*, 1995, **24**, 391.

184 M. D. Ward, J. A. McCleverty and J. C. Jeffery, *Coord. Chem. Rev.*, 2001, **222**, 251–272.

185 W.-T. Lee, I.-R. Jeon, S. Xu, D. A. Dickie and J. M. Smith, *Organometallics*, 2014, **33**, 5654–5659.

186 N. M. Scott and S. P. Nolan, *Eur. J. Inorg. Chem.*, 2005, **2005**, 1815–1828.

187 M.-T. Lee and C.-H. Hu, *Organometallics*, 2004, **23**, 976–983.

188 N. Tsoureas, A. Hamilton, M. F. Haddow, J. N. Harvey, A. G. Orpen and G. R. Owen, *Organometallics*, 2013, **32**, 2840–2856.

189 W. A. Herrmann, *Angew. Chem., Int. Ed.*, 2002, **41**, 1290–1309.

190 F. E. Hahn and M. C. Jahnke, *Angew. Chem., Int. Ed.*, 2008, **47**, 3122–3172.

191 M. N. Hopkinson, C. Richter, M. Schedler and F. Glorius, *Nature*, 2014, **510**, 485–496.

192 C. M. Crudden and D. P. Allen, *Coord. Chem. Rev.*, 2004, **248**, 2247–2273.

193 P. de Frémont, N. Marion and S. P. Nolan, *Coord. Chem. Rev.*, 2009, **253**, 862–892.

194 H. Jacobsen, A. Correa, A. Poater, C. Costabile and L. Cavallo, *Coord. Chem. Rev.*, 2009, **253**, 687–703.

195 G. Frenking, M. Solà and S. F. Vyboishchikov, *J. Organomet. Chem.*, 2005, **690**, 6178–6204.

196 S. F. Vyboishchikov and G. Frenking, *Chem. - Eur. J.*, 1998, **4**, 1428–1438.

197 G. Occhipinti and V. R. Jensen, *Organometallics*, 2011, **30**, 3522–3529.

198 O. Kühl, *Chem. Soc. Rev.*, 2007, **36**, 592–607.

199 V. K. Greenacre, M. B. Ansell, S. M. Roe and I. R. Crossley, *Eur. J. Inorg. Chem.*, 2014, **2014**, 5053–5062.

200 V. Greenacre, University of Sussex, 2016.

201 A. Sathyanarayana, B. P. R. Metla, N. Sampath and G. Prabusankar, *J. Organomet. Chem.*, 2014, **772**–**773**, 210–216.

202 G. Prabusankar, A. Sathyanarayana, G. Raju and C. Nagababu, *Asian J. Org. Chem.*, 2017, **6**, 1451–1459.

203 X. Wang, S. Liu, L. H. Weng and G. X. Jin, *Chem. - Eur. J.*, 2007, **13**, 188–195.

204 H. Brown and B. C. Rao, *J. Org. Chem.*, 1957, **22**, 1136–1137.

205 S. Huang, W. Zhang, T. Liu, K. Wang, X. Qi, J. Zhang and Q. Zhang, *Chem. - Asian J.*, 2016, **11**, 3528–3533.

206 H. C. Brown, J. R. Schwier and B. Singaram, *J. Org. Chem.*, 1978, **43**, 4395–4397.

207 H. C. Brown, J. R. Schwier and B. Singaram, *J. Org. Chem.*, 1979, **44**, 465–466.

208 B. Singaram and J. R. Schwier, *J. Organomet. Chem.*, 1978, **156**, C1–C4.

209 H. C. Brown, B. Nazer, J. S. Cha and J. A. Sikorski, *J. Org. Chem.*, 1986, **51**, 5264–5270.

210 H. C. Brown, T. E. Cole, M. Srebnik and K. W. Kim, *J. Org. Chem.*, 1986, **51**, 4925–4930.

211 T. E. Cole, R. K. Bakshi, M. Srebnik, B. Singaram and H. C. Brown, *Organometallics*, 1986, **5**, 2303–2307.

212 H. C. Brown and J. A. Soderquist, *J. Org. Chem.*, 1980, **45**, 846–849.

213 E. F. Knights and H. C. Brown, *J. Am. Chem. Soc.*, 1968, **90**, 5280–5281.

214 D. Morvan, J. F. Capon, F. Gloaguen, F. Y. Pétillon, P. Schollhammer, J. Talarmin, J. J. Yaouanc, F. Michaud and N. Kervarec, *J. Organomet. Chem.*, 2009, **694**, 2801–2807.

215 S. Arava and C. Diesendruck, *Synthesis* , 2017, **49**, 3535–3545.

216 H. M. J. Wang and I. J. B. Lin, *Organometallics*, 1998, **17**, 972–975.

217 Q. Li, X. Li, J. Yang, H.-B. Song and L.-F. Tang, *Polyhedron*, 2013, **59**, 29–37.

218 C.-X. Lin, X.-F. Kong, F.-B. Xu, Z.-Z. Zhang and Y.-F. Yuan, *Z. Anorg. Allg. Chem.*, 2013, **639**, 881–885.

219 Q.-X. Liu, L.-X. Zhao, X.-J. Zhao, Z.-X. Zhao, Z.-Q. Wang, A.-H. Chen and X.-G. Wang, *J. Organomet. Chem.*, 2013, **731**, 35–48.

220 D. Zhang, S. Zhou, Z. Li, Q. Wang and L. Weng, *Dalton Trans.*, 2013, **42**, 12020.

221 B. Khalili Najafabadi and J. F. Corrigan, *Dalton Trans.*, 2014, **43**, 2104–2111.

222 S. G. Resch, S. Dechert and F. Meyer, *Z. Anorg. Allg. Chem.*, 2019, **645**, 605–612.

223 H. U. Blaser, C. Malan, B. Pugin, F. Spindler, H. Steiner and M. Studer, *Adv. Synth. Catal.*, 2003, **345**, 103–151.

224 M. Heitbaum, F. Glorius and I. Escher, *Angew. Chem., Int. Ed.*, 2006, **45**, 4732–4762.

225 M. Slivarichova, M. F. Haddow, H. Othman and G. R. Owen, *Eur. J. Inorg. Chem.*, 2013, **2013**, 2782–2788.

226 G. Giordano, R. H. Crabtree, R. M. Heintz, D. Forster and D. E. Morris, in *Inorganic Syntheses*, 1979, vol. 19, pp. 218–220.

227 D. J. Pasto, J. Hickman and T.-C. Cheng, *J. Am. Chem. Soc.*, 1968, **90**, 6259–6260.

228 Ö. Seven, M. Bolte, H. Lerner and M. Wagner, *Organometallics*, 2014, **33**, 1291–1299.

229 I. P. Beletskaya and A. V. Cheprakov, *Coord. Chem. Rev.*, 2004, **248**, 2337–2364.

230 S. V. Ley and A. W. Thomas, *Angew. Chem., Int. Ed.*, 2003, **42**, 5400–5449.

231 F. Bellina and R. Rossi, *Adv. Synth. Catal.*, 2010, **352**, 1223–1276.

232 S. H. Kim, S. Y. Gwon, S. M. Burkinshaw and Y. A. Son, *Dyes Pigm.*, 2010, **87**, 268–271.

233 H.-J. Cristau, P. P. Cellier, J.-F. Spindler and M. Taillefer, *Chem. - Eur. J.*, 2004, **10**, 5607–5622.

234 M. Toure, O. Chuzel and J. L. Parrain, *Dalton Trans.*, 2015, **44**, 7139–7143.

235 J. Chatt and L. M. Venanzi, *J. Chem. Soc.*, 1957, 4735.

236 W. A. Herrmann, M. Elison, J. Fischer, C. Köcher and G. R. J. Artus, *Chem. - Eur. J.*, 1996, **2**, 772–780.

237 W. S. Sheldrick and B. Günther, *J. Organomet. Chem.*, 1989, **375**, 233–243.

238 C. Tejel, M. A. Ciriano, M. Bordonaba, J. A. López, F. J. Lahoz and L. A. Oro, *Inorg. Chem.*, 2002, **41**, 2348–2355.

239 R. Uson, L. A. Oro, J. A. Cabeza, H. E. Bryndza and M. P. Stepro, in *Inorganic Syntheses*, 1985, vol. 23, pp. 126–130.

240 J. J. Levison and S. D. Robinson, *J. Chem. Soc. A*, 1970, 96–99.

241 A. M. James, R. K. Laxman, F. R. Fronczek and A. W. Maverick, *Inorg. Chem.*, 1998, **37**, 3785–3791.

242 P. P. Power, K. Ruhlandt-Senge and S. C. Shoner, *Inorg. Chem.*, 1991, **30**, 5013–5015.

243 D. Enders and U. Reinhold, *Tetrahedron: Asymmetry*, 1997, **8**, 1895–1946.

244 I. Coldham, *J. Chem. Soc., Perkin Trans. 1*, 1998, **5**, 1343–1364.

245 R. Chinchilla, C. Nájera and M. Yus, *Tetrahedron*, 2005, **61**, 3139–3176.

246 H. C. Brown, T. E. Cole and M. Srebnik, *Organometallics*, 1985, **4**, 1788–1792.

247 V. César, N. Lugan and G. Lavigne, *J. Am. Chem. Soc.*, 2008, **130**, 11286–11287.

248 V. Lavallo, Y. Canac, C. Präsang, B. Donnadieu and G. Bertrand, *Angew. Chem., Int. Ed.*, 2005, **44**, 5705–5709.

249 J. Chu, D. Munz, R. Jazzar, M. Melaimi and G. Bertrand, *J. Am. Chem. Soc.*, 2016, **138**, 7884–7887.

250 M. Melaimi, R. Jazzar, M. Soleilhavoup and G. Bertrand, *Angew. Chem., Int. Ed.*, 2017, **56**, 10046–10068.

251 A. Iannetelli, G. Tizzard, S. J. Coles and G. R. Owen, *Inorg. Chem.*, 2018, **57**, 446–456.

252 M. Soleilhavoup and G. Bertrand, *Acc. Chem. Res.*, 2015, **48**, 256–266.